CHAPTER 4

RESULTS AND DISCUSSIONS

Part I

4.1 Characterization of the Raw Arsenic-Iron Hydroxide Sludge

4.1.1 Chemical Compositions of the Raw Sludge

By EPA method 3051 together with ICP-OES, arsenic and iron, two important chemical components of the five different recipes of synthesized arsenic-iron hydroxide sludge, were analyzed and are reported in Table 4.1 below.

Table 4.1 Chemical composition of the sludge S1 to S5

	Concentration in microwave digestion fluid		As-to-Fe ratio (M/M)	%As in sludge (weight basis)
	As (mg/L)	Fe(mg/L)		
S1	41.18	200.57	0.153	8.24
S2	35.73	202.13	0.132	7.15
S3	28.70	204.13	0.105	5.74
S4	28.01	206.81	0.101	5.60
S5	19.19	207.04	0.069	3.84

4.1.2 Particle Size Analysis of the Raw Sludge

Figure 4.1 (a) illustrates the particle size distribution curves of the four types of the dewatered arsenic-iron hydroxide sludge, SW1, SW3, SW4, and SW5 in semisolid liquid state. These distribution curves simulate the distribution of the dewatered sludge subjected to the leaching tests at time zero when no dissolution is supposed to take place. As shown in the curves, the distribution can be divided into 3 regions. Most of the distribution of the sludge ranges from 10 to 100 microns while some is from 1 to 10 microns, and only a little is below 1 microns.

On the other hand, Figure4.1 (b) depicts the particle size distribution curves of three types of the dried arsenic-iron hydroxide sludge, SD1, SD4, and SD5 which were dried by heat at 105 ^{o}C and crushed to achieve the finest particles possible to simulate the worst case of leaching. In the same way, these distribution curves simulate the distribution of the dried sludge subjected to leaching tests at time zero when no dissolution is supposed to occur. As shown in this figure, the distribution of the dried sludge ranges from 2 to 1000 microns, mostly from 100 to 1000 microns. It should be noticed that none of the SW samples have particle size larger than 100 micron.

The rational explanation of the increase of the particle size of the sludge after dried by heat is that although dewatered by vacuum filtration until no more free water could be extracted, the saturated surface dry sludge was still saturated with water. Since further dewatering by heating at 105 ^{o}C repelled almost all of water molecules, the semisolid liquid sludge shrinked, accumulated, and turned to denser and larger solid. Although crushed for more than 10 minutes, it was still impossible to reduce the sizes of the dried sludge to the original sizes before drying.

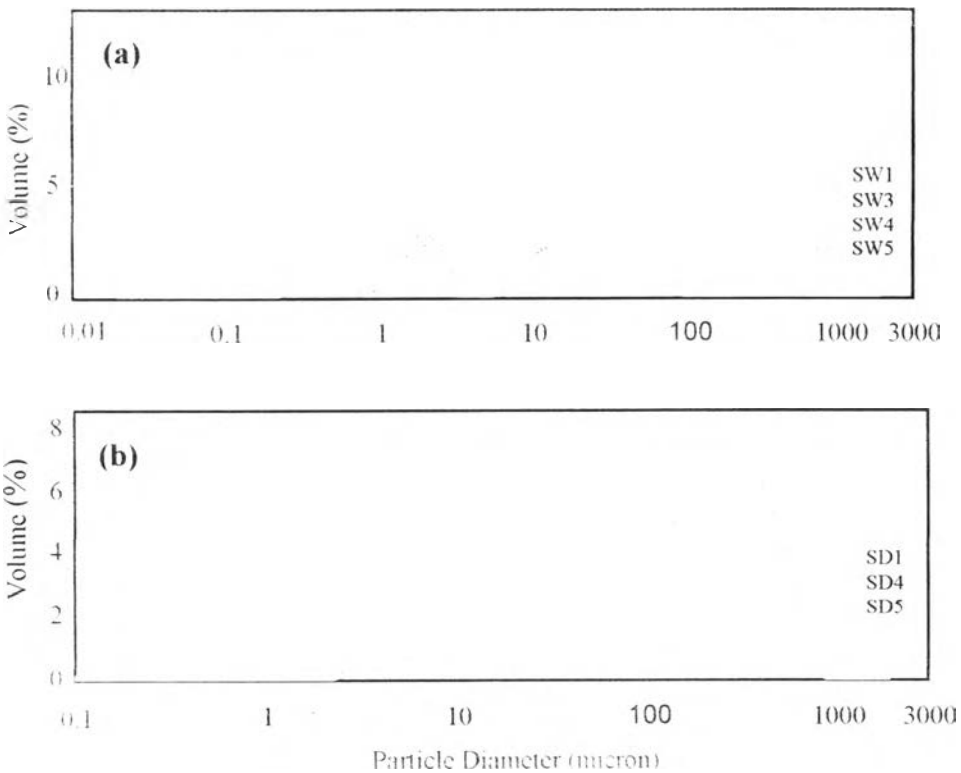

Figure 4.1 (a) Particle size distribution curves of SW1, SW3, SW4, and SW5 and (b) particle size distribution curves of SD1, SD4, and SD5

4.1.3 Vibrational Characterization of the Raw Sludge

The FT-IR spectra of pure amorphous iron hydroxide sludge, pure sodium arsenate hepta-hydrate, and pure sodium arsenite recorded from the wavenumber of 400 to 4000 cm^{-1} are shown in Figure 4.2 (a), (b), and (c), respectively.

Considering Figure 4.2 (a) illustrating the spectra of the pure amorphous iron hydroxide sludge synthesized without addition of arsenic, the adsorption bands appearing at 1345, 2182 (broad peak), and 3302 cm^{-1} are supposed to be responsible for hydrogen bonds (OH) of iron hydroxide. In the same way, the adsorption bands appearing at 449, 555, and 704 cm^{-1} are supposed to be responsible for Cl^- which sorbs onto iron hydroxide on the basis of outer-sphere complexation as discussed in Equation 2-22. The rest at 1516, 1657, and 3612 cm^{-1} are supposed to be responsible for water molecule left in the sludge (Bio-Rad Laboratories, 1998-1999).

On the other hand, as shown in Figure 4.2 (b), the adsorption bands appearing at 855 and 1658 cm^{-1} are in good agreement with the spectrum of Na_2HAsO_4 recently reported by several researchers. The band at 855 cm^{-1} could be assigned to v_3 vibration of the AsO_4^{-3} ion which is closely consistent with the values reported by Keller (1986) (855 cm^{-1}) and Hsia et al (1994) (860 cm^{-1}) while the band at 1658 cm^{-1} could be assigned to v_4 vibration of the AsO_4^{-3} ion which is closely consistent with the values reported by Keller (1986) (1636 cm^{-1}), Hsia et al (1994) (1637 cm^{-1}), and Yousuf et al (1998) (1641 cm^{-1}) (All references above are cited in Mollah et al., 1998). In the same way, in Figure 4.2 (c), the FT-IR spectrum of pure $NaAsO_2$ appearing at 826 cm^{-1} is due to the presence of As-OH groups (Raade et al., 1984 cited in Mollah et al., 1998).

Shown in Figure 4.3 (b) are the FT-IR spectra of the synthesized arsenic-iron sludge S1 to S5 together with the pure amorphous iron hydroxide. Generally, most of the adsorption bands of all the synthesized arsenic-iron sludge S1 to S5 resemble to those of the pure amorphous iron hydroxide throughout the whole wavenumber from 400 to 4000 cm^{-1} except those from 617 to 950 cm^{-1}. Figure4.3 (a) is enlargement of Figure 4.3 (b) from the wavenumber of 400 to 1000 cm^{-1} focusing on additional adsorption bands approximately at 761, 797, and 894 cm^{-1}.

The adsorption band at 797 cm^{-1} is in reasonable agreement with the earlier study of arsenite sorption onto iron and aluminum oxides by Suarez, Goldberg, and Su (1998 cited in Goldberg and Johnston, 2001). In contrast, the band at 894 cm^{-1} is possible to be either arsenite or arsenate sorbed onto iron hydroxide surface. Considering Figure 4.2 again, it is very obvious that, for the pure iron hydroxide sample, there is no adsorption band between the wavenumber of 704 to 1056 cm^{-1}, nevertheless, there are the adsorption bands at 826 and 855 cm^{-1} for sodium arsenite and sodium arsenate, respectively. By this reason, it has potential for the band at 894 cm^{-1} to be either Fe-O-As(III) or Fe-O-As(V) bonds which is a result of shifting either 826 or 855 cm^{-1} to 894 due to the lowering symmetry of arsenic ions as a result of interaction with iron hydroxide surface. The same phenomenon was observed by Arienzo et al. (2001 cited in Voegelin and Hug, 2003) who reported that the band at

1670 cm^{-1} of sodium arsenate shifted to 1748 cm^{-1} when arsenate interacted with iron oxide in electrochemical peroxidation process.

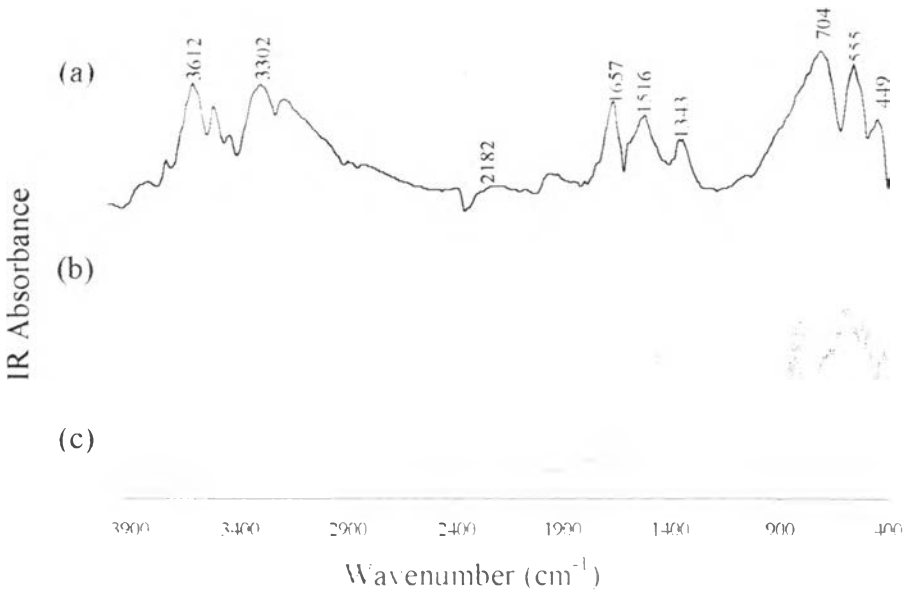

Figure 4.2 The FT-IR spectra of (a) pure amorphous iron hydroxide sludge, (b) pure sodium arsenate hepta-hydrate, and (c) pure sodium arsenite recorded from 400 to 4000 cm^{-1}

It should be noticed that although arsenite was used in the sludge synthesis, the presence of arsenate was also possible. According to the study of Sun and Doner in 1998 (cited in Goldberg and Johnston, 2001), it was found that oxidation of sorbed As(III) to As(V) on Fe(III)-oxide surfaces might be as high as 20%. In this study, the adsorption band at 761 cm^{-1} which is assigned to asymmetric stretching of As-OH groups of $H_2AsO_4^-$ may be one of the good witnesses to support the alteration of arsenic speciation. This band is in good agreement with the Raman spectrum of $H_2AsO_4^-$ in aqueous solution reported by Tossell (1997 cited in Goldberg and Johnston, 2001) (765 cm^{-1}).

However, the Raman as well as FT-IR spectrum of arsenic species in aqueous solution and in pure arsenic salt is generally different from that of arsenic species sorbed onto iron hydroxide surface due to the lowering symmetry as discussed in the last paragraph. Therefore, that the band of $H_2AsO_4^-$ sorbed onto iron hydroxide surface present in this study is almost not different from that of $H_2AsO_4^-$ in aqueous solution in literature implies that this bond between iron hydroxide and $H_2AsO_4^-$ is very weak or even corresponds to non-surface complexed As-O bonds.

The last point to which the author pays attention is that the bonds identified by FT-IR spectra in Figure 4.3 may not be all of the possible bonds. Especially for arsenite species, Goldberg and Johnston (2001) suggested that spectral methods used in their research including FT-IR were not as well-suited to observe more weakly held surface complexes that do not involve direct coordination of the As(III) complex with the surface through a As-O-X bond.

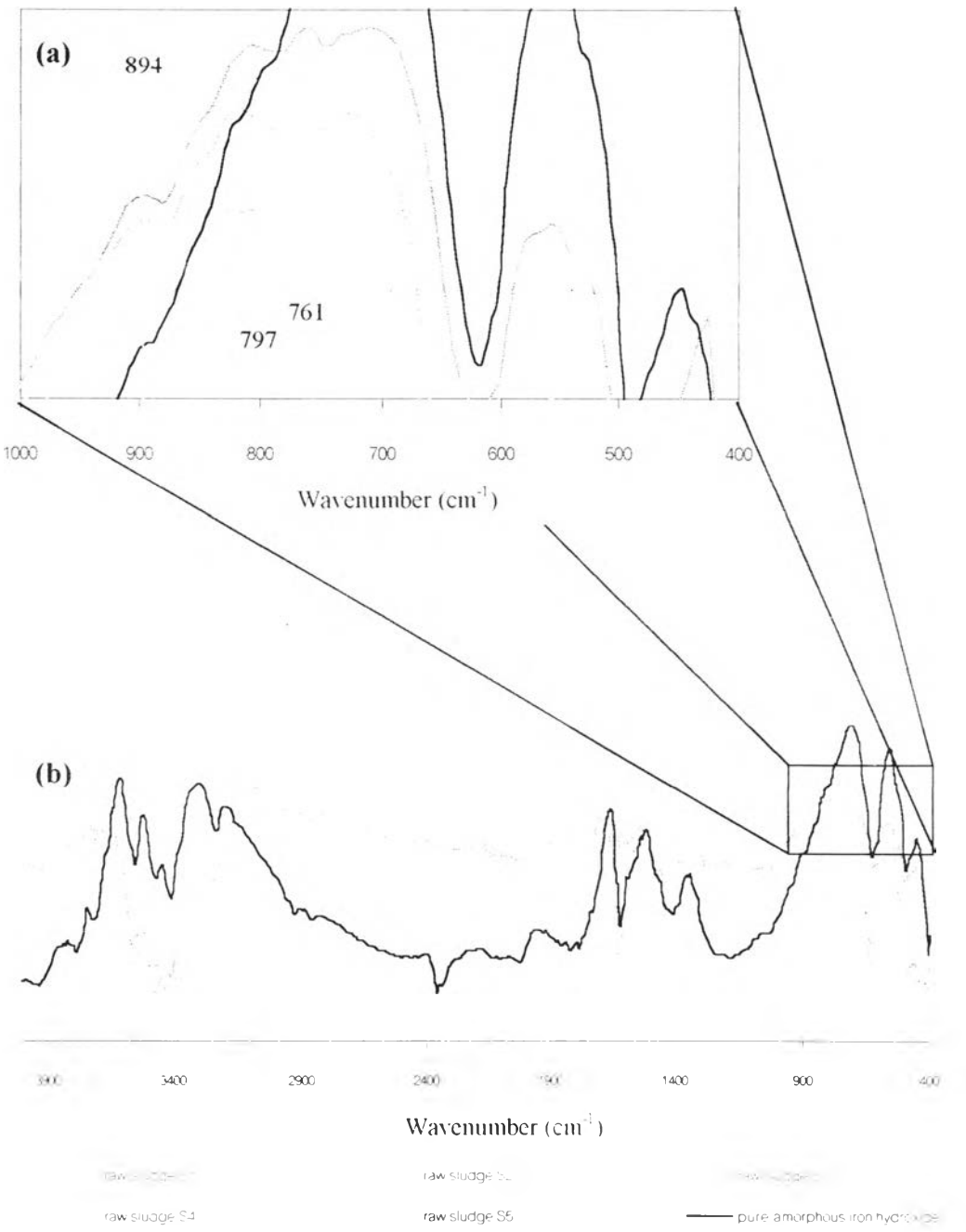

FIGURE 4.3 (a) the FT-IR spectra of synthesized arsenic-iron sludge S1 to S5 together with pure amorphous iron hydroxide focusing on the wavenumber from 400 to 1000 cm^{-1}. (b) the FT-IR spectra throughout the whole length from 400 to 4000

4.1.4 Microstructures of the Raw Sludge

The microstructures together with the x-ray dot maps and the EDS spectra of the pure amorphous iron hydroxide and the four types of the arsenic-containing sludge, S1, S2, S4, and S5 are shown in Figures 4.4, 4.5, 4.6, 4.7, 4.8, and 4.9, respectively. However, due to the fact that, naturally, dewatered coagulation residual is still saturated with water, further dewatering by heat is required in order to make it appropriate for SEM-EDS analysis. Consequently, since almost all of water is repelled by heat at 105 °C from an oven, the semisolid liquid sludge shrinks, accumulates, and turns to very dense residual from which it is almost impossible for us to study its actual microstructures. For this reason, almost all of the SEM photographs shown in the present study illustrate only the outside of the shrinking sludge. Furthermore, their x-ray dot maps reveal only the information regarding distribution of their components such as Fe, O, As, Na, and Cl from the outer surface to 10 μm deep down into the bulk sludge.

Despite SEM-EDS analysis having the drawback as discussed in the previous paragraph, the distribution of the components of the sludge provided by their x-ray dot maps is still useful for confirming the adsorption density of arsenic onto the sludge which was indirectly interpreted by the result of microwave assistant acid digestion described in section 4.1.1. Considering the x-ray dot maps expressing arsenic and iron together with the semi quantitative EDS analysis for each kind of the sludge shown in Table 4.2, it is evident that the densities of x-ray dots expressing arsenic decrease from S1 to S5. Similarly, the semi quantitative As-to-Fe ratios by atomic (count/count) from EDS analysis of S1 to S5 are in the same trend as their x-ray dot maps. In conclusion, these three groups of information indicate that the sludge S1 has the highest adsorption density while S2 has the second highest density, and so on.

Fortunately, although most of SEM photographs in this study cannot reveal actual microstructures of the arsenic-iron sludge due to accumulation mentioned in the previous paragraph, the SEM photograph of the sludge S3 can help provide insight into not only its microstructures but also arsenic binding mechanism. Illustrated in

Figure 4.10, the surface of the sludge can be categorized into two types: zone 1 and 2 covered by a number of sphere-like microstructures and zone 3 without the sphere-like covering.

According to its x-ray dot maps in Figure 4.12 together with the SEM photograph and EDS analysis in Figures 4.14 focusing on the spheres, it is evident that these spheres consist of Na and Cl with a little amount of arsenic. Moreover, it is still found that the zone 3 without the sphere-like covering consists of Fe, As, and O, but not Na and Cl. These x-ray dot maps resemble to two surface complexation mechanisms based on the triple-layer model (TLM), inner-sphere surface complexation and outer-sphere surface complexation.

TLM has been primarily applied to adsorbents having the layer of $\equiv OH_x$ groups all along the surface such as amorphous iron hydroxide. Figure 4.11 and 4.13 illustrate the surface structure of such an adsorbent when it is suspended in solution with the presence of Na^+, Cl^-, and arsenic species. As shown in the diagram and the figure, arsenic is presumed to bind directly to either a surface oxide ion or an underlying Fe ion (effectively replacing a surface $\equiv OH_x$ groups). Adsorption by this manner must lose at least the water of hydration on the side nearest the solid. The strong surface complexes formed by this reaction are known as inner-sphere complexes. A plane that runs through the centers of the surface oxide ions and any adsorbate bond either directly to them or to surface Fe ions is named surface plane or naught (O) plane which is supposed to correspond to the zoom 3 containing Fe, O and As in Figure 4.10.

On the other hand, other ions such as Na^+ and Cl^- as well as arsenic are presumed to bind to the surface via chemical bonds, but to retain all their waters of hydration. Therefore, separated from the surface by water molecule, these ions are supposed to form weak complexes called ion pair or outer-sphere complexes. A plane running through these ions is called the beta (β) plane which is supposed to correspond to the zoon 1 and 2 containing Na^+, Cl^-, and As in Figure 4.10.

In conclusion, from the combination of information of FT-IR and SEM-EDS, arsenic is supposed to form both inner and outer sphere complexes. This conclusion is, also, in good agreement with the several studies mentioned in literature review section

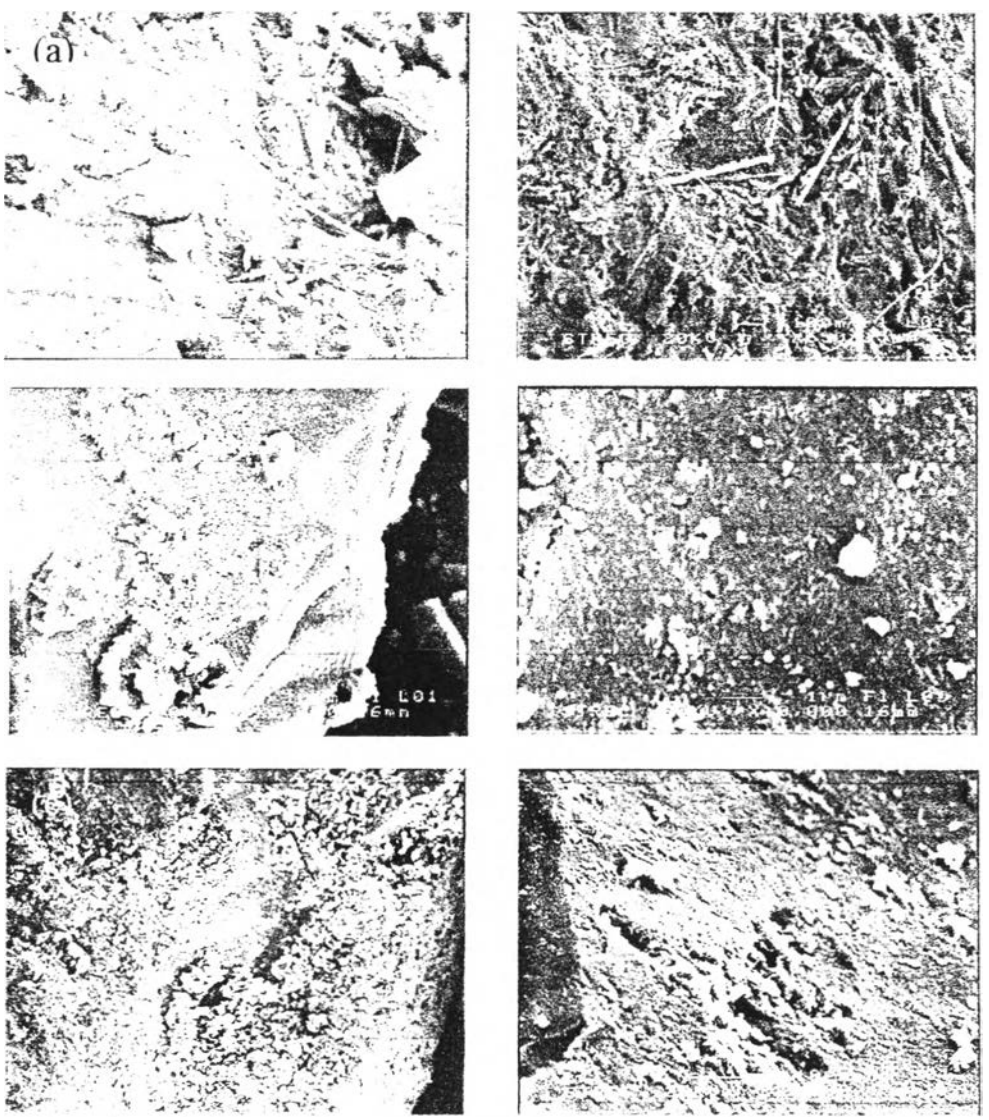

Figure 4.4 The SEM photographs of of (a) and (b) the pure amorphous iron hydroxide, (c) S1, (d) S2, (e) S4, and (f) S5

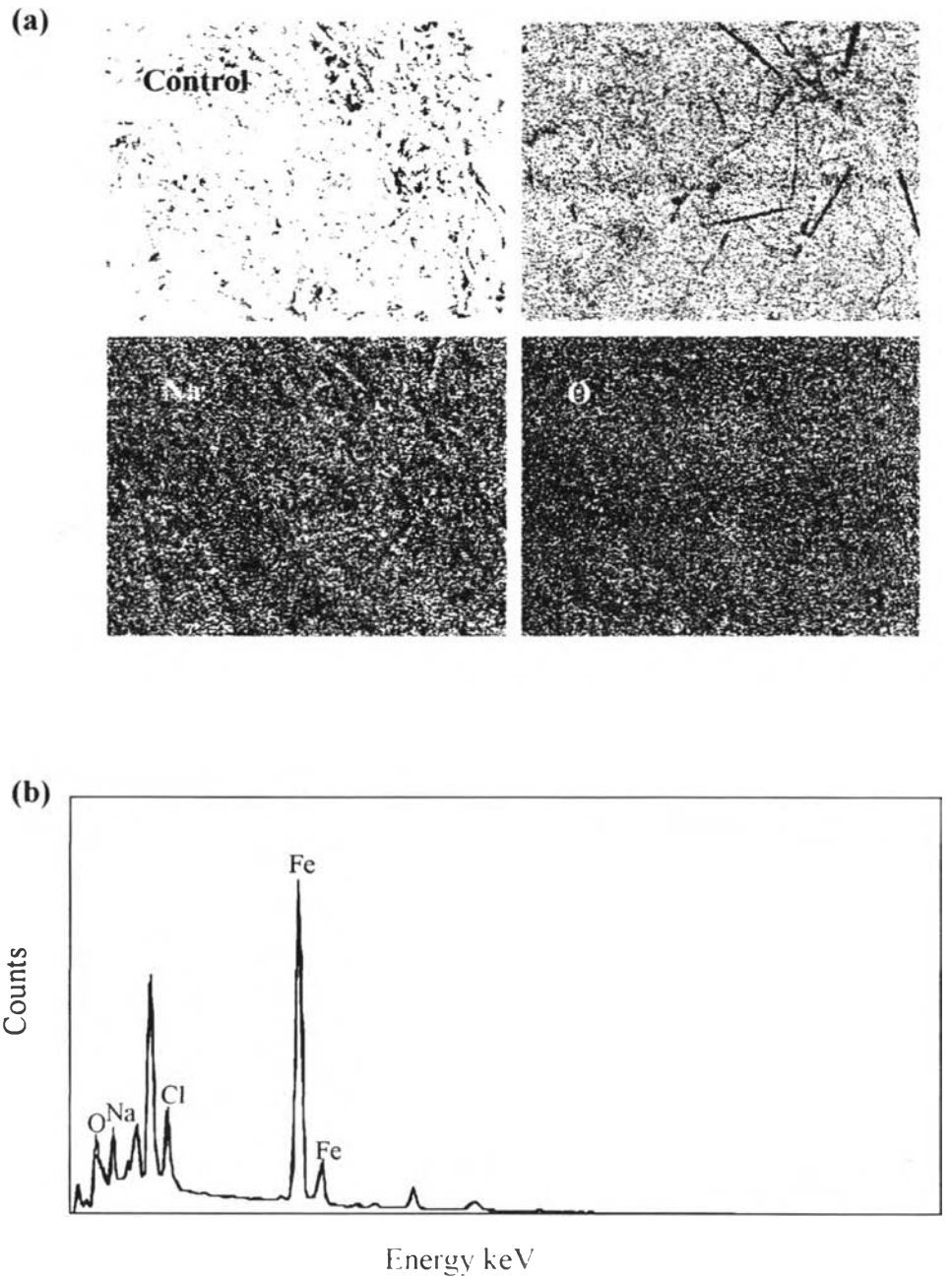

Figure 4.5 (a) The x-ray dot maps and (b) the EDS spectra of the pure amorphous iron hydroxide

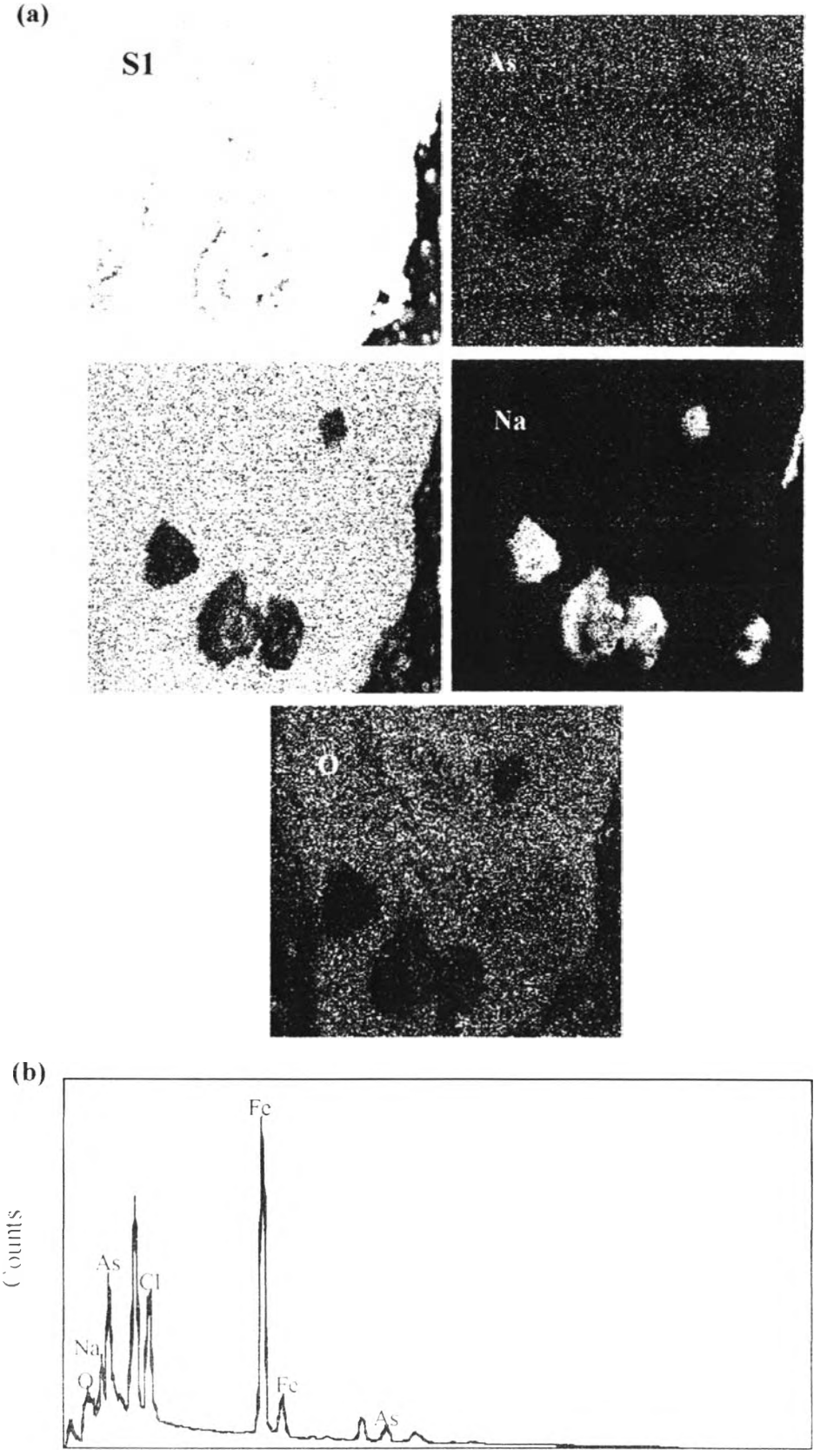

Figure 4.6 (a) the x-ray dot maps and (b) the EDS spectra of S1

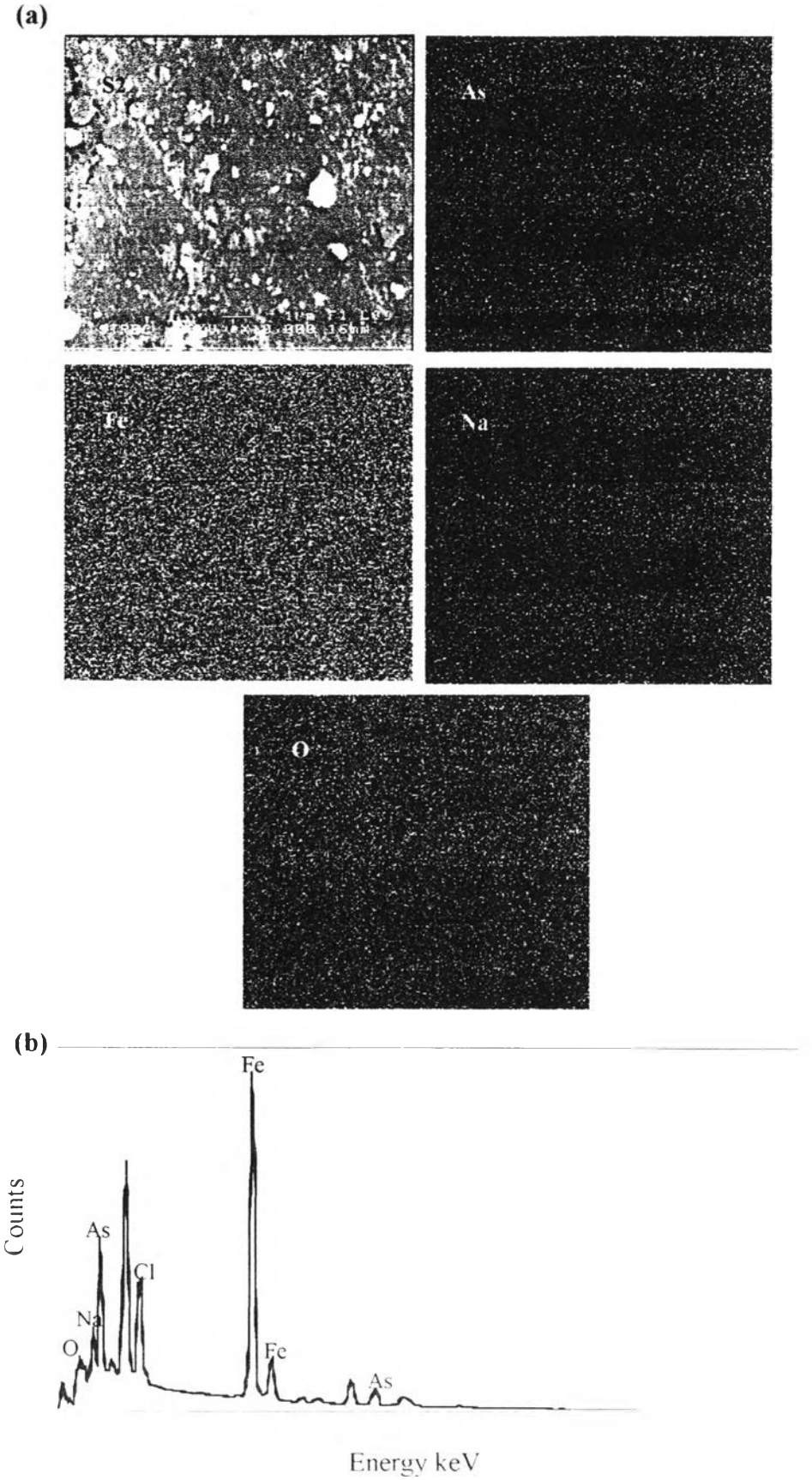

Figure 4.7 (a) the x-ray dot maps and (b) the EDS spectra of S2

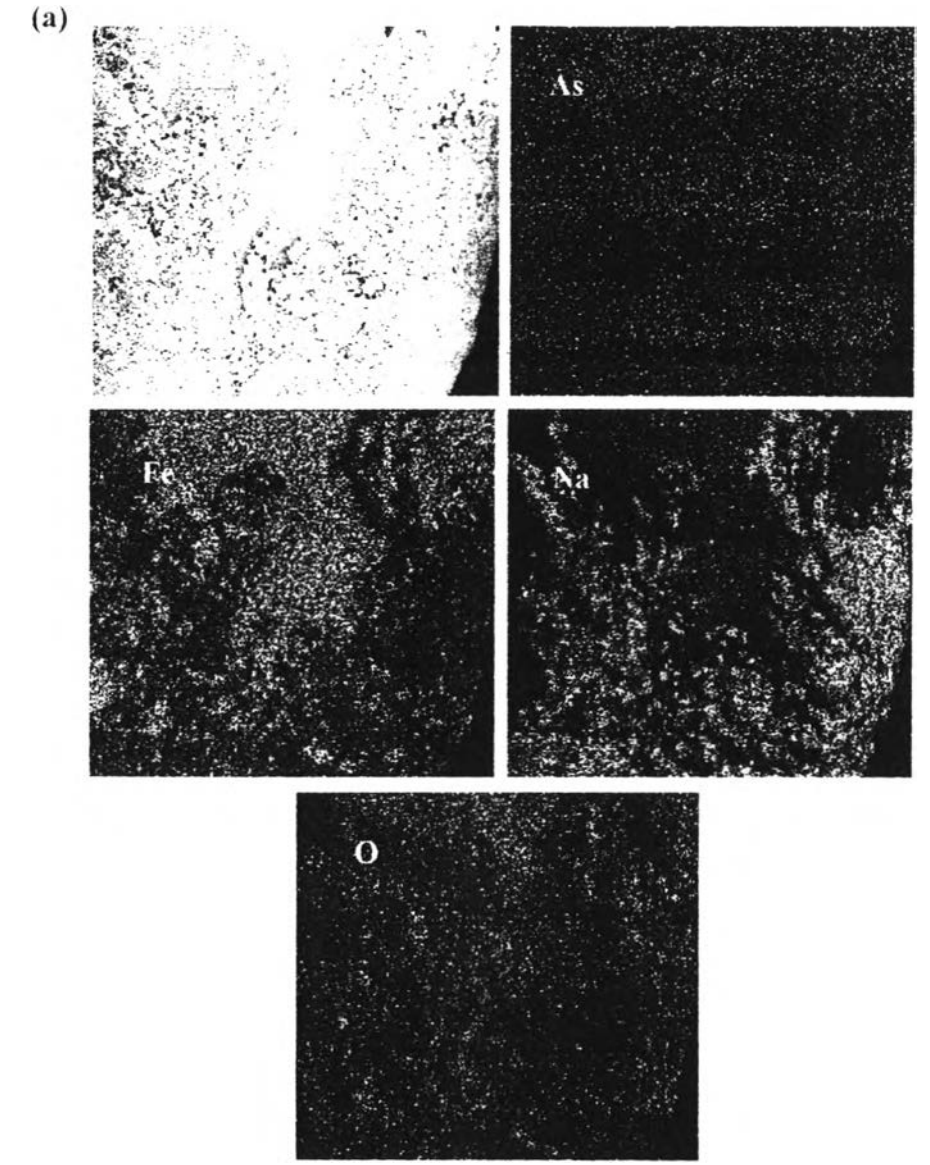

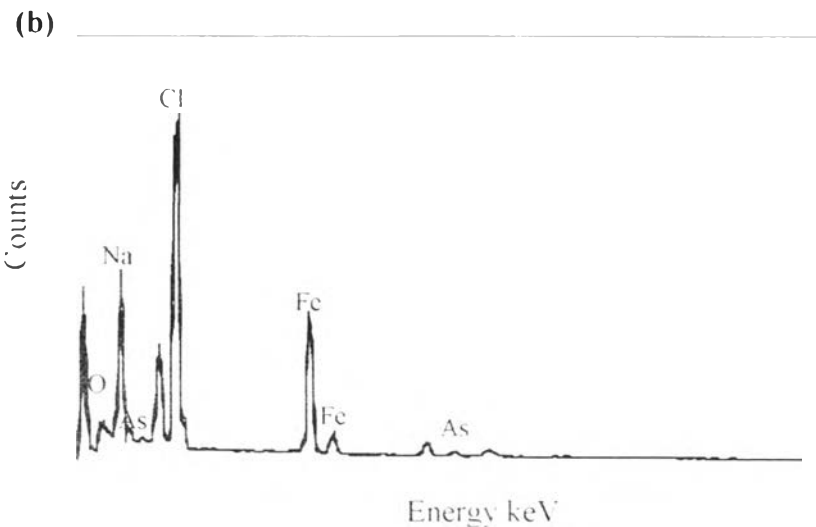

Figure 4.8 (a) the x-ray dot maps and (b) the EDS spectra of S4

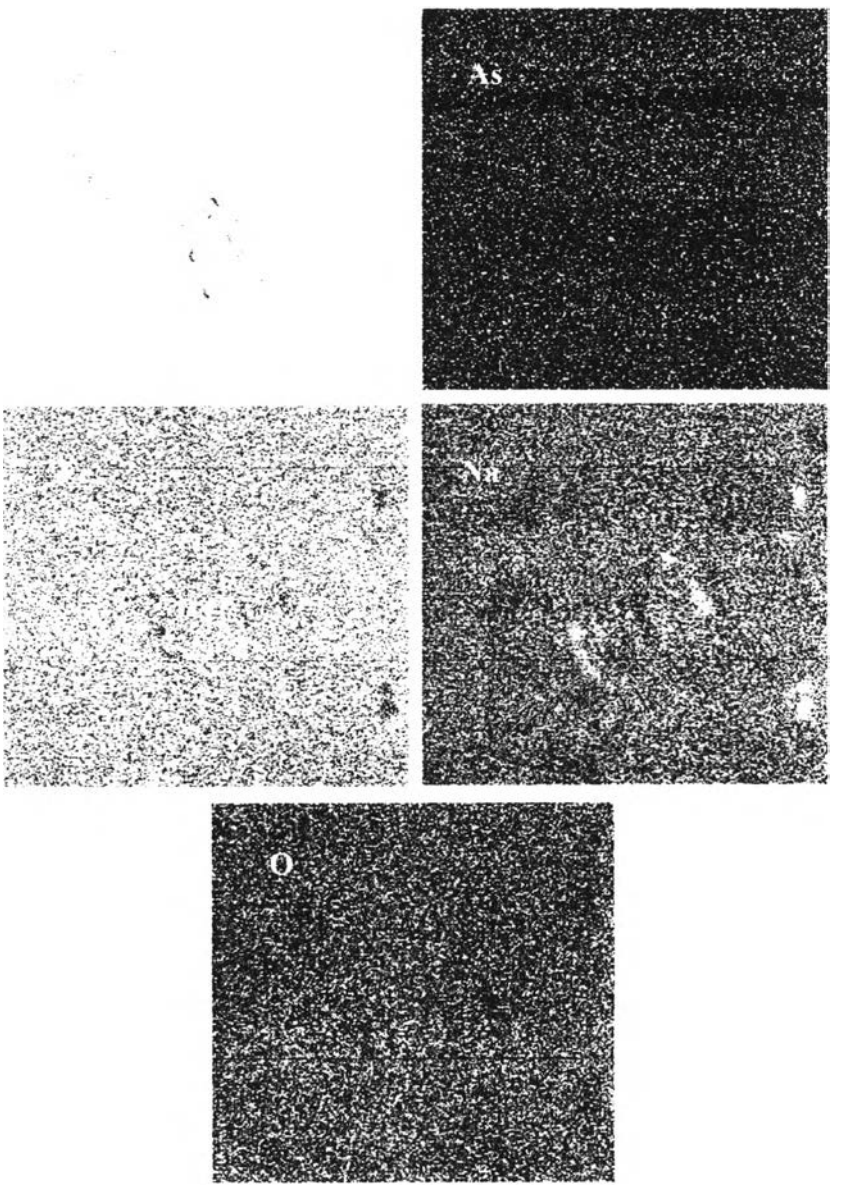

Figure 4.9 the X-Ray Dot Maps of S5

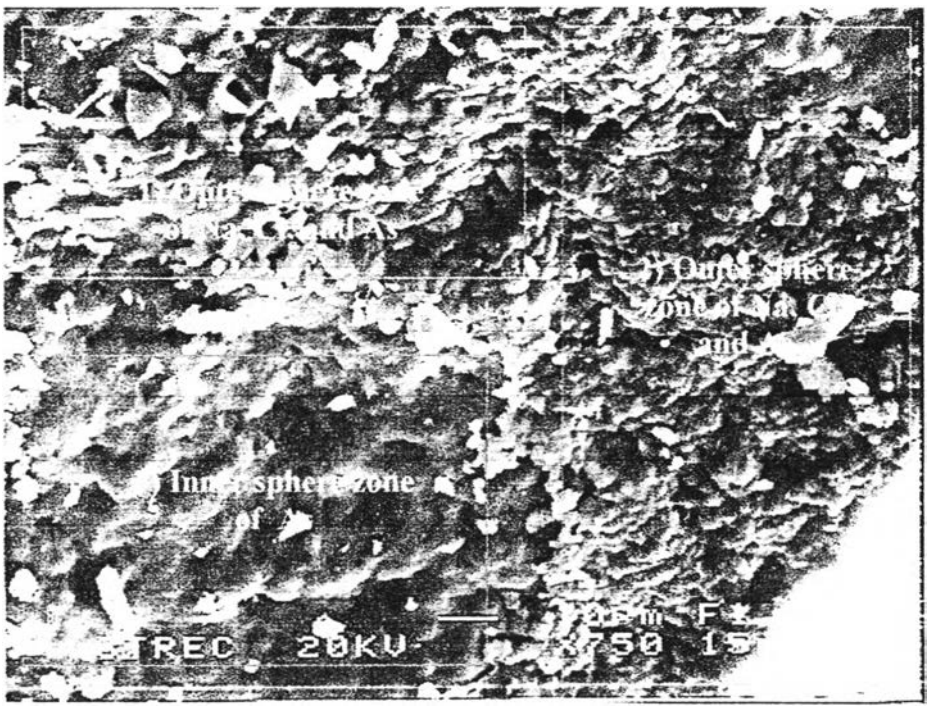

Figure 4.10 The SEM photograph of the sludge S3 expressing zones supposed to be inner-sphere and outer-sphere complexes

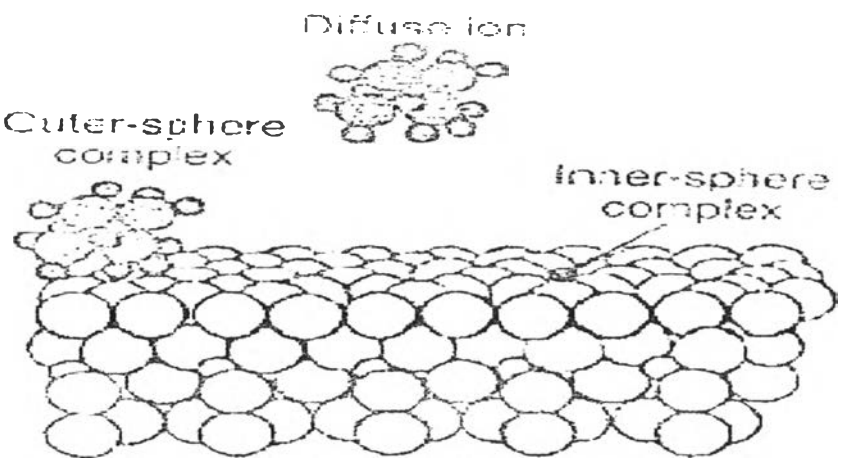

Figure 4.11 A hypothetical interfacial structure comprising a solid (open circles), an adsorbate that has lost the water molecules from its primary hydration sphere and binds directly to the surface, forming an inner- sphere complex (a single black circle), and adsorbate that is bonded to the surface but retains its water of hydration, forming an outer-sphere complex (a group of black circles attaching the surface), and an adsorbate that is attracted to the surface via electrostatic interactions, but is not bonded directly to the surface (a diffused ion) (Benjamin, 2002)

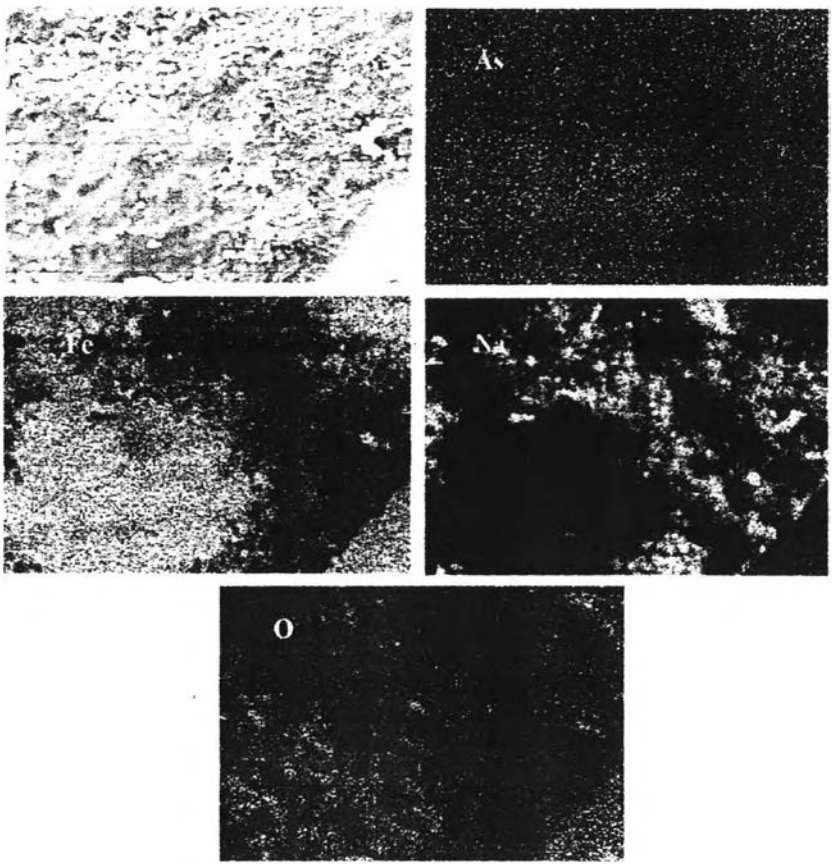

Figure 4.12 The x-ray dot maps of S3

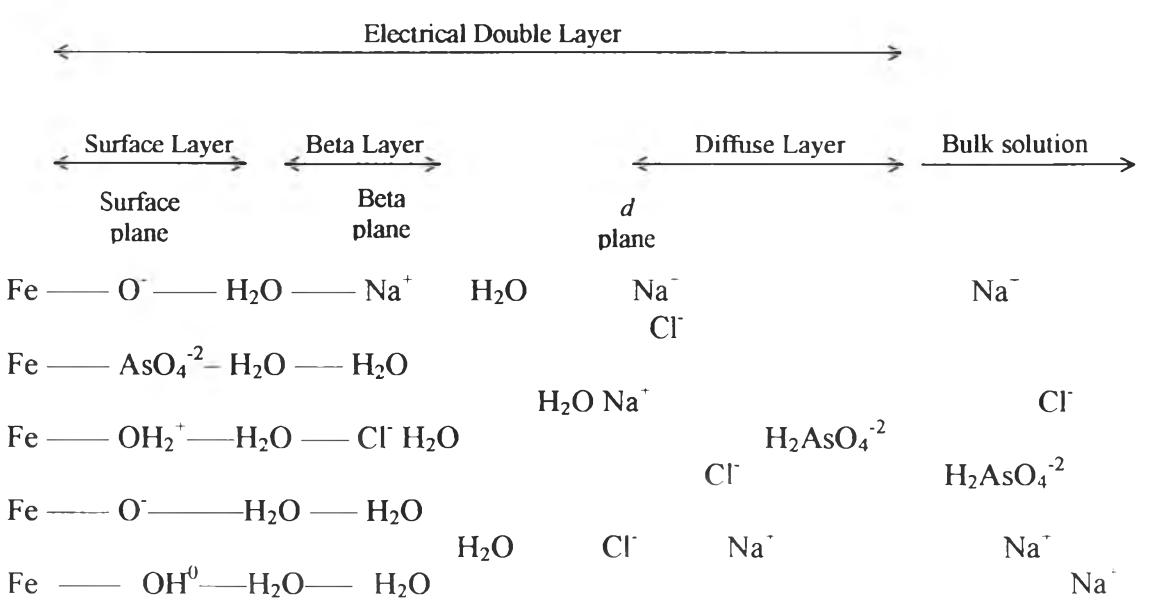

Figure 4.13 Schematic of the interfacial structure as envisioned in the Triple-Layer Model (adapted from Benjamin, 2002)

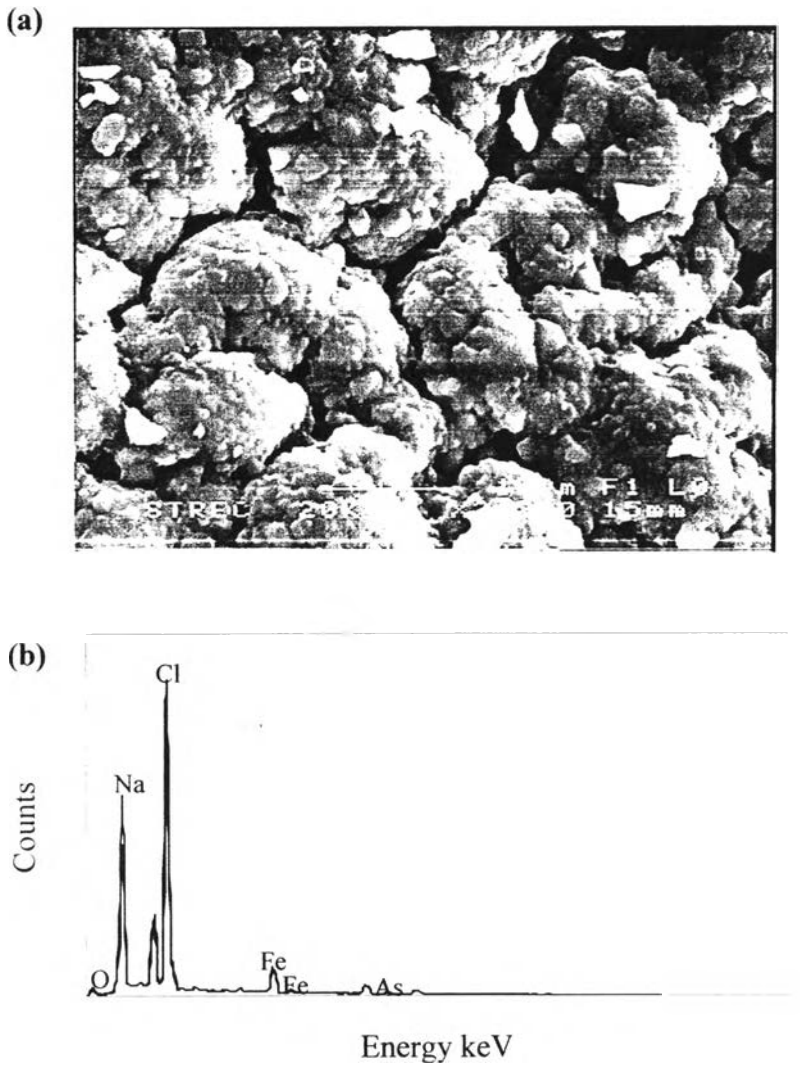

Figure 4.14 (a) the SEM photograph and (b) the EDS spectra of S3 zoomed in Zone 2

Table 4.2 Semi quantitative EDS analysis of the control sample and the five kinds of arsenic containing sludge

Sample	% by Atomic					
	Fe	As	O	Na	Cl	As/Fe
Pure iron sludge	36.87	-	35.51	11.83	6.69	0
S1	39.74	8.49	30.41	9.3	10.12	0.214
S2	35.84	7.34	30.87	10.51	11.28	0.205
S3	51.74	7.48	15.47	8.95	14.27	0.145
S4	15.05	2.05	28.5	31.02	23.23	0.136
S5	26.92	1.97	30.79	22.19	16.48	0.073

4.2 Characterization of the Leached Arsenic-Iron Hydroxide Sludge

4.2.1. Particle Size Analysis of the Leached Arsenic Sludge

It was observed that the particle size distribution of the leached SW1, SW3, SW4, and SW5 in the extraction liquid after 18 hours of TCLP was quite homogeneous in that most of the leached sludge suspended in the aqueous phase. The curves shown in Figure 4.15 are good evidence of homogeneity of the particle size distribution of leached SW samples. Most of the distribution of leached SW samples ranks from 2 to 0.1 microns. In comparison to the particle size distribution of the raw SW samples shown in Figure 4.1(a), it can be concluded that the extraction fluid together with the 18 hours' agitation of the TCLP can dissociate the dewatered sludge samples to become 1,000 times smaller than their original size.

Unlike that of the leached SW samples, the particle size distribution of leached SD samples is obviously inhomogeneous. It was roughly observed that two types of the leached SD samples remained after the TCLP. First, the fine particles of which particle size distribution curves are shown in Figure 4.16 (a). These fine particles suspended in the aqueous phase. Second, the coarse particles of which particle size distribution is shown in Figure 4.16 (c). These coarse particles settled on the bottom of the vessel.

In comparison to the particle size distribution of the raw SD samples, shown in Figure 4.1 (b), only some but not all of the dried sludge was dissociated to the particle size of 0.1 to 1 micro, the same degree of dissociation of the leached SW sludge; the particle size of the rest of the leached SD ranks from 1 to 100 microns. This implies that drying the sludge by heat until most of water molecules vaporize helps the sludge resist the dissociation by TCLP due to the fact that the denser the sludge, the higher dissociation resistance.

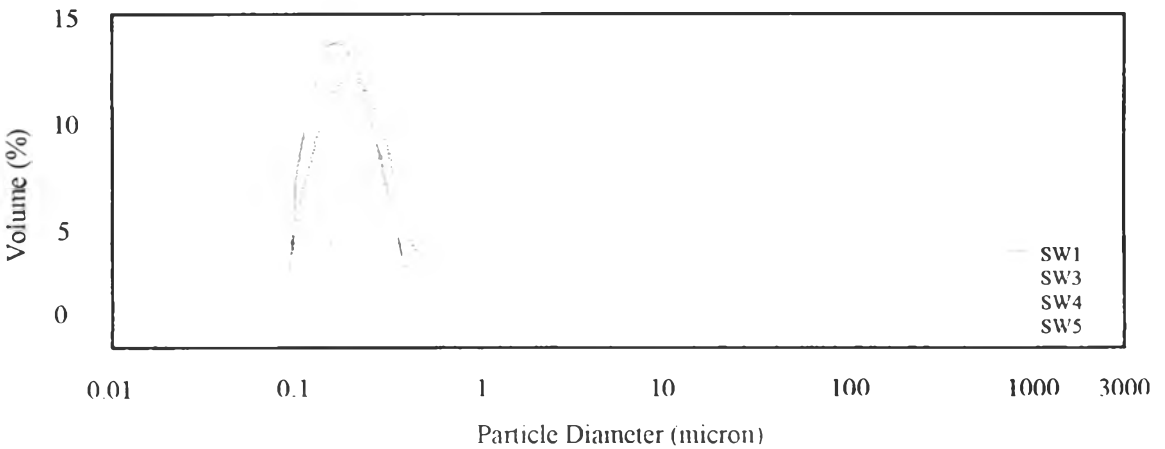

Figure 4.15 The particle size distribution curves of the leached SW1, SW3, SW4, and SW5 after subjected to TCLP

Another difference between the dissolution resistibility of two conditions of the sludge, SW and SD, may be described by the theory of the surface-controlled rate of dissolution. The dissolution kinetics based on a zero-order rate law is shown in following equation (Stumm and Morgan, 1996):

$$r = \frac{dC}{dt} = kA(Ms^{-1}) \qquad (4\text{-}1)$$

Where the dissolution rate r (Ms^{-1}) is proportional to the surface area of the mineral, A (m^2), and k, the reaction rate constant ($M\ m^{-2}s^{-1}$). Concerning the leaching condition, k is a function of an initial pH of extraction fluid and the constant rate of agitation. Owning to the fact the initial pH of the TCLP extraction fluid as well as the agitation rate to which SW and SD samples were subjected was the same, the major factor contributing to the different degrees of dissolution is the difference between the surface areas of the wet and the dried sludge which are implied in Figures 4.1(a) and (b). These figures indicate that the raw SW samples had much larger surface areas than the raw SD samples owning to the fact that the smaller the particle size, the larger the surface area. Therefore, according to Equation 4-1, it is reasonable that the dissolution rate of SW samples was much higher that of SD samples.

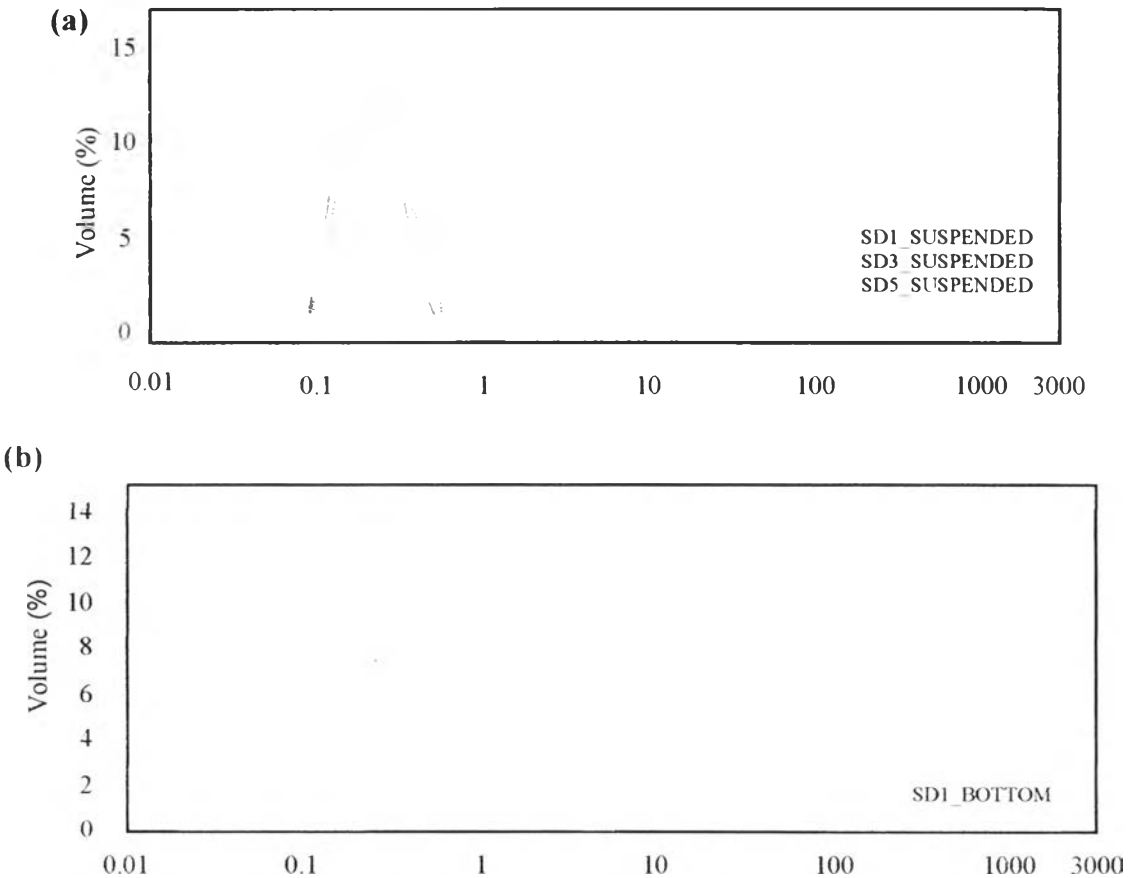

Figure 4.16 The particle distribution curves of (a) the fine particles of some leached SD samples suspended in aqueous phase and (b) the coarse particles settled on the bottom of the extraction vessel.

4.2.2 Vibrational Characterization of the Leached Arsenic Sludge

The FT-IR spectra of the leached SW samples (leached SW1 to SW5) after 18 hours of the TCLP are shown in Figure 4.17. It is obvious that the adsorption bands at 761, 797, and 894 cm^{-1} present in Figure 4.3, the original spectra of the raw sludge before leaching, become less in size or even absent from some leached SW samples shown in Figure 4.17. For example, the band at 761 cm^{-1} is absent from the spectra of the leached SW2 and SW3. Similarly, the band at 797 cm^{-1} is absent from the spectra of all leached SW samples while the band at 894 cm^{-1} is present in almost all of the leached SW samples except SW3. This observation is in good agreement with the property of the expected bond of each band. For example, the band at 894 cm^{-1} is supposed to represent the bond of either Fe-O-As(III) or Fe-O-As(V) which is believed to be more stable than As(III) or As(V) attached by very weak outer sphere surface complexation or even non-surface-complexed As-O at 761 and 797 cm^{-1}, respectively.

Moreover, the additional bands at 739, 826, and 838 cm^{-1} appeared after the leaching test. The band at 739 cm^{-1} is close to the Raman spectrum of $H_2AsO_4^-$ in aqueous solution reported by Tossell (1997 cited in Goldberg and Johnston, 2001) (742 cm^{-1}) while the band at 826 cm^{-1} is identical to the adsorption band of sodium arsenite shown in Figure 4.2(c). In the same way, the band at 838 cm^{-1} is assigned to the symmetric stretching of the Fe-O-As(V) recorded by Myneni (1998 cited in Jing et al., 2003) (834 cm^{-1}).

The decrease in intensity or even absence of the original bands which were present before the TCLP test and the appearance of the new bands after the TCLP test imply that the desorption and resorption of arsenic species on the sludge might take place during the leaching test. However, it should be noted that the new adsorption bands after leaching supposed to be responsible for resorption of arsenic are different from those of the original bands. This can be taken as a meaningful indicator of alteration of sorption behavior of arsenic. For example, arsenate species might be first desorbed out of the sludge and then resorbed onto the fresh formation of amorphous

ferric hydroxide from dissociated iron ions. Thus, the bond Fe-O-As is possible as indicated by the adsorption and at 838 cm^{-1}. Moreover, desorbed arsenate could sorb onto surface of the undissolved sludge on the basis of iron-pair or even non surface complexation, and so did desorbed arsenite. Thus, the bands at 739 and 826 cm^{-1} are good representatives of such sorption behaviors for arsenate and arsenite.

Similarly, the FT-IR spectra of the leached SD samples after 18 hours of the TCLP are shown in Figure 4.18. According to Figure 4.16, the leached SD samples can be divided into two groups based on their particle sizes, so two samples from each leached SD sample were sampled. One was the residuals settling on the bottom of an extraction vessel (SD_BOTTOM samples) and another was the residuals suspended into the aqueous phase (SD_SUSPENDED samples).

Figures 4.18 (b) and (c) illustrate the FT-IR spectra of SD_BOTTOM samples and SD_SUSPENDED samples from the wavanumber of 400 to 4000 cm^{-1}, respectively. Moreover, the enlargement of the spectra of SD_BOTTOM and SD_SUSPENDED samples from the wavenumber of 650 to 1250 cm^{-1} are shown in Figure 4.18 (a) and (d), respectively. It is noticeable that the shape of the spectra of SD_BOTTOM reminds that of the original sludge before leaching. This similarity corresponds to the conclusion drawn from particle size distribution of the leached SD samples shown in Figure 4.16 concerning the assumption that the drying by an heat improves resistibility of the sludge to chemical and mechanical weathering from the leaching test. The confirmation of the previous statement can be emphasized by considering the shape of adsorption bands of SD_SUSPENDED samples. The shape of almost all of SD_SUSPENDED adsorption bands except SD1_SUSPENDED resembles that of leached SW sludge. This similarity is in good agreement with the fact that the particle size distribution curves of the leached SW and the SD_SUSPENDED is almost identical.

Like the case of the leached SW discussed above, some adsorption bands of the raw, unleached sludge become less in size or even absent from some samples of both SD_BOTTOM and SD_SUSPENDED. For example, the intensity of the bands at 761 cm^{-1} decreases in the spectra of SD1_BOTTOM, SD3_BOTTOM, and

SD5_BOTTOM as well as SD1_SUSPENDED, SD4_SUSPENDED, SD5_SUSPENDED. Moreover, this band is absent from the spectra of SD2_BOTTOM and SD4_BOTTOM as well as SD2_SUSPENDED and SD3_SUSPENDED.

In the same way, the intensity of the bands at 797 cm^{-1} decreases in the spectra of SD3_BOTTOM as well as SD1_SUSPENDED while it is absent from the spectra of SD1_BOTTOM, SD2_BOTTOM, SD4_BOTTOM, SD5_BOTTOM, and SD4_BOTTOM as well as SD2_SUSPENDED, SD3_SUSPENDED, SD4_SUSPENDED, and SD5_SUSPENDED. In contrast, the adsorption band at 893 cm^{-1} exists in all samples but varies in height.

The adsorption bands at 734 and 742 cm^{-1} together with at 823 and 826 cm^{-1} close to the additional bands at 739 and 826 cm^{-1} present in leached SW are also present in some leached SD samples. For example, the band at 734 cm^{-1} is present in SD1_BOTTOM and SD5_BOTTOM while the band at 742 cm^{-1} is present in SD2_SUSPENDED and SD3_SUSPENDED. Furthermore, the adsorption bands at 823 and 826 seem to exist in all SD_BOTTOM and SD_SUSPENDED samples, respectively.

Unlike SW samples, both SD_BOTTOM and SD_SUSPENDED have additional bands at 719 and 853 cm^{-1} as well as 711 and 854 cm^{-1}, respectively. The adsorption band at 719 cm^{-1} of all SD_BOTTOM except SD5_BOTTOM as well as the band at 711 cm^{-1} of SD1_SUSPENDED and SD4_SUSPENDED is close to the Raman spectrum at 710 cm^{-1} of symmetric As-OH stretching of H_3AsO_3 recorded by Sprycha in 1984 (cited in Goldberg and Johnston, 2001). While The adsorption band at 853 cm^{-1} of SD1_BOTTOM and SD4_BOTTOM as well as the band at 854 cm^{-1} of all SD_SUSPENDED except SD1_SUSPENDED is close to the Raman spectrum at 858 cm^{-1} of asymmetric As-O stretching of $HAsO_4^{-2}$ recorded by Tossell in 1997 (cited in Goldberg and Johnston, 2001).

The change of FT-IR spectra of both SD_BOTTOM and SD_SUSPENDED leads to the same conclusion as SW discussed above; that is, the desorption and resorption of arsenic are supposed to be the main phenomena contributing to the present and absence of some adsorption bands as well as controlling arsenic mobility crossing solid and aqueous phase.

In conclusion, the author 's purpose of devoting several pages to describe the changes of FT-IR spectra due to the leaching test is to emphasize two important issues that are the desorption and the resorption might take place during the leaching test, and the resistibility to chemical and mechanical weathering from the leaching test can be improved by drying by means of heating at 105 ^{o}C until most of water vaporizes. In this study is none of quantitative analyses done owning to the fact that only small amount of the sludge was used for FT-IR analysis each time; thus, it cannot be claimed to be a good representative of the actual, heterogeneous system.

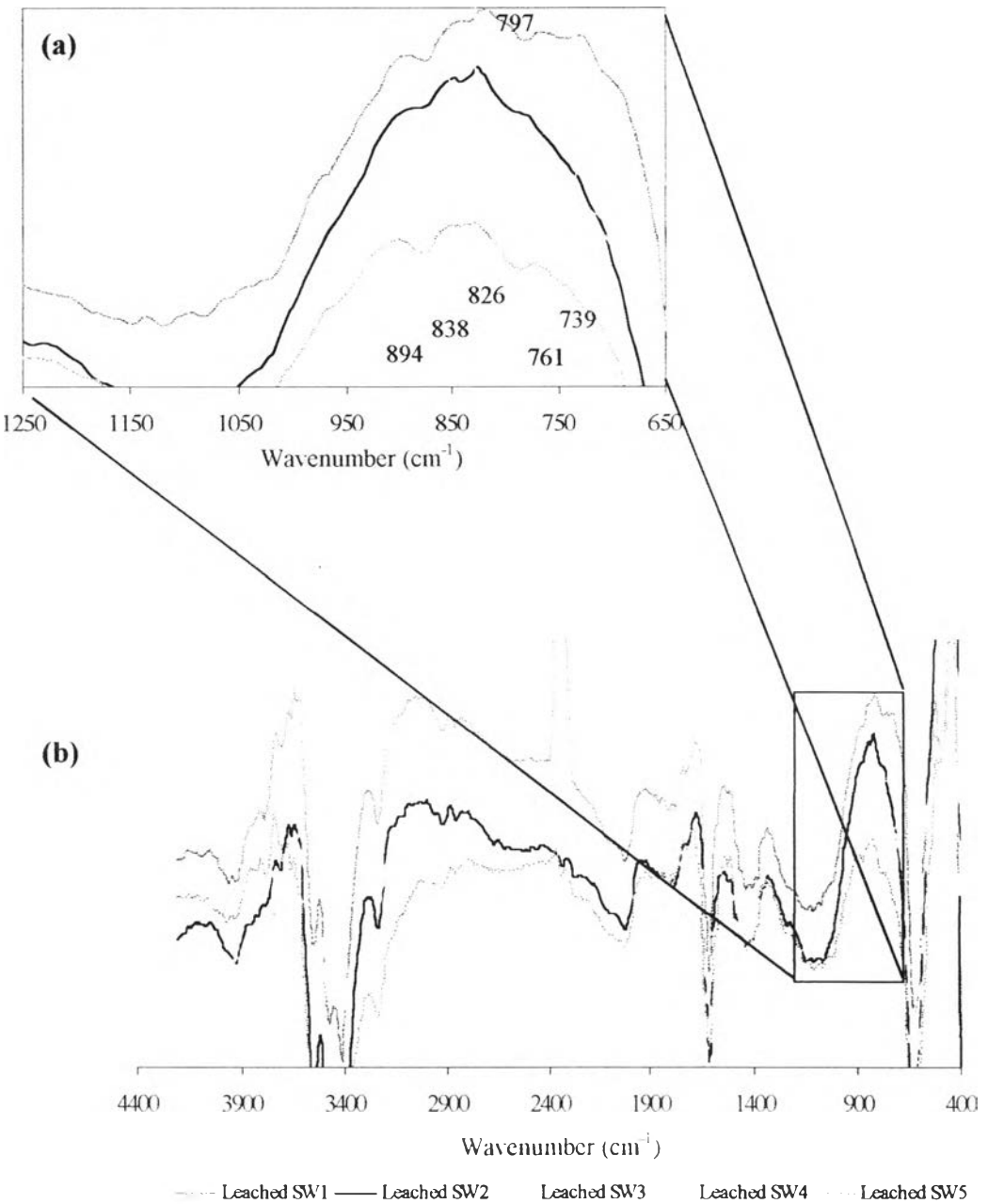

Figure 4.17 The FT-IR spectra of the leached SW samples (Leached SW1 to SW5) after 18 hours of the TCLP (a) focusing on the wavenumber from 650 to 1250 cm^{-1}, and (b) throughout the whole length from 400 to 4000 cm^{-1}

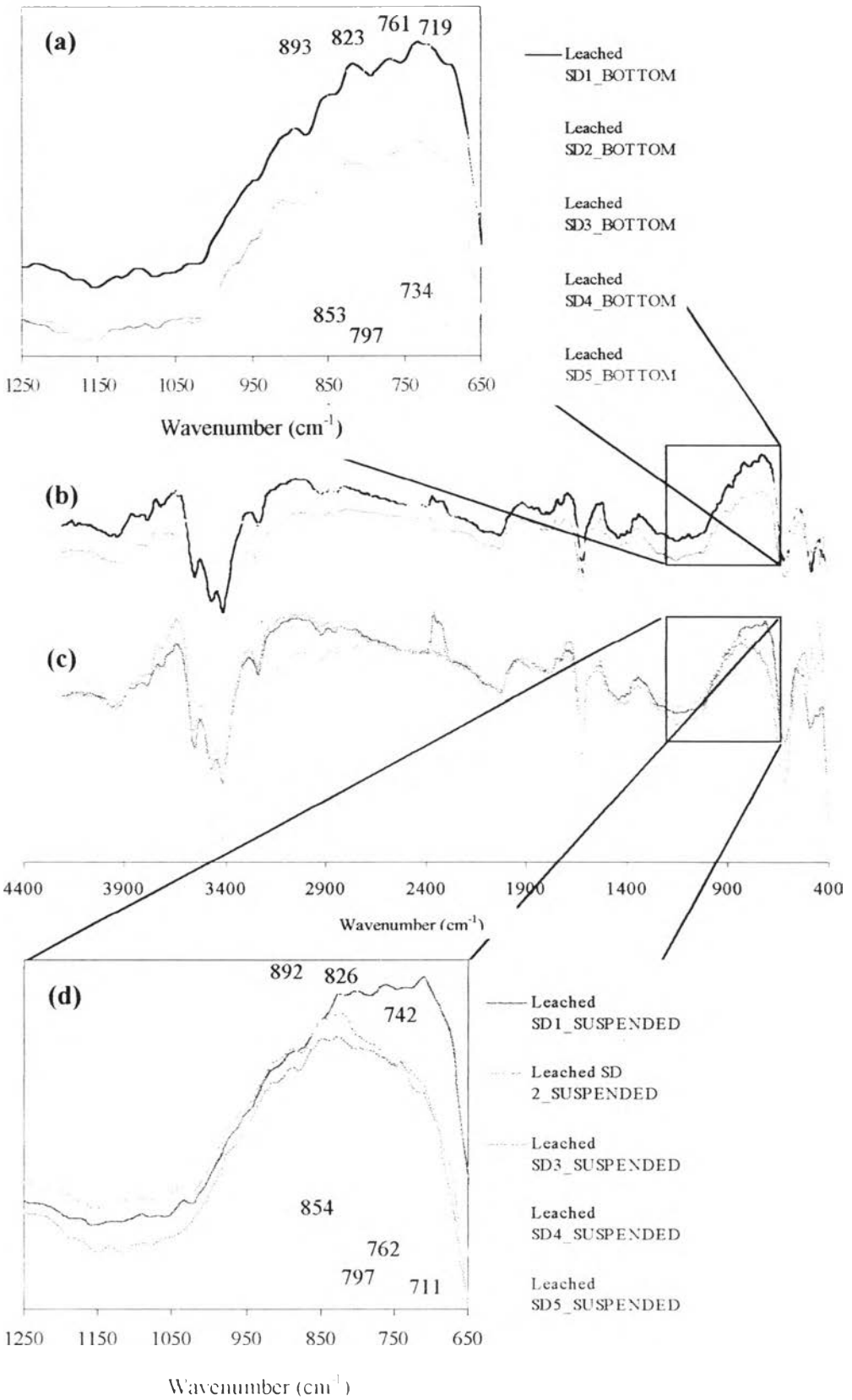

Figure 4.18 The FT-IR spectra of (a) the Leached SD_BOTTOM samples focusing on the wavenumber from 650 to 1250 cm^{-1}. (b) the Leached SD_BOTTOM samples throughout the whole length from 400 to 4000 cm^{-1}. (c) the Leached SD_SUSPENDED samples focusing on the wavenumber from 650 to 1250 cm^{-1}. (d) the Leached SD_BOTTOM samples throughout the whole length from 400 to 4000 cm^{-1}

4.2.3 Microstructures of Leached Arsenic Sludge

Due to the same drawback as FT-IR, it is not possible to conduct any reliable quantitative analysis from SEM-EDS. Therefore, the purpose of SEM-EDS investigation in this part is only to illustrate some physical characteristics of two different conditions of the leached sludge: SD_BOTTOM and leached SW.

The SEM photographs of SD3_BOTTOM, SD4_BOTTOM, leached CW (pure amorphous iron hydroxide dewatered by vacuum filtration and subjected to the leaching test), leached SW3, leached SW4, and leached SW5 together with their EDS spectra are shown in Figures 4.19 to 4.24. It is obvious that the microstructure of SD_BOTTOM samples is very different from that of CW and SW samples. Based on the photographic evidence, two different patterns of leached surface are identified. One is the shear plan-like surface found in SD3_BOTTOM, SD4_BOTTOM. Another is the accumulated sphere–like surface found in CW, SW3, SW4, and SW5. The shear plane-like surface of SD3_BOTTOM and SD4_BOTTOM is in good agreement with their particle size analysis in Figure 4.16 (c) and (d); that is, the dried sludge had the better weathering resistibility as the bulk dried sludge samples were still in relatively good shape and only partially dissociated as confirmed by the shear plane-like pattern in Figure 4.19 and 4.20. In contrast, the accumulated sphere–like surface of CW, SW3, SW4, and SW5 indicates that all of the wet sludge samples subjected to the leaching test might fully dissociated; then, it trended to accumulate to form larger, more stable floc as shown in Figure 4.21 to 4.24.

The mechanism leading to each surface patterns has its own advantages and disadvantages which play crucial roles on mobility of arsenic. For example, for the sludge dried by heat, only its outer surface was partially dissociated and only arsenic sorbed onto the outer layer of the sludge leached. Therefore, the arsenic covered inside the sludge was not mobile.

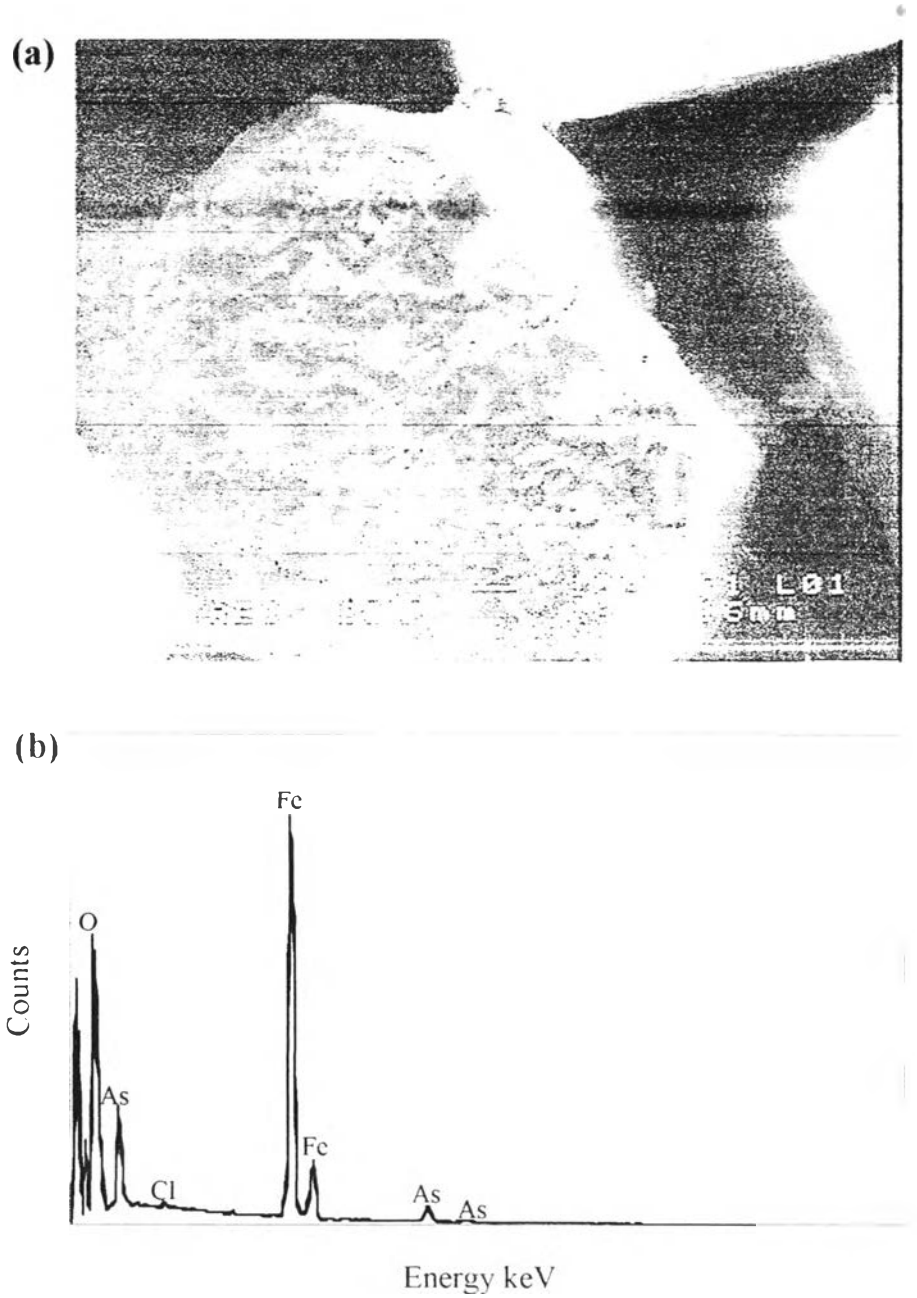

Figure 4.19 (a) the SEM photograph and (b) the EDS spectrum of SD3_BOTTOM

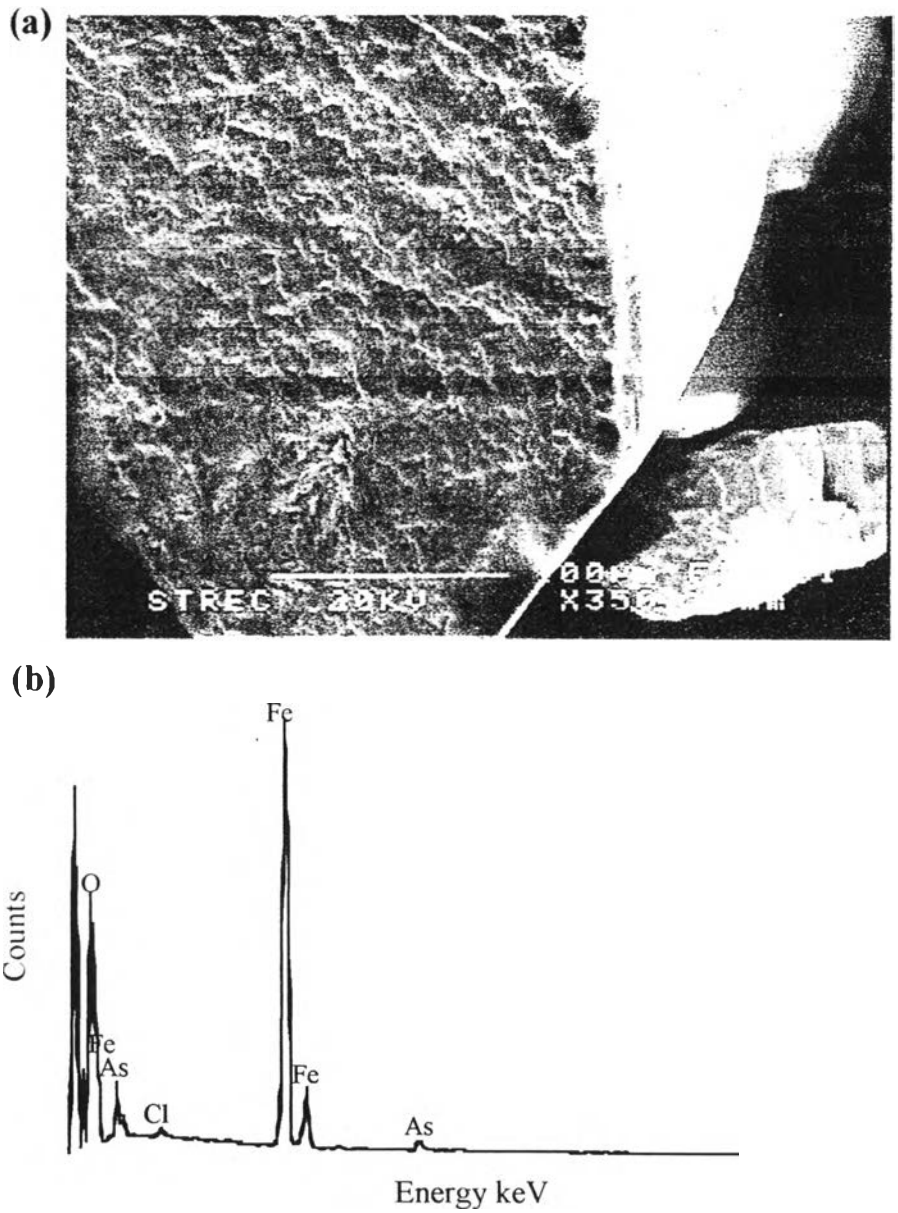

Figure 4.20 (a) the SEM photograph and (b) the EDS spectrum of SD4_BOTTOM

However, the potential for the desorbed arsenic in aqueous phase to resorb onto the dried, leached sludge was inferior to that to resorb onto the wet, leached sludge owning to the fact that the sorption efficiency is generally proportional to a surface area of a sorbent which is inversely proportional to particle size of sorbent. On the contrary, although the wet sludge samples were the better sites for arsenic to resorb, they were the worse sites of arsenic retention.

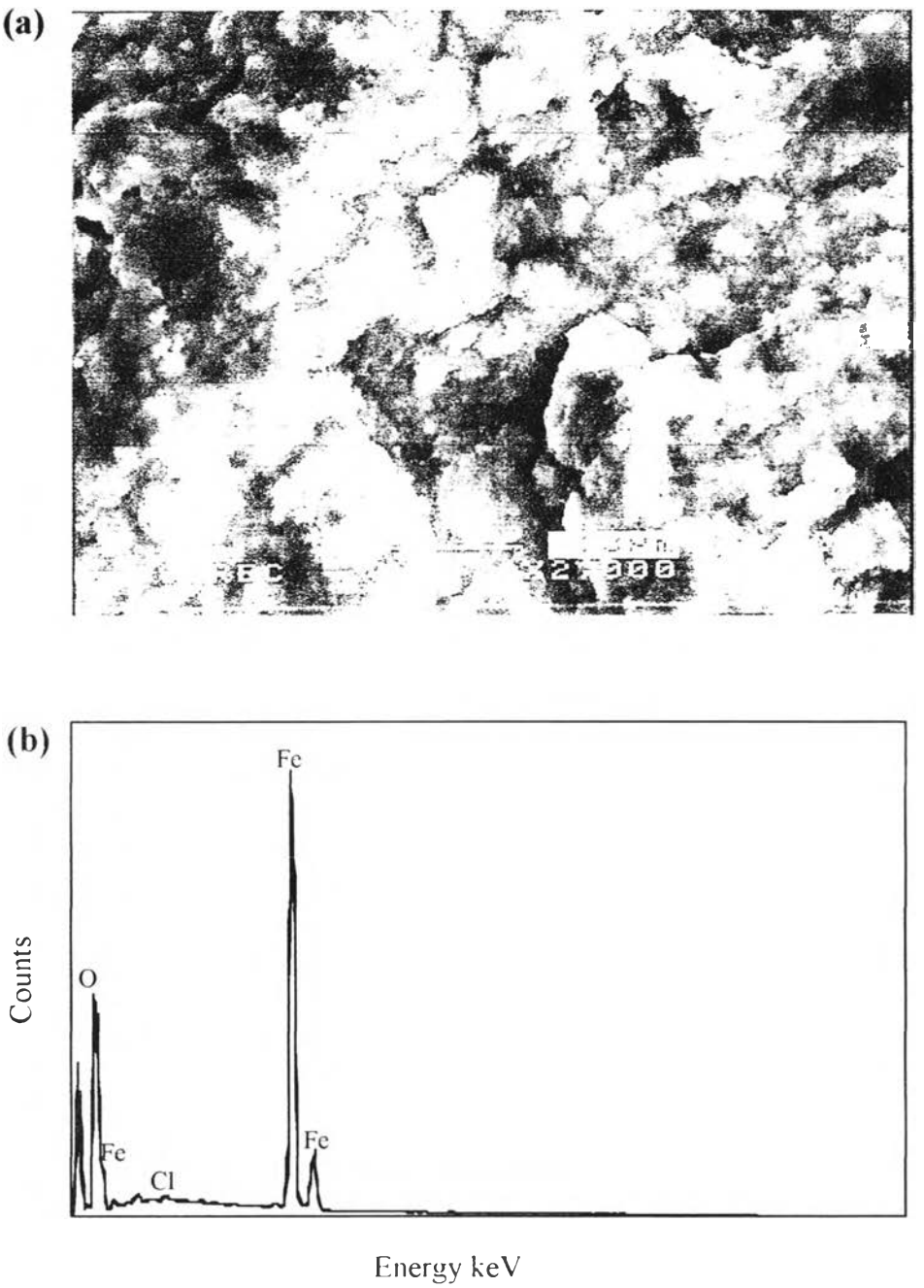

Figure 4.21 (a) The SEM photograph and (b) the EDS spectrum of CW (pure amorphous iron hydroxide sludge after the TCLP test)

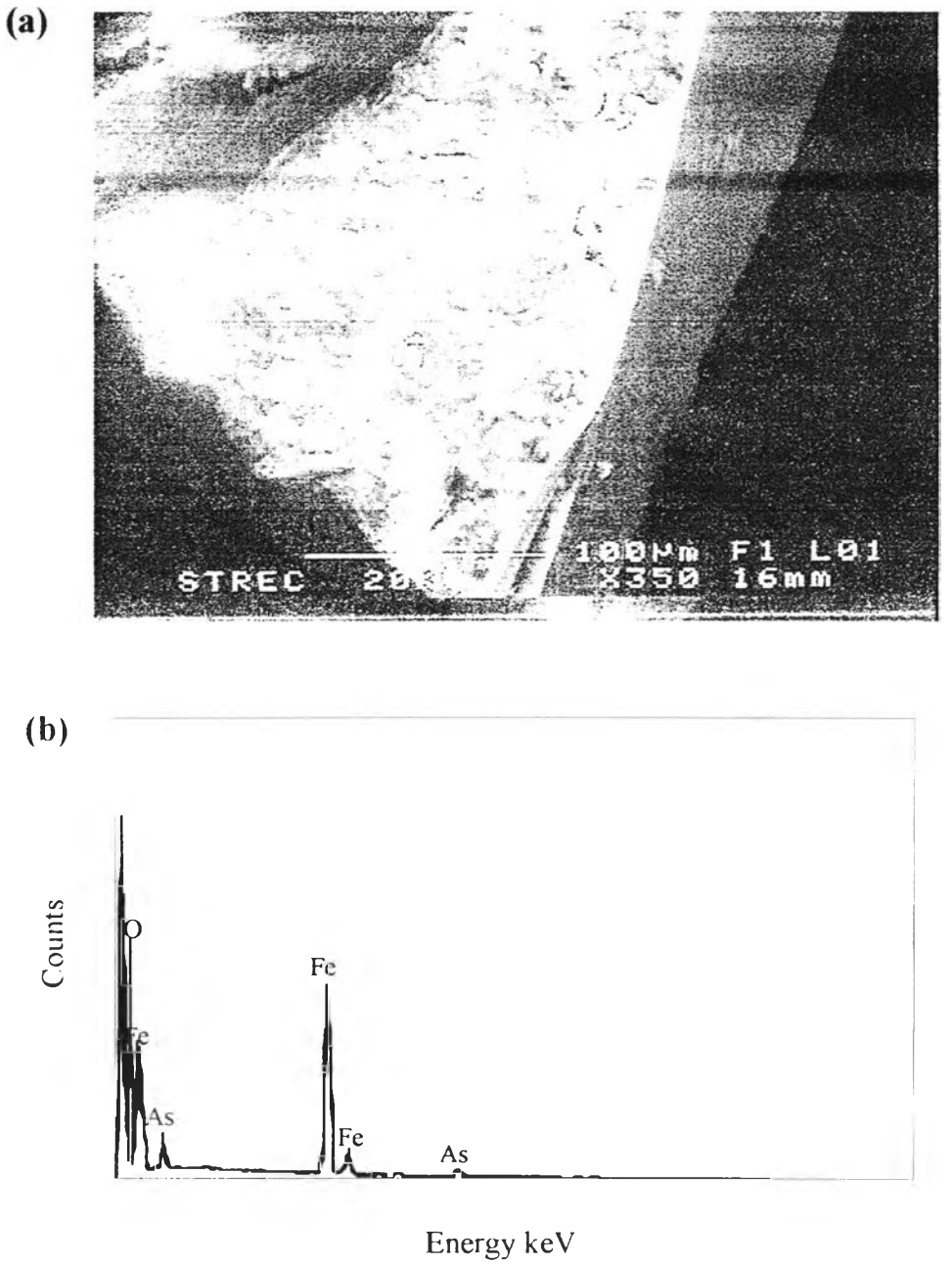

Figure 4.22 (a) The SEM photograph and (b) the EDS spectrum of Leached SW3

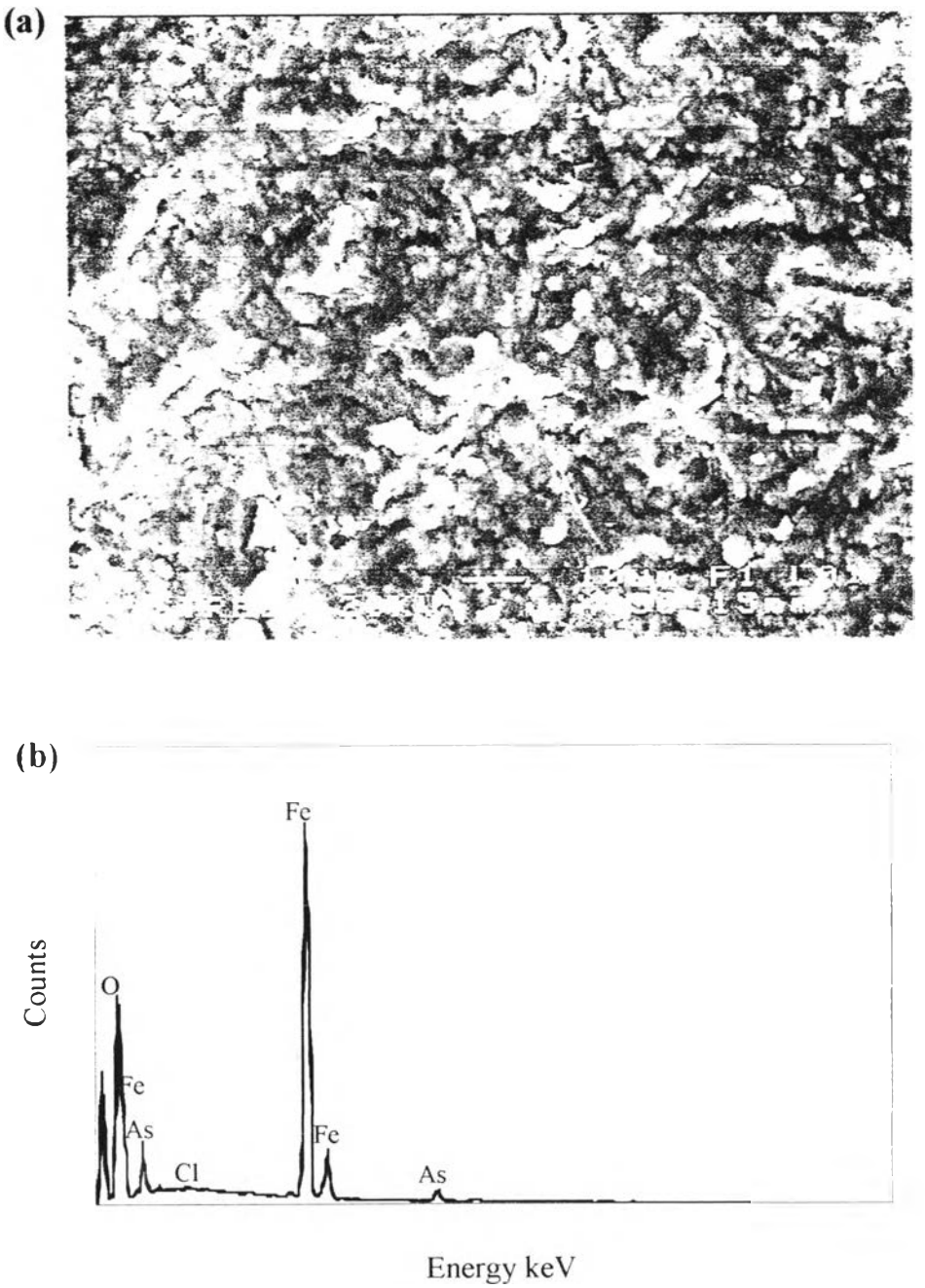

Figure 4.23 (a) The SEM photograph and (b) the EDS spectrum of Leached SW4

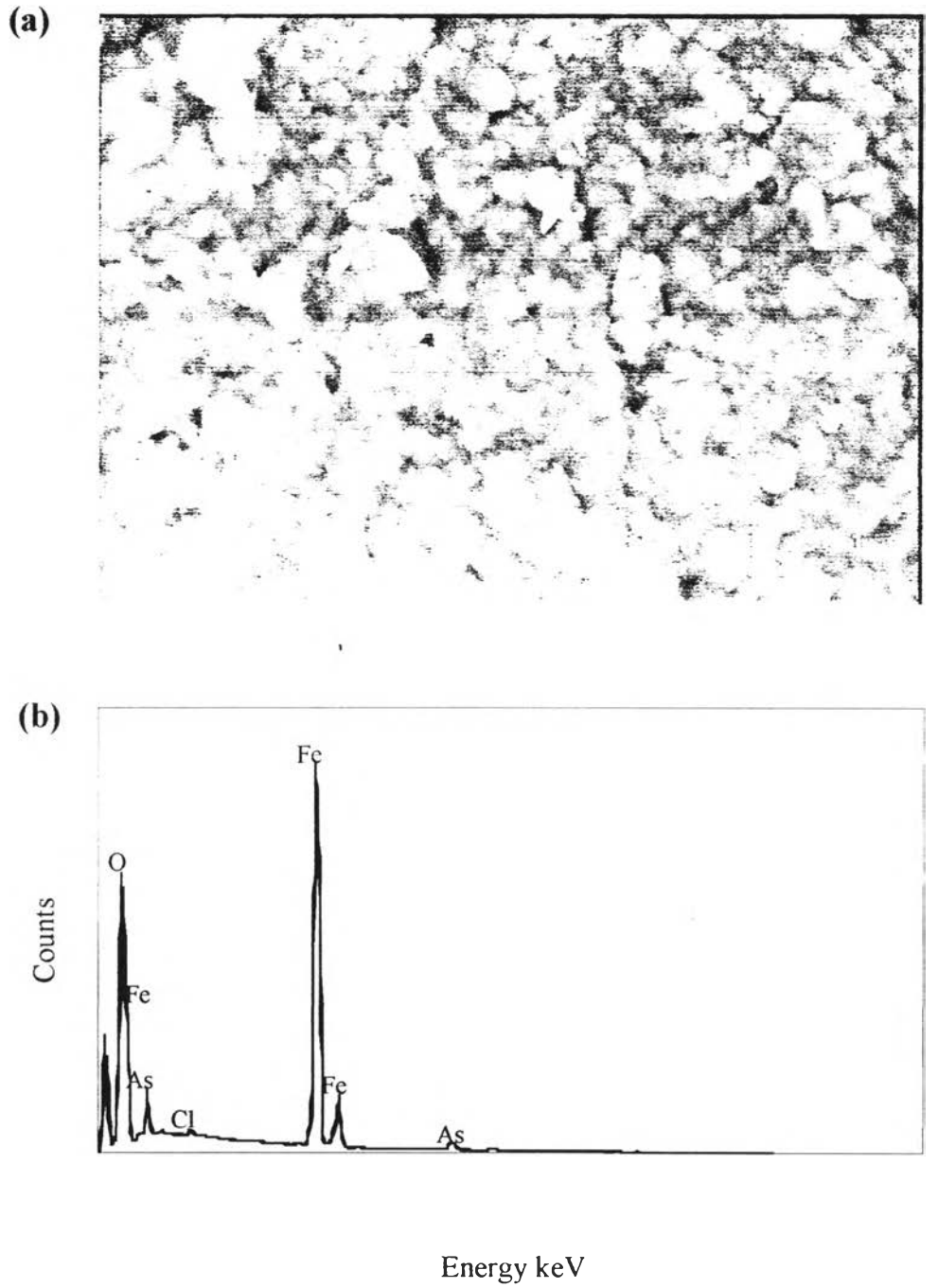

Figure 4.24 (a) The SEM photograph and (b) the EDS spectrum of Leached SW5

In conclusion, the dewatered sludge has the better resorption potential but has the lower weathering resistibility due to having smaller particle sizes and higher surface area while the opposition is true for the dried sludge.

4.3 Leachate Characteristics of the Arsenic-Containing Sludge

The results of the two types of extraction tests, TCLP and LP-NO.6, on the two different conditions of the raw arsenic-containing sludge, SW and SD samples,are shown in Table 4.3 and illustrated in Figure 4.25. Each symbol used in this figure consists of three sections e.g. SW_TCLP_Fe. The first section represents condition of the raw arsenic-containing sludge; the second section represents the leaching procedure to which the sludge was subjected; and the last section represents the element of concern. Therefore, SW_TCLP_Fe represents concentration of iron (mg/L) extracted from one of the SW samples subjected to the TCLP test while SD_NO6_As represents concentration of arsenic (mg/L) extracted from one of the SD samples subjected to the LP-NO.6 test, and so on. The symbols S1, S2, S3, S4, and S5 on the top of the figure are to identify the kind of the SW and SD samples.

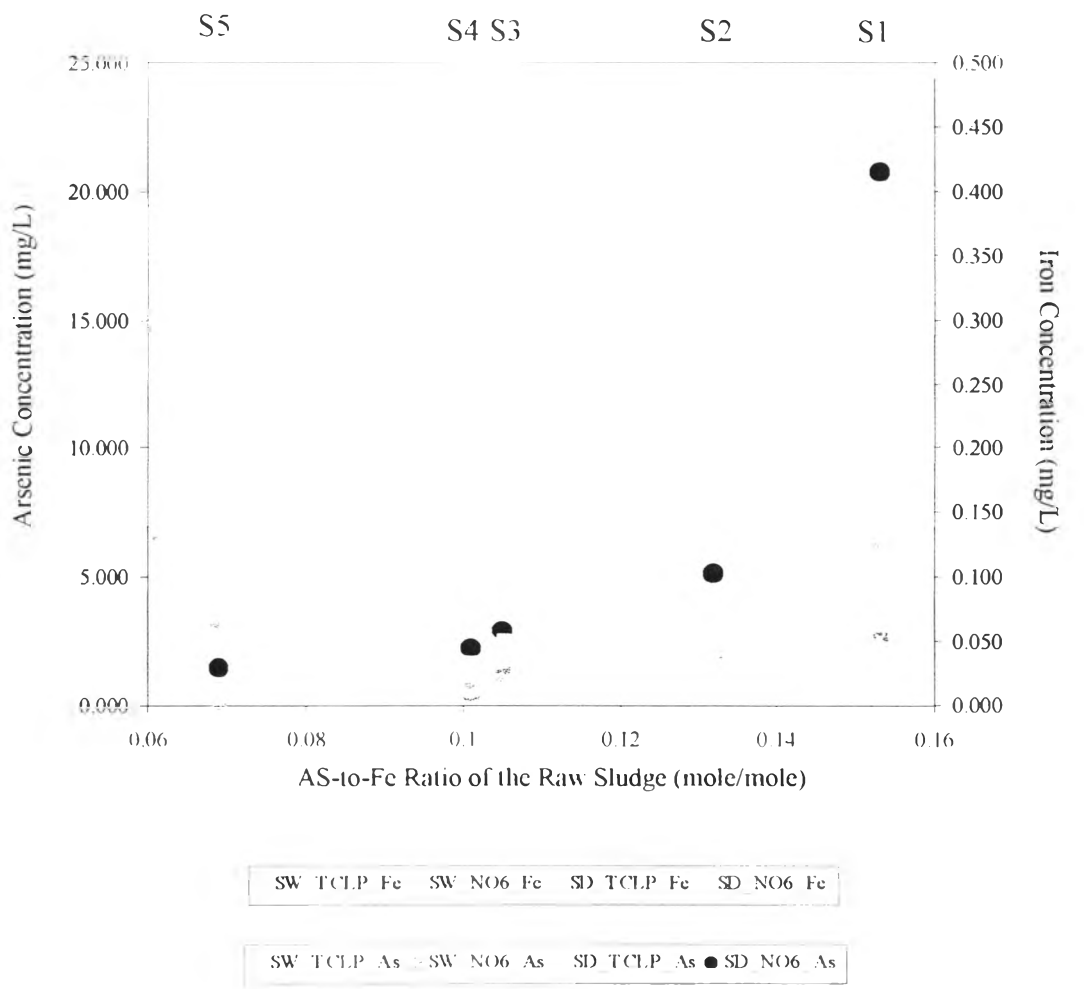

Figure 4.25 Concentrations of arsenic and iron in leachate of SW and SD samples subjected to the TCLP and LP-NO.6 test

Table 4.3 Concentrations of arsenic and iron in Leachate of SW and SD samples subjected to the TCLP and LP-NO.6 test.

	As-to-Fe Ratio of the Raw Sludge (mole/mole)	SW				SD			
		TCLP (mg/L)		LP-NO.6 (mg/L)		TCLP (mg/L)		LP-NO.6 (mg/L)	
		As	Fe	As	Fe	As	Fe	As	Fe
S1	0.153	2.54	0.05	2.62	0.01	20.70	0.12	20.75	0.05
S2	0.132	1.86	0.04	1.83	0.03	5.13	0.06	5.14	0.06
S3	0.105	1.05	0.04	1.58	0.05	2.82	0.02	2.94	0.08
S4	0.101	0.40	0.01	0.52	0.06	2.32	0.02	2.26	0.08
S5	0.069	0.26	0.01	0.23	0.01	1.37	0.06	1.48	0.45

According to the FT-IR results discussed in the section 4.2.2, it is possible that resorption of desorbed arsenic onto remaining and/or newly forming iron hydroxide surfaces may be one of the major mechanisms responsible for the immobilization of arsenic on the sludge. To verify this assumption, it is essential to examine the relationship between adsorption density of arsenic to iron ($q_{As/Fe}$) and the dissolved concentration of arsenic at equilibrium after 18 hours of leaching tests (c_{As}).

First of all, considering SW samples subjected to the TCLP test, the data from Table 4.1 together with Table 4.3 can be modified to empirically derive the relationship between $q_{As/Fe}$ and c_{As} at equilibrium as shown in Table 4.4. In addition, Figure 4.26 illustrates $q_{As/Fe}$ as a function of c_{As} at equilibrium of the leached SW samples. It is found that the relationship between $q_{As/Fe}$ and c_{As} at equilibrium corresponds to the Langmuir Isotherm, an adsorption isotherm. Being in good agreement with the FT-IR results in the previous section, this observation indicates that resorption of desorbed arsenic onto remaining and/or newly forming iron hydroxide surfaces existed.

Based on the combination of the available information from the vibrational characterization in the section 4.2.2 and the adsorption isotherm in this section, the possible mechanisms of arsenic remobilization and immobilization from the arsenic-containing sludge can be divided into two following parts:

1) Desorption

According to the solubility chart of amorphous $Fe(OH)_3$ as a function of pH at 25 $^{\circ}$ C in Figure 4.27(a), when the arsenic-containing sludge was subjected to the extraction liquid of the TCLP test of which pH was 4.93±0.05, it might dissolve due to the fact that the solubility of $Fe(OH)_3$ trends to increase when pH decreases. Schematic representation of iron oxide dissolution promoted by proton (H^+) is also illustrated in Figure 4.27(b). Although proton-promoted dissolution is generally considered slow, the agitation at 30 rpm according to TCLP may help enhance the rate of this phenomenon.

The dissolution of $Fe(OH)_3$ means the destruction of binding sites for arsenic; therefore, arsenic either inner or outer-spherically complexed with those iron hydroxide surfaces was expected to be released. Consequently, the dissolution of $Fe(OH)_3$ is believed to have a hand in desorption of arsenic.

Moreover, considering the study of Dixit and Hering in 2003 regarding the arsenic sorption efficiency as a function of pH shown in Figure 4.28, it is clearly seen that the sorption efficiency of arsenite, the main arsenic species supposed to exist in the sludge in this study, becomes lower when the pH decreases. In contrast, the sorption efficiency of arsenate, the minor arsenic species supposed to exist in the sludge in this study, becomes higher when the pH decreases. For this reason, arsenite either inner or outer-spherically complexed with the iron hydroxide surfaces of which arsenic sorption efficiency is relatively high at pH 7 was supposed to be desorbed when subjected to the extraction liquid at pH around 4.93±0.05 because of reduction of sorption efficiency. While arsenate was not supposed to be desorbed by this mechanism; in contrast, arsenate desorbed by dissolution of iron hydroxide surfaces was supposed to be resorbed onto available surfaces due to effect of pH promoting higher sorption efficiency.

2) Resorption

It is important to keep in mind that, during desorption of arsenic and dissolution of $Fe(OH)_3$, resorption of arsenic as well as reformation of $Fe(OH)_3$ might happen simultaneously. According to proton-promoted dissolution diagram of $Fe(OH)_3$ in Figure 4.27(b), dissolution of one mole of Fe^{3+} in the extraction fluid consumed three moles of H^+. In the same way, the desorption of arsenic consumed H^+ as shown in Equation 2-9 to 2-13 and 2-23 to 2-29. Therefore, in such condition, pH of the system was supposed to relatively increase; the solubility of $Fe(OH)_3$ consequently, relatively decreased while the sorption efficiency of arsenic was relatively higher ; and, finally, because of the reduction of solubility as well as the increase of sorption efficiency , the dissolved ferric ions trended to reform $Fe(OH)_3$ and desorbed arsenic trended to be resorbed onto these newly forming iron hydroxide surfaces or even onto the remaining, undissolved iron oxide surfaces.

Table 4.4 Calculation of $q_{As/Fe}$ and c_{As} at equilibrium for SW samples subjected to TCLP test

	Amount of As and Fe (mmole) per 1g of the raw, dry sludge[a]		Amount of As and Fe (mmole) per 100g of the raw, dry sludge[b]		% Solid per wet sludge[c]	Amount of As and Fe (mmole) per 100g of the wet, raw sludge[d]		As/Fe of the raw ,wet sludge (mmole/mmole)[e]	Total amount of As and Fe leaching out (mmole) after the TCLP[f]		Total amount of As and Fe remaining in the sludge(mmole) after TCLP[g]		Adsorption Density ($q_{As/Fe}$) (mmole/mmole)[h]
	As	Fe	As	Fe		As^{d1}	Fe^{d2}		As ($2*c_{As}$)	Fe	As^{g1}	Fe^{g2}	
S1	1.099	7.183	109.931	718.284	21.89	24.064	157.232	0.153	0.068	0.002	1.182	8.161	0.145
S2	0.954	7.239	95.390	723.855	21.89	20.881	158.452	0.132	0.050	0.001	2.560	19.803	0.129
S3	0.766	7.310	76.615	731.017	21.89	16.771	160.020	0.105	0.028	0.001	2.708	26.107	0.104
S4	0.748	7.406	74.776	740.631	21.89	16.368	162.124	0.101	0.011	0.000	8.001	79.353	0.101
S5	0.512	7.415	51.233	741.454	21.89	11.215	162.304	0.069	0.007	0.000	4.150	60.162	0.069

[a] is from multiplying (Concentration of As and Fe from microwave digested fluid in Table 4.1) by 2 because 0.5 g of the sludge was used for microwave assistant digestion. [b] is from multiplying [a] by 100 because 100 g of the sludge was used for the TCLP test. [c] is from drying the SW samples at 105 °C for 24 hours and then dividing the remaining solid (g) by an initial weight of the SW(g). [d] is from multiplying [b] by [c] /100 . [e] is from dividing [d1] by [d2]. [f] is from multiplying the TCLP results in Table 4.3 by 2 because 2 liters of the extraction fluid was used in the TCLP test. [g] is from subtracting [f] from [d]. [h] is from dividing [g1] by

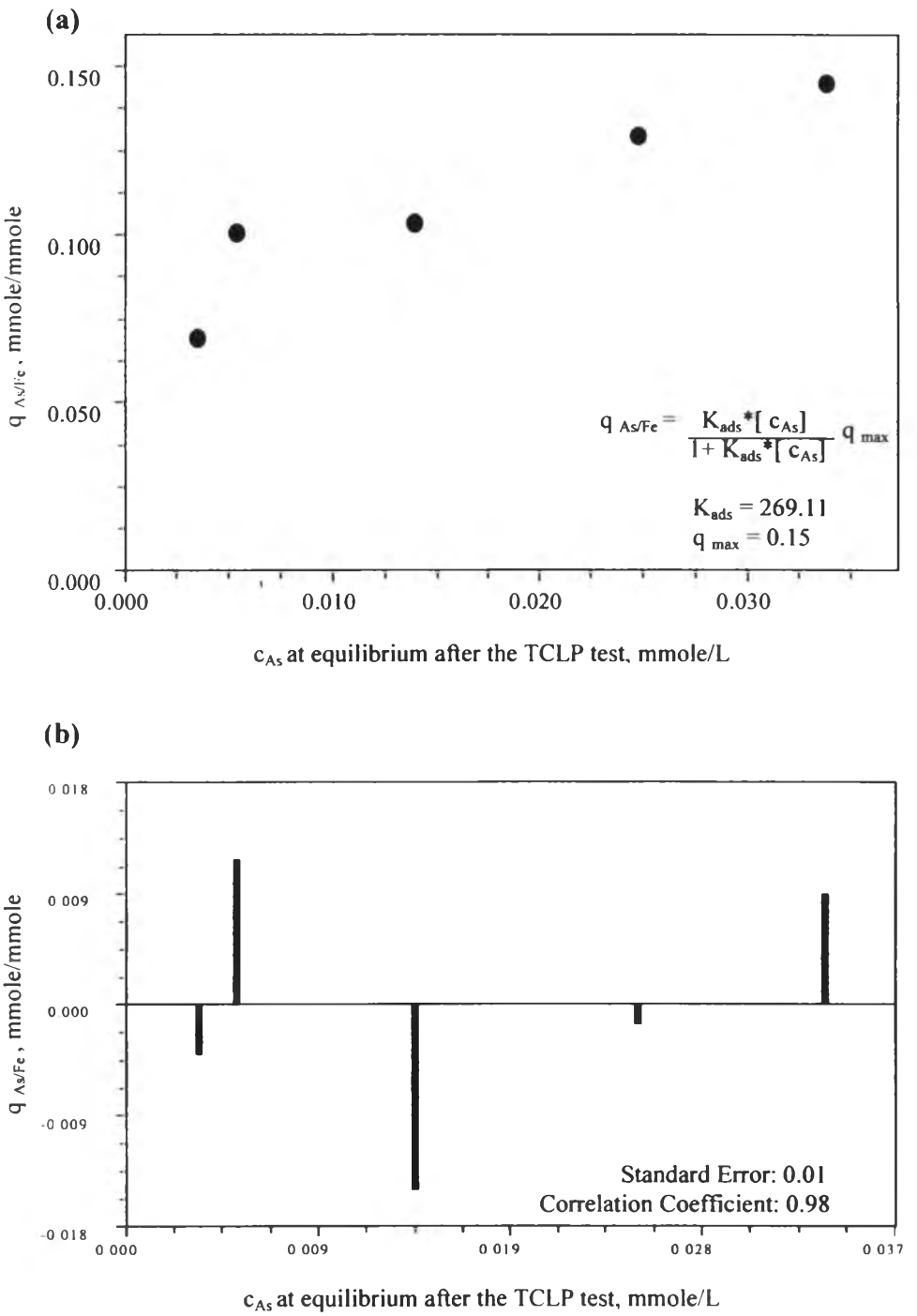

Figure 4.26 Graphical representation of (a) the relationship between adsorption density of arsenic to iron ($q_{As/Fe}$) and the dissolve concentration of arsenic of leached SW samples at equilibrium after the TCLP test (c_{As}) empirically matched with the Langmuir Isotherm of which K_{ads} and q max are 269.11 l./mmole and 0.15mmole/mnole, respectively, and (b) the residuals of the model as well as standard error and correlation coefficient.

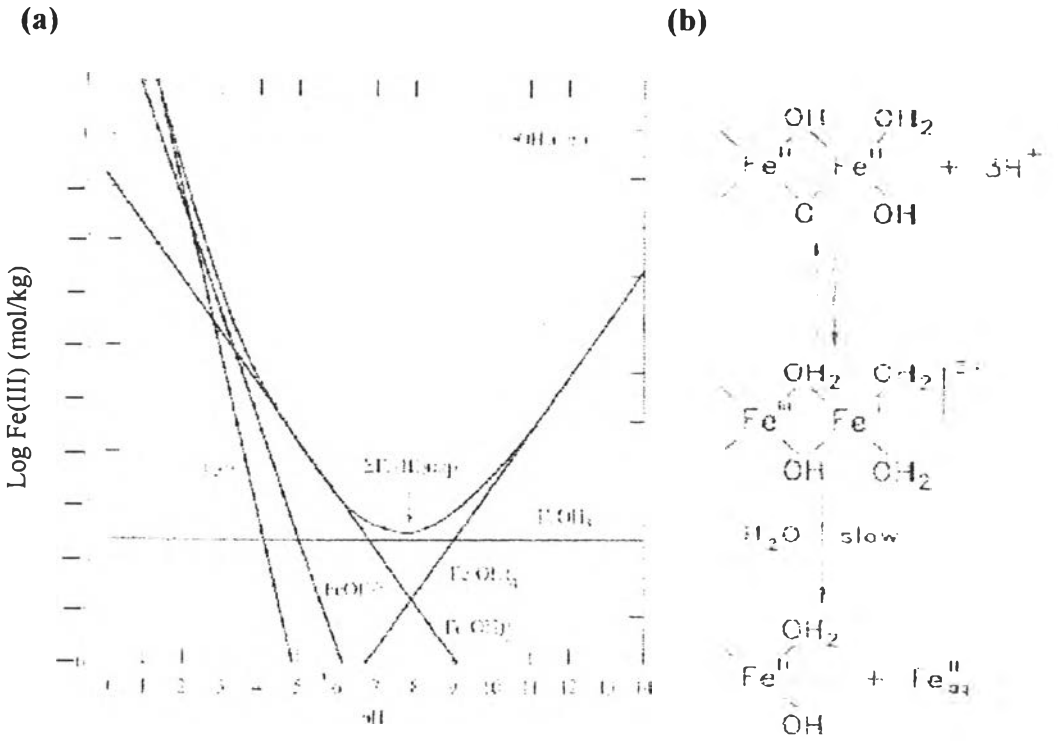

Figure 4.27 (a) Solubility of amorphous $Fe(OH)_3$, $K_{sp}= 10^{-37.1}$, as a function of pH at 25°C(Langmuir, 1997), (b) schematic representation of iron oxide dissolution promoted by proton (Morel and Hering, 1993)

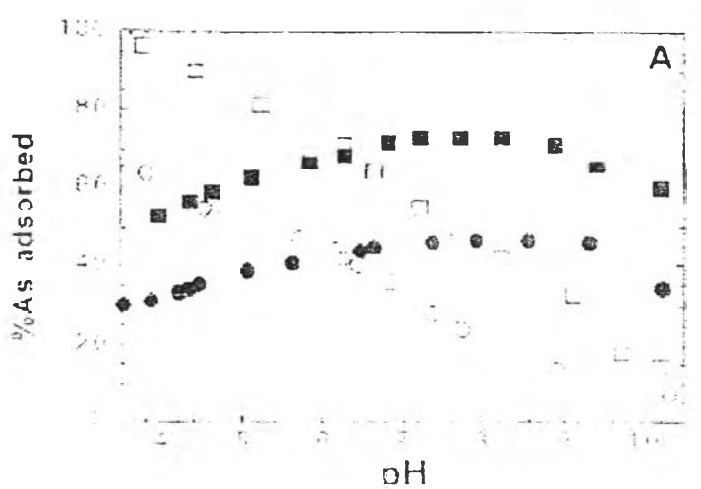

Figure 4.28 Comparison of As(V) and As(III) sorption edges on hydrous ferric oxide(HFO). The total arsenic concentrations shown are 100μM (circles) and 50 μ M(squares). Open symbols represent As(V) and closed symbols As(III) (Dixit and Hering, 2003)

The dissolution and reformation of $Fe(OH)_3$ as well as the desorption and resorption of arsenic is supposed to occur back and forth until the system reached the equilibrium point. One of the evidence supporting this assumption is final pH of the extraction fluid of each kind of sludge shown in Figure 4.29. It is clearly seen that final pH values of the extraction fluid are higher than 4.93 and 5 for both TCLP and LP-No.6, respectively.

Moreover, this assumption is also believed to be true for SD samples subjected to TCLP, witness the fact that, the relationship between $q_{As/Fe}$ and c_{As} at equilibrium of the leached SD samples calculated in Table 4.5 and illustrated in Figure 4.30 also corresponds to the Langmuir Isotherm.

However, considering Figure 4.31(a) comparing total amount of leached arsenic (mg) per two liters of leachate extracted from SD samples and that (mg) extracted from SW samples normalized by percentage of solid in dewatered sludge, it is evident that, at the equivalent amount of arsenic (mg) in the sludge, arsenic leached from SW1 was lower than that from SD1. In contrast, arsenic leached from SW2, SW3, SW4 was higher than that from SD2, SD3, and SD4, respectively, while arsenic leached from SW5 was insignificantly different from SD5.

As mentioned before, the disadvantage of drying the sludge before the leaching test is the lower surface for arsenic resorption while its advantage is increasing weathering resistibility. Figure 4.31 (a) indicates that the disadvantage of drying the sludge of which arsenic adsorption density is relative high, for example, 0.152 of S1 outweighs its advantage. In contrast, the advantage of drying the sludge of which arsenic adsorption density is moderate, for example, 0.132, 0.105, and 0.101 of S2, S3, S4, respectively, outweighs its disadvantage. Moreover, influence of the advantage and the disadvantage of drying trends to play insignificant role on the leachability of the sludge of which adsorption density is relatively low such as 0.069 of S5. However, both the dewatered and the dried arsenic-iron hydroxide sludge had high immobilization efficiency as illustrated in Figure 4.31 (b).

Similarly, the desorption and resorption are believed to be responsible for remobilization and immobilization of arsenic from both SW and SD samples subjected to LP-No.6. The evidences supporting this assumption are shown in Tables 4.6 and 4.7 as well as in Figures 4.32 and 4.33.

Table 4.5 Calculation of $q_{As/Fe}$ and c_{As} at equilibrium for SD samples subjected to TCLP

	Amount of As and Fe (mmole) per 1g of the raw, dry sludge[a]		Amount of As and Fe (mmole) per 100g of the raw, dry sludge[b]		% Solid per dry sludge[c]	Amount of As and Fe (mmole) per 100g of the dry, raw sludge[d]		As/Fe of the raw -dry sludge (mmole/mmole)[e]	Total amount of As and Fe leaching out (mmole) after the TCLP[f]		Total amount of As and Fe remaining in the sludge(mmole) after TCLP[g]		Adsorption Density ($q_{As/Fe}$) (mmole/mmole)[h]
	As	Fe	As	Fe		As^{d1}	Fe^{d2}		As ($2*c_{As}$)	Fe	As^{g1}	Fe^{g2}	
S1	1.099	7.183	109.931	718.284	100	109.931	718.284	0.153	0.553	0.004	109.378	718.279	0.152
S2	0.954	7.239	95.390	723.855	100	95.390	723.855	0.132	0.137	0.002	95.253	723.852	0.132
S3	0.766	7.310	76.615	731.017	100	76.615	731.017	0.105	0.075	0.001	76.540	731.017	0.105
S4	0.748	7.406	74.776	740.631	100	74.776	740.631	0.101	0.062	0.001	74.714	740.630	0.101
S5	0.512	7.415	51.233	741.454	100	51.233	741.454	0.069	0.037	0.002	51.197	741.452	0.069

[a] is from multiplying (Concentration of As and Fe from microwave digested fluid in Table 4.1) by 2 because 0.5 g of the sludge was used for microwave assistant digestion. [b] is from multiplying [a] by 100 because 100 g of the sludge was used for the TCLP test. [c] is 100 for all SD samples. [d] is from multiplying [b] by [c]/100. [e] is from dividing [d1] by [d2]. [f] is from multiplying the TCLP results in Table 4.3 by 2 because 2 liters of the extraction fluid was used in the TCLP test. [g] is from subtracting [f] from [d]. [h] is from dividing [g1]

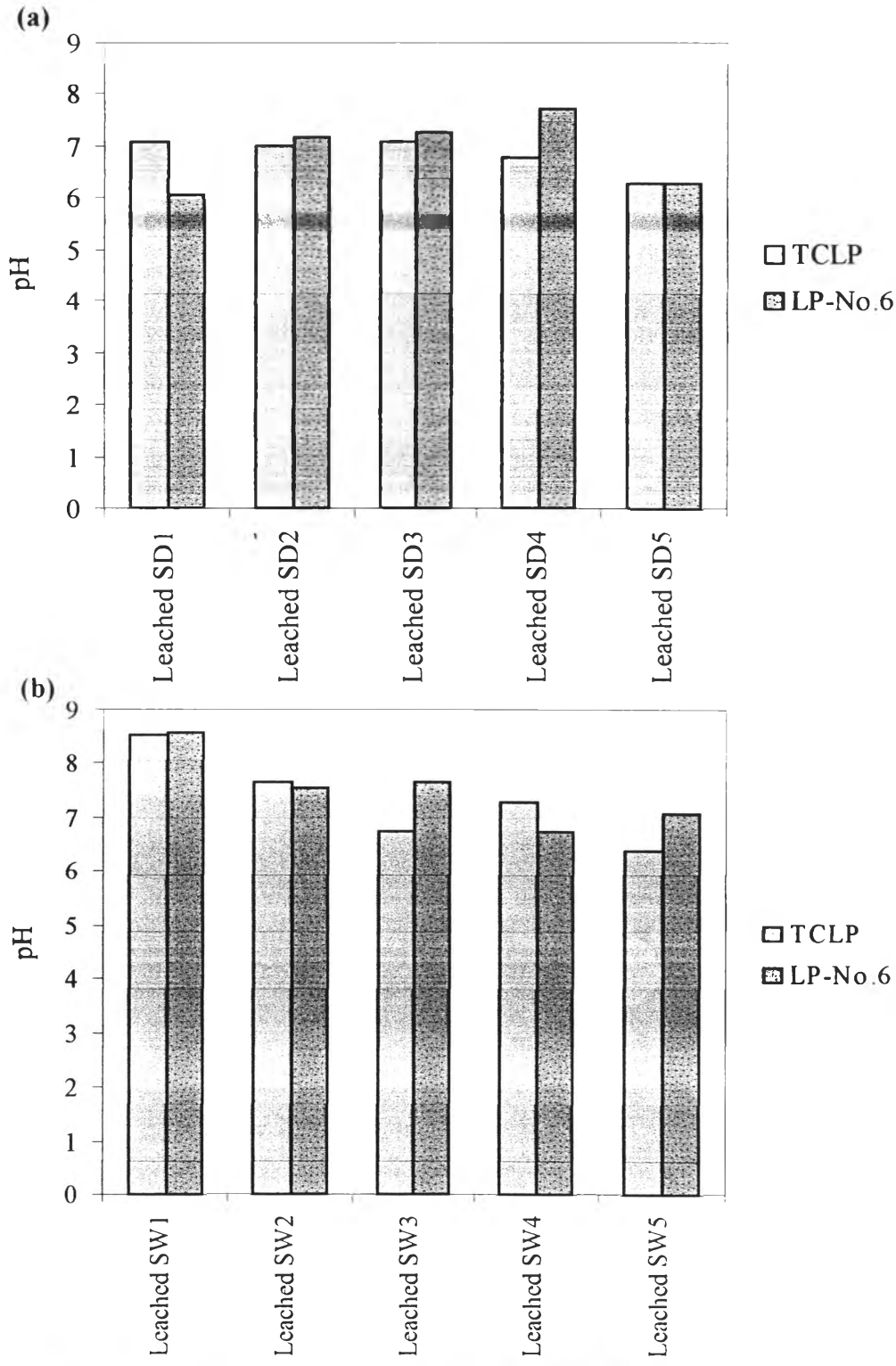

Figure 4.29 Final pH of the extraction fluid of the the TCLP and LP-No.6 (a) for SD samples and (b) for SW samples

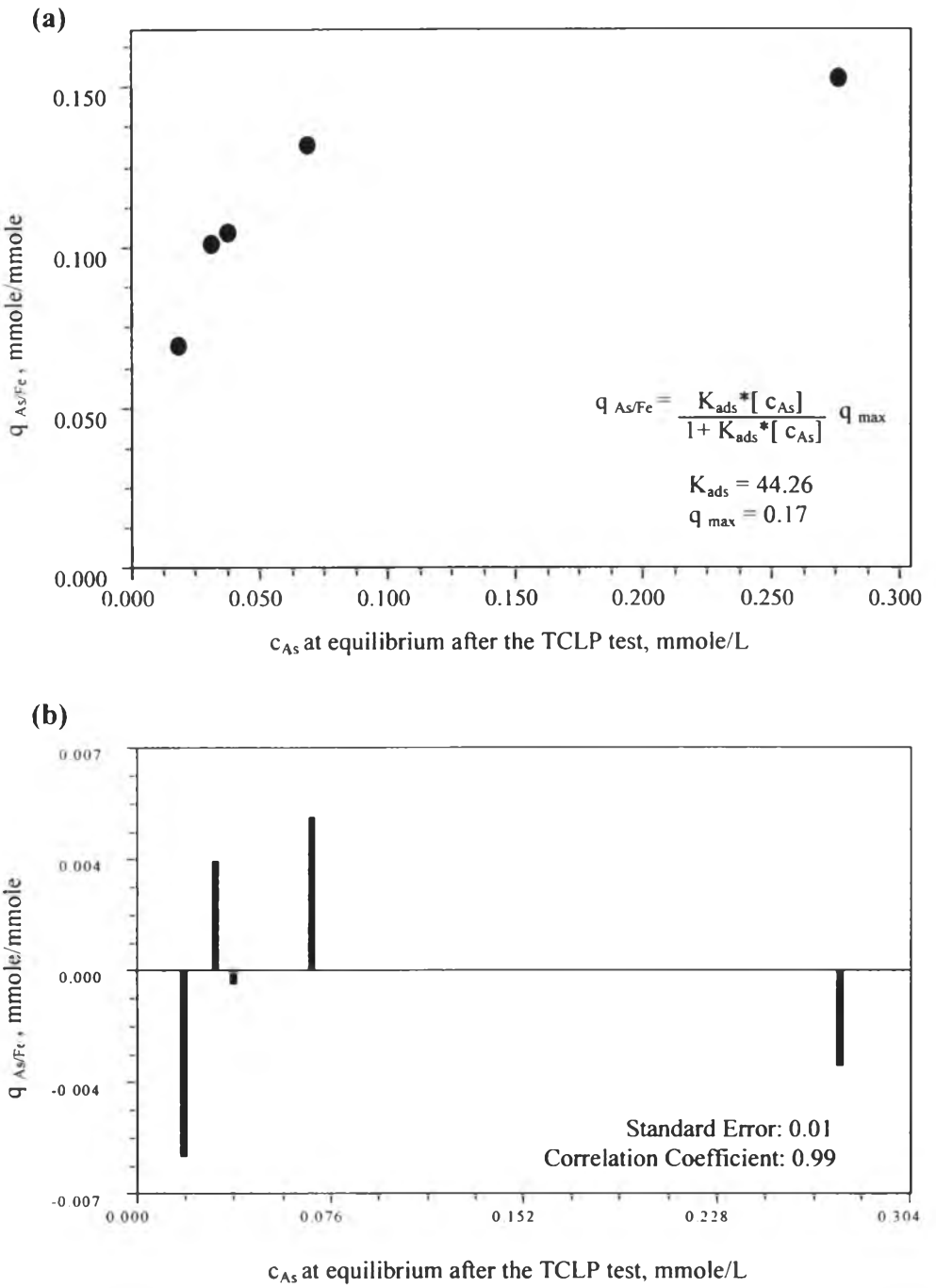

Figure 4.30 Graphical representation of (a) the relationship between adsorption density of arsenic to iron ($q_{As/Fe}$) and the dissolve concentration of arsenic of leached SD samples at equilibrium after the TCLP test (c_{As}) empirically matched with the Langmuir Isotherm of which K_{ads} and q max are 44.26 L/mmole and 0.17 mmole/mnole, respectively, and (b) the residuals of the model as well as Standard Error and Correlation Coefficient.

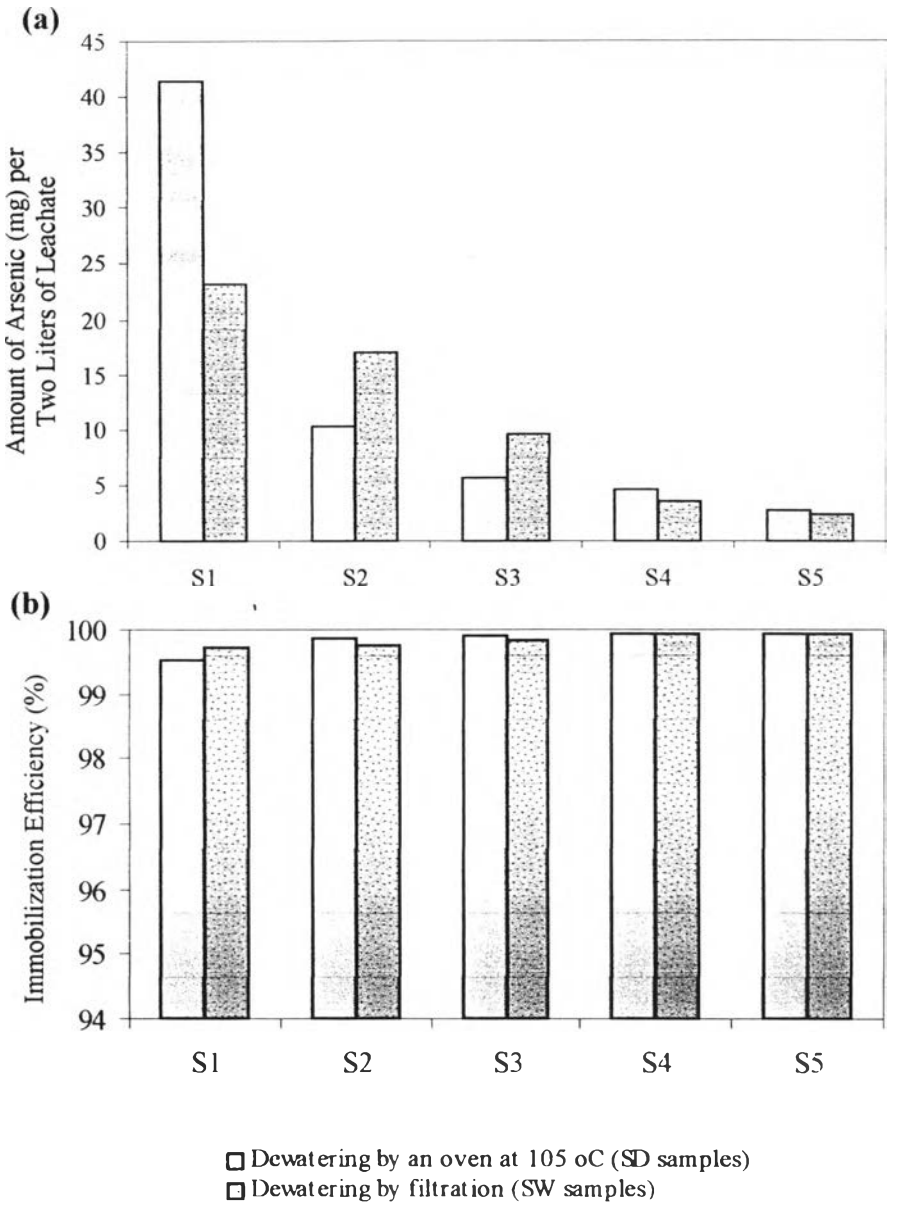

Figure 4.31 (a) Relationship of total amount of arsenic (mg) per two liters of leachate extracting from SD samples and that (mg) from SW samples normalized by % solid per wet sludge, and (b) comparison between immobilization efficiency of SD samples and that of SW samples

Table 4.6 Calculation of $q_{As/Fe}$ and c_{As} at equilibrium for SW samples subjected to the LP-No.6 test

	Amount of As and Fe (mmole) per 1g of the raw, dry sludge[a]		Amount of As and Fe (mmole) per 100g of the raw, dry sludge[b]		% Solid per wet sludge[c]	Amount of As and Fe (mmole) per 100g of the wet, raw sludge[d]		As/Fe of the raw ,wet sludge (mmole/mmole)[e]	Total amount of As and Fe leaching out (mmole) after the LP-No.6[f]		Total amount of As and Fe remaining in the sludge(mmole) after LP-No.6[g]		Adsorption Density ($q_{As/Fe}$) (mmole/mmole)[h]
	As	Fe	As	Fe		As [d1]	Fe[d2]		As ($2*c_{As}$)	Fe	As [g1]	Fe [g2]	
S1	1.099	7.183	109.931	718.284	21.89	24.064	157.232	0.153	0.070	0.000	1.179	8.162	0.144
S2	0.954	7.239	95.390	723.855	21.89	20.881	158.452	0.132	0.049	0.001	2.561	19.804	0.129
S3	0.766	7.310	76.615	731.017	21.89	16.771	160.020	0.105	0.042	0.002	2.694	26.106	0.103
S4	0.748	7.406	74.776	740.631	21.89	16.368	162.124	0.101	0.014	0.002	7.998	79.351	0.101
S5	0.512	7.415	51.233	741.454	21.89	11.215	162.304	0.069	0.006	0.000	4.151	60.161	0.069

[a] is from multiplying (Concentration of As and Fe from microwave digested fluid in Table 4.1) by 2 because 0.5 g of the sludge was used for microwave assistant digestion. [b] is from multiplying [a] by 100 because 100 g of the sludge was used for the LP-No.6 test. [c] is from drying the SW samples at 105 °C for 24 hours and then dividing the remaining solid (g) by an initial weight of the SW(g). [d] is from multiplying [b] by [c]/100. [e] is from dividing [d1] by [d2]. [f] is from multiplying the LP-No.6 results in Table 4.3 by 2 because 2 liters of the extraction fluid was used in the TCLP test. [g] is from subtracting [f] from [d]. [h] is from dividing [g1] by [g2].

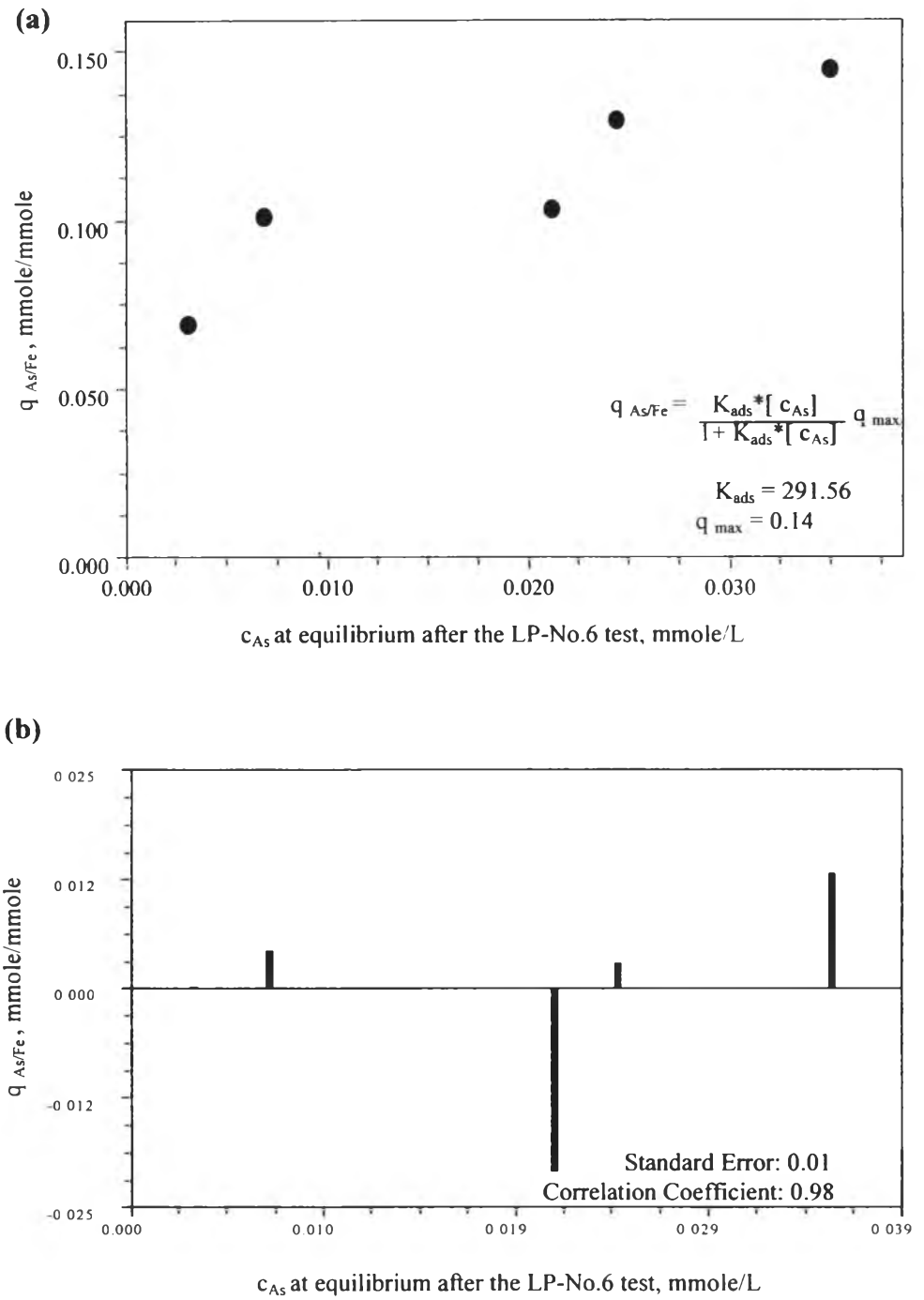

Figure 4.32 Graphical representation of (a) the relationship between adsorption density of arsenic to iron ($q_{As/Fe}$) and the dissolve concentration of arsenic of leached SW samples at equilibrium after the LP-No.6 test (c_{As}) empirically matched with the Langmuir Isotherm of which K_{ads} and q max are 291.56 L/mmole and 0.14 mmole/mnole, respectively, and (b) the residuals of the model as well as Standard Error and Correlation Coefficient.

ต้นฉบับ หน้าขาดหาย

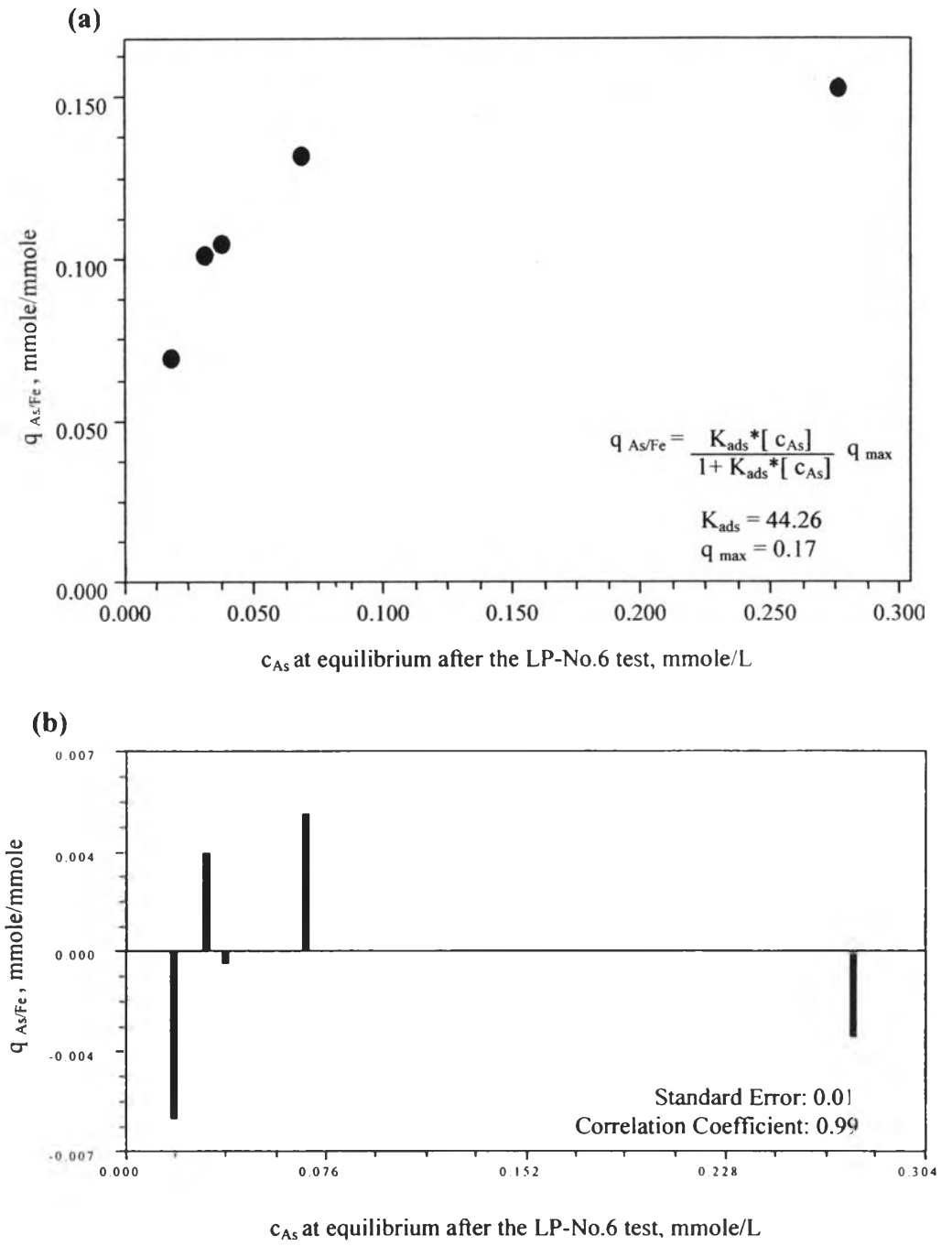

Figure 4.33 Graphical representation of (a) the relationship between adsorption density of arsenic to iron ($q_{As/Fe}$) and the dissolve concentration of arsenic of leached SD samples at equilibrium after the LP-No.6 test (c_{As}) empirically matched with the Langmuir Isotherm of which K_{ads} and q max are 44.26 L/mmole and 0.17 mmole/mnole, respectively, and (b) the residuals of the model as well as standard error and correlation coefficient.

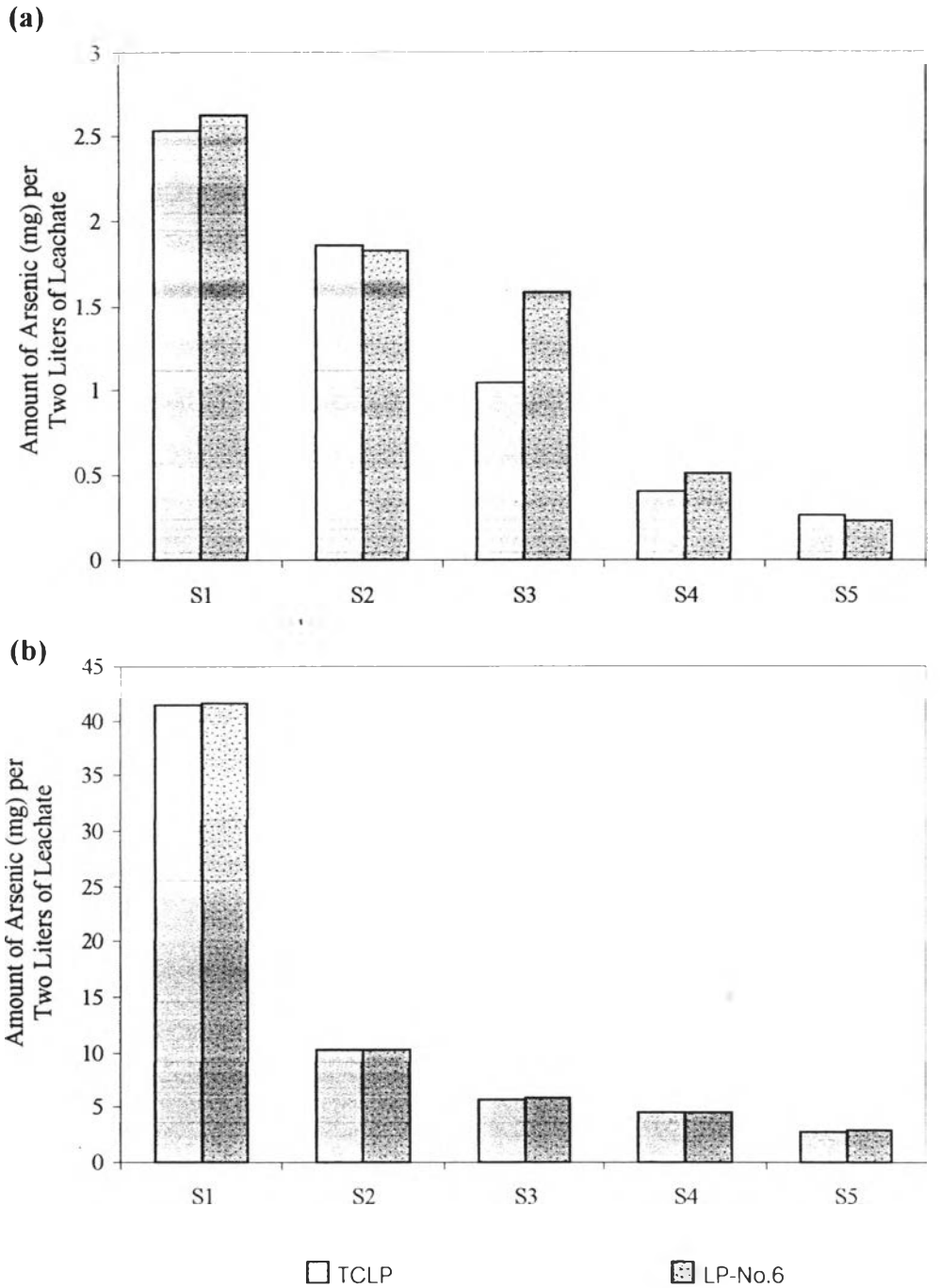

Figure 4.34 (a) comparison between total amount of arsenic (mg) per two liters of leachate extracting from SW samples subjected to the TCLP and that subjected to LP-No.6, (b) comparison between total amount of arsenic (mg) per two liters of leachate extracting from SD samples subjected to the TCLP and that subjected to LP-No.6

In addition, Figures 4.34 (a) compares total amount of arsenic (mg) per two liters of leachate extracted from SD samples by the TCLP and LP-No.6 while Figure 4.34 (b) compares that extracted from SW samples by the two leaching procedures. These two figures reveal that extractabilities of the two procedures are not significantly different from one another. To clarify this issue, the factors controlling leachability have to be considered in detail. The factors affecting leachability of waste can be categorized into two broad categories: (1) those which are determined by the property of waste itself and (2) those which are a function of the leaching test or disposal environment (Conner, 1993). Under the assumption of homogeneity, the internal factors such as chemical, physical and biological property of two waste samples for the same recipe (S1, S2, S3, S4, or S5) and the same condition (SD or SW) subjected to TCLP and LP-No.6 were identical. In the same way, except pH of extraction fluid, almost all of external factors of the two leaching procedures including surface area of waste, nature of the extraction vessel, the agitation technique, the ratio of extraction fluid to waste, the time of contract, temperature, and the method used to separate extract from solid were the same.

However, as mentioned before, the most important difference between these two extraction procedures is that the extraction fluid of TCLP is made with water and acetic acid while that of NO.6-LP fluid is made with 80% of sulfuric acid and 20% of nitric acid in deionized (DI) water. To examine the influence of this difference on extractability, it is essential to review possible reactions of these chemicals against the sludge. The three most possible reactions are metal-ligand complexation, precipitation as sulfide compounds, and competitive surface complexation between sulfate ion and arsenic oxyanions.

Mixed with water in forms of CH_3COOH, H_2SO_4, and HNO_3, acetic, sulfuric, and nitric acid subsequently dissociate as H^+ and CH_3COO^-. SO_4^{-2} together with HSO_4^- and NO_3^-, respectively. Both CH_3COO^- as well as NO_3^- , HSO_4^- , and SO_4^{-2} ions can reduce the likelihood that metal will bind directly to an adsorbent surface because these dissolved ligands can bind to dissolved, positive-charged metal ions. Then less dissolved metal is available to bind to the surface (Benjamin, 2002)

However, this metal-ligand complexation is unlikely to happened with the case of arsenic due to the fact that although classified as a metal when in its zero-valent oxidation state, arsenic is more stable as oxyanion than as a cation when it is in aqueous phase.

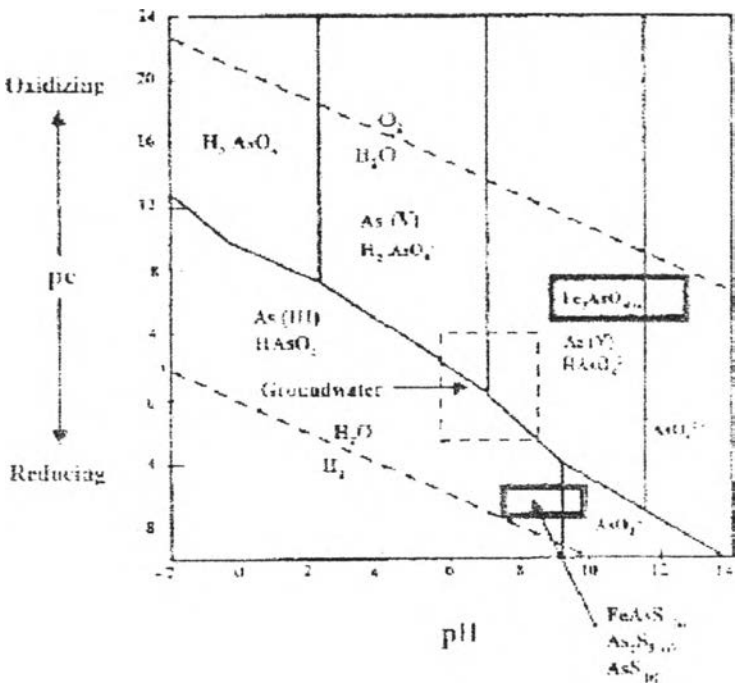

Figure 4.35 Predominance or pe-pH Diagram of Various As(V) and As(III) Species Including Precipitates (SenGupta and Greenleaf, 2002)

Unlike CH_3COO^- and NO_3^- ions, HSO_4^- and SO_4^{-2} ions can both negatively and positively influence over leachability of the sludge by two others phenomena besides metal-ligand complexation.

One is precipitation as sulfide compounds such $FeAsS_{(s)}$ and $As_2S_{3(s)}$. Under reduced environmental, dissolved SO_4^{-2} and As(V) can be reduced to dissolved sulfide (either H_2S or HS^-, depending on pH) and As(III), respectively. Consequently, the formation of As(III)-sulfide phases such as such $FeAsS_{(s)}$ and $As_2S_{3(s)}$ may take place (Inkeep, McDermott, and Fendorf, 2002) as shown in Figure 4.35. These solids have been suggested as important sinks for As(III) in reduced condition; as a result, in the

presence of the formation of such compounds, concentration of arsenic in solution unsurprisingly decreases. However, such phenomenon is unlikely to exist in the leaching tests owning to the fact that both the TCLP and LP-No.6 are generally performed without playing attention to headspace in the extraction vessel or the exclusion of oxygen from the extraction system. For this reason, in the presence of oxygen, the oxidized condition probably exists in the leaching tests rather than reduced environment. Therefore, dissolved SO_4^{-2} and As(V) cannot be reduced to dissolved sulfide and As(III) and the formation of As(III)-sulfide phases is in vain.

Another is surface complexation of SO_4^{-2} onto amorphous iron oxide surface. SO_4^{-2} ions can be sorbed onto amorphous iron oxide surface. The presence of SO_4^{-2} ions may reduce arsenic sorption/resorption efficiency due to the fact that competitive sorption between SO_4^{-2} ions and dissolved arsenic oxyanions may take place. By sorption of SO_4^{-2} ions, it is possible that the fewer binding sites on amorphous iron oxide surface are available for arsenic because SO_4^{-2} ions occupies them. Consequently, arsenic resorption on the surface becomes worse because of insufficient binding sites and arsenic mobility seems to be increase. However, this phenomenon is also unlikely to play a crucial role on leachability of arsenic according to the study of Meng, Bang, and Korfiatis in 2000. Their study suggested that sulfate binding affinity for ferric hydroxide surface was much weaker than As(V) and As (III).

In conclusion, none of these three reactions are supposed to influence the extractability of arsenic by both the TCLP and LP-No.6. Therefore, the difference among types of acid used to produce the extraction fluid of the two extraction procedures is unlikely to present a significant role controlling the desorption and resorption of arsenic in the sludge. For this reason, only pH controls the rate of the desorption and resorption directly related to the leachability of arsenic. Owning to the fact that the initial pH values of the extraction fluid of the two leaching procedures are insignificantly different, it is unsurprising that the leachabilities of arsenic by these two procedures are similar.

PART II

4.4 Batch Coagulation/Co-precipitation Tests of Arsenic Removal by Ferric Chloride.

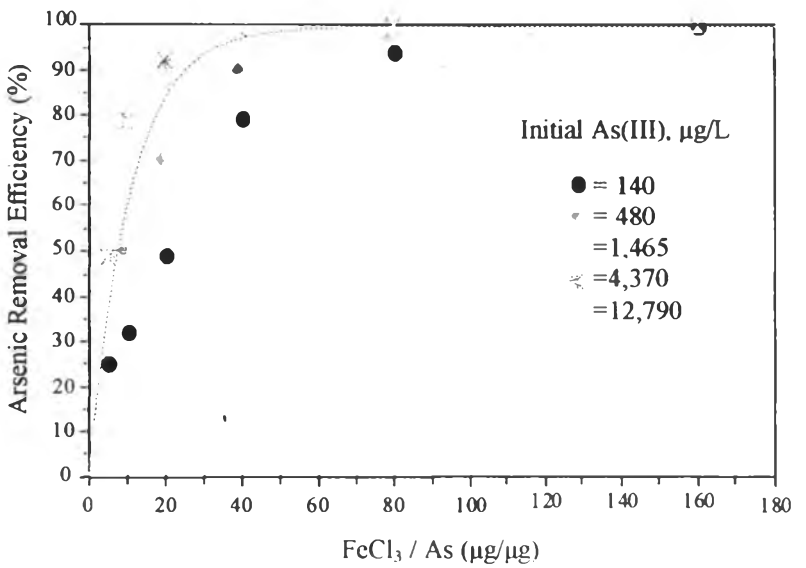

Figure 4.36 Effect of initial arsenic concentrations and $FeCl_3$ / As ratios on arsenic removal efficiency at pH 7

The series of the results from the jar tests conducted with varying initial As (III) concentrations from 140 to 12,790 µg/L and $FeCl_3$/ As ratios by weight from 5 to 160 at pH 7 are illustrated in Figure 4.36. It is found that the removal efficiency of As (III) is strongly under the influence of initial As(III) concentrations and $FeCl_3$/As ratios. This observation is in good agreement with a number of recent studies. However, owning to the fact that the discussions regarding this graph are available in a great deal of publication together with the fact that the objective of this part is not to discuss the arsenic removal mechanism by ferric chloride coagulation but to examine the variation in the property of the sludge as well as its potential to be classified as hazardous waste as the functions of initial arsenic concentrations and finished water targets, the explanation about influence of initial As(III) concentration and $FeCl_3$/ As ratios on the effectiveness of As(III) removal will not be discussed here. However, for the readers who wish to gain better understanding of this issue, reviewing the articles

titled *Adsorption of Arsenic onto Hydrous Ferric Oxide: Effects ofAdsorbate/Adsorbent Ratios and Co-Occorring Solution* by Wikie and Hering (1996) or *Low-Cost Technique of Arsenic Removal from Water and Its Removal Mechanism* by Mamtaz and Bache is recommended.

As discussed in Chapter 2, the factors controlling amount and properties of the sludge are initial arsenic concentrations, finished water targets, and background coagulant demands. Therefore, to achieve the objectives of Part II, three empirical models have been built from the results of the jar tests shown above. The first model, which will be discussed in Section 4.5.1, is the empirical model to predict the coagulant demand for each initial arsenic concentration to achieve a finished water target. The second model, which will be discussed in Section 4.5.2, is the empirical model to calculate the most important property of the sludge, As-to-Fe ratio (mmole/mmole), in order to predict arsenic leachability of the sludge produced from the removal process for each initial arsenic concentration and coagulant demand. Finally, the empirical models concerning As-to-Fe ratios (mmole/mmole) in the sludge and leachate concentrations of arsenic by TCLP and LP-NO.6 discussed in Part I are applied in Section 4.5.3 to evaluate the potential of the sludge from different initial arsenic concentrations, finished water targets, and background coagulant demands to be classified as hazardous waste.

4.5 Linear Regression Analysis

4.5.1 The Empirical Model Describing Relationship among Removal Effieiency of As(III), Initial As(III) Concentrations, and $FeCl_3$ /As Ratios

The series of jar test results plotted in Figure 4.36 were input to SPSS 11.0.0, a statistical program, to build the first empirical model. In this regression analysis, the dependent variable was the natural logarithm of As(III) removal efficiency (%), while the natural logarithms of initial As(III) concentrations (μg/L) and $FeCl_3$/As ratios (by weight) were set as the independent variables. The model and coefficient summaries are shown in Tables 4.8 and 4.9. According to this table, it can be concluded that the first empirical model is:

As(III) removal (%) =

$$13.37\,(\text{Initial As(III)},\ \mu g/L)^{0.104}\,(FeCl_3/\text{As(III)},\text{by weight})^{0.28} \qquad (4\text{-}2)$$

This equation is valid for As(III) concentration of 140 to 12,790 μg/L, $FeCl_3$ /As(III) by weight from 5 to 160 at pH 7. The contour line expressing the removal efficiency at each initial arsenic concentration and $FeCl_3$/As ratio is illustrated in Figure 4.37.

This model is beneficial to roughly determine a coagulant demand when an initial As(III) concentration and a MCL of arsenic are known. For example, according to Table 2.9 in Chapter 2, the highest concentration of arsenic in groundwater at West Bengal is 3,200 μg/L and the MCL of arsenic for drinking water in West Bengal is 50 μg/L. Therefore, the removal efficiency required to produce drinking water from this contaminated is 98.44%. Thus, by substituting *As(III) removal (%)* and *Initial As(III)* in the equation with 98.44% and 3,200 μg/L, respectively, *$FeCl_3$ As(III)* is 62.32. Thus, $FeCl_3$ required to remove As at this concentration is 199.43 mg/L.

As shown in Table 2.8 in Chapter 2, MCLs of arsenic are different from country to country. Therefore, if two countries have been contaminated with the same level of arsenic but have different MCLs, the $FeCl_3$/As(III) required to produce drinking water for each country is likely to be different from one another. By the same procedure discussed in the previous paragraph, the $FeCl_3$/As(III) required to produce drinking water complying with two different MCLs, 0.01 and 0.05 ng/L from the contaminated water of which arsenic concentration ranges from 150 to 12,000 μg/L can be calculated and depicted in Table 4.10 and Figure 4.38.

Table 4.8 Summary of the empirical model describing relationship among effectiveness of As(III) removal, initial As(III) concentration, and $FeCl_3$ /As ratios

Model	R	R Square	Adjusted R Square	Std. Error of the Estimate
1	.877	.769	.752	.2141

Table 4.9 Coefficient summary of the empirical model describing relationship among effectiveness of As(III) removal, initial As(III) concentration, and $FeCl_3$ /As ratios

Model	Unstandardized Coefficients		Sig.	Correlations		Collinearity Statistics	
	B	Std. Error		Zero-order	Partial	Tolerance	VIF
(Constant)	2.593	0.213	0	-	-	-	-
Ln initial As	0.104	0.025	0	0.391	0.631	1	1
Ln Fe:As	0.28	0.033	0	0.785	0.853	1	1

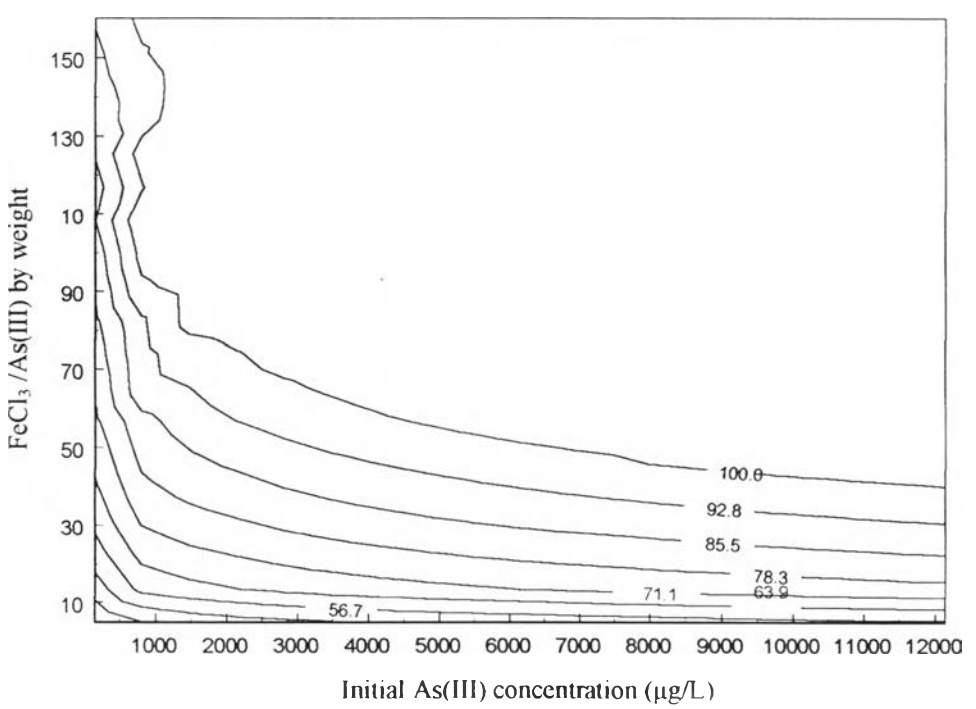

Figure 4.37 The contour line expressing the removal efficiency (%) at each initial arsenic concentration and $FeCl_3$ /As ratio

Table 4.10 FeCl3 /As ratios (by weight) and effectiveness of As(III) removal (%) required for removal of arsenic contaminated water of which initial As(III) concentration ranges from 150 to 12,000(μg/L) to comply with two different MCLs: 10 and 50 μg/L

Initial As(III) Concentration (μg/L)	MCL=10 μg/L		MCL=50 μg/L	
	$FeCl_3$ /As Ratios Required (by Weight)	Effectiveness of As(III) Removal Required (%)	$FeCl_3$ /As Ratios Required (by Weight)	Effectiveness of As(III) Removal Required (%)
12,000	40.23	99.92	39.75	99.58
8,500	45.67	99.88	44.91	99.41
5,000	55.45	99.8	53.89	99.00
1,500	85.29	99.33	77.39	96.67
500	122.28	98.00	90.18	90.00
150	160.58	93.33	48.29	66.67

4.5.2 The Empirical Model Describing Relationship among As-to-Fe ratios in the Sludge produced from the Arsenic Removal Process, Initial As(III) Concentrations, and $FeCl_3$ /As Ratios

As discussed in the previous section, $FeCl_3$ /As ratios (by weight) required in producing drinking water in accordance with two different MCLs from arsenic contaminated water can be calculated. The mission of this section is to examine the important property, As-to Fe ratios, of the sludge produced from such removal processes. This property is helpful for sludge classification, which will be discussed in the next section.

From the series of jar test results plotted in Figure 4.36, As-to-Fe ratios of the sludge produced from coagulation with variation of initial As(III) concentrations and coagulant demands ($FeCl_3$ /As ratios) were calculated under mass balance concept.

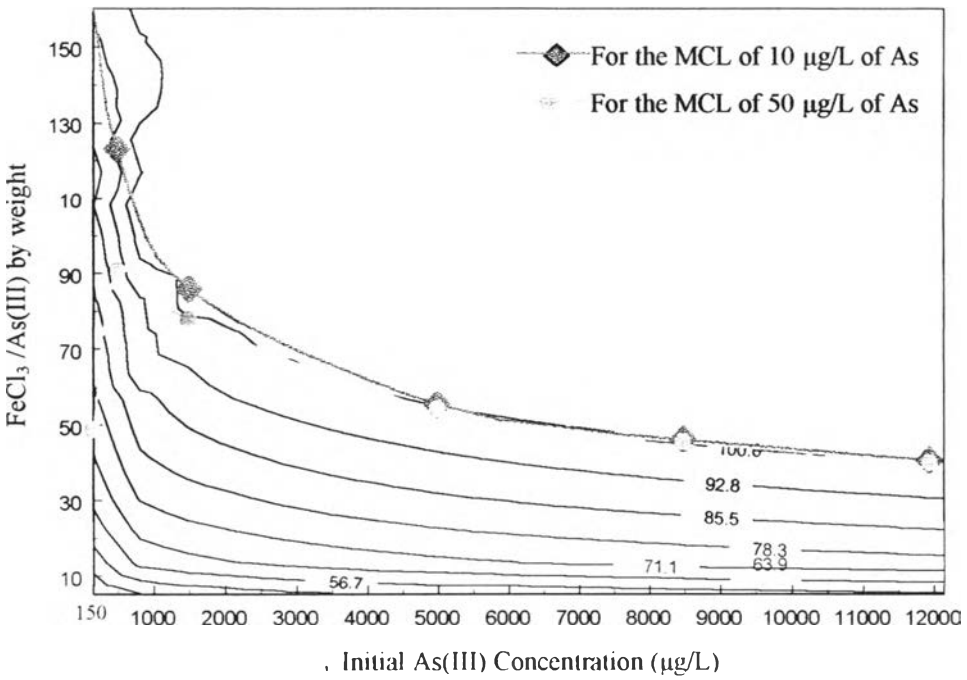

Figure 4.38 Plotting of $FeCl_3$ /As ratios (by Weight) and effectiveness of As(III) removal (%) required for removal of arsenic contaminated water of which initial As (III) concentration ranges from 150 to 12,000(µg/L) to comply with two different MCLs: 10(blue-filled rectangles) and 50 µg/L(red-filled circles)

The regression analysis was conducted by SPSS 11.0.0 to build the second empirical model, the model describing relationship among As-to-Fe ratios in the sludge produced from the arsenic removal processes, initial As(III) concentration, and $FeCl_3$ /As ratios.

In this regression analysis, the dependent variable was the natural logarithm of As-to-Fe ratios (mmole/mmole) of the sludge produced from the coagulation, while the natural logarithms of initial As(III) concentrations (µg/L) and $FeCl_3$/As ratios (by weight) were set as the independent variables. The model and coefficient summaries are shown in Tables 4.11 and 4.12. According to this Table, it can be concluded that the second empirical model is:

As-to-Fe ratios of the sludge produced from coagulation (mmole/mmole)

$$= 0.129\ (\text{Initial As(III)},\ \mu g/L)^{0.119}\ (FeCl_3/\text{As(III)},\text{by weight})^{-0.722} \qquad (4\text{-}3)$$

This equation is valid for As(III) concentration of 140 to 12,790 μg/L, $FeCl_3$ /As(III) by weight from 5 to 160 at pH 7. The contour line expressing the As-to-Fe ratios of the sludge produced from coagulation varying in initial arsenic concentrations and $FeCl_3$/As ratios is illustrated in Figure 4.39.

This model is beneficial to roughly determine As-to-Fe ratios (mmole/mmole) of the sludge produced from the coagulation when initial As(III) concentrations and $FeCl_3$/As ratios are known. For example, as discussed in the previous, in order to produce drinking water from groundwater contaminated by arsenic in West Bengal of which highest arsenic concentration is 3,200 μg/L, 199.43 mg/L of $FeCl_3$ is required to lessen such high arsenic concentration to 50 μg/L, the MCL of West Bengal. $FeCl_3$/As(III) corresponding to 199.43 mg/L of $FeCl_3$ is 62.32. Thus, by substituting *$FeCl_3$ As(III)* and *Initial As(III)* in the equation 4-3 with 62.32 and 3,200 μg/L, respectively, *As-to-Fe ratios of the sludge* is 0.017 mmole/mmole.

By the same procedure discussed in the previous paragraph, As-to-Fe ratios of the sludge produced from the coagulation of initial As(III) concentrations and $FeCl_3$/As(III) ratios in Table 4.10 can be calculated and depicted in Table 4.13 and Figure 4.40.

Table 4.11 Summary of the empirical model describing relationship among As-to-Fe in the sludge produced from the arsenic removal process, initial As(III) concentration, and $FeCl_3$ /As ratios

Model	R	R Square	Adjusted R Square	Std. Error of the Estimate
2	.975	.951	.947	.2091

Table 4.12 Coefficient summary of the empirical model describing relationship among As-to-Fe in the sludge produced from the arsenic removal process, initial As (III) concentration, and $FeCl_3$ /As ratios

Model	Unstandardized Coefficient		Sig.	Correlation		Collinearity Statistics	
	B	Std. Error		Zero-order	Partial	Tolerance	VIF
(Constant)	-2.048	.192	0	-	-	-	-
Ln initial	.119	.024	0	.182	.691	.999	1.001
Ln Fe:As	-.722	.032	0	-.952	-.974	.999	1.001

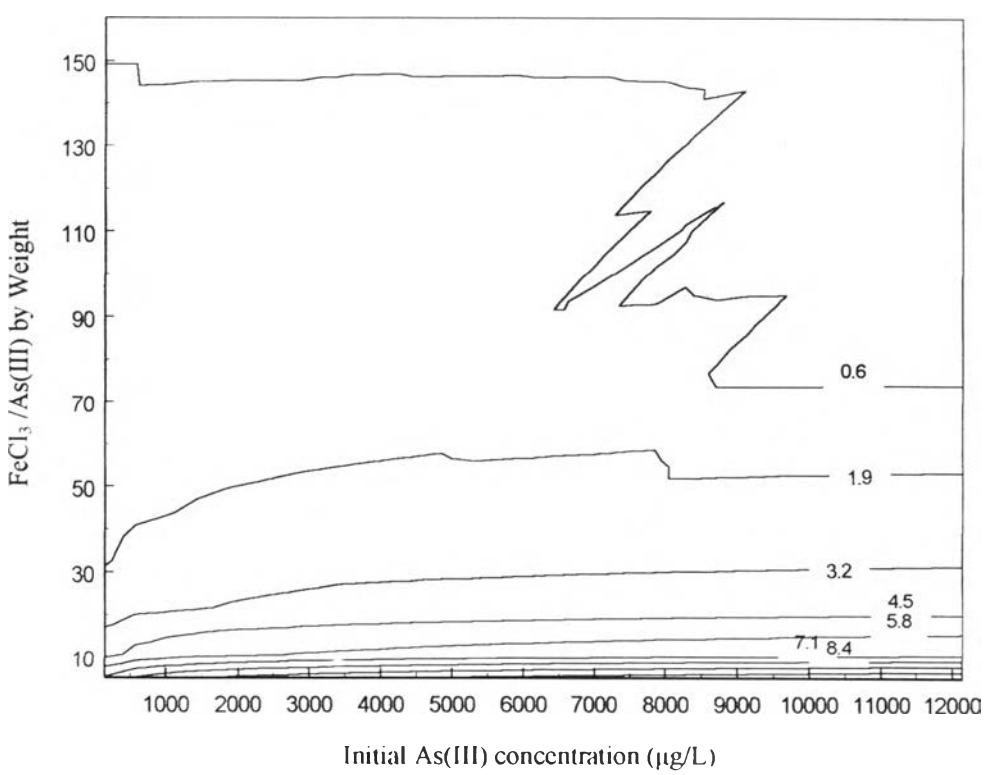

Figure 4.39 The As-to-Fe ratios (10^{-2} mmole/mmole) of the sludge produced from coagulation varying in initial arsenic concentrations and $FeCl_3$/As ratios

Table 4.13 The As-to-Fe ratios (mmole/mmole) of the sludge produced from coagulation process to treat contaminated water of which initial As(III) concentration ranges from 150 to 12,000 (μg/L) to comply with two different MCLs: 10 and 50 μg/L

Initial As(III) Concentration (μg/L)	MCL=10 μg/L		MCL=50 μg/L	
	$FeCl_3$ /As Ratio Required (by Weight)	As-to-Fe Ratio (mmole/mmole) of the Sludge	$FeCl_3$ /As Ratios Required (by Weight)	As-to-Fe Ratio (mmole/mmole) of the Sludge
12.000	40.23	0.027	39.75	0.028
8.500	45.67	0.024	44.91	0.024
5.000	55.45	0.020	53.89	0.020
1.500	85.29	0.012	77.39	0.013
500	122.28	0.008	90.18	0.010
150	160.58	0.006	48.29	0.014

4.5.3 The Application of the Empirical Model Describing Relationship between As-to-Fe Ratios (mmole/mmole) of the Sludge and Their Leachate Concentrations of Arsenic by TCLP and LP-NO.6

In this section, the empirical models describing the relationship between As-to-Fe ratios (mmole/mmole) of the sludge and leachate concentrations of arsenic by both TCLP and LP-NO.6 discussed in Part I are applied to evaluate whether or not the sludge as a result of producing drinking water complying with two different MCLs, 10 and 50 μg/L of arsenic, by the coagulation of contaminated water of which initial As(III) concentration ranges from 150 to 12,000(μg/L) is classified as hazardous waste.

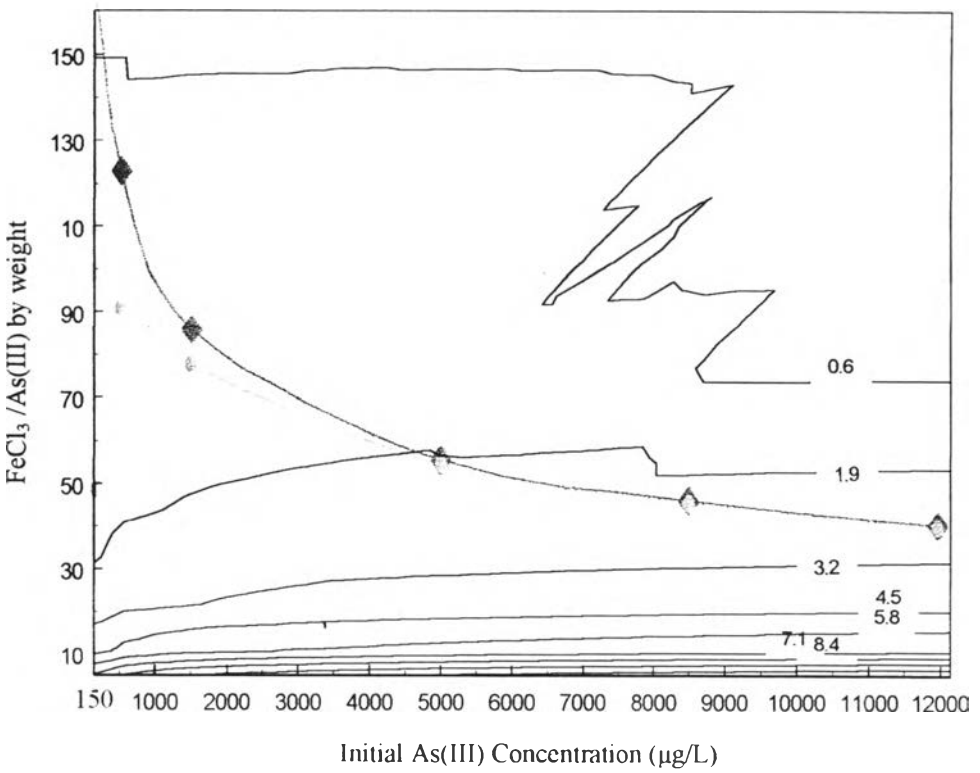

Figure 4.40 Plotting of the As-to-Fe ratios (10^{-2} mmole/mmole) of the sludge produced from coagulation process to treat contaminated water of which initial As (III) concentration ranges from 150 to 12,000(μg/L) to comply with two different MCLs: 10 (blue-filled rectangles) and 50 μg/L (red-filled circles)

For the countries, such as the United States, which use the TCLP to evaluate the potential to be hazardous waste of the sludge, the empirical model illustrated in Figure 4.26 of Part I can be applied for roughly estimating concentration of arsenic in leachate of the dewatered sludge (approximately 21.9% solid). Figure 4.41(a) illustrates the application of this model for the As-to-Fe ratios (mmole/mmole) of the sludge shown in Table 4.13 to estimate their corresponding leachate concentrations of arsenic.

As mentioned in Chapter 2, the regulatory limits of leachate concentration of arsenic in the countries of which MCLs of arsenic for drinking water are 10 and 50 μg/L are generally 1 mg/L (0.0133 mmole/L) and 5 mg/L (0.0667 mmole/L), respectively. Therefore, the dewatered sludge produced from the coagulation of contaminated water of which initial As(III) concentration ranges from 150 to 12,000 (μg/L) to the final target of 10 μg/L is unlikely to be hazardous waste based on its leachate concentration of arsenic as shown by the red-filleds circle in this figure. Similarly, the dewatered sludge produced from coagulation of contaminated water of which initial As(III) concentration ranges from 150 to 12,000 (μg/L) to the final target of 50 μg/L is also unlikely to be hazardous based on its leachate concentration of arsenic as shown by the blue-filled circles in the same figure.

To reduce volume of the sludge, drying by heat can be applied to the sludge as discussed in Part I. The model illustrated in Figure 4.30 of Part I can be applied for roughly estimating concentration of arsenic in leachate of the dried sludge (100% solid). Figure 4.41(b) illustrates the application of this model for the As-to-Fe ratios (mmole/mmole) of the sludge shown in Table 4.13 to estimate their corresponding leachate concentrations of arsenic by TCLP.

Like the case of the dewatered sludge discussed above, the dried sludge produced from the coagulation of contaminated water of which initial As(III) concentration ranges from 150 to 12,000 (μg/L) to the final target of both 10 and 50 μg/L is unlikely to be hazardous waste based on its leachate concentration of arsenic as shown by the red-filled circles and blue-filled rectangles illustrated in Figure 4.41 (b), respectively.

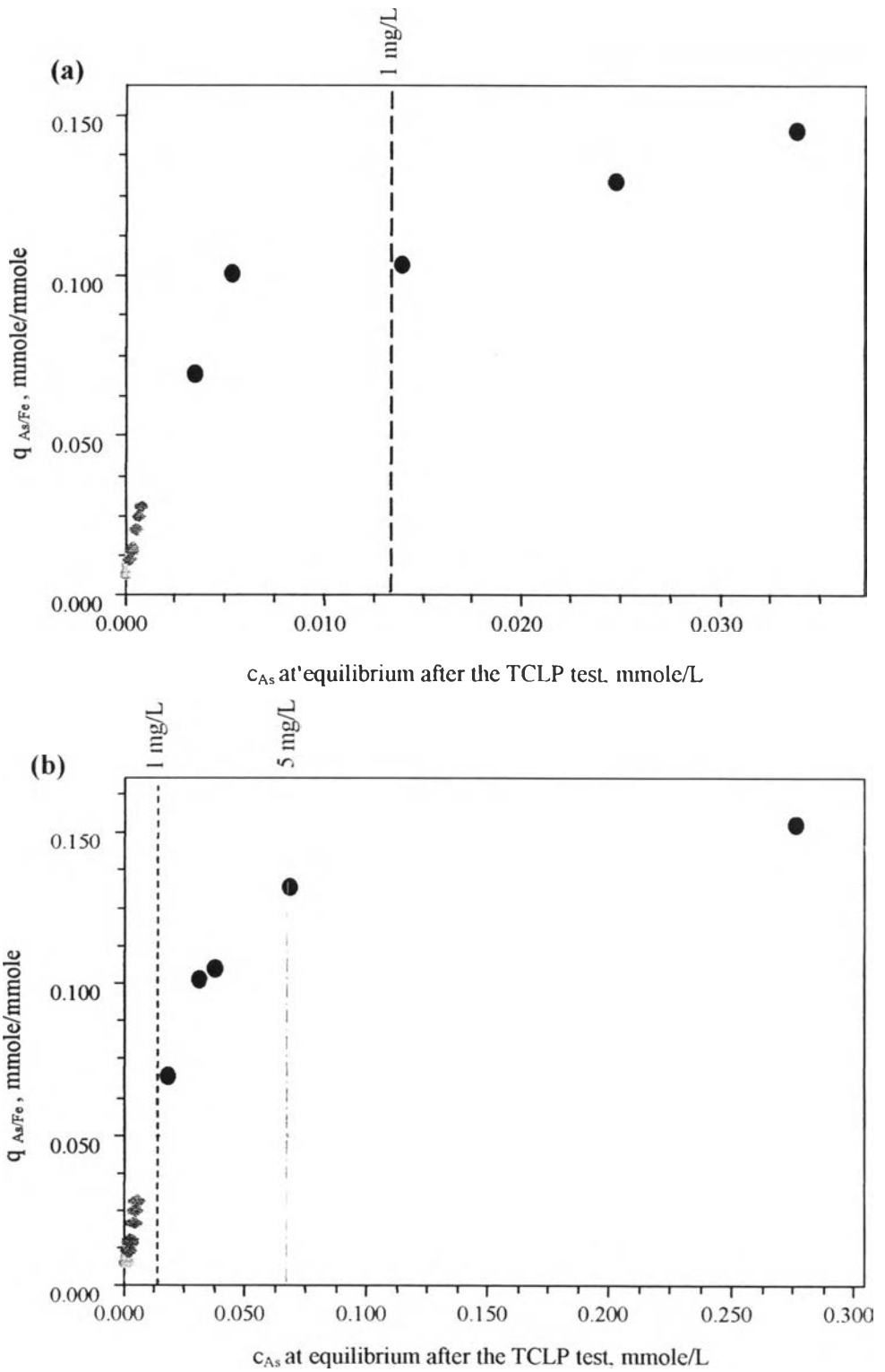

Figure 4.41 (a) Application of the empirical model in Figure 4.26 to estimate leachate concentration of arsenic from the dewatered sludge (approximately 21.9% solid) subjected to the TCLP and (b) application of the empirical model in Figure 4.30 to Estimate Leachate Concentration of Arsenic from the Dried Sludge (100% solid) subjected to the TCLP. The red-filled circles represent the sludge for MCL of 10 μg/L while blue-filled rectangles represent the sludge for MCL of 50 μg/L

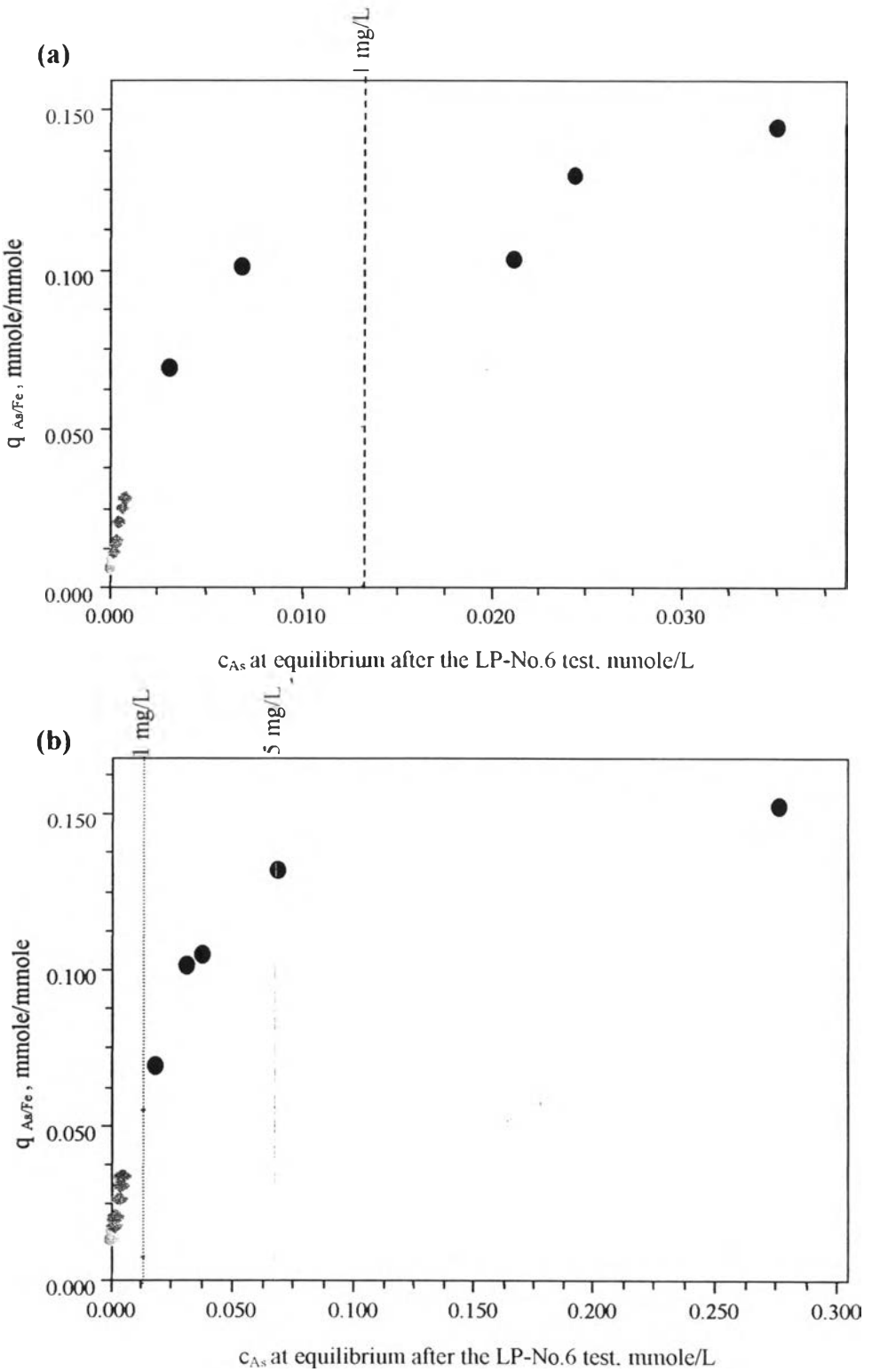

Figure 4.42 (a) Application of the empirical model in Figure 4.32 to estimate leachate concentration of arsenic from the dewatered sludge (21.9% solid) subjected to LP-No.6 and (b) application of the empirical model in Figure 4.33 to estimate leachate concentration of arsenic from the dried sludge (100% solid) subjected to LP-No.6. The red-rilled circles represent the sludge for MCL of 10 μ g/L while blue-filled rectangles represent the sludge for MCL of 50 μg/L

As mentioned in Chapter 2 that Thailand has developed its own leaching procedure, the empirical models illustrated in Figures 4.32 and 4.33 of Part I can be applied for roughly estimating arsenic concentration in leachate of the dewatered and dried sludge. Figure 4.42 (a) and (b) illustrates the application of this model for the As-to-Fe ratios (mmole/mmole) of the sludge shown in Table 4.13 to estimate their corresponding leachate concentrations of arsenic. The blue-filled rectangles represent the sludge produced from the coagulation of contaminated water of which initial As (III) concentrations range from 150 to 12,000 μg/L to the final target of 50 μg/L, the present MCL of arsenic for drinking water in Thailand . It is clearly seen that both the dewatered and the dried sludge are unlikely to be hazardous waste. In the same way, if the MCL of arsenic for drinking water in Thailand is reduced to 10 μg/L in the future, the sludge is also unlikely to be hazardous waste as simulated by the red-filled circles in the same figure, but the volume of the sludge produced is supposed to serious increase.

In conclusion, both the dewatered and the dried arsenic-containing sludge from the coagulation process of contaminated water of which initial As(III) concentrations range from 150 to 12,000 (μg/L) to the final targets of 10 and 50 μg/L are supposed to be classified as non-hazardous waste by both the TCLP and LP-No.6. It should be noticed that, in this study, the wide range (from 150 to 12,000 μg/L) of initial As(III) was examined; however, none of the sludge produced is supposed to be hazardous. This implies that the initial arsenic concentration is not the most important factor controlling if the sludge will be hazardous waste.

According to Figure 4.36, it is clearly seen that the curves expressing relationship between $FeCl_3$ / As ratios and arsenic removal efficiency for every initial arsenic concentration can be divide into three sections as shown in Figure 4.43. The first section is from removal efficiency of 0 to 60 %. The slope of this section is quite steep. The second section is from removal efficiency of 60 to 95 %. The slope of this section is flatter than the first section. The third section is from removal efficiency of 95 to 100 %. The slope of this section is flattest. This means that to increase removal efficiency from 0 to 60 % requires relatively low increase of coagulant per one

percentage of increasing removal efficiency while to increase removal efficiency from 60 to 95 % requires relatively higher increase of coagulant per one percentage of increasing removal efficiency. Thus, to increase removal efficiency from 95 to 100 % requires highest increase of coagulant per one percentage of increasing removal efficiency. The more the coagulant demand, the more the sludge produced, the less As to Fe ratio the sludge, the lower the amount of arsenic per a binding site, the better retention of arsenic the sludge, and the lower the leachate concentration of arsenic. Therefore, the most important factor controlling if the sludge will be hazardous waste is probably the final target of finished water. As shown in Table 4.10 that the removal efficiencies required to produce drinking water of which MCLs are 10 and 50 μg/L from contaminated water of which initial As(III) concentrations range from 150 to 12,000 μg/L are from 66.67 to 99.92 % -most of them are from 96.67 to 99.92. Consequently, to reach such high removal efficiencies, a great deal of coagulant was consumed. Thus, the sludge produced was so stable that it was non-hazardous waste as discussed above.

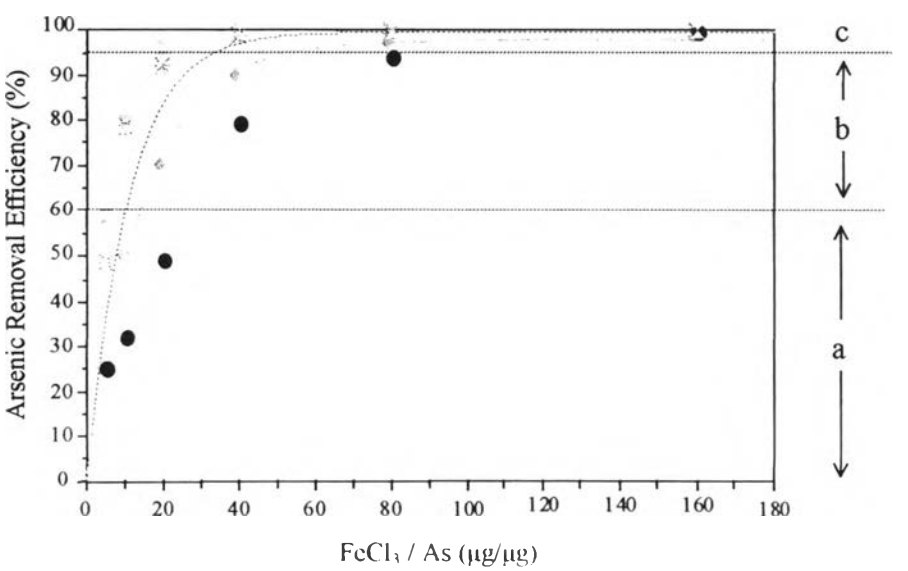

Figure 4.43 The curves between $FeCl_3$ / As ratios and arsenic removal efficiency focused on three different slopes

One of the best examples to clarify the influence of the final targets of finished water on degree of hazard of the sludge is variation of the sludge produced from the coagulation of waste brine from Ion Exchange. As mentioned in Chapter 2, concentration of arsenic in waste brine from Ion Exchange is around 10 mg/L which is generally much greater than TBLLs. Therefore, to discharge Ion Exchange residuals to a sanitary sewer, the pretreatment of such residuals by coagulation with ferric chloride may be an advisable alternative. However, TBLLs vary from location to location as shown in Table 2.15. According to that table, TBLLs range from 51 to 2,000 μg/L. For this reason, coagulant demands required to comply with TBLLs vary from place to place, and property of the sludge varies from place to place as well.

Table 4.14 Simulation of removal efficiency required to comply with different TBLLs from 50 to 3000 μg/L as well as As-to-Fe of the sludge produced from each TBLLs and estimated concentration of arsenic in leachate by the TCLP

Finished Water Target (TBLL) (μg/L)	Removal Efficiency Required (%)	As-to Fe Ratios of the sudge (mmole/mmole)	Estimated Concentration of Arsenic in Leachate by the TCLP (mmole/L)	
			Dewatered Sludge	Dried Sludge
50	99.5	0.0258	0.0008	0.0041
100	99	0.0261	0.0008	0.0042
500	95	0.0291	0.0009	0.0047
1000	90	0.0334	0.0011	0.006
1500	85	0.0387	0.0013	0.0068
2000	80	0.0453	0.0016	0.0083
3000	70	0.0639	0.0027	0.0138

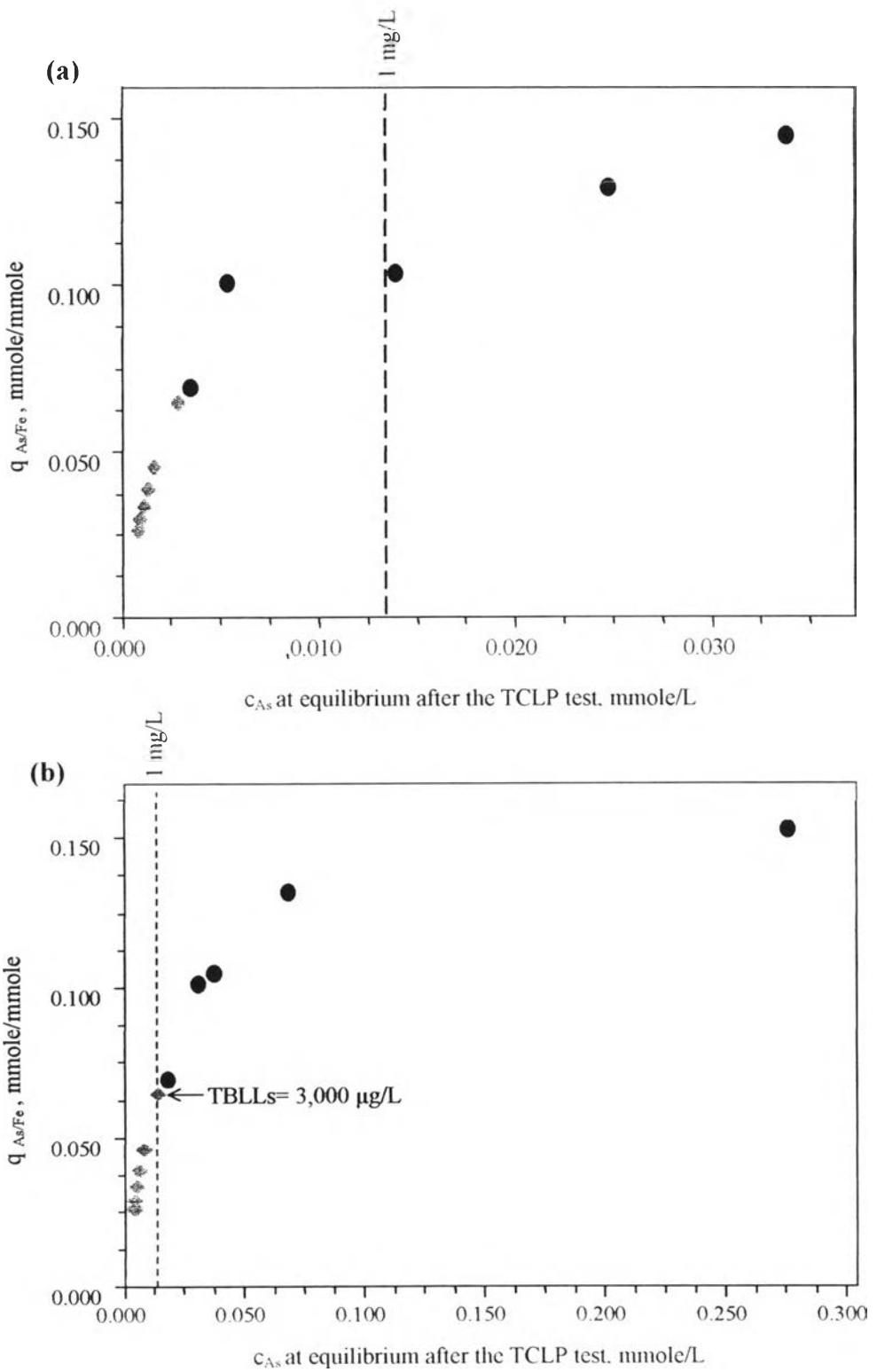

Figure 4.44 (a) Application of the empirical model in Figure 4.26 to estimate leachate concentration of arsenic from the dewatered sludge (approximately 21.9% solid) produced from treatment of Ion Exchange brine of which initial arsenic concentration is 10,000 µg/L by coagulation to different TBLLs from 50 to 3,000 µg/L (b) application of the empirical model in Figure 4.30 to estimate leachate concentration of arsenic from the dried sludge (100% solid) of the same samples. The leaching procedure used in this figure is the TCLP

Table 4.14 simulates the removal efficiencies required to comply with different TBLLs from 50 to 3000 μg/L as well As-to-Fe ratios of the sludge produced from each TBLL. Figures 4.44 (a) and (b) simulate leachate concentration of arsenic as a result of subjecting the sludge from each TBLLs to the TCLP. It is found that, for both the dewatered and dried sludge, the higher the TBLLs, the more the aesenic concentration in leachate of the sludge, and the more, the potential for the sludge to become hazardous waste. Moreover, it is found that the dried sludge produced from the TBLL of 3,000 μg/L can be classified as hazardous waste.

PART III

4.6 Physical Properties and Phase Analyses of the Solidified/Stabilized Arsenic-Iron Hydroxide Sludge

4.6.1 Compressive Strength of the Solidified/Stabilized Sludge

The results of unconfined compressive strength (UCS) tests of all the solidified/stabilized waste forms are shown in Table 4.15 In addition, Figure 4.45 illustrates the relationship between the waste-to-binder ratio and the UCS. It is clearly seen that, for the recipes both with and without the addition of lime, the more the sludge is added, the lower the compressive strength. In other words, the substitution of Portland cement with the sludge causes some negative effects to some of the mechanical properties of the solidified products.

Obviously, the addition of the sludge means cement replacement which means reducing amount of Portland cement undergoing hydration that is directly responsible for development of compressive strength. Therefore, it is unsurprising that the more cement is replaced, the more the strength reduction as shown in Figure 4.46. This explanation is also applicable to clarify why, at the same percentage of sludge addition, the solidified matrices with forty percent of lime have lower compressive strength than those without lime as shown Figure 4.45.

However, it is possible that the addition of sludge might present other physically and/or chemically negative effects to the strength property of the solidified products, so the strength reduction shown in Figure 4.46 might be the combination of cement replacement and unknown physically and/or chemically negative effects from the addition of the sludge. For further understanding, the physically negative effect was examined by SEM-EDS and will be discussed in Section 4.82 while the chemically negative effect was investigated by XRD and will be discussed in Section 4.83.

Table 4.15 UCS(ksc) of the recipes with and without lime

Notation	Average UCS (ksc)	Notation	Average UCS (ksc)
the recipes without lime		the recipes with lime	
CW4-S00-L00	461.06	CW9-S00-L04	95.06
SW4-S15-L00	428.81	SW9-S15-L04	73.02
SW4-S25-L00	371.82	SW9-S25-L04	54.67
SW4-S50-L00	269.77	SW9-S50-L04	43.77
SW4-S100-L00	144.84	SW9-S100-L04	28.81

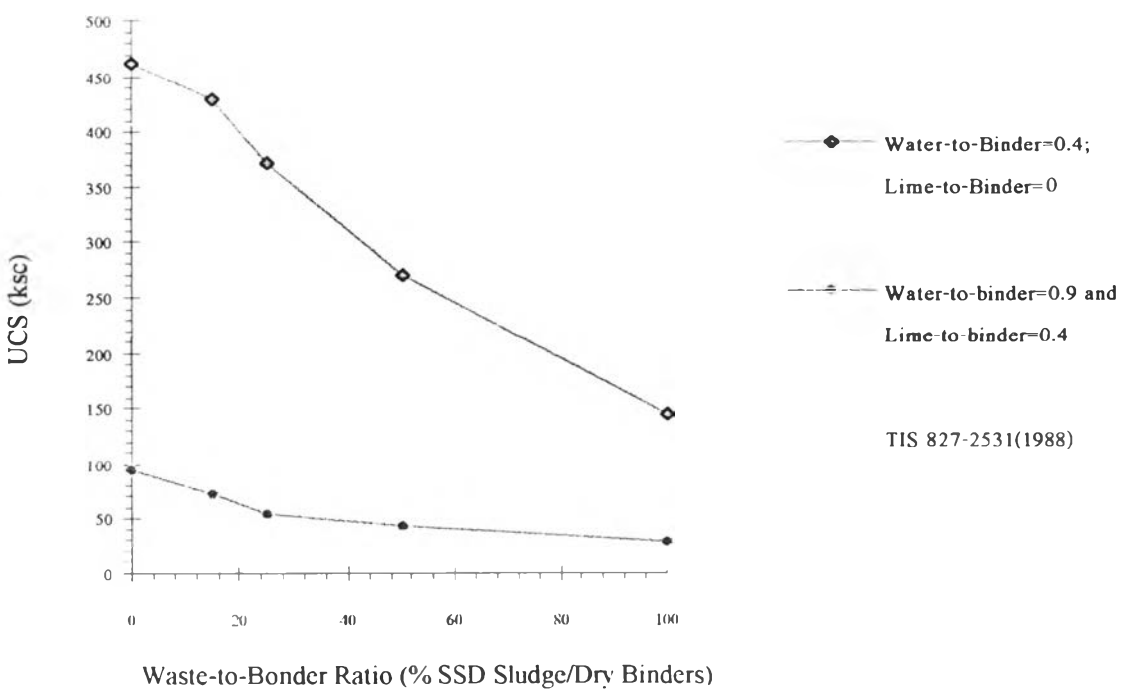

Figure 4.45 Relationship between waste-to-binder ratio and UCS

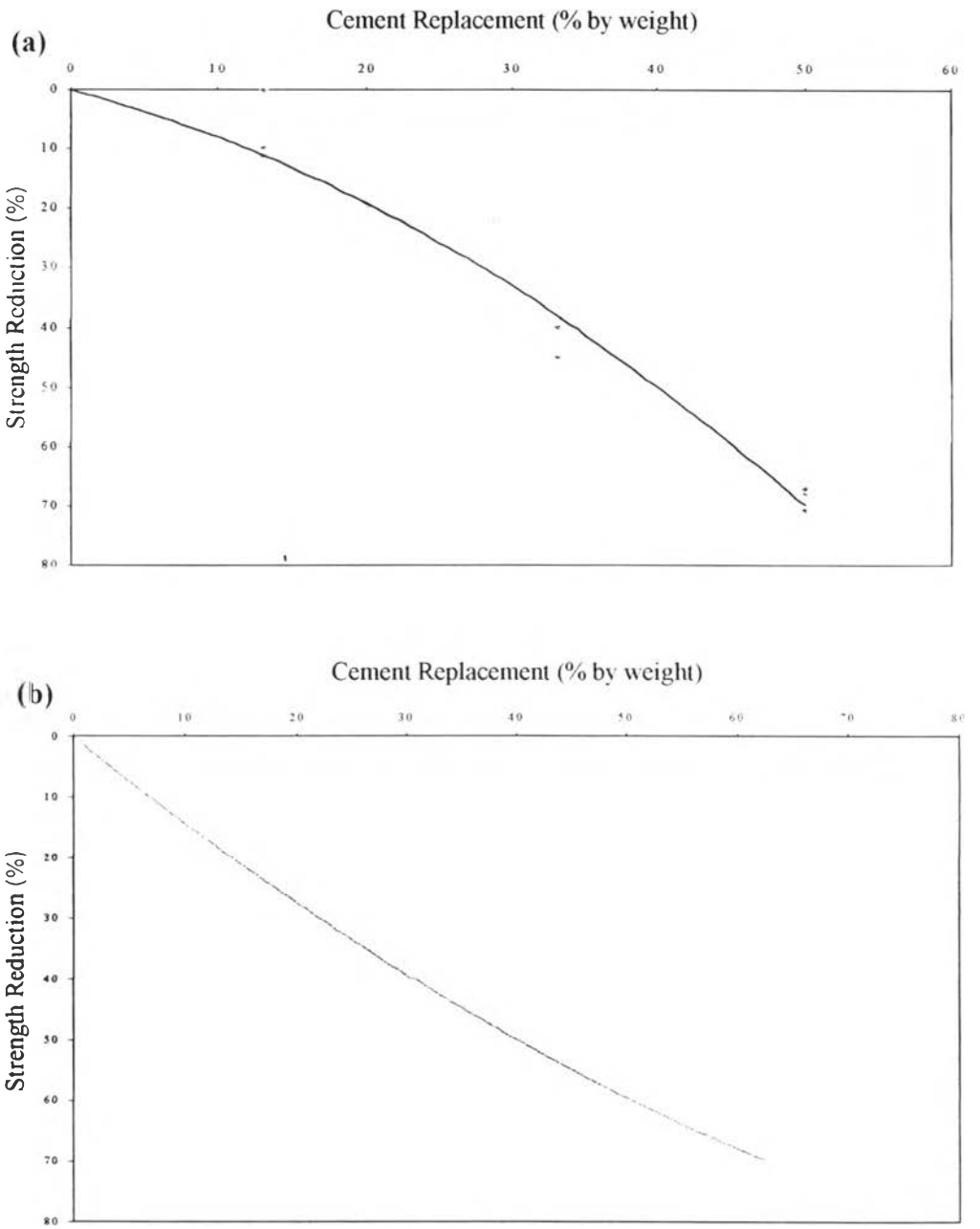

Figure 4.46 The relationship between strength reduction (%) and cement replacement (%) of (a) S/S at water-to binder ratio 0.4 and lime-to-binder ratio 0 and (b) of S/S at water-to binder ratio 0.9 and lime-to-binder ratio 0.4

4.6.2 SEM-EDS Application for Examining Macroencapsulation of the Solidified /Stabilized Sludge

As shown in Figure 4.1(a), the particle size of the dried sludge can be as large as 1 mm. Therefore, when mixed with Portland cement to produce the solidified products, the sludge was physically entrapped in the larger structural matrix. This mechanism is called macroencapsulation. Some of SEM photographs together with their x-ray dot maps illustrating macroencapsulation are shown in Figures 4.47, 4.48, and 4.49. The clusters of x-ray dots of Fe briefly illustrate location of the sludge in the cross section of the solidified sample.

The definition of USC is the ultimate force per baring area, so the maximum force, which each solidified product can stand, can be calculated by multiplying UCS by its baring area. Consequently, it is clearly seen that the larger the bearing area, the more the ultimate force which the product can stand. For this reason, macroencapsulation is supposed to be one of physical factors reducing the UCS of the mortars. Figure 4.50 simulating cross sectional areas of solidified products varying amount of sludge addition is to explain why addition and macroencapsulation of the sludge causes physically negative effect to UCS.

As shown in Figure 4.50, under the assumption that the addition of the sludge does not cause chemically negative effects to hydration process, the actual UCS of hydrated cement minerals at the same age should be the same regardless amount of sludge added. In this figure, the actual UCS of hydrated cement minerals at the age of 28 days is abbreviated to UA. Owning to the fact that the strength property of sludge is relatively low in comparison to that of hydrated products, the sludge is not supposed to maintain the strength of the matrix. Therefore, the area of sludge encapsulated in the matrix is considered as a void. For this reason, the actual bearing area of the matrix at one plane is the area of the whole matrix at that plane subtracted by the area of macroencapsulation in the same plane. Consequently, the actual, ultimate force that each matrix can stand can be calculated by multiplying the actual UCS of hydrated cement minerals with its actual bearing area. It is clearly seen that the more the sludge is added, the lower the actual bearing area, and the lower ultimate

force that the matrix can stand. However, in order to calculate measured UCS of the whole matrix, the ultimate force is divided by the measured bearing area which is area of the whole matrix (around 5 x 5 cm^2) without subtraction of the area of macroencapsulation in that plane. For this reason, the relationship between waste-to-binder ratios and UCS is expressed as the declining trend-line as shown in Figure 4.45 in spite of the fact that the strength values of hydrated cement minerals of the matrices varying in waste-to-binder ratio may not different from one another.

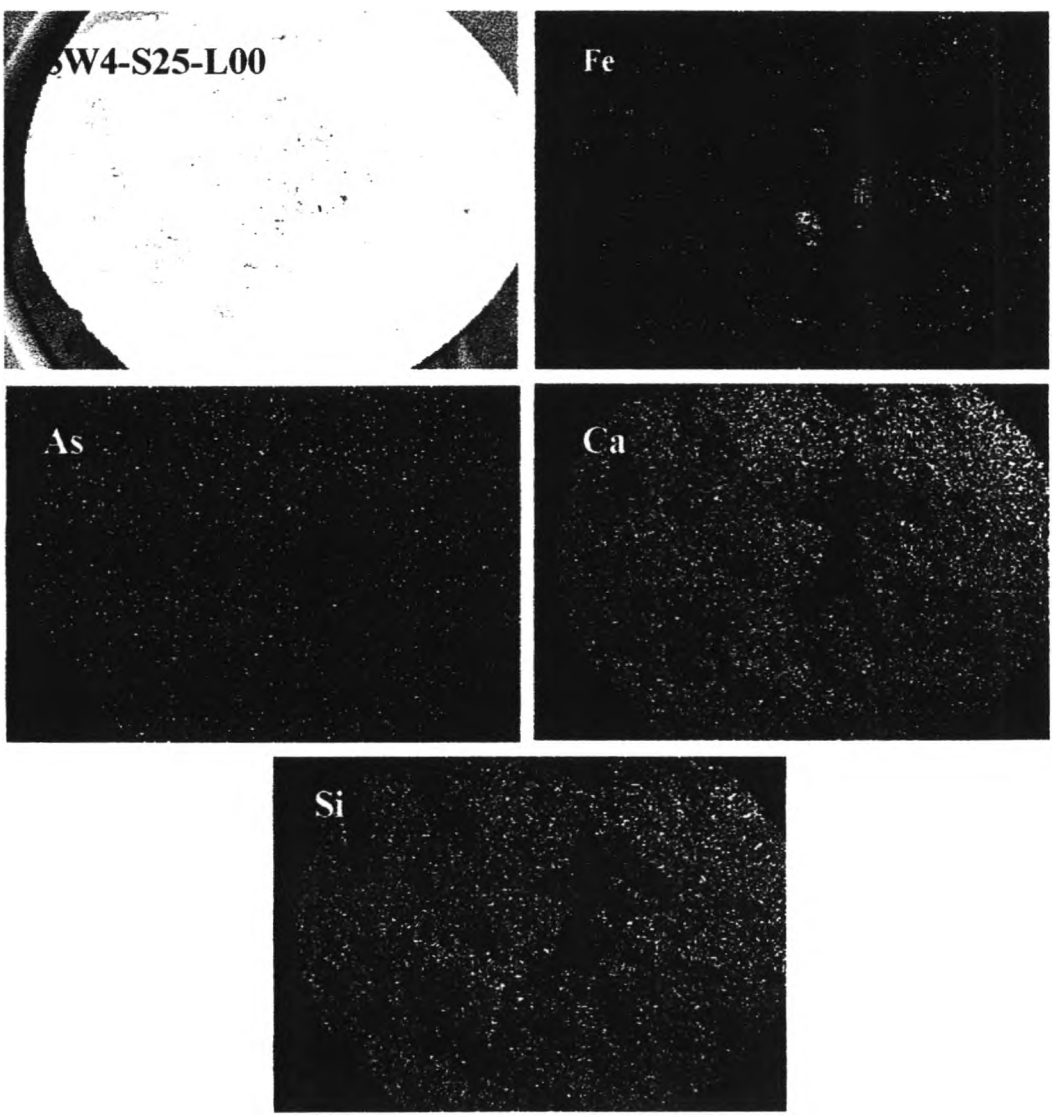

Figure 4.47 The x-ray dot maps of SW4-S25-L00 at the age of 28 days. The clusters of x-ray dots for Fe briefly illustrate location of the sludge in the cross section of the solidified sample

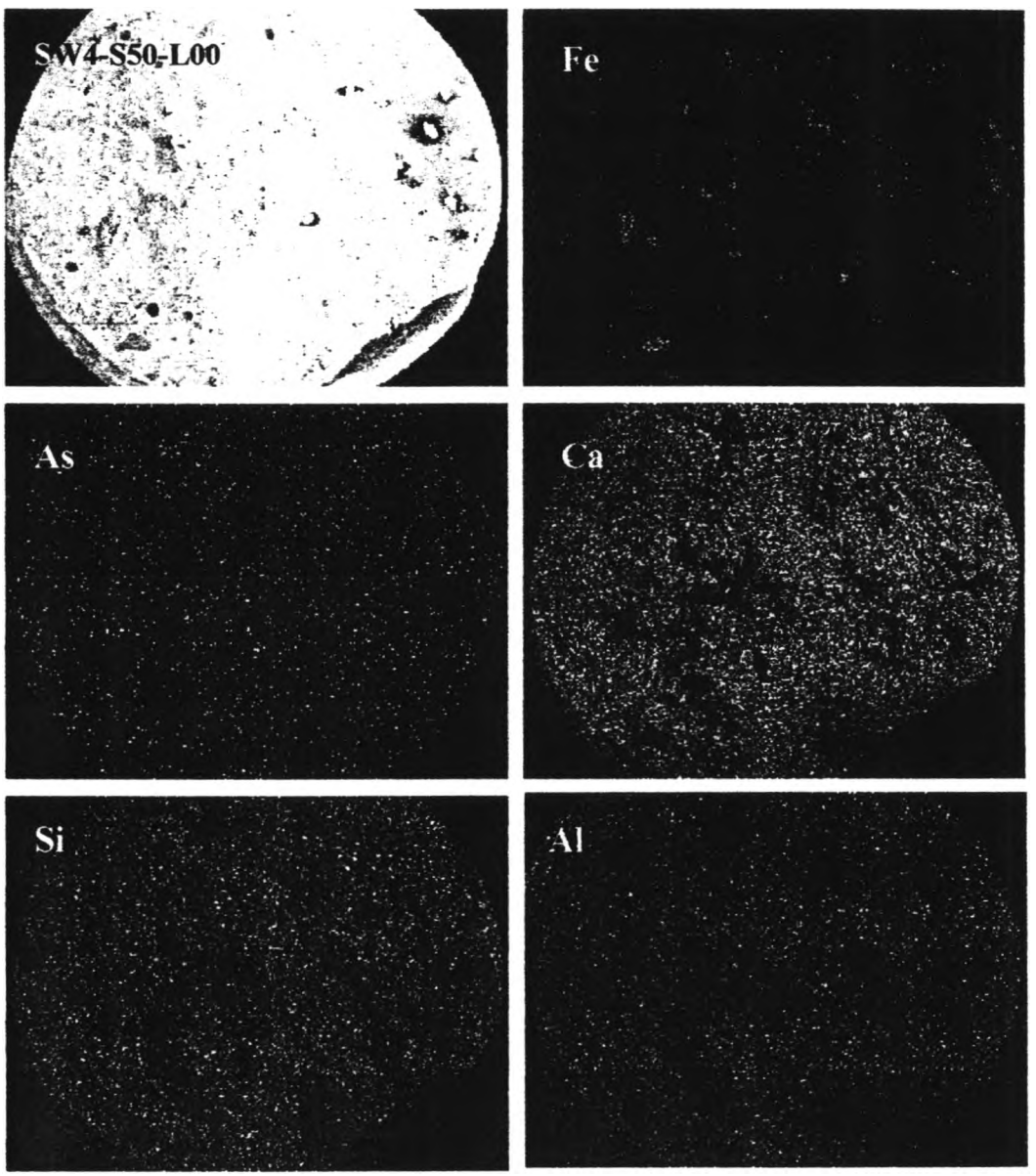

Figure 4.48 The x-ray dot maps of SW4-S50-L00 at the age of 28 days. The clusters of x-ray dots for Fe briefly illustrate location of the sludge in the cross section of the solidified sample.

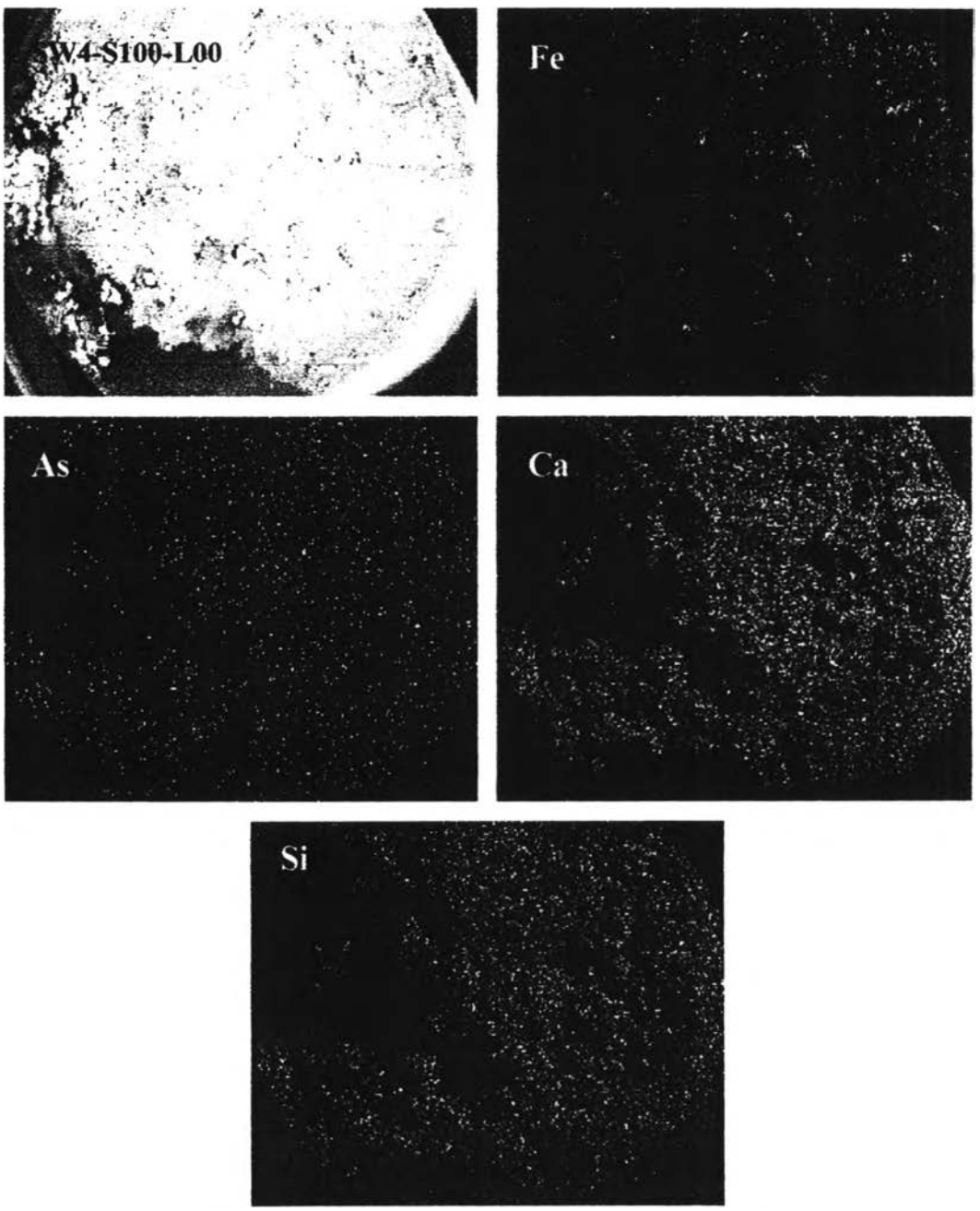

Figure 4.49 The x-ray dot maps of SW4-S100-L00 at the age of 28 days. The clusters of x-ray dots for Fe briefly illustrate location of the sludge in the cross section of the solidified sample.

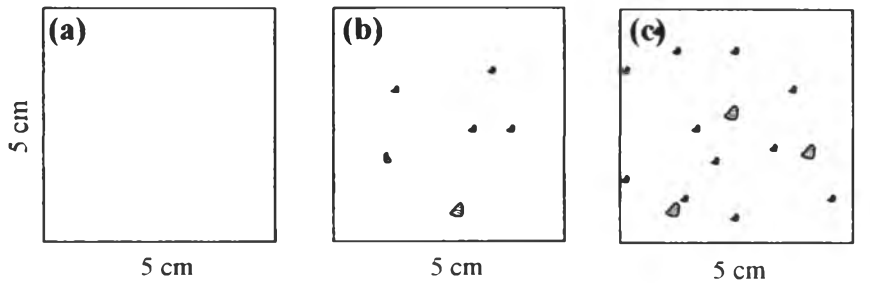

Amount of sludge addition

None | little | Much more

Actual USC of cement (ksc)

UA = UA = UA

Actual bearing Area (cm^2)

AR1 = 5x5 cm^2 > AR2 = (5x5 cm^2)- (area of sludge encapsulated in the matrix) > AR3 = (5x5 cm^2)- (area of sludge encapsulated in the matrix)

Actual ultimate force (kg)

UA x AR1 > UA x AR2 > UA x AR3

Measured bearing Area (cm^2)

AM1 = AM2 = AM3 = 5 x 5 cm^2

Measured USC of the solidified waste (ksc)

$$\frac{UA \times AR1}{AM1} > \frac{UA \times AR2}{AM2} > \frac{UA \times AR3}{AM3}$$

Figure 4.50 Schematic view and calculation explaining how addition and macroencapsulation of sludge physically decline USC of the mortars. The gray rectangles represent the whole cross sectional area of the matrices while the red dots represent the dried iron–arsenic sludge.

4.6.3 XRD Application for Phase Analysis of the Solidified /Stabilized Waste

The assumption used to explain Figure 4.50, which is that addition of the sludge does not cause chemically negative effects to hydration process, may be either right or wrong because of the fact that the arsenic containing sludge in the present study can be either an inert or an active substitute. An inert substitute is the substance of which addition results in only reducing amount of Portland cement undergoing

hydration that is directly responsible for development of compressive strength as discussed before. Therefore, the chemical reaction between such a substitute and Portland cement or its by-products is unlikely to occur. In contrast, if the substitute is classified as an active substitute, it means that the substitute can react with cement components or hydration by-products to form a new compound that may positively or negatively affect some properties of solidified products. This is very important because the substitution with some waste such as high silica-alumina fly ash is well known for increasing the long-term compressive strength while substitution with other waste, such as waste containing borate and phosphate, tends to respond in an opposite way.

In regards to the importance of this issue, the sets of XRD spectra shown in Figures 4.51, 4.52, and 4.53 are here to indirectly identify the type, among inert, positively active, and negatively active agents, as which the sludge is classified. The XRD patterns of CW4-S00-L00 and CW9-S00-L04 shown in Figure 4.51 are set as references, control samples without addition of the sludge while the XRD patterns of the solidified samples both without and with the addition of lime are shown in Figures 4.52 and 4.53, respectively.

By making a comparison between the spectra of both the references and the solidified samples with and without the addition of lime, it is found that they all have several things in common such as the set of peaks near 4.92, 3.12, 2.63, 1.92, and 1.80 Å (18.0, 28.6, 34.0, 47.2, and 50.6° 2θ) corresponding to $Ca(OH)_2$, Portlandite. In addition, the set of peaks near 3.03, 2.75, 2.61 (overlap with 2.63 Å of Portlandite), and 2.18 Å (29.4, 32.5, 34.4, and 41.4° 2θ) corresponding to Ca_3SiO_5, Alite, as well as that near 2.7494 (overlap with 2.7485 Å of Alite), 2.1897 (overlap with 2.1804 Å of Alite), and 1.9346 Å (overlap with 1.9223 Å of Portlandite) (32.5, 41.2, 46.9° 2θ) corresponding to Ca_2SiO_4, Belite, is present in all samples but varying in intensities. Considering the three detected phases mentioned above, the first is one of hydration by-productions while the last two compounds are two out of four major components of Portland cement.

However, it should be noticed that the additional strong peak, approximately, at 7.9 Å (11.2° 2θ) appears in almost all the S/S recipes but two references and SW4-S025-L00. This obvious difference between the spectra of the mixtures with and without the addition of the sludge can be taken as a good indicator that the waste is not inert in the cementitious environment. This peak suggests that some foreign compounds besides the common phases, which are reactants or products of hydration in pure cement or a mixture of cement and lime such as those found in CW4-S00-L00 and CW9-S00-L04, might be formed due to the addition of the sludge. The foreign compounds are supposed to be a result of the reaction between some of the sludge components such as As, Fe, O as well as H and some of the additives components such as Ca, Si, Al, Fe, and O.

The formation of several compounds is possible in the system with the presence of the chemical species mentioned in the previous paragraph. However, the compounds responsible for *d* spacing of 7.9 Å (11.2° 2θ) should be arsenic containing compounds such as calcium-arsenic, silicon-arsenic, or aluminum-arsenic compounds because three out of four major components of the sludge except arsenic are similar to those of cement and lime, and they are expected to form indifferent phases from those of cement and lime. According to the literature review, the set of compounds between Ca and As seems to receive the most attention. Based on the diffraction data from JCPDS-International Centre (1996), all calcium-arsenic compounds can be classified into 10 major groups: calcium arsenate compounds, calcium arsenate hydrate compounds, calcium arsenite, calcium hydrogen arsenate compounds, calcium hydrogen arsenate hydrate compounds, calcium arsenate hydroxide compounds, calcium arsenate hydroxide hydrate compounds, calcium hydroxide arsenate compounds, and calcium hydroxide arsenate hydrate compounds. Each major group is composed of several compounds different in XRD spectra, chemical property, and degree of hydrate. However, of all these calcium arsenic compounds, only four compounds from four major groups; namely, calcium arsenate hydroxide hydrate, calcium hydroxide arsenate hydrate, calcium hydrogen arsenate hydrate, and calcium arsenate hydrate express potential for being the compound(s) which results in *d* spacing around 7.9 Å. The diffraction patterns of them are illustrated in Figures 4.52 (d) and 4.53 (d). It is clearly seen that overlap of these diffraction patterns with some

d values of portlandite, alite, and belite makes the identification of calcium-arsenic phases more complex and uncertain.

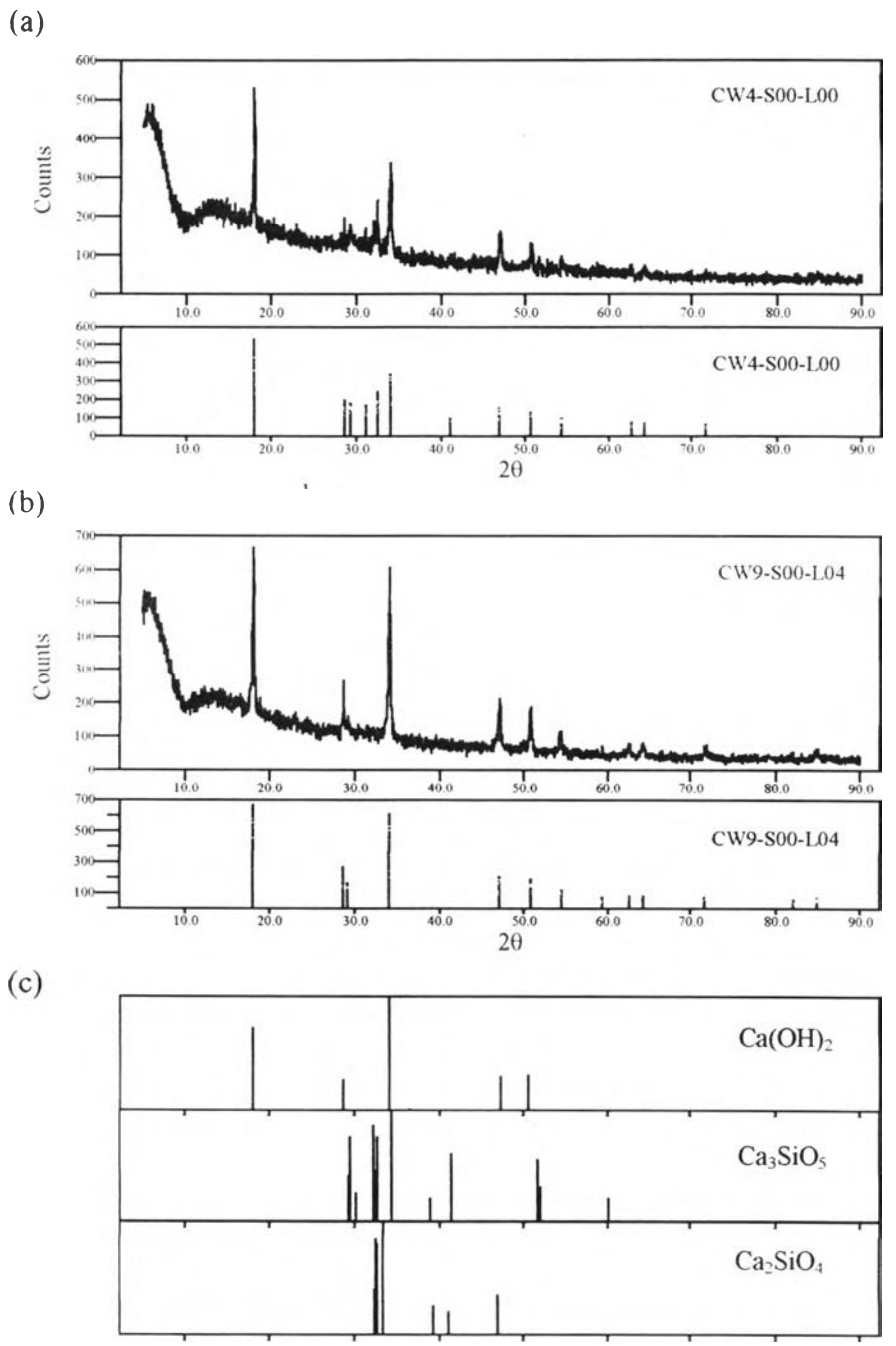

Figure 4.51 X-ray diffraction patterns for (a) CW4-S00-L00 and (b) CW9-S00-L04 as well as their possible phases illustrated in (c) according to 1996 JCPDS-International Center for Diffraction Data

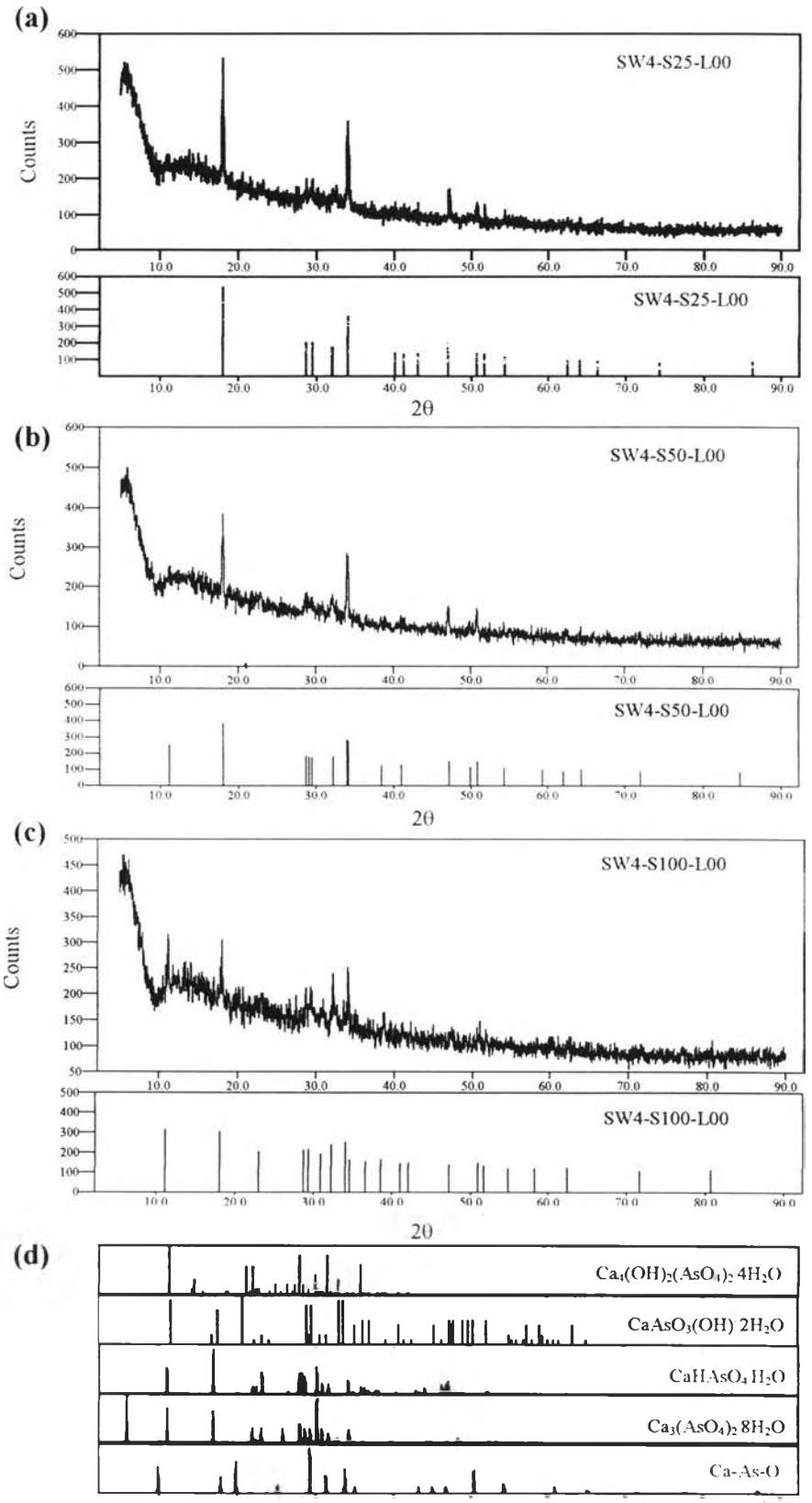

Figure 4.52 X-ray diffraction patterns for (a) SW4-S25-L00, (b) SW4-S50-L00, and (c) SW4-S100-L00 as well as their possible phases, besides $Ca(OH)_2$, Ca_3SiO_5, and Ca_2SiO_4, illustrated in (d) according to 1996 JCPDS-International Center for Diffraction Data

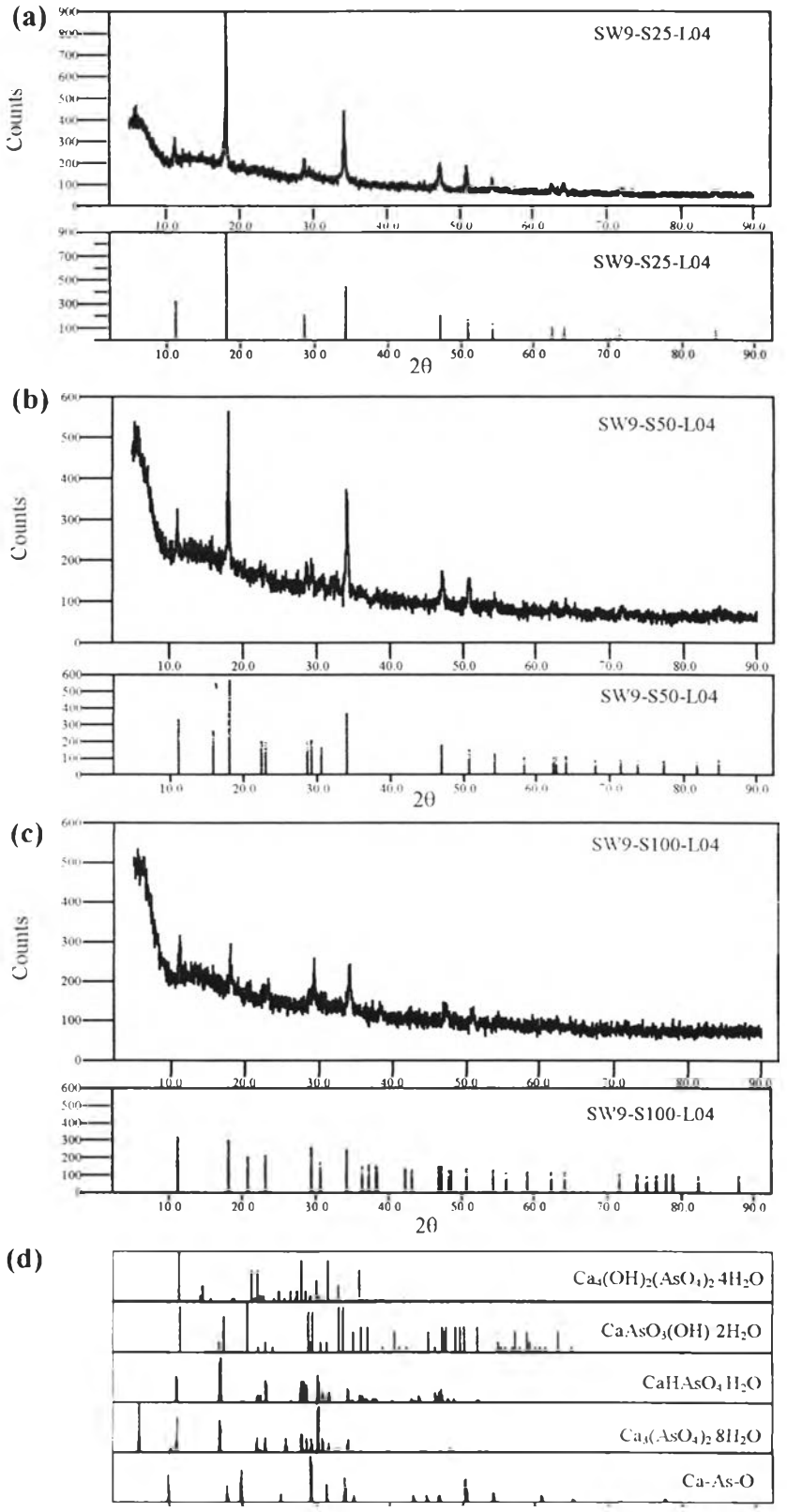

Figure 4.53 X-ray diffraction patterns for (a) SW9-S25-L04, (b) SW9-S50-L04, and (c) SW9-S100-L04 as well as their possible phases, besides $Ca(OH)_2$, Ca_3SiO_5, and Ca_2SiO_4, illustrated in (d) according to 1996 JCPDS-International Center for Diffraction Data

Nevertheless, it is certain about the fact that the peak at 7.9 Å (11.2° 2θ) is not a result of only one of the four compounds but the combination between, at least two of them. To clarify this, the diffraction pattern of SW4-S50-L00 is used as an example. First of all, considering the diffraction pattern of calcium arsenate hydroxide hydrate, $Ca_4(OH)_2(AsO_4)_2 4H_2O$, it is found that the peak at 7.90 Å (11.2° 2θ) of SW4-S50-L00 can be closely matched with the highest peak (I_{100}) at 7.82 Å of $Ca_4(OH)_2(AsO_4)_2 4H_2O$; however, in order to conclude that $Ca_4(OH)_2(AsO_4)_2 4H_2O$ is the only calcium-arsenic compound present in SW4-S50-L00, its second highest peak(I_{80}) at 2.83 Å, of which the calculated intensity is around 202.4 counts (80x253/100) which is higher than the background at this *d* spacing (around 139 counts), should obviously appear in SW4-S50-L00, but it does not. One of the possible explanations for this disagreement is that $Ca_4(OH)_2(AsO_4)_2 4H_2O$ is only partially responsible for the peak at 7.90 Å (11.2° 2θ). For example, as the background level at 2.83 Å where the second highest peak (I_{80}) of $Ca_4(OH)_2(AsO_4)_2 4H_2O$ is located is 139 counts, the possible intensity of the peak of $Ca_4(OH)_2(AsO_4)_2 4H_2O$ at 2.83 Å can rank from 0 to 139 counts to not exceed the background level. By this reason, the possible intensity of $Ca_4(OH)_2(AsO_4)_2 4H_2O$ at 7.90 Å (11.2° 2θ) should rank from 0 to 173.75, or from 0 to 68.68% of the actual intensity at this *d* spacing of SW4-S50-L00. This suggests that there must be at least one of the other three calcium-arsenic compounds present in SW4-S50-L00, so that the peak at 7.90 Å (11.2° 2θ) is overlapped to correspond to the actual intensity as shown in the spectrum of SW4-S50-L00.

Similarly, considering the diffraction patterns of calcium hydroxide arsenate hydrate ($CaAsO_3(OH) 2H_2O$), calcium hydrogen arsenate hydrate ($CaHAsO_4 H_2O$), and calcium arsenate hydrate ($Ca_3(AsO_4)_2 8H_2O$) it is found that the peak at 7.90 Å (11.2° 2θ) of SW4-S50-L00 can be closely matched with the second highest peak(I_{90}) at 7.70 Å of $CaAsO_3(OH) 2H_2O$, the third highest peak(I_{60}) at 8.06 Å of $CaHAsO_4 H_2O$, and the third highest peak(I_{60}) at 7.99 of $Ca_3(AsO_4)_2 8H_2O$. However, like the case of $Ca_4(OH)_2(AsO_4)_2 4H_2O$, it is still impossible to conclude that any of these three compounds is the only calcium-arsenic compound present in SW4-S50-L00 due to disagreement of diffraction pattern. By the same calculation concept used in the previous paragraph, the possible intensities of ($CaAsO_3(OH) 2H_2O$), ($CaHAsO_4 H_2O$), and ($Ca_3(AsO_4)_2 8H_2O$) at 7.90 Å (11.2° 2θ) can rank from 0 to

135.9 counts (0 to 53.71%), 0 to 126 counts(0 to 49.80%), and 0 to 93 counts (0 to 36.76%), respectively.

Like the case of SW4-S50-L00 discussed above, the possible way to fit the spectra of other S/S samples is based on the concept that at least two out of four of calcium-arsenic compounds were formed in the sample. The phrase " at least two out of four" expresses the possibility that it could be the set of two, three, or four. The sets of two have six possible cases such as combination of $Ca_4(OH)_2(AsO_4)_2 \cdot 4H_2O$ and $CaAsO_3(OH) \cdot 2H_2O$, $(Ca_4)_2(AsO_4)_2 \cdot 4H_2O$ and $CaHAsO_4 \cdot H_2O$, $CaAsO_3(OH) \cdot 2H_2O$ and $Ca_3(AsO_4)_2 \cdot 8H_2O$, and so on. The sets of three have three possible cases such as the combination of $Ca_4(OH)_2(AsO_4)_2 \cdot 4H_2O$, $CaAsO_3(OH) \cdot 2H_2O$, and $CaHAsO_4 \cdot H_2O$, and so on. Finally, the set of four has only one possible case which is the combination of $Ca_4(OH)_2(AsO_4)_2 \cdot 4H_2O$, $CaAsO_3(OH) \cdot 2H_2O$, $CaHAsO_4 \cdot H_2O$, and $Ca_3(AsO_4)_2 \cdot 8H_2O$.

Although there are 10 possible cases to fit the spectrum of each S/S recipe, there is only one best-fit case and it can be roughly solved and evaluated by submitting all 10 possible cases of each S/S recipes to this set of equations:

$$I_{Aj} = \Sigma I_{Ej} \qquad (4\text{-}4)$$

When

I_{Aj} is an actual (or as close as possible) intensity (counts) of a sample at j Å

I_{Ej} is an estimated intensity (counts) of all phases, both the phases of calcium-arsenic and common cement products such as $Ca(OH)_2$, Ca_3SiO_5, and Ca_2SiO_4 present at j Å.

For example, to find the best-fit for SW4-S50-L00, considering the set of two, the first case, the combination of $Ca_4(OH)_2(AsO_4)_2 \cdot 4H_2O$ and $CaAsO_3(OH) \cdot 2H_2O$, is subjected to the Equation 4-4 as shown below.

at 7.89 Å (11.2 2θ)

$$253 = I_{100\ of\ Ca4(OH)2(AsO4)2.4H2O} + 0.9 I_{100\ of\ CaAsO3(OH).2H2O}$$

at 4.91 Å

$$269 = 0.72\ I_{100\ of\ Ca(OH)2} + 0.7\ I_{100\ of\ CaAsO3(OH).2H2O}$$

at 3.10 Å

$$183 = 0.27\ I_{100\ of\ Ca(OH)2} + 0.2\ I_{100\ of\ Ca4(OH)2(AsO4)2.4H2O} + 0.8\ I_{100\ of\ CaAsO3(OH).2H2O}$$

By solving these equation simultaneously,

it is found that: $I_{100\ of\ Ca(OH)2}$ is equal to 287.88 counts.

$I_{100\ of\ Ca4(OH)2(AsO4)2.4H2O}$ is equal to 173.64 counts.

$I_{100\ of\ CaAsO3(OH).2H2O}$ is equal to 88.19 counts.

By making a comparison between Figure 4.54 (a) and (b), it is clearly seen that the intensities of both at the same values of *d* spacing, with an exception at 4.91 Å, are insignificantly different. However, the obvious difference between the intensity of the simulated spectrum (a) and that of the actual one (b) may be a result of there being many other phases such as some hydration products, which could not be identified but exist in the sample, and may overlay at this d spacing.

However, this may not be the best-fit simulation for SW4-S50-L00; it is only an example to demonstrate how to estimate the best-fit simulation for each S/S sample. To obtain the actual answer, it is necessary to calculate the best-fit simulation for each S/S recipe from the ten possible cases and select only one simulation that gives the minimum difference between the calculated intensity and the actual one. However, the determination of the best-fit simulation for each S/S is not done here because it requires plenty of time to do and is far beyond the scope of this study. Moreover, it contains many uncertainties and inaccuracies because of the presence of many other phases that could not be identified.

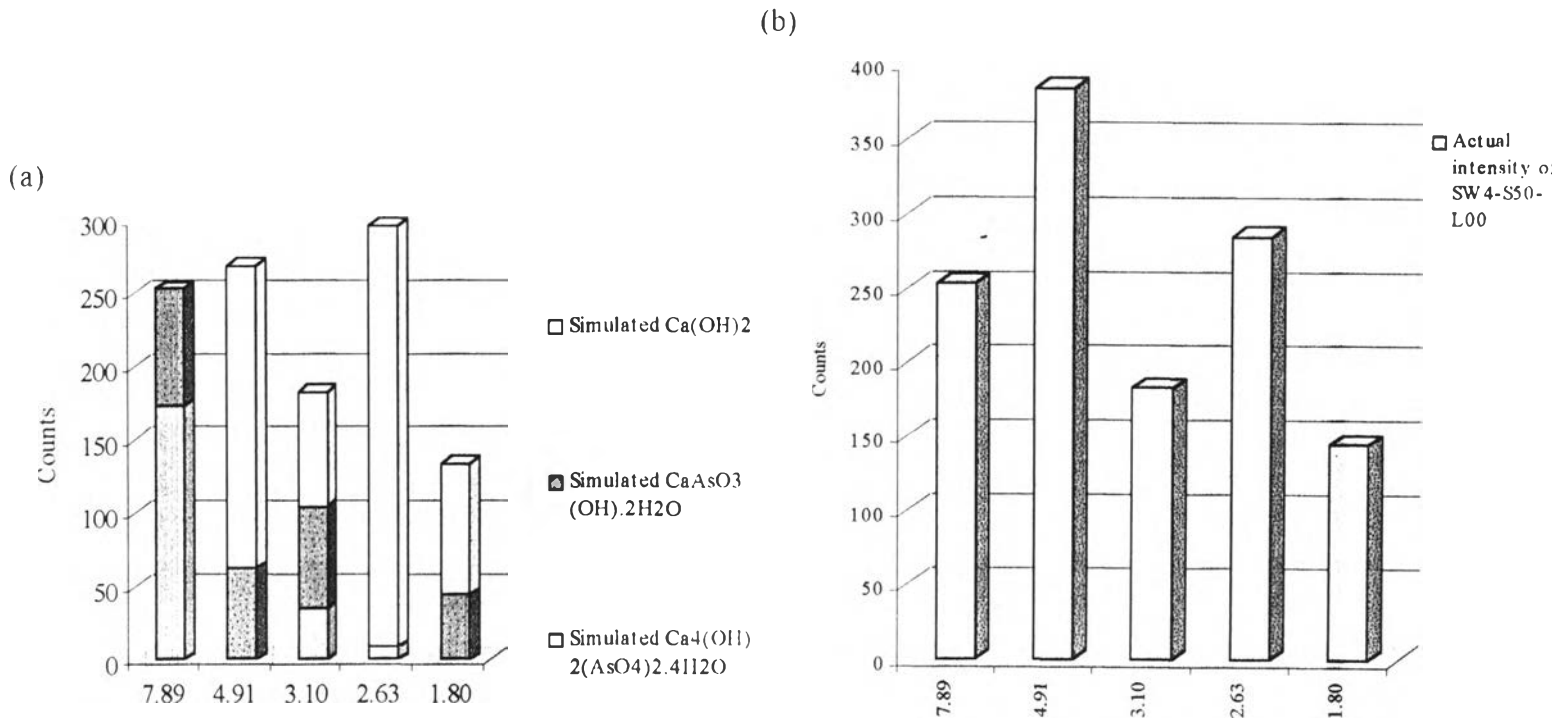

Figure 4.54 Histograms comparing (a) the intensities of the spectrum simulated by calculation with (b) the intensities of actual spectra of SW4-S50-L00 at the same selected *d* spacing .

Although the phases of calcium-arsenic compounds cannot be thoroughly characterized, it does not undermine the potential of the available data to investigate the effect of the sludge on the mechanical property of the solidified/stabilized matrix, namely unconfined compressive strength (UCS), due to two important aspects which all the four calcium-arsenic compounds have in common. Firstly, all the four are formed in the presence of calcium and arsenic. Secondly, it is possible that all may be slightly soluble or insoluble because several compounds in this group with the same elements and closely related structures were proved slightly soluble or insoluble by several recent researches. For example, pK_{sp} of $Ca_4(OH)_2(AsO_4)_2 \cdot 4H_2O$ is 28.1 and pK_{sp} of $CaHAsO_4 \cdot H_2O$ is 4.74, while pK_{sp} of $Ca_3(AsO_4)_2 \cdot 3^2/_3H_2O$ and $Ca_3(AsO_4)_2 \cdot 4^1/_4H_2O$ of which components remind $Ca_3(AsO_4)_2 \cdot 8H_2O$ are 21.02 and 21.15, respectively.

By these reasons, it makes sense to examine the effect of the group of calcium-arsenic compounds, instead of individual species, on the USC by means of semi-quantitative X-ray diffraction. Generally, it is accepted that the intensity of the diffraction spectrum at particular *d*-spacing is related to the amount of phases present at that *d*-spacing. As a result, the intensity of the diffraction at 7.90 Å (11.2° 2θ) is related the amount of the group of calcium-arsenic compounds present in the sample, or in other words the higher the intensity, the more the amount of calcium-arsenic compounds. In the same way, the intensity of the diffraction at 2.74 Å is related to the amount of remaining Ca_3SiO_5 and Ca_2SiO_4.

As the UCS of a solidified/stabilized waste form is directly under the influence of the hydration reaction, it is not possible to understand how the sludge effects the UCS without the understanding of the hydration reaction as well as hydration inhibition. Despite the fact that Portland cement is regarded as a common and cheap construction material, its reaction with water, known as the hydration reaction, is much more complex than its appearance. It is true that the mechanisms of the reaction are still under debate, but the overall course of hydration kinetics is generally accepted (Glasser, 1993:5.) as shown in Figure 4.55. As a raw material, unhydrated Portland cement is composed of 35-55% of Ca_3SiO_5 (C_3S), 15-35% of Ca_2SiO_4 (C_2S), 7-15% of $Ca_3Al_2O_6$ (C_3A), and 5-10% of Ca_2AlFeO_5 (C4AF) (Glasser, 1993:5). As

soon as it reacts with water, unhydrated clinker is subjected to both direct and indirect hydration reactions. By direct reaction, hydration occurs by the direct attack of water on the cement grains. On the other hand, there are several reactions involved in indirect hydration such as dissolution and precipitation, by colloid formation, ripening and coagulation with subsequent agglomeration, and deposition of newly formed solid (Glasser, 1993:8) depicted in Figure 4.56. However, of all these processes, dissolution and precipitation, known as through-solution, seems to have the greatest influence during the initial set and hardening. Repeatedly, under the cycle of dissolution and precipitation, both major and minor components of anhydrous solid cement such as calcium, silica, aluminum, iron, sulfate ion dissolve, become supersaturated in the aqueous phase, and finally reprecipitate, mainly as hydrate (Glasser, 1993: 4-9)

By dissolution and precipitation, the cement grains become coated with a thin layer of an almost amorphous gel-like material, which acts as diffusion membranes. At first, this membrane slows down the rate of hydration; however, due to its permeable property, the water outside the membrane flows inwards and some ions inside the cement particles such as Ca^{2+} and OH^- flow outwards (Glasser, 1993: 4-9)

These abundant sources of Ca^{2+} and OH^- results in an excess of $Ca(OH)_2$ and, finally, precipitation of portlandite on the fluid side of the membrane. In the meantime, an excess of silicate ions on the gain side of the membrane produces an osmotic pressure which periodically ruptures the membrane and allows a secondary growth of C-S-H as the acceleration stage of hydration.

As shown in Figure 4.55, in approximately 28 days, roughly two thirds of the cement will have hydrated, and in 1 year 95 to 98% of cement will have hydrated. The two major products of hydration are tobermorite gel (C-S-H gel) and $Ca(OH)_2$; most modern cements yield about 20 to 25% $Ca(OH)_2$ and 60 to 70 % C-S-H with approximately 5-15% of other minor phases. The idealized equations that express the formation of these two phases are as follows:

$$2(Ca_3SiO_5) + 6H_2O \longrightarrow 3CaO\,2SiO_2\,3H_2O(C\text{-}S\text{-}H) + 3Ca(OH)_2$$

$$2(Ca_2SiO_4) + 4H_2O \longrightarrow 3CaO\,2SiO_2\,3H_2O(C\text{-}S\text{-}H) + Ca(OH)_2$$

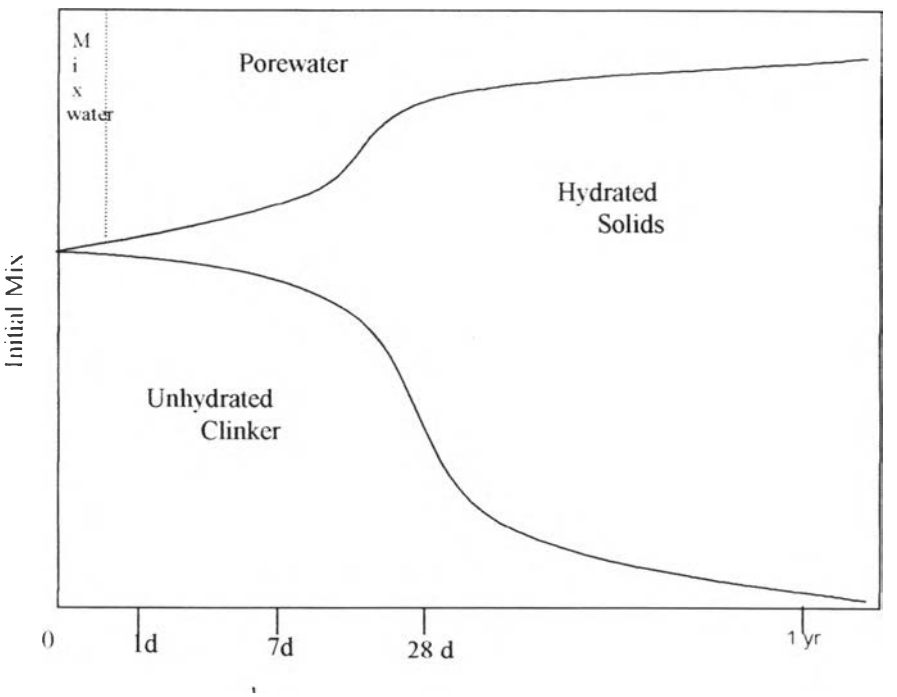

Figure 4.55 Schematic showing the overall course of cement hydration (Glasser, 1993)

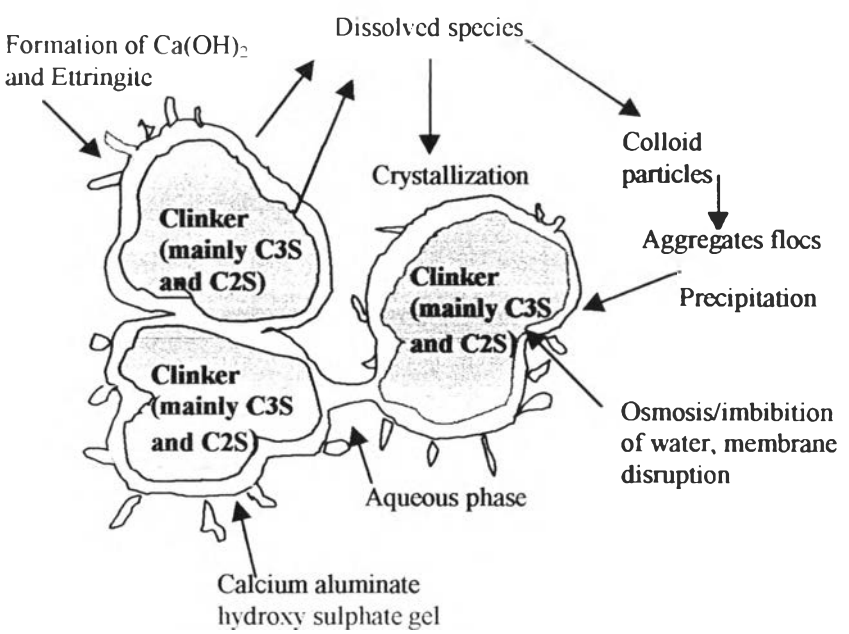

Figure 4.56 Schematic view of hydration process occurring during the first few hours or days (Glasser, 1993)

The stoichiometry of these two equations can be taken as a clear sign of the relationship between Ca_3SiO_5 together with Ca_2SiO_4 and C-S-H. Moreover, it is generally accepted that the UCS of a cementitious material including solidified/stabilized wastes is the function of C-S-H because C-S-H tends to fill pores, enhance bonding, and finally increase the UCS (Glasser, 1993). As a result, the inverse relationship between the UCS and amount of Ca_3SiO_5 as well as Ca_2SiO_4 present in any sample after an interval of curing time in which hydration has started is suggested.

It is now clearly seen that the presence of the sludge affects the USC of the matrix, as shown in Figure 4.45. However, that figure does not reveal the clear evidence of if the reduction of the UCS is only a result of the substitution with inert sludge, which reduces the amount of Ca_3SiO_5 and Ca_2SiO_4 undergoing hydration to produce C-S-H and increase strength property or the reduction is also under influence of other negative chemical reactions. Moreover, even though x-ray diffraction patterns of the S/S samples suggests possibility of the formation of calcium-arsenic compounds, they do not help in determination of if the compounds cause negative effect to the hydration reaction. Consequently, perhaps using the inverse relationship between the amount of Ca_3SiO_5 together with Ca_2SiO_4 left after the particular time of the hydration and the hydration progress is the best method available. This can be done by plotting intensities of Ca_3SiO_5 and Ca_2SiO_4 at 2.74 Å (32.5° 2θ) for both the references and the S/S samples at the age of 28 days, and the hydration progress can be inferred.

First, considering the set of the S/S recipes without lime, its plotting is illustrated in Figure 4.57. As the intensities shown in this figure are not significantly different from each other, this may mislead the reviewers to conclude that the sludge is inert and there is no negative chemical reaction between cement and sludge components. However, it should be noted that the amount of cement initially added into each S/S recipes is different from one another as shown in Table 3.2 As a result, in order to make a more reasonable comparison among the intensities at 2.74 Å of S/S samples, they should be divided by normalized factors which are calculated by dividing the amount of cement(g) added into each S/S sample (SW4-S25-L00, SW4-

S50-L00, and SW4-S100-L00) by the amount of cement added into a reference sample (CW4-S00-L00) as shown Table 4.16. The plotting of normalized intensities are also shown in Figure 4.58.

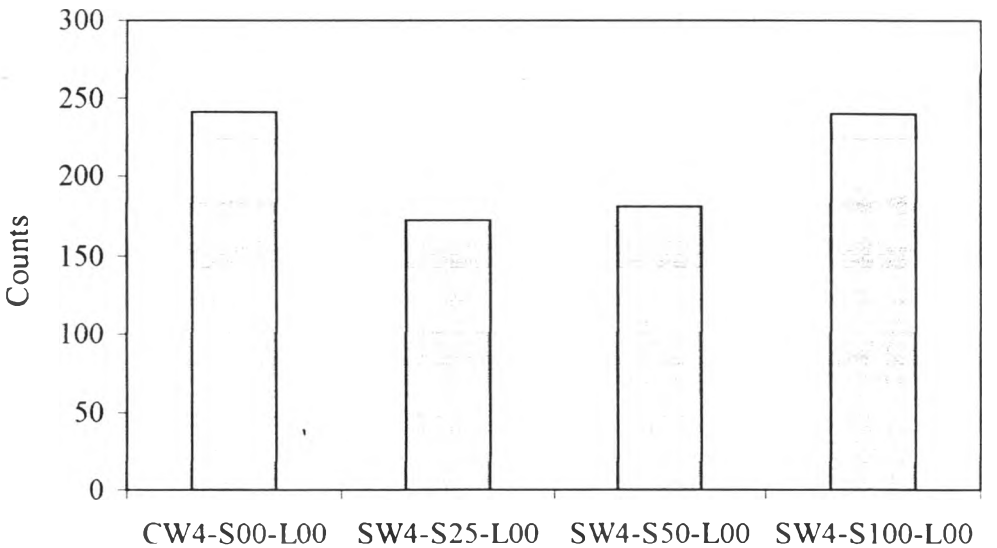

Figure 4.57 Histograms illustrating observed intensities at 2.74 Å (32.5 2θ) for both the control and S/S recipes without lime

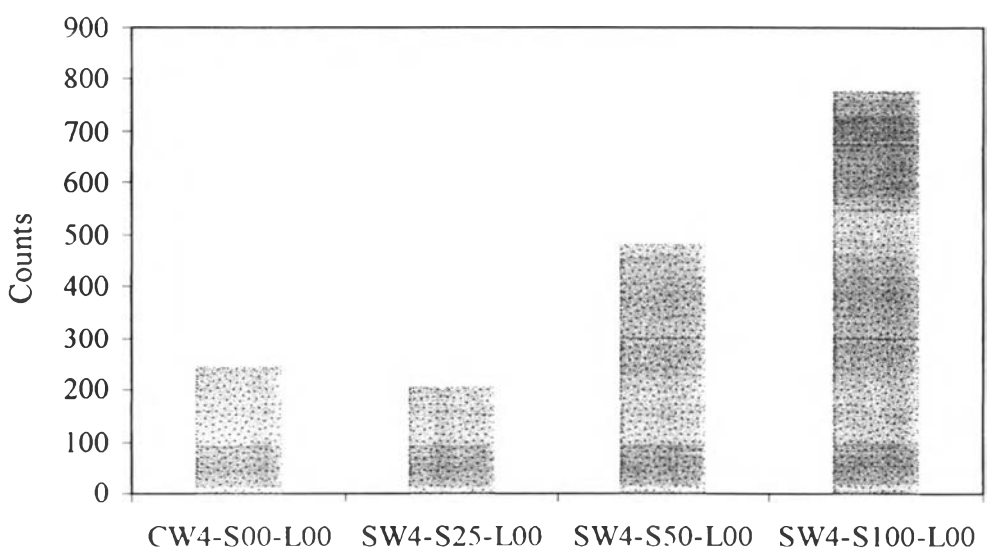

Figure 4.58 Histograms illustrating normalized intensities at 2.74 Å (32.5 2θ) for both the control and S/S recipes without lime

Table 4.16 Normalized factor, observed intensities, and normalized intensities for all samples without lime at 2.74 Å(32.5° 2θ).

S/S recipe	*d* spacing (Å)	*Cement(g) 15 g of sample*	Normalized Factor	Observed Ints. (Counts)	Normalized Ints. (Counts)
CW4-S00-L00	2.748	10.75	1.000	241	241.000
SW4-S25-L00	2.781	9	0.837	172	205.444
SW4-S50-L00	2.774	4	0.372	180	483.750
SW4-S100-L00	2.781	3.33	0.310	240	774.775

In regard to the inverse relationship between the amount of Ca_3SiO_5 together with Ca_2SiO_4 left after the particular time of hydration and hydration progress, if the substitute is inert, the rate of hydration must be the same regardless of the amount of substitute added. In other words, no matter how much sludge is added, the normalized intensities of Ca_3SiO_5 and Ca_2SiO_4 in the S/S samples should be insignificantly different from that of the control sample. By this reason, the intensities at 2.75 Å of S/S samples would have been insignificantly different from those of the control sample, if the sludge were inert.

Oppositely, the results shown in Figure 4.58 imply the potential that the sludge is not inert and possible to causes hydration inhibition. It is clear seen that the more the sludge added, the higher the normalized intensities at 2.75 Å are, or the lower the hydration development is. However, it should be noticed that the intensities at 2.75 Å of CW4-S00-L00 and SW4-S25-L00 are insignificantly different from one another in comparison to that of SW4-S50-L00 or SW4-S100-L00. This may be explained by examining the presence and absence of calcium-arsenic compounds in the S/S samples. As shown in Figure 4.52, no peak at 7.90 Å appears in SW4-S25-L00 which suggests that either no calcium-arsenic compound was formed in the sample or that too little amount of these compounds was formed because of the fact that the intensity was lower than the background. While in the same figure, the peaks at 7.90 Å appears

ต้นฉบับ หน้าขาดหาย

hydration development. In conclusion, the reduction of the UCS in these two recipes as shown in Figure 4.46(a) is supposed to be a result of the reduction of the amount of cement undergoing hydration by substitution with the sludge coupled with the reduction of bearing area due to macroencapsulation of the sludge and the negative chemical mechanisms from the group of calcium-arsenic compounds.

In order to gain insight into the mechanism of how calcium-arsenic compounds contribute to hydration interference, it is worth reviewing mechanisms of cement hydration inhibition. There are four possible models for any chemical to inhibit cement hydration: calcium complexation, nucleation poisoning, suface adsorption, and protective coating/osmotic bursting (Bishop, Bott, and Barron, 2003) Firstly, as mentioned before, in the pure system of Ca_3SiO_5 and Ca_2SiO_4, the lime concentration in the solutions is the crucial factor in determining the precipitation of C-S-H, if any chemical that can cause complexation with calcium is present in the mixture during hydration, the hydration inhabitation by calcium complexation takes place and brings about an adverse effect upon the UCS of that mixture. Calcium complexation involves either removing calcium from solution by forming insoluble compounds or chelating calcium in the solution to prevent C-S-H formation (Bishop et al., 2003). The second way for a chemical to inhibit cement hydration is by nucleation poisoning. In this model, the chemical blocks the growth of C-S-H or Ca $(OH)_2$ crystals through inhibiting agglomerates of calcium ions from forming the necessary nucleites (Bishop et al., 2003). In a related manner to nucleation poisoning, in cement inhibition by suface adsorption, the third model, the chemical or compound can directly sorb onto the surface of both the anhydrous and (more likely) the partially hydrated cement surfaces and, therefore, blocks further hydration (Bishop et al., 2003). The final possible mechanism is that the retarder may form a semipermeble layer at the surface of the cement grain and slow down the migration. This inhibition mechanism is called protective coating/osmotic bursting. It lengthens the introduction period of hydration but does not stop hydration because osmosis will drive water through the semipermeble membrane toward the unhydrated mineral, and eventually the flow of water creates higher pressure inside the protective coating and the layer bursts. Consequently, hydration is allowed to continue at a normal rate (Bishop et al., 2003)

According to the chemical and physical characteristics of calcium-arsenic compounds, it is possible that these compounds may be able to have a hand in three out of four cement inhibition mechanisms: calcium complexation, surface adsorption, and protective coating/osmotic bursting. As discussed before, all of the four calcium-arsenic compounds have one thing in common, which is that all are formed in the presence of calcium and arsenic. As shown in Figure 4.28 in Part I, when the sludge is added into the aqueous solution of the cementitious environment of which pH is above 12, some of arsenite and almost all of arsenate at the surface of the dried sludge are supposed to be desorbed out of the iron hydroxide sludge and react with Ca^{2+} or $Ca(OH)_2$ available in the solution to form calcium-arsenic compounds as shown in Figure 4.59. It should be noticed that the fact that in such basic condition was arsenate supposed to desorb more than arsenite is in good agreement with the results from XRD in that all four calcium-arsenic compound possibly present in the matrix is calcium-arsenate compound. Based on the chemical formula of the compounds, it is revealed that one mole of arsenic consumes a mole of calcium in order to form $CaAsO_3(OH)2H_2O$ as well as $CaHAsO_4H_2O$, while one mole of arsenic consumes two moles and one and a half moles of calcium to form $Ca_4(OH)_2(AsO_4)_2 4H_2O$ and $Ca_3(AsO_4)_2 8H_2O$, respectively. In addition, because of the fact that these compounds are insoluble compounds ($Ca_4(OH)_2(AsO_4)_2 4H_2O$ of which pK_{sp} is 28.1 and $CaHAsO_4H_2O$ of which pK_{sp} is 4.74) or expected to be insoluble compounds($Ca_3(AsO_4)_2 8H_2O$ and $CaAsO_3(OH)2H_2O$), their formation acts as cement hydration inhibition based on calcium complexation model by means of removing calcium from solution by forming insoluble compounds.

These arsenic compounds can interfere with the hydration reaction not only by their chemical reaction but also by their physical characteristics. Witness the fact that the morphology of some calcium-arsenic compounds recorded by SEM coupled with EDS and shown in Figures 4.60 and 4.61 expresses the potential to act as being cement hydration inhibitor by either surface adsorption or protective coating/osmotic bursting. The morphology shown in Figure 4.16 is in a good agreement with some of those recorded by Bother and Brown (1999a), who investigated the morphologies of $Ca_4(OH)_2(AsO_4)_2 4H_2O$, $Ca_3(AsO_4)_2 3^2/_3H_2O$, $Ca_3(AsO_4)_2 4^1/_4H_2O$, and

$Ca_5(AsO_4)_3OH$ by SEM micrographs, in that the morphologies of several of calcium-arsenic compounds except for $Ca_5(AsO_4)_3OH$ were plate or leafy crystals with the high potential to disturb the hydration progress. As depicted in Figure 4.59, in the aqueous solution of the cementitious system where hydration was in progress, when Ca^{2+} or $Ca(OH)_2$ from dissolution of Ca_3SiO_5 and Ca_2SiO_4 or from hydration by-product reacted with arsenic desorbed out of the sludge, the results were insoluble calcium-arsenic compounds, which might precipitate onto the surface of unhydrated or partially hydrated cement grain. Figures 4.62 and 4.63 depict the morphologies of hydrated and unhydrated cement clinkers, respectively. Several hydration by-products are also shown in Figure 4.62; however, it should be noticed that they disappear in Figure 4.60. The possible explanation is that the precipitated calcium-arsenic compounds might wrap all unhydrated or partially hydrated microstructures. According to EDS in Figure 4.61, it is found that this calcium arsenic layer is composed of 1.80% Al, 2.83% Si, 16.26% Fe, 20.52% As, 26.31% Ca, and 30.6% O by atomic. It should be noticed that the ratio among Al, Si, and Ca from EDS suggests that it is impossible for layer to be only C-S-H or one of the other hydrated structures. In addition, the ratio between Fe and As of this EDS also proves that it is impossible for this layer to be only iron hydroxide containing arsenic because its Fe to As ratio is very different from that of the sludge depicted in Figure 4.64. The model simulating the possible arrangement of the calcium-arsenic compounds, hydrated or unhydrated cement gain, and the iron sludge is depicted in Figure 4.59. Because of the fact that the penetration limit of EDS is around 10 μm, and some components of C-S-H or other hydrated structures such as Al and Si were detected in this penetration limit, the thickness of the calcium-arsenic layer might be less than 10 μm.

It is known that a secondary growth of C-S-H in the acceleration stage of hydration will occur when the excess of silicate ions on the gain side of the membrane produces an osmotic pressure that periodically ruptures the membrane. This excessive of silicate ions will exist if the water outside the membrane flows inwards and some ions inside the cement particles such as Ca^{2+} and OH^- flow outwards. However, under the condition of the calcium-arsenic layer, the cement hydration inhibition in the mode of surface adsorption may take place. The water outside the layer may not be able to flow inwards and Ca^{2+} and OH^- may not be able to flow outwards by the

insoluble property of the layer, then the hydration of these warped cement gains is stopped. On the other hand, the layer may just slow down the rate of the inward flow and outward flow which just lengthen the period of producing an osmotic pressure that ruptures the membrane. Thus, the cement hydration inhibition is shifted from surface adsorption mode to protective coating/osmotic bursting mode.

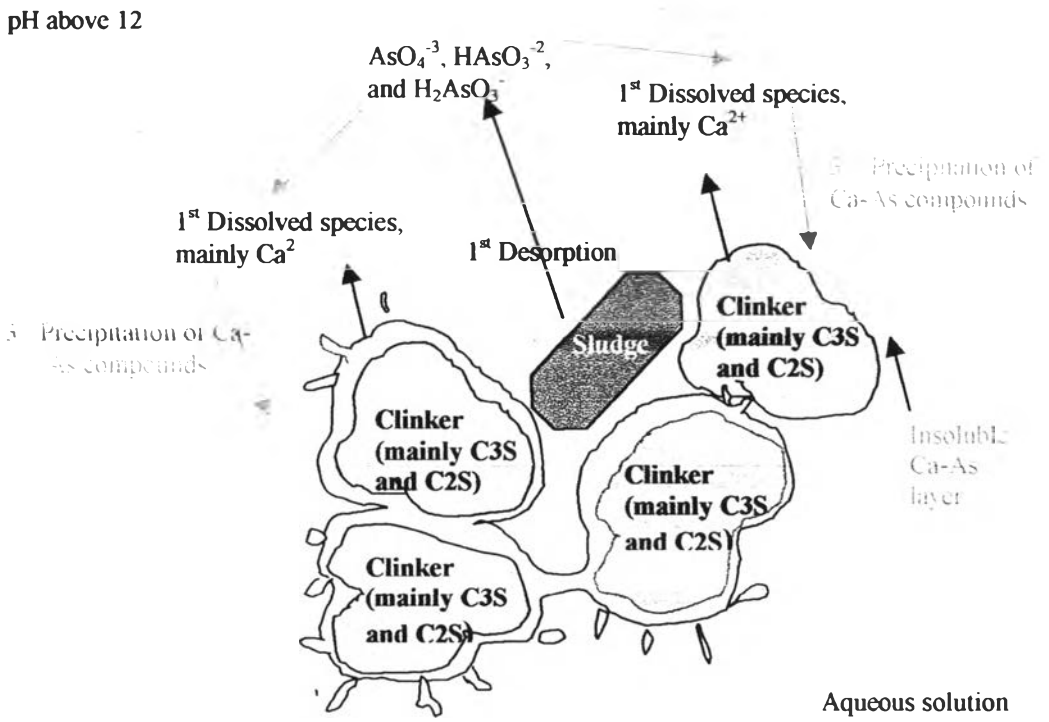

Figure 4.59 Three steps of the formation of the insoluble calcium-arsenic layer in a cement environment

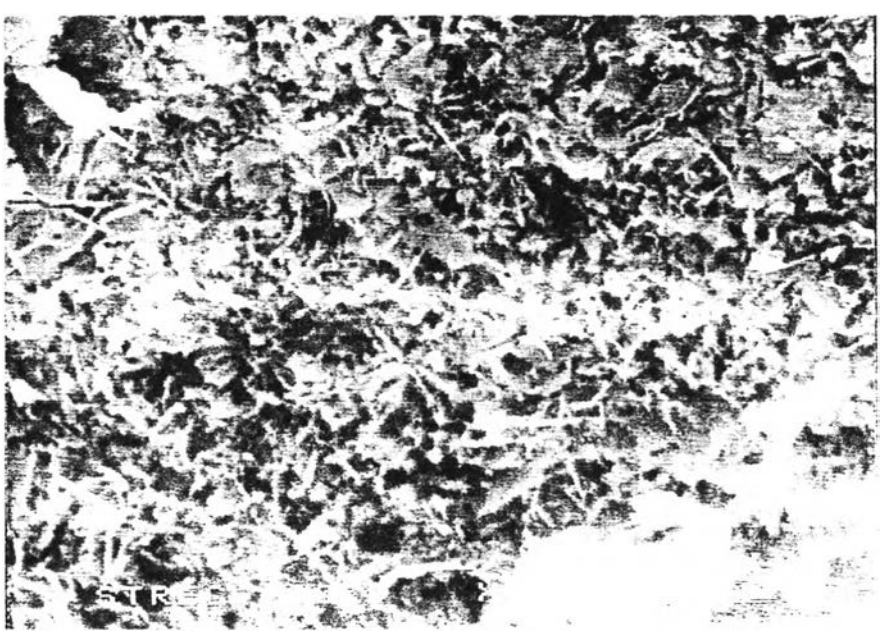

Figure 4.60 SEM micrograph depicting the leafy crystals of insoluble calcium arsenic compound which may act as the insoluble layer covering hydrated and unhydrated cement gains

Figure 4.61 EDS spectra of the calcium-arsenic compound shown in Figure 4.16

(a)

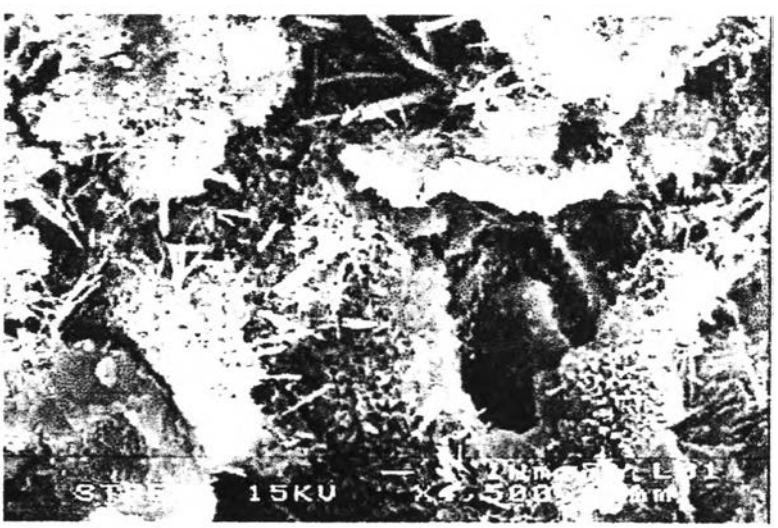

(b)

Figure 4.62 (a) SEM micrograph of hydrated cement without the addition of the sludge, (b) Its EDS spectra showing the presence of C-S-H as well as other possible hydrated phases

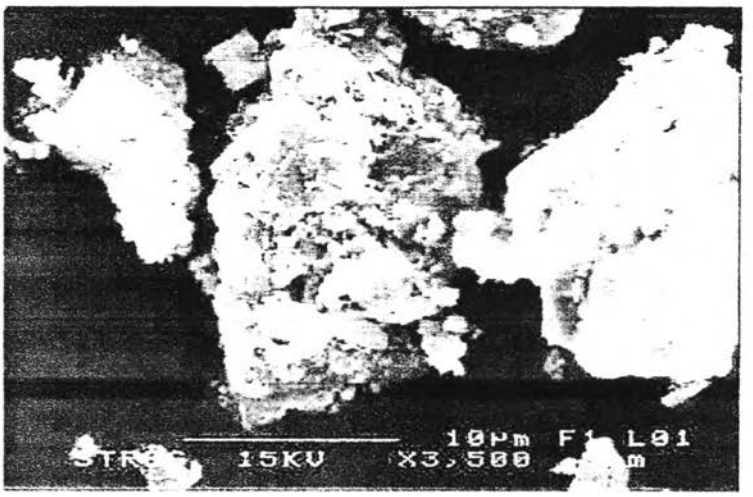

Figure 4.63 SEM micrograph of unhydrated portland cement

(a)

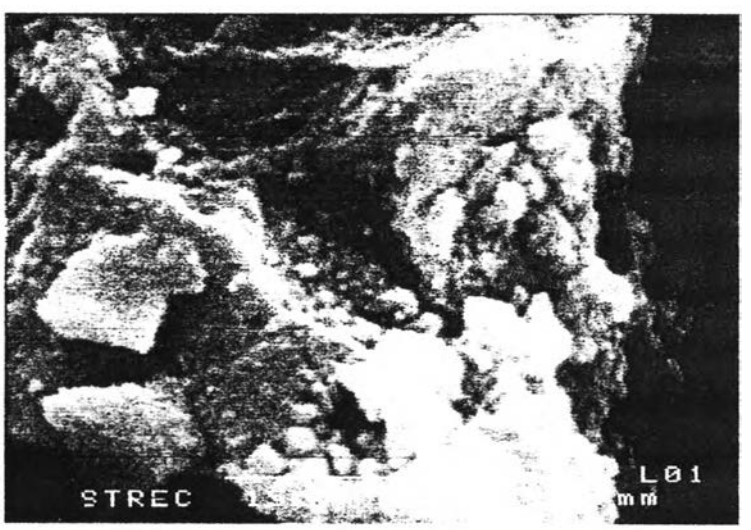

(b)

Figure 4.64 (a) SEM micrograph of iron hydroxide sorbing arsenic, (b) its EDS specta illustrating its components, which are 26.44% Na, 13.67% Cl, 44.79% Fe, and 15.11% As by atomic

Another evidence to confirm the hydration inhibition by calcium-arsenic compounds is the inverse relationship between the normalized intensities at 2.74 A represent Ca_3SiO_5 and Ca_2SiO_4 and the intensities at 7.90 Å represent calcium-arsenic compounds of SW4-S50-L00 and SW4-S100-L00. The normalized intensities at 2.74 Å and the intensities at 7.90 Å of SW4-S50-L00 are 484 and 253 counts, respectively. While The normalized intensities at 2.74 Å and the intensities at 7.90 Å of SW4-S100-L00 are 775 and 315 counts, respectively. This observation suggests that the more the amount of calcium-arsenic compounds formed in the matrices, the more the hydration inhibition.

In contrast to the XRD spectra of the S/S recipes without lime, the XRD spectra of the S/S recipes with lime cannot be used to indirectly examine the hydration inhibition by means of plotting the inverse relationship between the amount of Ca_3SiO_5 together with Ca_2SiO_4 left after the particular time of the hydration and the hydration progress as discussed above due to the fact that the intensities at 2.74 A of all S/S samples are lower than background as shown in Figure 4.53. Owning to the fact that, in these recipes was 40 percent of Portland cement replaced by lime, the amount of Ca_3SiO_5 and Ca_2SiO_4 left after 28 days of the hydration might be too small to be detected by XRD. However, the presence of the intensities at 7.90 Å for all samples implies the existence of the group of calcium-arsenic compounds in the matrices. Therefore, the hydration inhibition in surface adsorption and protective coating/osmotic bursting mode is possible. On the other hand, on the ground that 40 percent of Portland cement in these recipes was replaced by lime, Ca^{2+} is supposed to be sufficient for formation of both C-S-H and calcium-arsenic compounds. As a result, the hydration inhibition in calcium complexation mode is not supposed to occur. In conclusion, the reduction of the USC of the S/S samples with lime is likely to be a result of the reduction of the amount of cement undergoing hydration by substitution with the sludge coupled with the reduction of bearing area due to macroencapsulation of the sludge and the hydration inhibition in the mode of surface adsorption and protective coating/osmotic bursting.

Last but not least, according to Figure 4.52, it is found that the intensities at 7.90 Å of SW4-S25-L00 is lower than 260 counts while those of SW4-S50-L00 and SW4-S100-L00 are 253 and 315 counts, respectively. In contrast to Figure 4.53, it is found that the intensities at 7.90 Å of SW9-S25-L40, SW9-S50-L40 and SW9-S100-L40 are 319, 326, and 316 counts, respectively. This observation suggests that both the amounts of sludge and calcium added play crucial role on formation of calcium-arsenic compounds in different environments. For example, in the calcium-limited environment such as in the matrix of the S/S recipes without addition of lime, increasing the amount of sludge added is the major factor controlling the formation of calcium-arsenic compounds. Owning to the fact that the source of Ca^{2-} in such environment was only dissolution of cement minerals and hydration by-products, the competition for Ca^{2-} between the formation of C-S-H and that of calcium-arsenic compounds was possible to take place. Therefore, the more the amount of the sludge added, the higher intensities at 7.90 Å, and the more the amount of calcium-arsenic compounds formed.

On the other hand, in the calcium-excessive environment such as in the matrix of the S/S recipes with addition of lime, increasing the amount of sludge added almost play no role on the formation of calcium-arsenic compounds. Owning to the fact that the source of Ca^{2-} in such environment was both dissolution of cement minerals and hydration by-products as well as lime added, the competition for Ca^{2-} between the formation of C-S-H and that of calcium-arsenic compounds was unlikely to take place. Therefore, all of arsenic desorbing from the sludge was supposed to form calcium-arsenic compounds to reach its saturated state. As discussed above that the intensities at 7.90 Å of all the S/S sample with lime are around 320 counts, the largest amount of calcium-arsenic compounds (grams) formed per two grams of the S/S samples subjected to XRD is the amount which gives the intensity of around 320 counts. Unfortunately, the calibration curve was not done in the study; therefore, it is not possible to figure out that amount here.

4.6.4 FT-IR Application for Examination of Hydration Inhibition

Although the XRD results discussed in the previous topic suggest the possibility of the hydration inhibition in the presence of calcium-arsenic compounds, FT-IR results of the same samples are discussed here to examine the same issue by considering the polymerization of the orthosilicates in cement.

The FT-IR spectrum of unhydrate cement is illustrated in Figure 4.65. The adsorption bands at 443, 516, 921 cm^{-1} which are in good agreement with those (460, 525, and 925 cm^{-1}) reported by Cocke and Mollah (1992) are due to in-plane Si-O bending, out-of-plane Si-O bending, and asymmetric Si-O stretching of alite, respectively. Moreover, the band at 1141 cm^{-1} which is in good agreement with that (1145 cm^{-1}) reported by Cocke and Mollah (1992) are due to S-O stretching vibration of SO_4^{-2}.

Figure 4.66 illustrates FT-IR spectra of the control sample and the S/S recipes without lime throughout the whole length from 400 to 4000 cm^{-1}. While Figure 4.67 focuses on the same spectra at the wavenumber from 800 to 1100 cm^{-1}. According to Figure 4.67 (a), the band at 875 cm^{-1} which is in good agreement with that (875 cm^{-1}) reported by Cocke and Mollah (1998) is due to vibration of CO_3^{-2} from carbonate. In addition, the band at 972 cm^{-1} in this Figure is due to the formation of C-S-H. This band, 972 cm^{-1}, is supposed to shift from the band at 921 cm^{-1} due to the polymerization of the orthosilicates in cement by hydration. Therefore, the shifting of Si-O asymmetric stretching band of CW4-S00-L00, the control sample without lime, due to hydration at the age of 28 days is 51 cm^{-1}. In contrast, the Si-O asymmetric stretching bands of SW4-S25-L00, SW4-S50-L00, and SW4-S100-L00 are shifted to 964, 968, and 966 cm^{-1}, respectively. Therefore, the shifting due to hydration in the presence of the sludge are 43, 47, and 45 cm^{-1}, respectively. Thus, the smaller shifting of Si-O asymmetric stretching bands of the S/S recipes without lime in comparison to that of the control sample indicates that the hydration of cement is retarded in the presence of the arsenic-iron hydroxide sludge. The retardation of the S/S samples corresponds to the additional band at 856 cm^{-1} which is in good agreement with that

(860 cm^{-1}) reported by Jing et al. (2003). This band represents As(V)-O-Ca bonds (Jing et al.,2003); therefore, it can be a good evidence to confirm the existence of calcium-arsenic compounds.

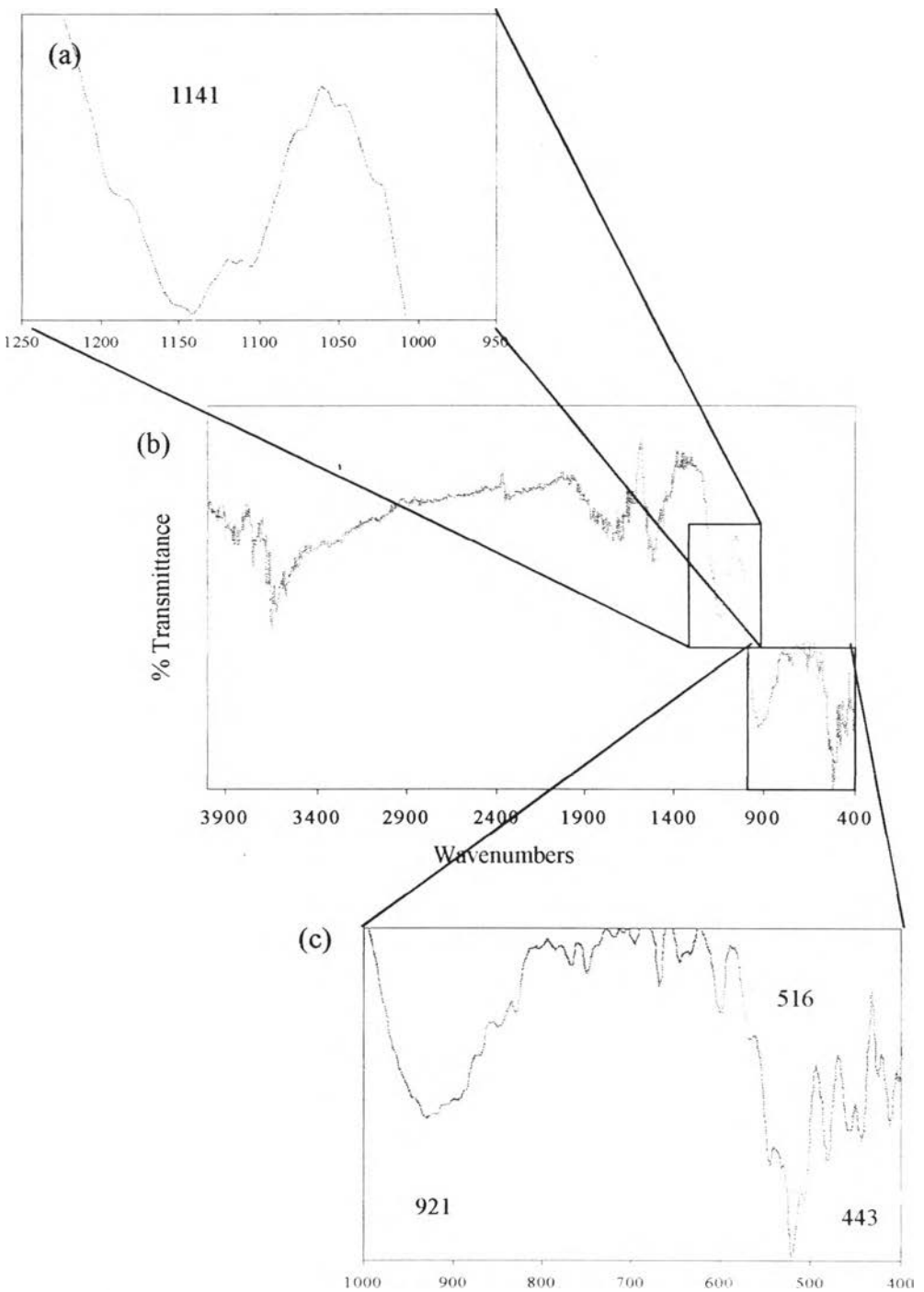

FIGURE 4.65 The FT-IR spectrum of unhydrated portland cement (a) focusing on the wavenumber from 950 to 1250 cm^{-1}, (b) throughout the whole length from 400 to 4000 cm^{-1}, and (c) focusing on the wavenumber from 400 to 1000 cm^{-1}

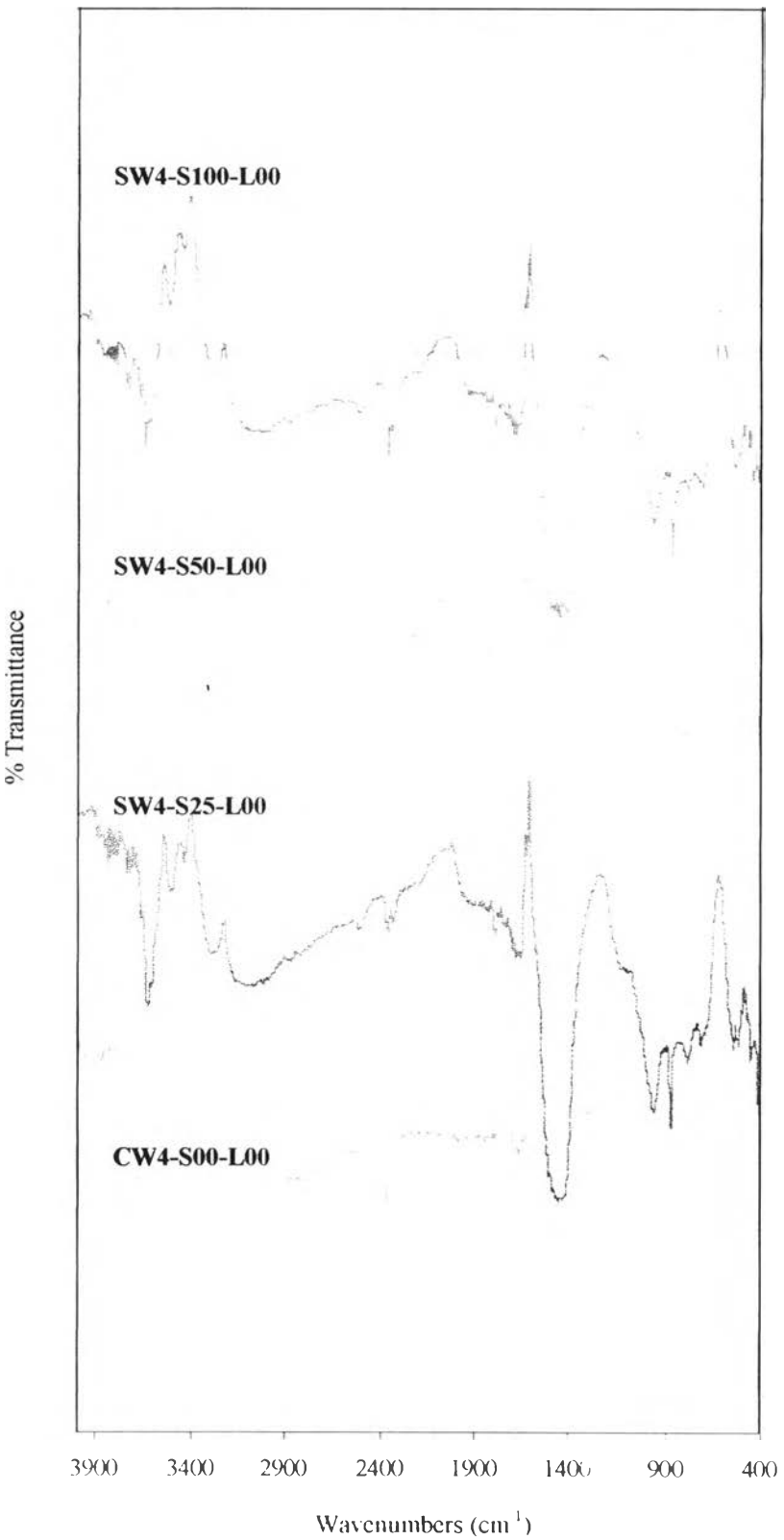

FIGURE 4.66 The FT-IR spectrum of the control and S/S recipes without lime throughout the whole length from 400 to 4000 cm^{-1}

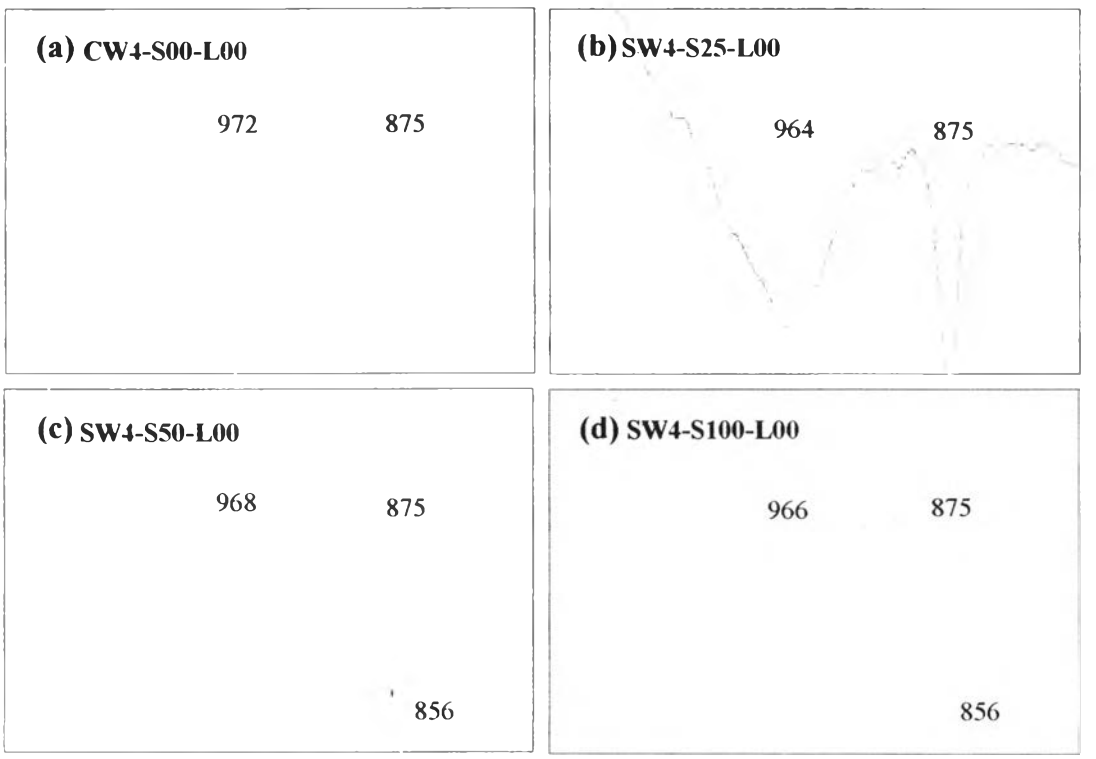

FIGURE 4.67 The FT-IR spectrum of the control and S/S recipes without lime focusing on the wavenumber From 800 to 1100 cm^{-1}

In the same way, Figure 4.68 illustrates FT-IR spectra of the control sample and the S/S recipes with lime throughout the whole length from 400 to 4000 cm^{-1}. While

Figure 4.69 focuses on the same spectra at the wavenumber from 800 to 1100 cm^{-1}. According to Figure 4.69, the band at 875 cm^{-1} due to vibration of CO_3^{-2} from carbonate is present in all the samples. In addition, the band at 968 cm^{-1} in Figure 4.69 (a) is due to the formation of C-S-H. Therefore, the shifting of Si-O asymmetric stretching band of CW4-S00-L04, the control sample with lime, due to hydration at the age of 28 days is 47 cm^{-1}. While the Si-O asymmetric stretching bands of SW9-S25-L04, SW9-S50-L04, and SW9-S100-L04 are shifted to 956, 968, and 968 cm^{-1}, respectively. Therefore, the shifting due to hydration in the presence of the sludge are 35, 47, and 47 cm^{-1}, respectively. Unlike that of the S/S samples without lime discussed in the previous paragraph, only the band of SW9-S25-L04 indicates the possibility of retardation by calcium-arsenic compounds. This contrasts with the conclusion drawn from XRD. However, the results from XRD are more reliable than

FT-IR because of the fact that the amount of sample required for XRD analysis is around 2 g while that for FT-IR is only 5 mg. Therefore, the samples used for FT-IR might not be the good representative of the whole matrix of the solidified wastes. In the same way, that the additional band at 856 cm^{-1} representing As-O-Ca bonds is obvious for of SW9-S25-L04 while it is not clear for SW9-S50-L04 and SW9-S100-L04 is supposed to be due to poor sampling as well.

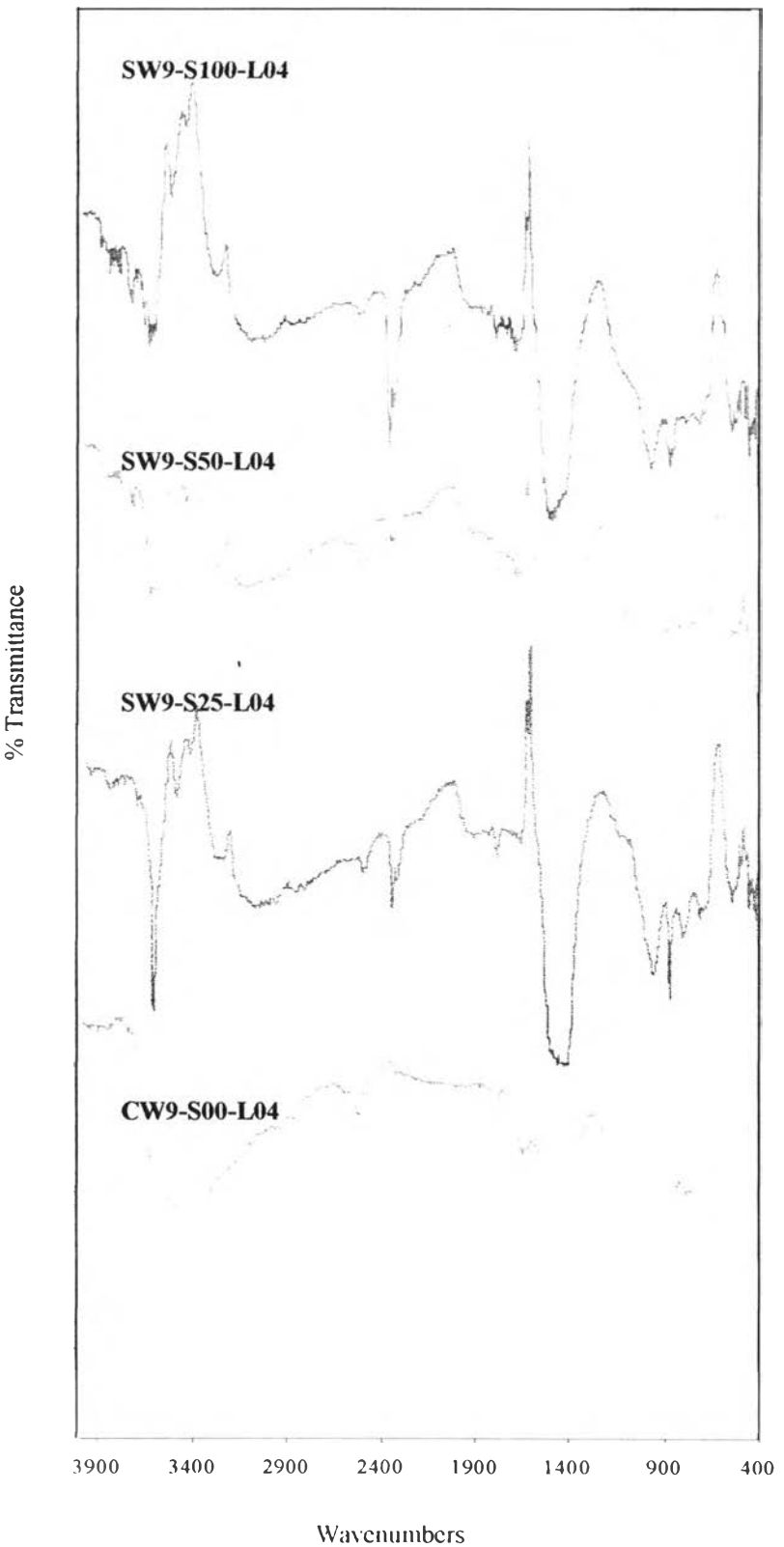

FIGURE 4.68 The FT-IR spectrum of the control and S/S recipes with lime throughout the whole length from 400 to 4000 cm^{-1}

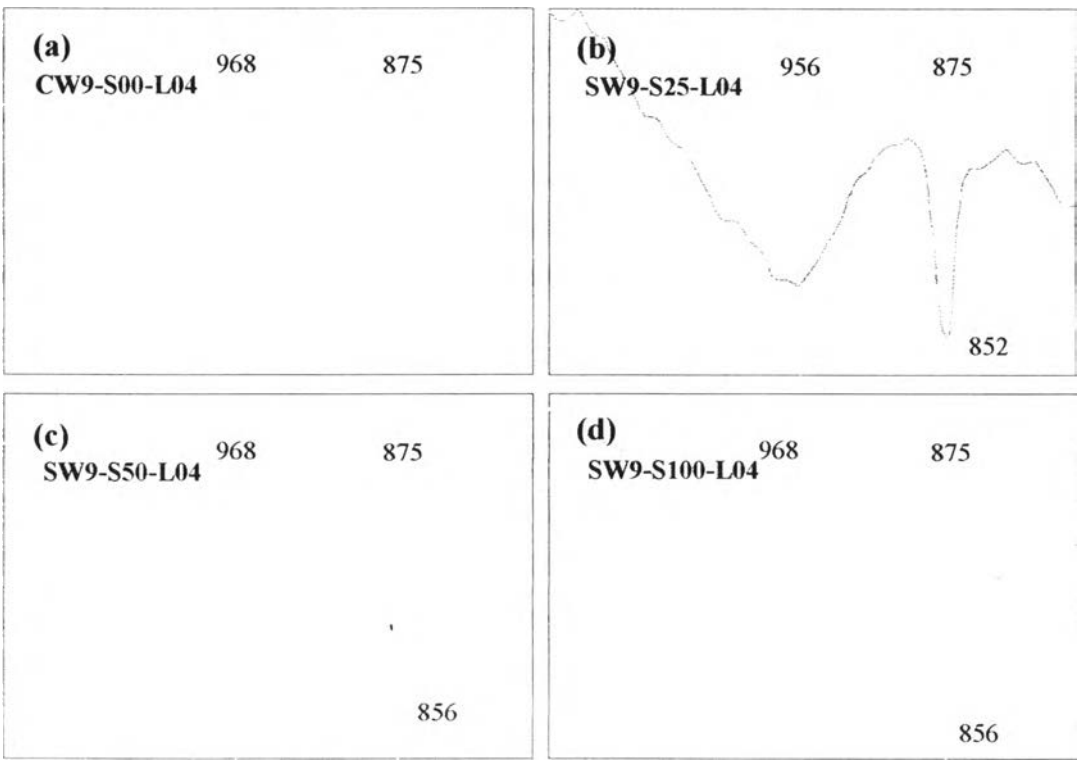

FIGURE 4.69 The FT-IR spectrum of the control and S/S recipes with lime focusing on the wavenumber from 800 to 1100 cm^{-1}

4.7 Leachability of the Solidified/Stabilized Sludge

The extraction results from the two types of leaching procedures on the eight different solidification/stabilization recipes as well as two control samples are shown in Tables 4.17 and 4.18 and illustrated in Figures 4.70 and 4.71 in which the concentrations (mg/L) of Ca, As, and Fe are given along with pH of leachate. According to the available data, it is found that two interesting issues should be taken into consideration.

The first issue raises when the comparison between concentrations of arsenic in leachate of the same S/S recipe subjected to the TCLP and LP-No.6 is made. Considering Figure 4.70, it can be clearly seen that, for all S/S recipes, the concentration of arsenic in the leachate subjected to TCLP is not significantly different from that submitted to NO.6-LP of the same recipe. For further understanding toward this issue, the remobilization and immobilization of arsenic in the extraction fluid is discussed here. As mentioned in the previous section, some of arsenic originally sorbed onto surface of the macroencapsulated sludge might desorb due to high pH of the cementitious environment in the solidified/stabilized matrices. However, owning to the fact that desorption of arsenic in the cement matrices was supposed to occur only at the interface between pore fluid and the sludge; therefore, a great deal of arsenic sorbed inward the sludge which pore fluid could not reach remained unleached. However, before subjected to the leaching test, the solidified products were pulverized by grinding to a particle size smaller than 9.5 mm. This procedure reduced the role of macroencapsulation on waste immobilization because most of the macroencapsulation was supposed to be destroyed. As a result, the bare sludge was supposed to confront with extremely chemical and mechanical weathering from the extraction tests. The sludge was supposed to be dissociated by weathering; then, the particle size of sludge was supposed to become smaller. The smaller the particle of the sludge, the higher the surface to contact with the extraction fluid, and the more potential of arsenic todesorb. As discussed before, the desorption of arsenic from iron hydroxide is function of pH as shown in Figure 4.28 in Part I. Therefore, the fact that pH of leachate from

Table 4.17 Leachate pH and leachate concentration (mg/l) of S/S samples subjected to Lp-No.6

S/S recipe	Leachate	Leachate concentration(mg/L)		
	pH	As	Ca	Fe
CW4-S00-L00	12.03	-	1050.00	0.007
SW4-S15-L00	12.07	0.3	1083.45	0.008
SW4-S25-L00	12.1	0.65	1105.20	0.005
SW4-S50-L00	12.24	1.09	1161.90	0.005
SW4-S100-L00	12.14	1.88	1083.75	0.007
CW9-S00-L04	12.12	-	1244.55	0.008
SW9-S15-L04	12.35	0.36	1237.30	0.108
SW9-S25-L04	12.23	0.58	1238.95	0.009
SW9-S50-L04	12.33	1.19	1240.05	0.006
SW9-S100-L04	12.2	1.85	1220.00	0.012

Table 4.18 Leachate pH and leachate concentration (mg/l) of S/S samples subjected to TCLP

S/S recipe	Leachate	Leachate concentration(mg/L)		
	pH	As	Ca	Fe
CW4-S00-L00	12.14	-	1105	0.007
SW4-S15-L00	12.28	0.36	1096	0.001
SW4-S25-L00	12.34	0.68	1109	0.001
SW4-S50-L00	12.37	1.12	1175.2	0.002
SW4-S100-L00	12.23	1.89	1070.1	0.030
CW9-S00-L04	12.20	-	1255.3	0.008
SW9-S15-L04	12.36	0.33	1262.85	0.002
SW9-S25-L04	12.29	0.58	1255.3	0.003
SW9-S50-L04	12.28	1.21	1250.5	0.002
SW9-S100-L04	12.33	1.88	1256.6	0.003

all S/S samples by both the TCLP and LP.-No.6 is almost the same, around 12, implies that remobilization of arsenic as a result of chemical and mechanical weathering of TCLP and LP-No.6 should be similar.

However, the chemical and mechanical weathering of TCLP and LP-No.6 promoted not only remobilization of arsenic but also immobilization of arsenic. According to the literature reviewed in Chapter 2, the main immobilization mechanism of arsenic in leachate of solidified products is formation of solubility-limiting phases, calcium-arsenic compounds, which are believed to be the different compounds from those formed in the cement matrices. For this reason, calcium is the major factor controlling immobilization of arsenic. During the leaching tests, not only arsenic but also calcium ion was leached by chemical and mechanical weathering. This can be taken as a clear sign of how chemical and mechanical weathering of the leaching procedures promotes immobilization of arsenic. As shown in Figure 4.70, it is evident that concentration of calcium in leachate of all S/S samples by the TCLP is insignificantly different from that by LP-No.6. This means that potential of arsenic to be immobilized by formation of calcium-arsenic compounds in the extraction fluid of the TCLP is the same as that of that LP-No.6 .

In conclusion, the potential for arsenic to mobilize from the sludge and to be immobilized by reacting with calcium due to chemical and mechanical weathering of TCLP is not different from that due to LP-No.6. Therefore, it is reasonable that why leachate concentration of arsenic from the TCLP is not significantly different from that of LP-No.6 as shown in Figure 4.70. However, the immobilization of arsenic by precipitation of solubility-limiting phases described in the previous three paragraphs is simplified to explain the first issue. In deed, the immobilized mechanism in this case is more complex than what is shown in the earlier discussions. Considering Figure 4.70, it is evident that leaching of arsenic from solidified/stabilized waste shows direct correlation to sludge content. This correlation violates concept of solubility product for metal species in terms of the equilibrium constant governing arsenic immobilization by formation of calcium-arsenic compounds in the leachate of S/S waste mentioned above. Therefore, the second issue rises from this point

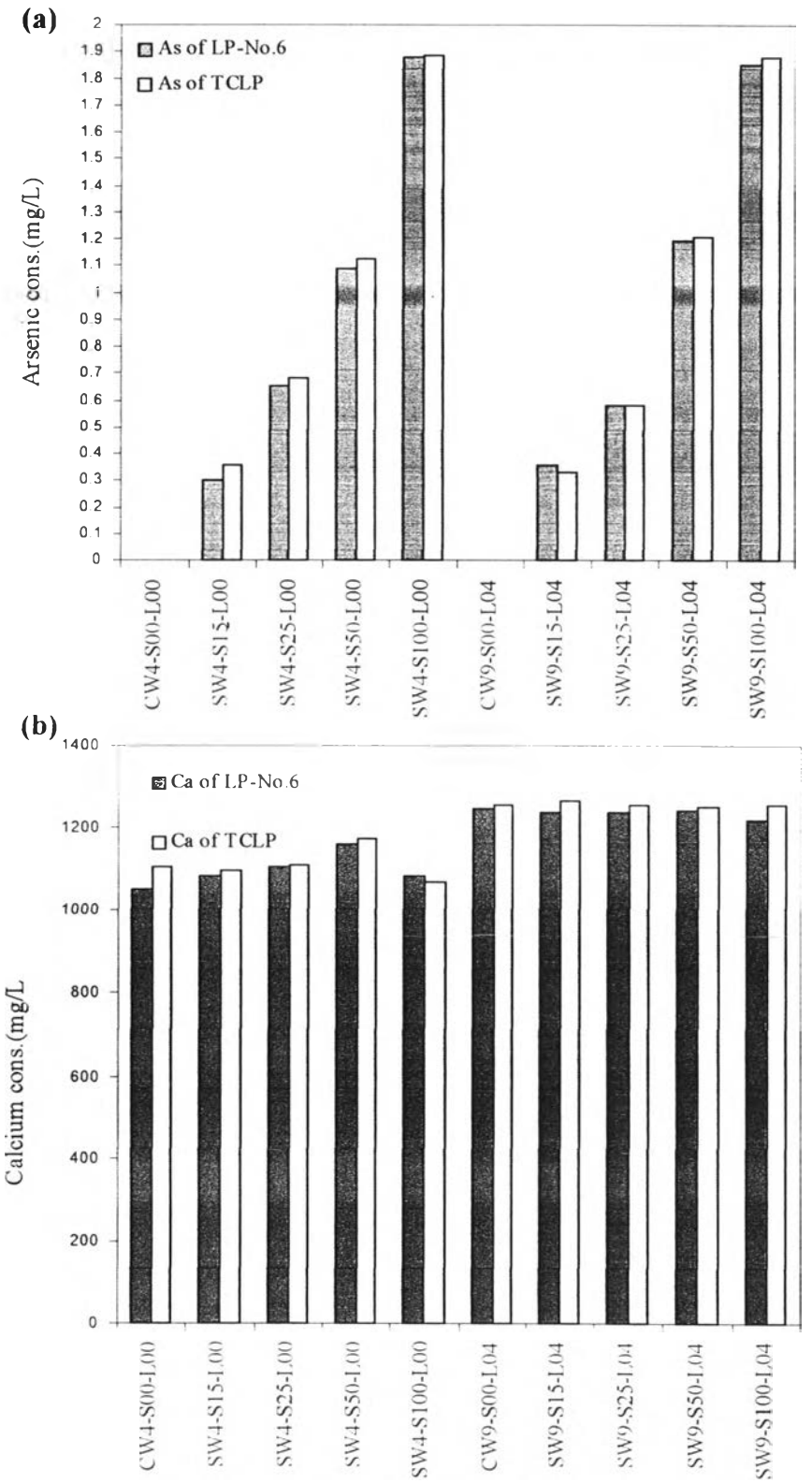

Figure 4.70 Histograms illustrating concentration of (a)arsenic and (b) calcium in leachate of all S/S recipes extracted by the TCLP and LP-No.6

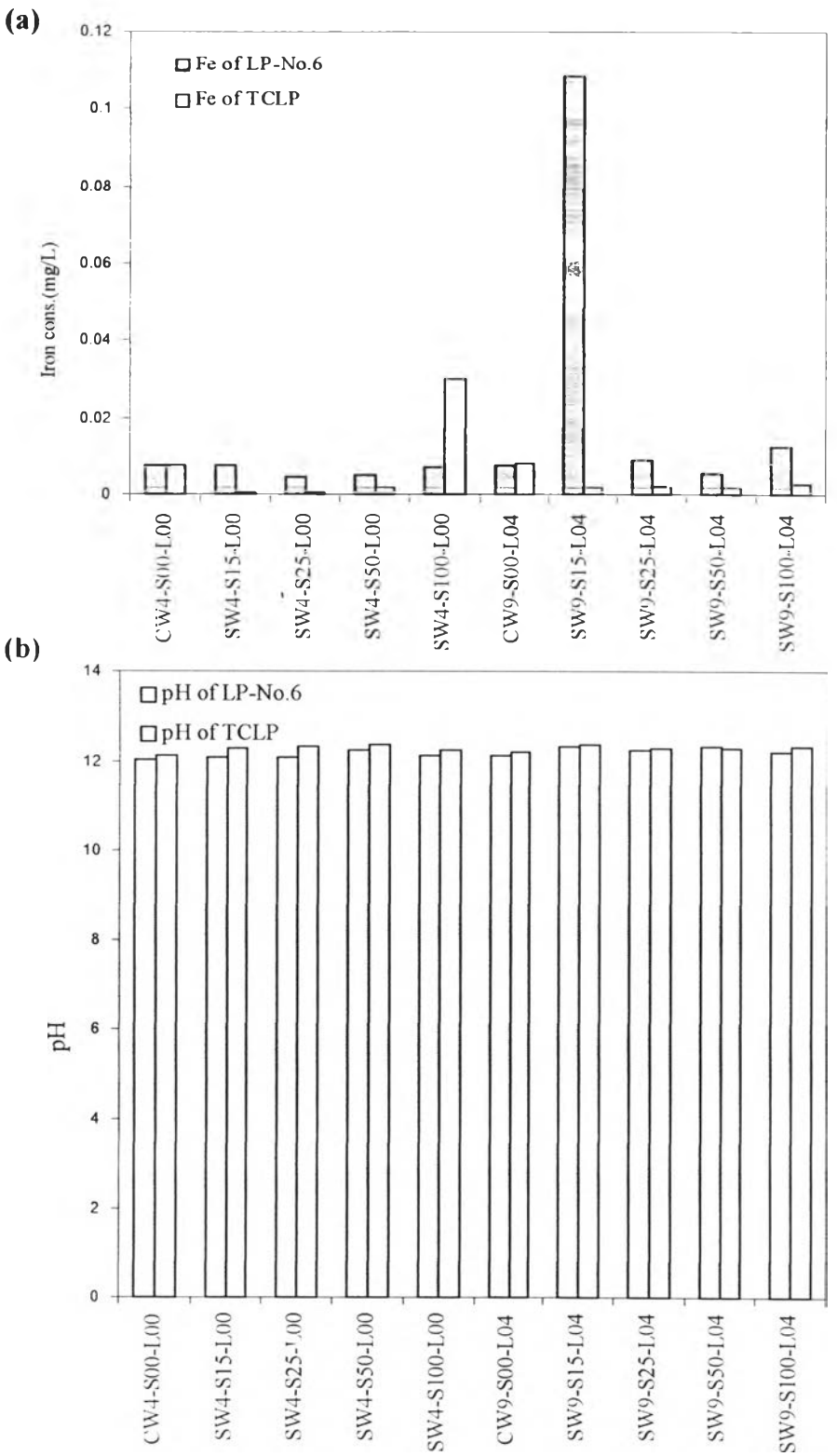

Figure 4.71 Histograms illustrating concentration of (a) iron in leachate of all S/S recipes and (b) their pH extracted by the TCLP and LP-No.6

To understand how this correlation violates the solubility product concept as well as to find the possible explanation for the issue, it is worthwhile to apply the general theory of equilibrium to the formation of a calcium-arsenic compound during leaching tests.

In the leaching tests, not only does calcium leach out of $Ca(OH)_2$ as well as other hydration products but also arsenic leaches out of the sludge which once was encapsulated in the solidified matrix. As discussed in Part I and II, although arsenite was used to synthesizing the sludge in the present study, both arsenite and arsenate seemed to exist in the sludge. Therefore, both of them were possible to transfer from the sludge to the extraction fluids.

Consequently, under equilibrium the reaction between calcium ion and arsenate can be expressed as:

$$\text{calcium-arsenate compound}_{(s)} \longleftrightarrow \text{calcium ion}_{(aq)} + \text{arsenate}_{(aq)} \qquad (4\text{-}7)$$

There, the dissociation constant is expressed as:

$$K_d = \frac{[\text{calcium ion}]\times[\text{arsenate}]}{[\text{calcium-arsenate compound}]} \qquad (4\text{-}8)$$

Based on MINEQL$^+$, at the high concentration of calcium shown in Figure 4.70, arsenate should not be present in aqueous phase but precipitate as calcium arsenate compound.

In the same way, under equilibrium the reaction between calcium ion and arsenite can be expressed as:

$$\text{calcium-arsenite compound}_{(s)} \longleftrightarrow \text{calcium ion}_{(aq)} + \text{arsenite}_{(aq)} \qquad (4\text{-}9)$$

There, the dissociation constant is expressed as:

$$K_d = \frac{[\text{calcium ion}]x[\text{arsenite}]}{[\text{calcium-arsenite compound}]} \quad (4\text{-}10)$$

In the above equation, the concentration of calcium-arsenite compound, which is in solid phase, is constant. Multiplying both sides of Equation (4-10) by [calcium-arsenite compound] results in a different value for K_d which is known as K_{sp}, the solubility product:

$$K_{sp} = [\text{calcium ion}]x[\text{arsenite}] \quad (4\text{-}11)$$

This equation concludes that, for dissociation of solids such as metal compounds including the arsenite compound, the concentration of metal ion in the leaching solution is not affected by the concentration of the solid metal compound in the waste.

According to recent study (Vandecasteele et al., 2002; Palfy et al.,1998; and Dutré and Vandecasteele,1998) the possible form of calcium-arsenite compound is $CaHAsO_3$ of which K_{sp}, without consideration of activity coefficients, is $1.07x10^{-7}$. For this reason, the matter of that increased amount of sludge addition may result in increasing potential for arsenite leaching out during the extraction tests is not the main factor controlling arsenite concentration in leachate, but the real controlling factor is calcium ion. Based on Equation (4-11), concentration of arsenite in each S/S recipe can be approximately calculated as :

$$\frac{[\text{arsenite}]}{[\text{calcium ion}]} = 1.07x10^{-7} \quad (4\text{-}12)$$

By this equation, at the $[Ca^{2+}]$ around 1171.325 mg/L, the average calcium concentration of all leachate, arsenic concentration should be only around 0.274 mg/L regardless of the amount of the sludge added. Therefore, the difference between the

calculated value and the observed values suggests that there be another factor beside the formation of $CaHAsO_3$ controlling immobility or mobility of arsenic in leachate.

This governing factor may be pH. By considering formation of $CaHAsO_3$, it is found that the presence of Ca^{2+} and $HAsO_3^{-2}$ is required to form this compound, and the factor determining how many percent of total arsenite ion present in form of $HAsO_3^{-2}$ is pH. Calculated by MINEQL$^+$, it is found that at around pH 12, the average pH of all leachates in the present study, only around 43.88 % of total arsenite leached is in the form of $HAsO_3^{-2}$ which means that other 56.12 % of arsenic from the sludge is in the form which cannot form $CaHAsO_3$. By this reason, it is not surprising that why there is a close relationship between the increasing amount of sludge and the increasing concentration of arsenic in leachate.

4.8 Evaluation of Utilization Potential

Generally speaking, there are two matters of concern regarding utilization of a solidified waste form as construction materials. First, the solidified product must not pose any threat to the environment during utilization. The leachabilities of the solidified products following both the TCLP and NO.6-LP can be used as a rough indicator to address this issue due to the fact that according to this leaching procedure the macroencapsulation of solidified products is destroyed, thus the simulation is believed to represent the worst-case scenario. Based on this criterion, the utilization of the solidified/stabilized arsenic iron sludge is supposed to pose no unacceptable threat to the environment because of the fact that, as shown in Figure 4.70, the concentrations of arsenic in the leachate pass the regulatory limit with a wide margin for both the TCLP and LP-No.6 in case that MCL of arsenic for drinking is 50 μg/L and the maximum allowable concentration of arsenic in leachate is 5 mg/L. However, if MCL of arsenic for drinking water is 10 μg/L, substitution of dried sludge is limited to 25% in comparison to the binders to comply with the maximum allowable concentration of arsenic in leachate, which is 1 mg/L.

ต้นฉบับ หน้าขาดหาย

PART IV

4.9 Morphologies of the Solidified/Stabilized Sludge

Although all the solidified/stabilized waste forms listed in Table 3.3 were subjected to SEM-EDS for the purpose of investigating their morphological development at 3, 7, 14 and 28 days, it is more meaningful to discuss the results in order to understand arsenic immobilization potential by each kind of hydration by-product than only to present the results in chronological order. Therefore, in this section, the results are organized and discussed in such a manner.

4.9.1 Calcium Silicate Hydrate (C-S-H)

Hydration reaction discussed in Chapter 2 as well as illustrated in Figure 2.7 is the origin of C-S-H. This hydration by-product not only has a direct influence on strength of the solidified matrices but also potentially has a hand in waste immobilization as shown in Figure 4.72 and Figure 4.73 as well as in Table 4.19, the evidences of arsenic sorbed on C-S-H microstructures.

Sorption potential of metals on C-S-H is supposed to be controlled by an important characteristic of C-S-H. The fact that C-S-H has a very high specific surface area with irregular hydrogen bonding can facilitate sorption of both water and other alien ions such as metal ions (Glasser, 1993). Figure 4.74 shows hypothetical reconstruction of the nanostructure of a C-S-H gel of which specific surface area could be as high as 50 m^2g^{-1}(Glasser, 1993). The blocks of layer-structured calcium silicate material with silicon in a low state of polymerization depicted in Figure 4.74 contain strong unsatisfied surface charges causing strong bonding to water molecules as well as to other C-S-H nanoparticles. The irregular stacking of solid blocks creates a large volume of micropores, which range in equivalent spherical diameter from a few to a few tens of nanometers. Consequently, the large specific surface created,

Table 4.19 Semi quantitative EDS analysis of SW9-S25-L00 and SW4-S25-L04 at the age of 7 days focusing on C-S-H structures

Sample	Age (days)	Atomic (%)										
		Ca	Si	O	Fe	As	Na	Mg	Al	K	Cl	Total
SW9-S25-L00	7	10.70	7.09	71.88	0.66	1.19	5.31	0.94	0.98	1.00	0.25	100.00
SW4-S25-L04	7	17.22	5.31	71.53	1.67	1.20	-	0.18	2.89	-	-	100.00

a)

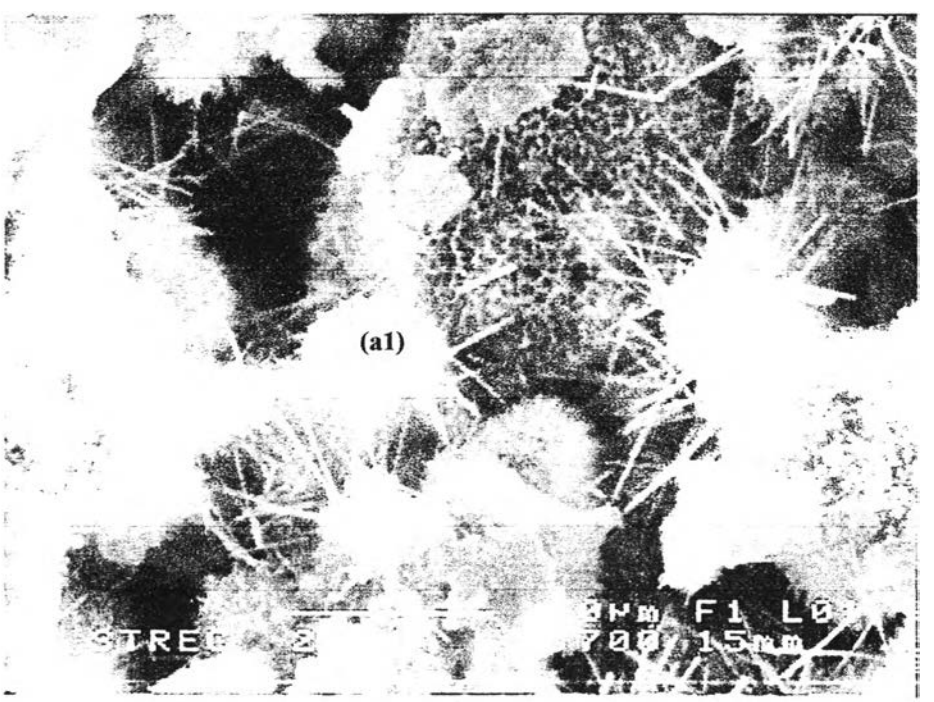

b)

Figure 4.72 (a) SEM photographs of SW9-S25-L00 at the age of 7 days (b) EDS spectrum focusing on C-S-H microstructure (a1) to investigate arsenic sorption potential.

a)

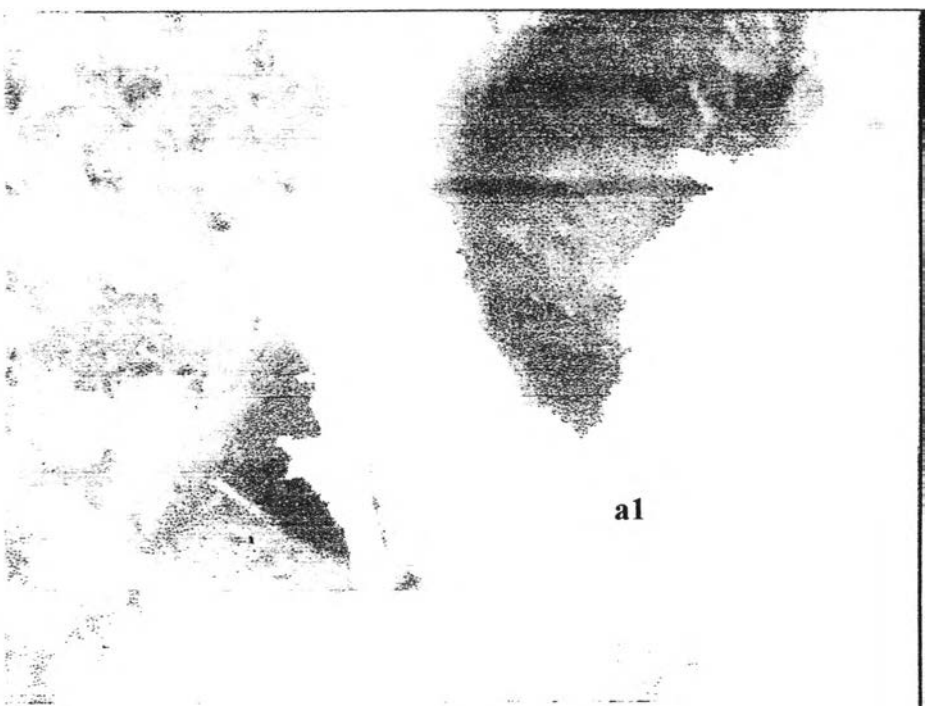

b)

Figure 4.73 (a) SEM photographs of SW4-S25-L04 at the age of 7 days (b) EDS spectrum focusing on C-S-H microstructure (a1) to investigate arsenic sorption potential.

with its high density of irregular hydrogen bonding, promotes a strong potential for sorption (Glasser, 1993).

In addition, the surface charge of C-S-H varies with its composition; Ca-rich C-S-H has a positive surface charge and trends to sorb anions such as oxyanions in alkaline condition. In contrast, as Ca:Si ratio decreases, the surface gradually lessens, passing through zero at a Ca:Si ratio about 1.2 and eventually becoming negative at lower rations (Glasser, 1993). For this reason, as shown in Table 4.19 that Ca:Si ratios of C-S-H structures in Figures 4.72 and 4.73 are 1.51 and 3.24, respectively, the surface charge of these C-S-H structures is supposed to be positive, so arsenic oxyanion with negative charge trends to sorb on them as shown in Table 4.19.

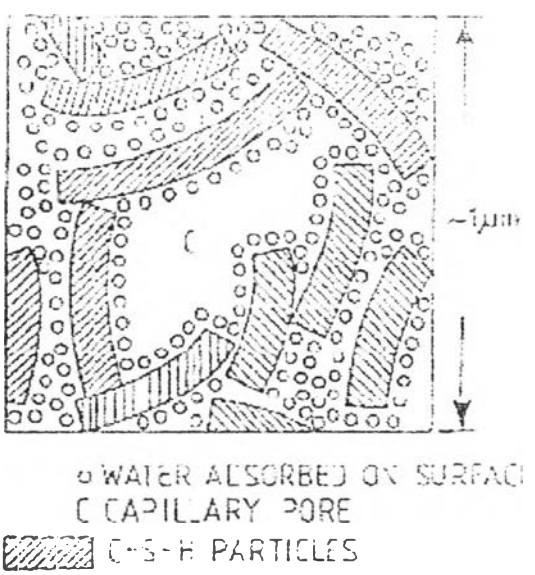

Figure 4.74 Hypothetical reconstruction of the nanostructure of a C-S-H gel (Glasser, 1993)

However, the sorption by C-S-H is unlikely to be unstable during a leaching test owning to the fact that although C-S-H has high resistivity to leaching, the semiprotective residual leaving after stead-state of a leaching test is insoluble $SiO_2 \cdot nH_2O$ rather than C-S-H (Glasser, 1993). This implies that after the leaching tests, the remaining C-S-H was in form of $SiO_2 \cdot nH_2O$, which was supposed to have negative surface charge; therefore, desorption of arsenic on C-S-H might take place and resorption of arsenic from leachate onto $SiO_2 \cdot nH_2O$ seemed to be impossible.

4.9.2 Ettringite, Monosulfoaluminate, and Other Hydrated Calcium Aluminates/Ferrite

Figures 4.75 and 4.76 illustrate the needle-like microstructure of ettringite [$Ca_6Al_2(SO_4)_3(OH)_{12} \cdot 26H_2O$], a hydration by-product of tricalcium aluminate in the presence of sulfate ions. The formation of ettringite is shown in Figure 2.7. It is well known that this hydration by-product has serious repercussion to the strength of the solidified matrices; nevertheless, ettringite was proved having potential to immobilize oxyanions especially As (V) ions (Myneni, Traina, Logan, and Waychunas; 1997).

As shown in Figure 4.77, the ettringite crystal structure consists of columns of $\{ Ca_6[Al(OH)_6]_2 \cdot 24H_2O \}^{6+}$ with the intercolumn space (channels) occupied by anions such as SO_4^{-2}, H_2O molecules. The column H_2O molecules form H-bonds with channel ions and hold the columns together through electrostatic interaction. Thus oxoanion immobilization by ettringite results in channel substitution by replacing SO_4^{-2} or H_2O and/or formation of complexes with surface functional groups by replacing OH or H_2O (Myneni et al., 1997).

Considering the components of ettringite shown in Table 4.20, it should be noted that atomic (%) of S in ettringite structure is only 0.01 and 0.29%, respectively. This implies that arsenic leached out of the sludge might be immobilized by replacing SO_4^{-2} in channel substitution.

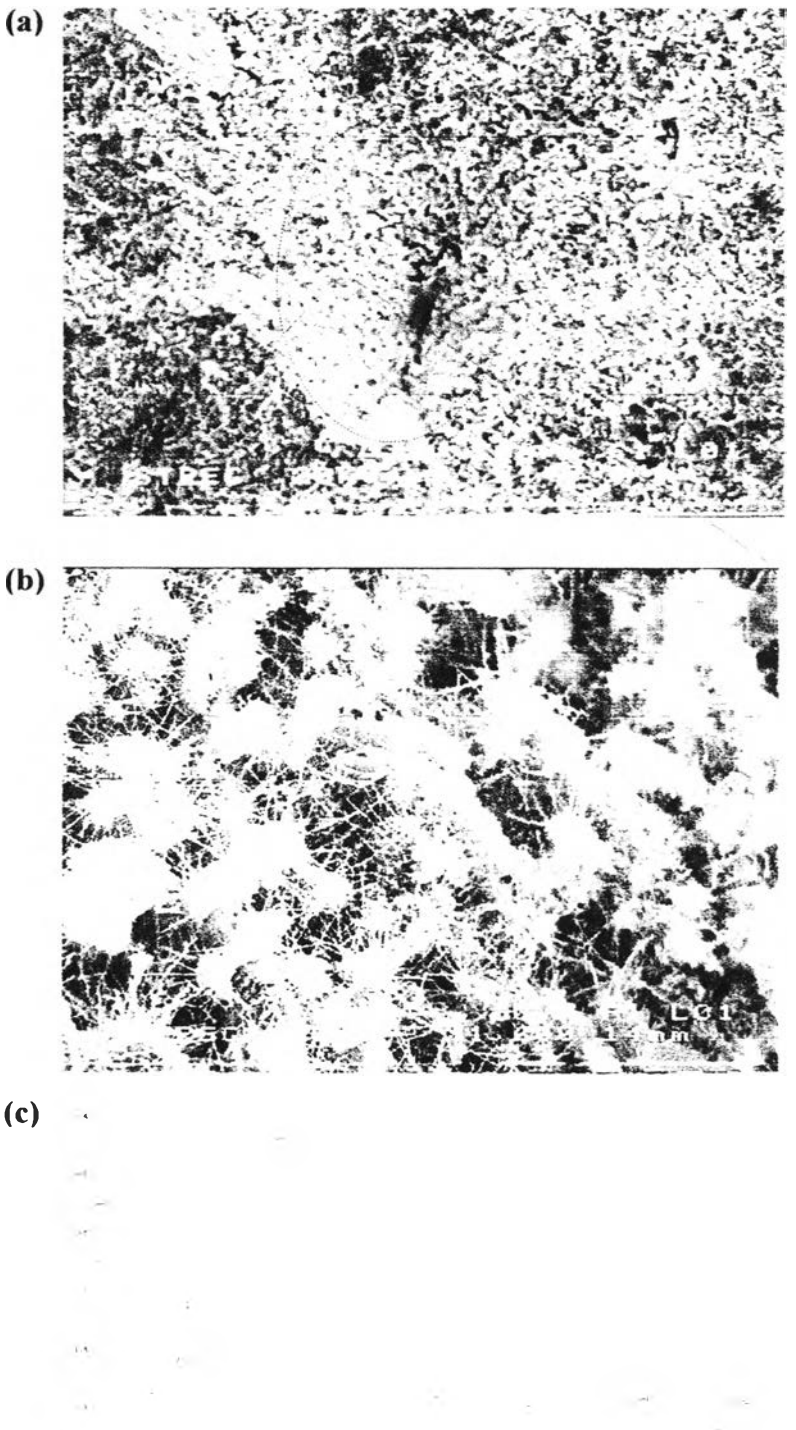

Figure 4.75 (a) SEM photographs of SW6-S25-L04 at the age of 7 days focusing on the hole once encapsulating the arsenic containing sludge, (b) SEM photographs zooming on microstructures at the interface of the sludge and cement, and (c) EDS spectrum focusing on ettringite microstructure to investigate arsenic immobilization potential.

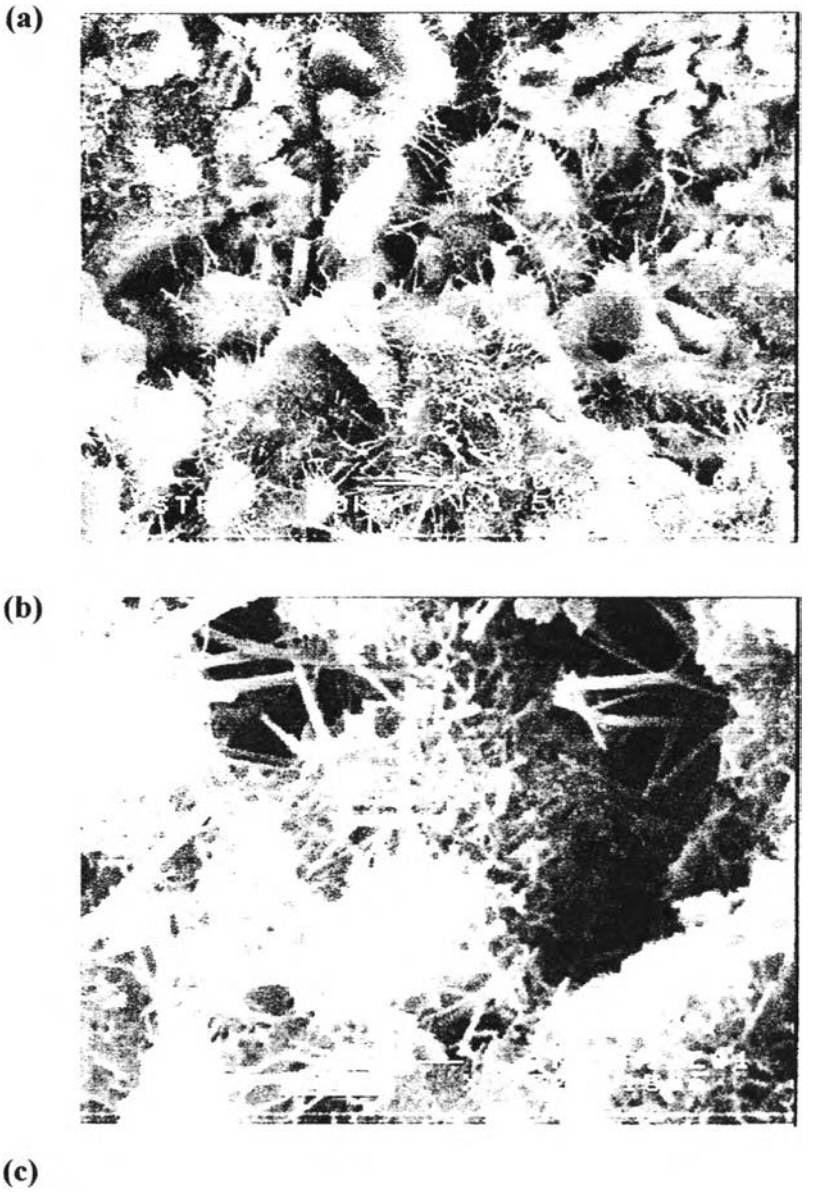

Figure 4.76 (a) SEM photographs of SW4-S25-L00 at the age of 7 days, (b) SEM photographs zooming on needle-like microstructure of ettringite, and (c) EDS spectrum pointing at ettringite microstructure to investigate arsenic immobilization potential.

Table 4.20 Semi quantitative EDS analysis of SW6-S25-L04 and SW4-S25-L00 at the age of 28 and 7 days focusing on ettringite structures

Sample	Age (days)	Atomic (%)												
		Ca	Si	O	Fe	As	S	Na	Mg	Al	K	C	Cl	Total
SW6-S25-L04	28	11.93	4.96	66.70	1.36	2.06	0.01	0.90	-	1.93	0.22	9.74	0.19	100.00
SW4-S25-L00	7	18.60	10.12	64.63	0.71	0.30	0.29	1.83	0.79	1.78	0.52	-	0.43	100.00

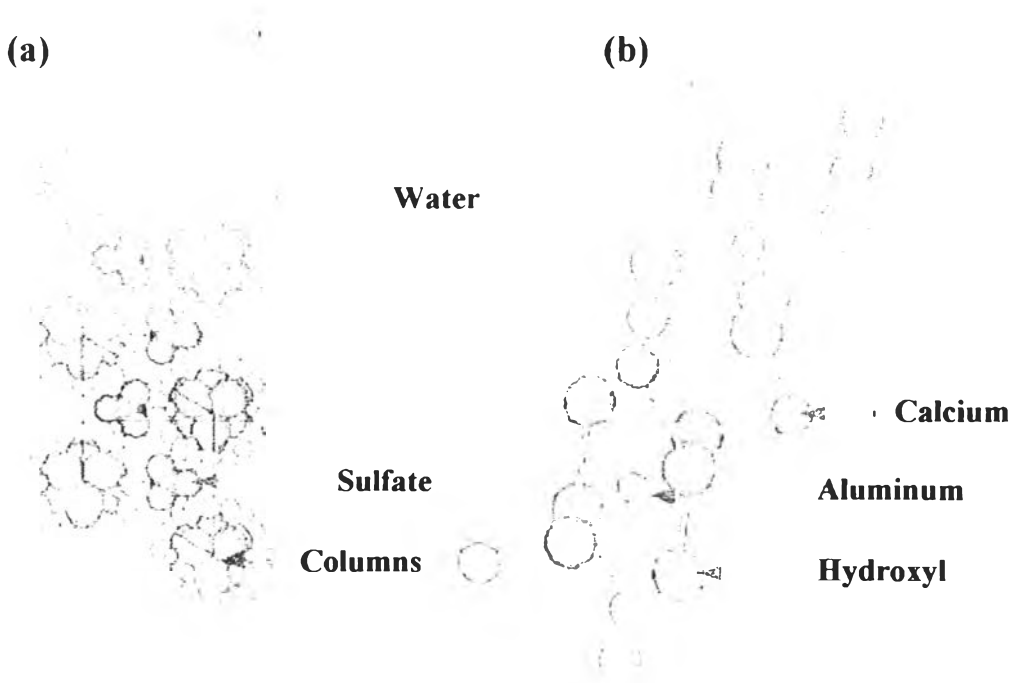

FIGURE 4.77 Structure of ettringite. (a) Perpendicular to c-axis [(001) plane], showing columns and channels. (b) structure of a single column showing all polyhedra and part of Ca polyhedra. Calcium-coordinated H_2O is removed for clarity. (Myneni et al., 1997)

It should be noted that although having the same structure, ettringite of SW6-S25-L04 and SW4-S25-L00 retained different amounts of arsenic, which were 2.06 and 0.3% atomic, respectively. The sharp distinction of these two samples, which might be responsible for the different retention of arsenic, is arsenic availability. For example, ettringite of SW6-S25-L04 was formed at interface between cement paste and the arsenic containing sludge, so there was abundance of arsenic to be crystallochemically incorporated by ettringite. In contrast, ettringite of SW4-S25-L00 was far from the sludge; limited amount of arsenic might available there. Therefore, even though crystallochemically incorporating all arsenic available, ettringite in SW4-S25-L00 might not reach its maximum arsenic immobilization capacity.

However, the question of stability of arsenic immobilized by ettringite during a leaching test is still open. Owning to the fact that ettringite is markedly lower stability at pH < 10.7 (Myneni et al.,1997), some of arsenic is possible to release when ettringite is initially mixed with extraction fluid at pH 5. However, dissolution of $Ca(OH)_2$ as well as C-S-H will provide Ca^{2+} buffer and gradually increase pH from 5 to around 12.4, at which ettringite becomes stable , when the system reaches equilibrium state. As a result, the factor controlling remobilization and immobilization of arsenic in ettringite is supposed to be the faster phenomenon, between dissolution of ettringite and dissolution of $Ca(OH)_2$ together with C-S-H. Moreover, during LP-No.6 test, arsenic crystallochemically incorporated by ettringite might desorb due to SO_4^{-2} in the extraction fluid; SO_4^{-2} having greater charge and smaller size (Myneni et al., 1997) may substitute inside ettringite channels and replace arsenic.

It should be noticed that ettringite is a stable hydration product only while there is an ample supply of sulfate available, as shown in Table 4.21. If sulfate is all consumed before $3CaO.Al_2O_3$ or $4CaO.Al_2O_3.Fe_2O_3$ has completely hydrated, ettringite trends to transform to another calcium sulfoaluminate hydrate containing less sulfate, simply called monosulfoaluminate (Mindess, Young, and Darwin, 2003). When first formed monosulfoaluminate trends to form cluster or rosettes of irregular plates. Later, these trend to grown into well-develop, but very thin, hexagonal plates.

Figure 4.78 illustrates SEM photographs of monosulfoaluminate found in this study. Unfortunately, EDS could not be applied to reliably investigate their compositions because they located in a cavity obstructed by several hydrated structures. However, theoretically, monosulfoaluminate, like ettringite, should be able to immobilize arsenic due to the fact that it also consists of SO_4^{-2} which arseic ion can replace. This assumption is in good agreement with recent study of Baur and Johnson (2003), who investigated sorption of selenite and selenate- oxyanions of which several properties corresponds to that of arsenic-and concluded that selenite and selenate were effectively sorbed by a cement where monosulfate was present in significant amount.

According to both the available results of this study and the literature, sulfate substitute is one of the important binding mechanisms of arsenic in cementitious environment. This assumption can be confirmed by considering other hydrated calcium aluminates or ferrites structures formed without SO_4^{-2} shown in Figures 4.79 and 4.80 as well as Table 4.22. It is found that insignificant amount of arsenic was detected in such structures.

Table 4.21 Formation of Hydration Products from $3CaO.Al_2O_3$ (Mindess et al., 2003)

$Ca\ SO_4.H_2O$ / $3CaO.Al_2O_3$ Molar Ratio	Hydration Products Formed
3.0	Ettringite
3.0-1.0	Ettringite+ monosulfoaluminate
1.0	Monosulfoaluminate
<1.0	Monosulfoaluminate solid solution
0.0	Hydrogarnet

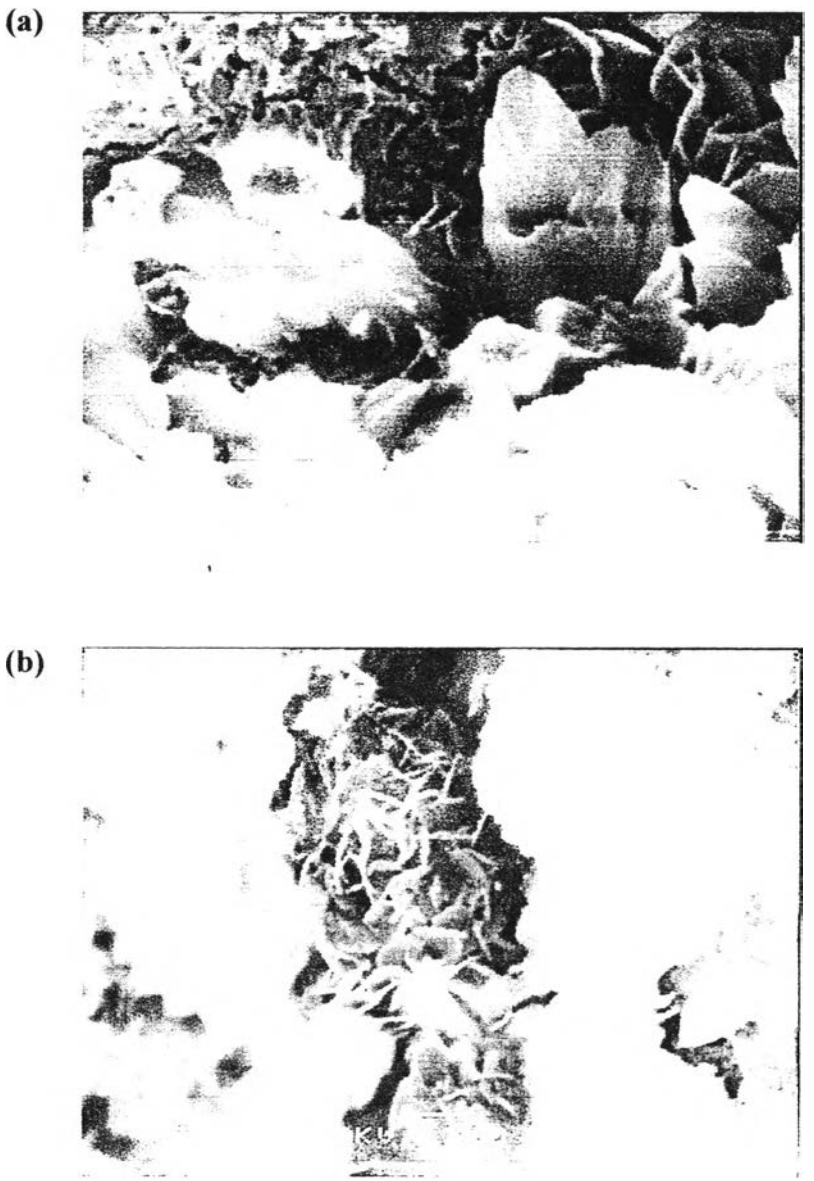

Figure 4.78 (a) SEM photographs of SW4-S25-L04 at the age of 3 days, (b) SEM photographs of SW6-S25-L04 at the age of 14 days. Both focus on rosette-like morphology of monosulfoaluminate

Table 4.22 Semi quantitative EDS analysis of SW4-S25-L04 and SW9-S25-L04 at the age of 7 days focusing on hexagonal-plate morphology of hydrated calcium alluminate/Ferrite and ill-defined morphology of hydrated calcium alluminate

Sample	Age (days)	Atomic (%)										
		Ca	Si	O	Fe	As	Na	Mg	Al	K	Cl	Total
SW4-S25-L04	7	18.59	1.62	74.06	2.44	0.13*	-	0.31	2.84	-	-	100.00
SW9-S25-L04	7	18.62	0.39	73.37	0.16	0.03*	0.54	0.17	5.00	0.05	1.68	100.00

*= <2sigma

(a)

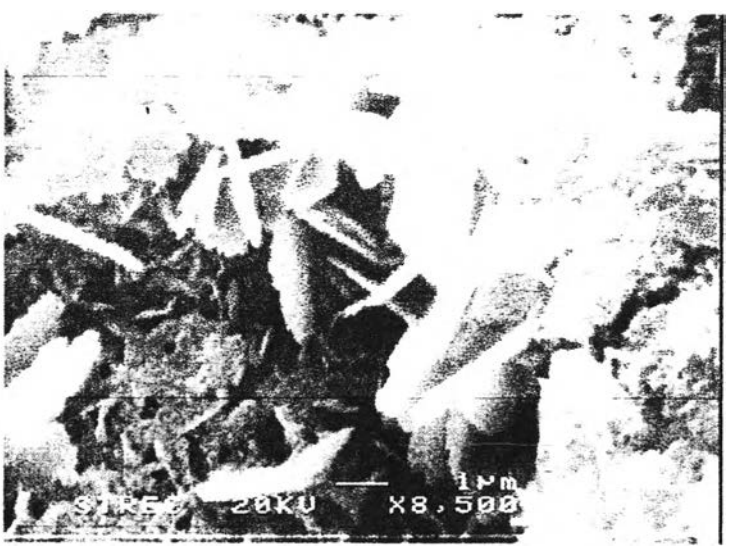

(b)

Figure 4.79 (a) SEM photographs of SW4-S25-L04 at the age of 7 days focusing on hexagonal-plate morphology of hydrated calcium alluminate/ferrite, (b) EDS spectrum pointing at hexagonal-plate structure to investigate arsenic immobilization potential

(a)

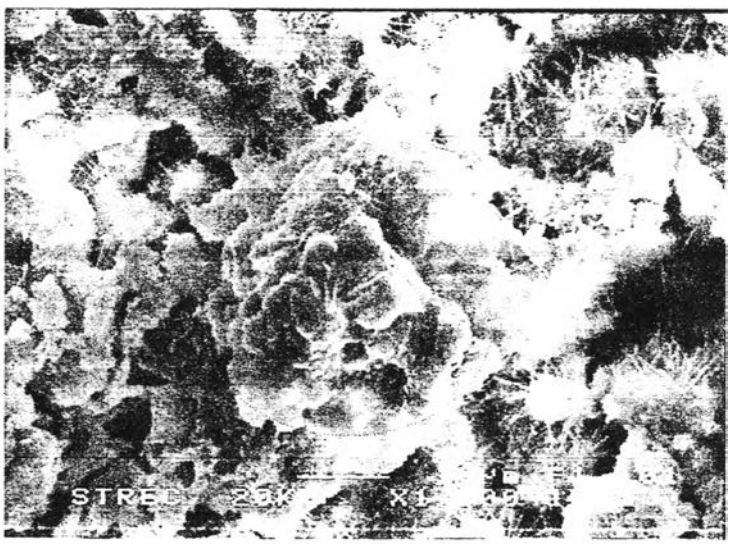

(b)

Figure 4.80 (a) SEM photographs of SW9-S25-L04 at the age of 7 days focusing on ill-defined morphology of hydrated calcium alluminate, (b) EDS spectrum pointing at ill-defined structure to investigate srsenic immobilization potential.

4.9.3 Calcium Hydroxide [$Ca(OH)_2$]

Although produced from $2CaO\,SiO_2$ and $3CaO\,SiO_2$ during hydration reaction like C-S-H, $Ca(OH)_2$, a well crystallized material with a definite stoichiometry, appears to have little potential for both sorption and crystallochemical incorporation of arsenic. As shown in Figure 4.81 and Table 4.23, only insignificant amount of arsenic is supposed to be either sorbed or crystallochemical incorporated into

$Ca(OH)_2$. This may be a result of that the surface of $Ca(OH)_2$ does not have positive charge like that of C-S-H, nor does it contain SO_4^{-2} for arsenic to substitute.

4.9.4 Calcium-Arsenic Compounds

While crystallized $Ca(OH)_2$ discussed in the previous section seems inefficient in binding arsenic by both sorption and lattice inclusion, calcium ion saturating in pore fluid from both hydration and addition of powder of hydrated lime as an additive seems considerably beneficial for arsenic immobilization by reacting with arsenic to form calcium-arsenic compounds, solubility limiting phases.

As discussed in Part III regarding remobilization of arsenic from the sludge in cementitious environment, arsenic is supposed to concentrate both at the surface of the sludge encapsulated into cement matrix and to distribute in aqueous phase of pore structure as shown in Figure 4.82. Therefore, calcium-to-arsenic ratio at the interface between cement paste and the sludge may differ from that between calcium ion and arsenic oxyanion dissolved in pore water. For this reason, as mentioned in Part III as well as in literature, it is possible that more than one type of calcium-arsenic compounds is formed in such environment.

Table 4.23 Semi quantitative EDS analysis of SW6-S25-L04 at the age of 7 days focusing on calcium hydroxide

Sample	Age (days)	Atomic (%)										
		Ca	Si	O	Fe	As	Na	Mg	Al	K	Cl	Total
SW6-S25-L04	7	30.73	2.11	65.04	0.08*	0.10*	0.86	0.23*	0.42	0.23	0.20	99.59

*= <2sigma

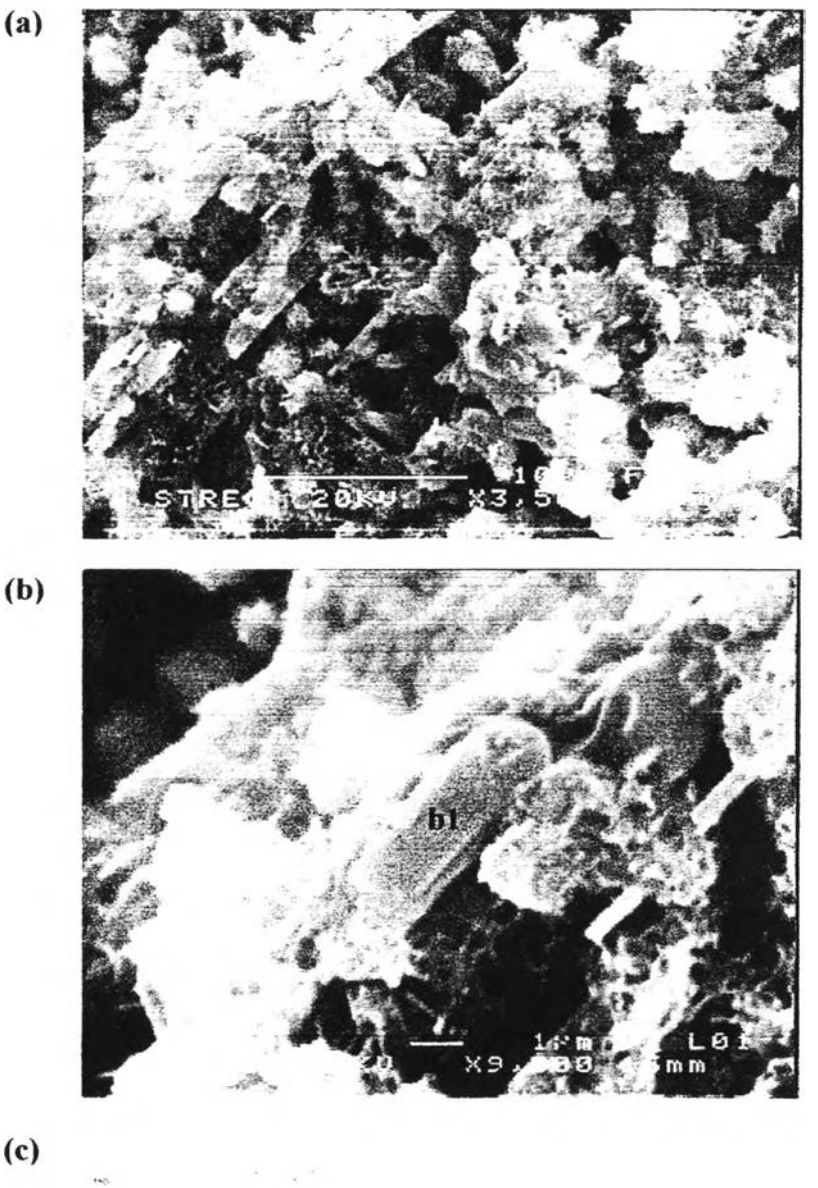

Figure 4.81 (a) SEM photograph of SW6-S25-L04 at the age of 7 days, (b) the same SEM photograph zooming on $Ca(OH)_2$ microstructures, and (c) EDS spectrum pointing on b1 representing $Ca(OH)_2$ to investigate arsenic immobilization potential.

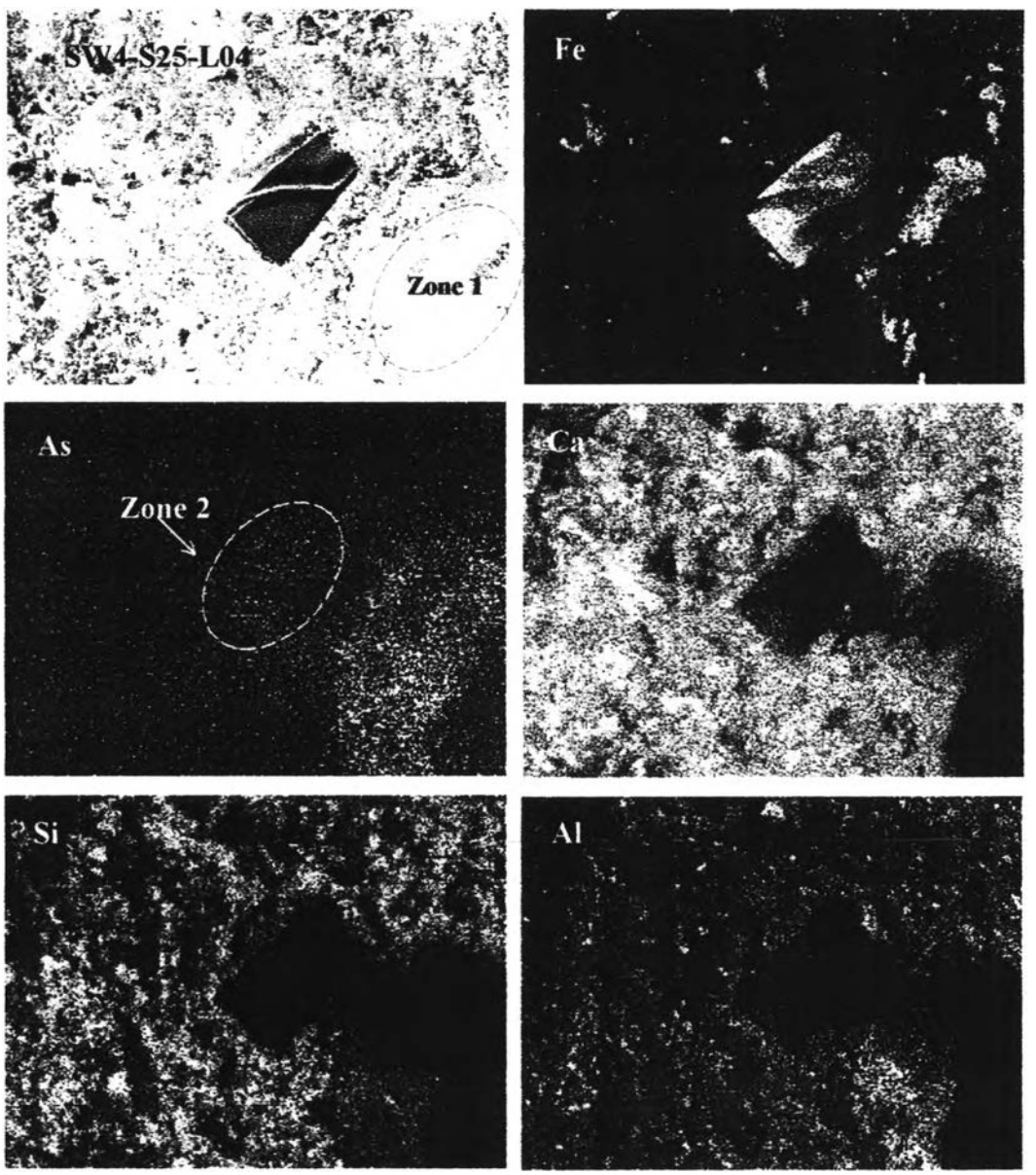

Figure 4.82 The x-ray dot maps of SW4-S25-L04 at the age of 7 days comparing arsenic distribution between Zone 1 where arsenic desorbing from the sludge locates and Zone 2 where arsenic remaining onto the surface of the sludge locates.

Figure 4.83 illustrates one of the possible calcium-arsenic compounds forming in the solidified/ stabilized matrices. Considering its morphology, this compound should be the same calcium-arsenic compound shown in Figure 4.60 of which presumed formation mechanism is depicted in Figure 4.59. This compound was found in zone 1 in Figure 4.82, so it is supposed to form by precipitation between calcium and arsenic ion dissolved in pore water.

In contrast, Figure 4.84 shows another type of calcium-arsenic compound. Unlike the calcium-arsenic compound discussed in previous paragraph, this compound located at the interface between cement paste and the sludge. Moreover, its grass leaf-like morphology is completely different from leafy crystals of the calcium-arsenic compound shown in Figure 4.83.

(a)

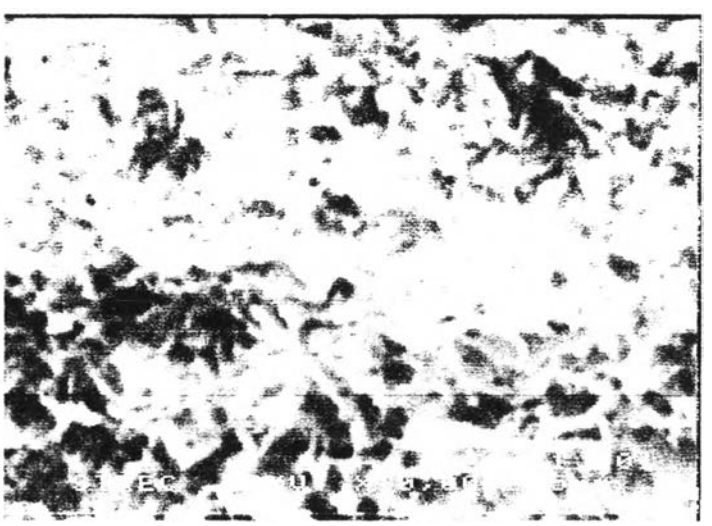

(b)

Figure 4.83 (a) SEM photograph of SW4-S25-L04 at the age of 7 days focusing on one of the possible calcium-arsenic compound and (b) its EDS spectrum

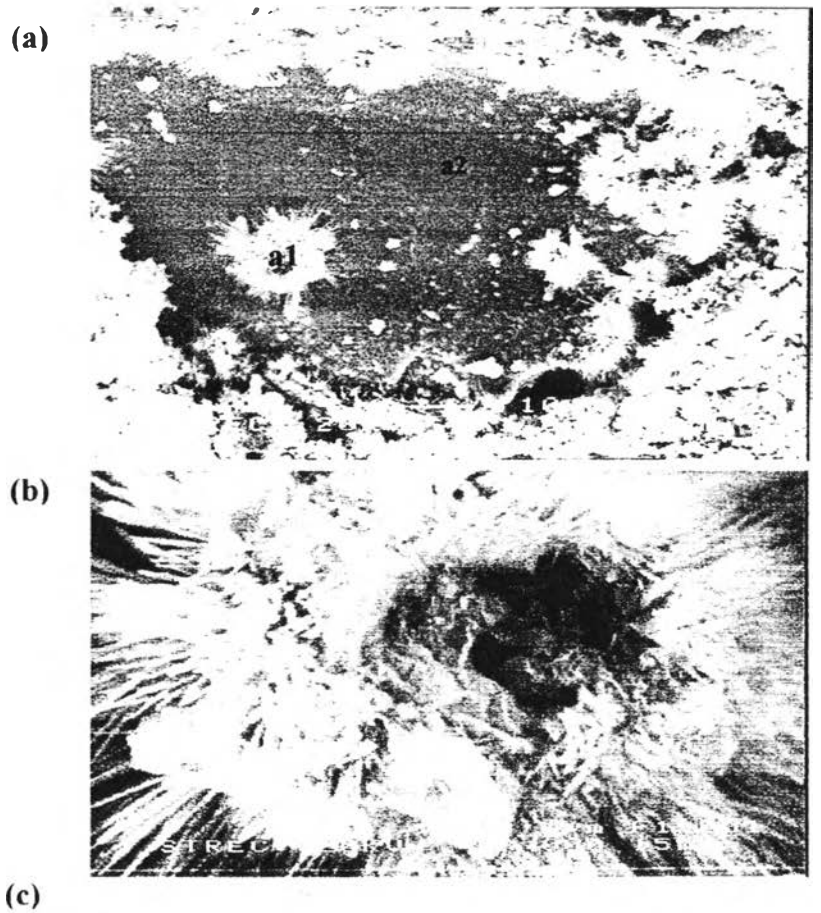

Figure 4.84 (a) SEM photograph of SW4-S25-L04 at the age of 28 days, (b) the same SEM photograph zooming on another calcium arsenic compound, and (c) EDS spectrum pointing on (a1) the calcium arsenic compound, and (d) EDS spectrum pointing on (a2) the arsenic-containing sludge. Comparing (c) and (d) is a clear evidence of arsenic transformation from the sludge to calcium arsenic compound

The most important difference between these two calcium arsenic compounds is the fact that the former was detected at the age of seven days while the latter was detected at the age of twenty-eight days. The former is supposed to be a result of interaction between calcium ion from either hydration reaction or addition of calcium hydroxide powder and arsenic(V) desorbed due to the influence of pH discussed in Part III because desorption of arsenic under the influence of pH is supposed to not consume so long time. In contrast, the latter is supposed to be result of the interaction between calcium ion from either hydration reaction or/and addition of calcium hydroxide powder and desorbed arsenic (V) that was oxidized from arsenic (III) at the surface of the sludge. Oxidation of As(III) to As(V) is possible in cementitious environment because of the fact that, normally, E_h of cement pore fluid is from +100 to + 200 mV. Generally, the principle electroactive species in pore fluid are believed to be oxygen dissolved in mix water and perhaps traces of sulfite, SO_3^{-2}, formed by condensation of kiln vapors which contact the cement during cement clinker cooling (Glasser, 1993). Therefore, the oxidation may gradually take place; that is why the latter form of calcium-arsenic compound was found at the age of 28 days while it was absent at the early age as shown in Figure 4.85. In addition, Figure 4.86 shows the x-ray dot maps of Figure 4.84 to emphasize transformation of arsenic from surface of the sludge to the calcium-arsenic compound. It is clearly seen that the density of arsenic on the surface of the sludge is less than that in calcium-arsenic compound.

In the same way, Figure 4.88 illustrates the grass leaf-like morphology of the calcium arsenic compound detected at the interface between cement paste and the arsenic containing sludge. This figure is analogous to Figure 4.75 but they were recorded at different age; however, it should be noticed that, from the age of 7 days in Figure 4.75 to 28 days in Figure 4.88, ettringite disappeared while calcium arsenic compound was present. This is also a good evidence of transformation of arsenic from the sludge and the formation of the calcium arsenic compound.

In addition to the identifiable compounds discussed above, there are some abnormal morphologies observed at the interface between the sludge and cement paste.

For example, shown in Figure 4.87 is the thin layer of the unidentified compound supposed to be one of the calcium-arsenic compounds. This layer covered the sludge so close that EDS could not distinguish between compositions of the layer and the sludge.

In conclusion, all the possible calcium-arsenic compounds observed in this study together with their morphologies and compositions are summarized in Table 4.24.

Table 4.24 Summation of all the possible calcium-arsenic compounds observed in this study together with their morphologies and compositions by EDS

Sample	Age (days)	Atomic (%)											Ca/As	Morphology
		Ca	Si	O	Fe	As	Na	Mg	Al	K	Cl	Total		
SW4-S25-L04	7	25.24	2.01	44.28	3.25	22.73	0.44	0.16	1.30	0.43	0 17	100	1.11	leafy crystals
SW4-S25-L04	28	16.54	1.56	67.26	3.89	10.31	-	-	-	0.29	0.14	100	1.60	grass leaf-like
SW4-S25-L00	28	38.87	1.96	10.5	3.35	44.68	-	-	-	0.65	-	100	0.87	grass leaf-like

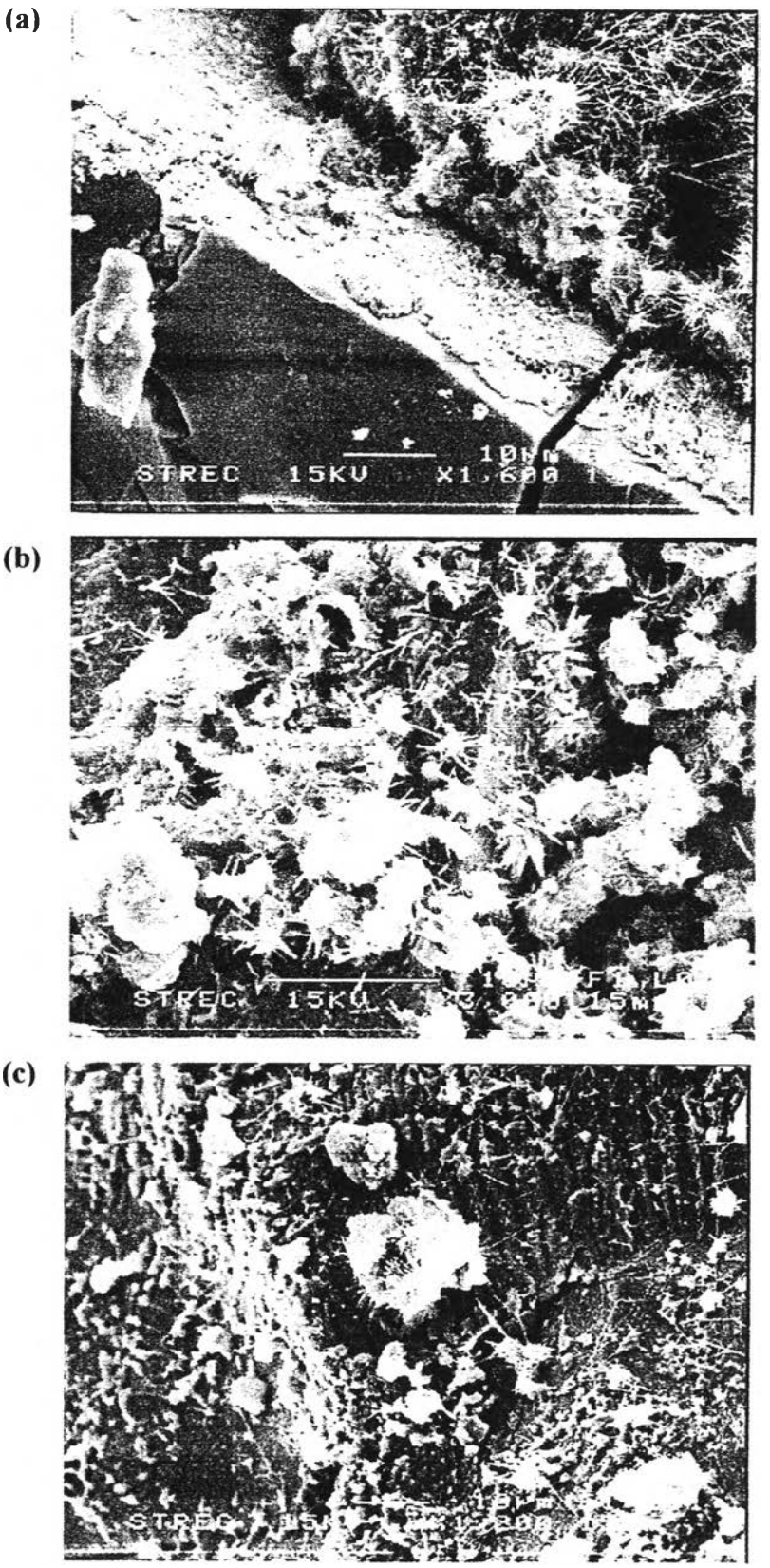

Figure 4.85 SEM Photograph Illustrating Several Hydrated Phases Interfacing with the Arsenic-Iron sludge at the Early Age (3 days) of (a) SW4-S25-L00, (b) SW6-S25-L04, and (c) SW9-S25-L00. It should be noted that there are no calcium-arsenic compound shown in Figure 4.84

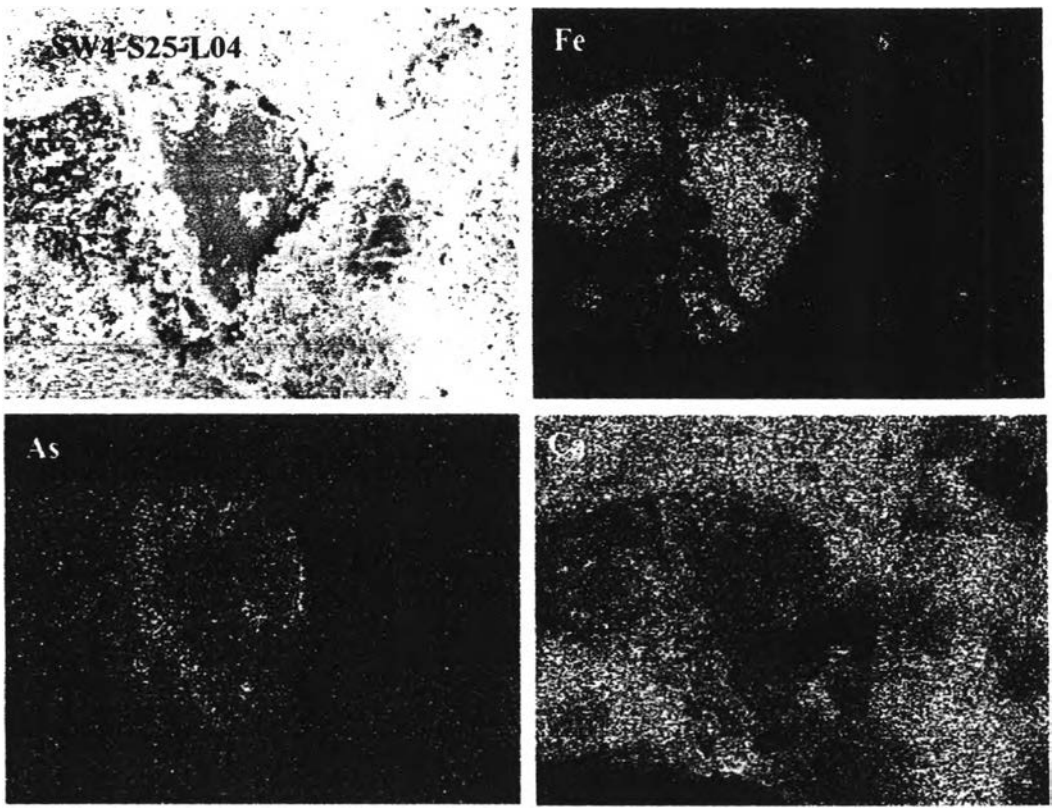

Figure 4.86 The x-ray dot maps of SW4-S25-L04 at the age of 28 days focusing on the arsenic compound formed at the interface zone. It is evident that that density of arsenic on the surface of the sludge is less than that in calcium-arsenic compound. Therefore, transformation of arsenic from surface of the sludge to calcium-arsenic compound is supposed to take place.

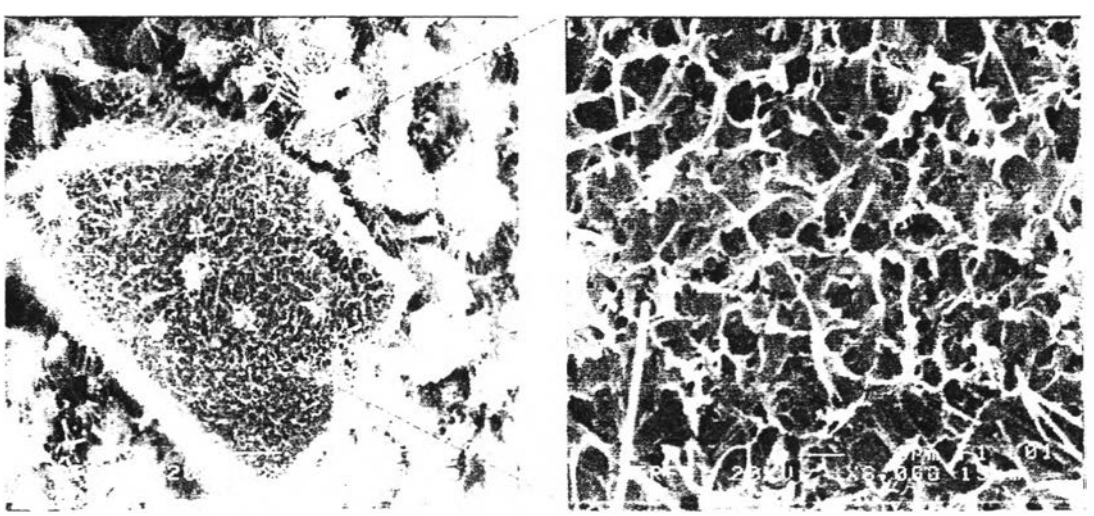

Figure 4.87 (a) SEM photograph of SW4-S25-L00 at the age of 28 days and (b) the same SEM photograph zooming on the thin layer covering the Sludge

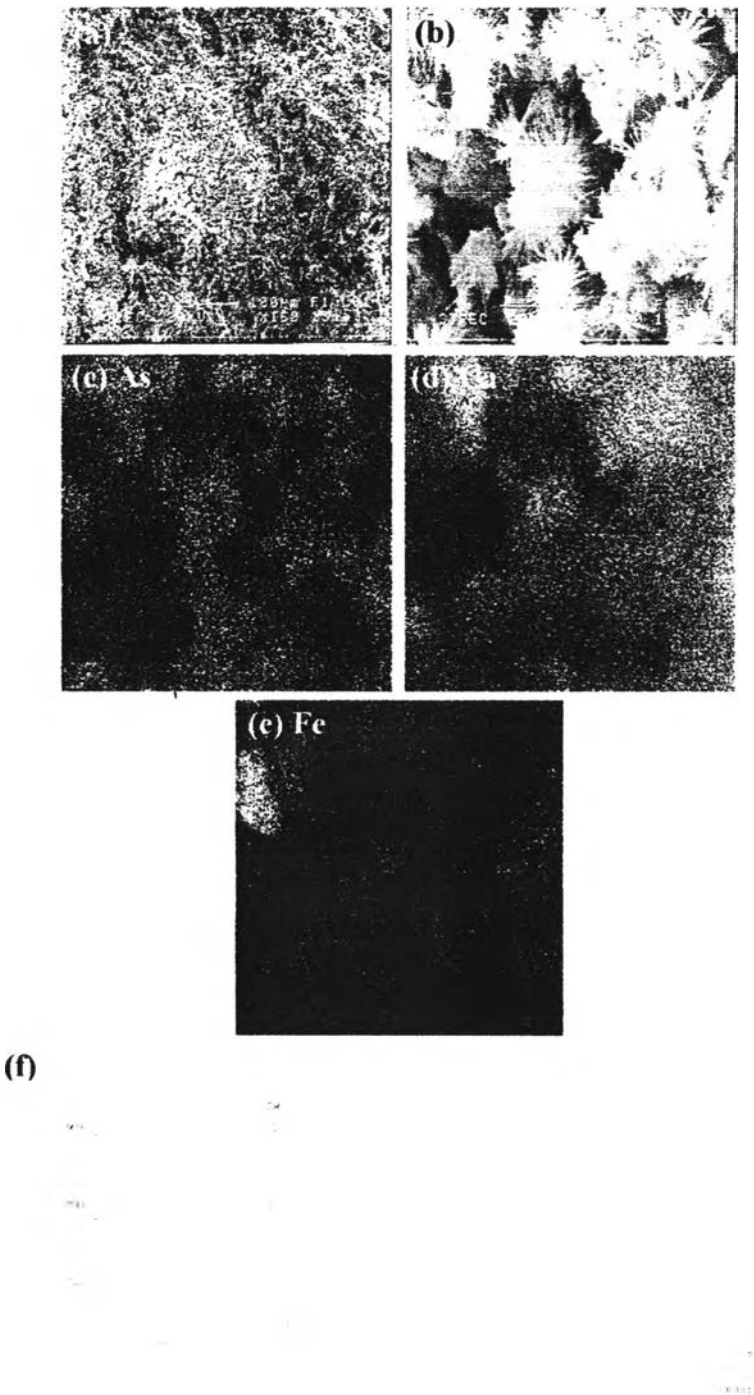

Figure 4.88 (a) SEM photograph of SW4-S25-L00 at the age of 28 days, (b) the same SEM photograph zooming on grass leaf-like microstructures of the calcium arsenic compound, (c), (d) as well as (e) the x-ray dot maps of (b) focusing on As, Ca and Fe respectively, and (f) EDS spectrum pointing on the calcium-arsenic compound to investigate arsenic immobilization potential

PART V

4.10 XRD Application for Examining Hydration Development and the Formation of Calcium-Arsenic Compounds

The XRD spectra of all the control samples for the S/S recipes without the addition of lime are shown in Figures 4.89 to 4.91. The results are shown in chronological order from the age of 3 to 28 days. In the same way, The XRD spectra of the S/S samples without addition of lime are also shown in Figures 4.92 to 4.94.

In these twenty-four spectra of both the control samples and the S/S samples at all ages appears the set of peaks near 4.92, 3.12, 2.63, 1.92, and 1.80 Å (18.0, 28.6, 34.0, 47.2. and 50.6° 2θ) corresponding to $Ca(OH)_2$, Portlandite. In addition, the set of peaks near 3.03, 2.75, 2.60 (overlap with 2.63 Å of Portlandite), and 2.18 Å (29.4, 32.5, 34.4. and 41.4° 2θ) corresponding to Ca_3SiO_5, Alite. as well as that near 2.7494 (overlap with 2.7485 Å of Alite), 2.1897 (overlap with 2.18 Å of Alite), and 1.93 Å (overlap with 1.92 Å of Portlandite) (32.5, 41.2, 46.9° 2θ) corresponding to Ca_2SiO_4, Belite, is present in all samples but varying in intensities. However, there is no sign of the additional peak at at 7.9 Å (11.2° 2θ) in the S/S samples without lime. However, as discussed in Part IV, some SEM photographs of the calcium-arsenic compounds were recorded from the S/S sample without addition of lime. Therefore, it is possible that the calcium-arsenic compounds were formed in the S/S samples without the addition of lime, but their amount might be too little to be detected by XRD.

As discussed in Part III, the indirect method to examine the presence of the calcium-arsenic compounds is comparing the normalized intensities at 2.74 Å of the S/S samples with the intensities at the same *d* spacing of their control samples. If the normalized intensities at 2.74 Å of the S/S samples are more than that of their control samples, the hydration inhibition is supposed to take place, and the calcium-arsenic compounds are supposed to exist in the solidified matrices

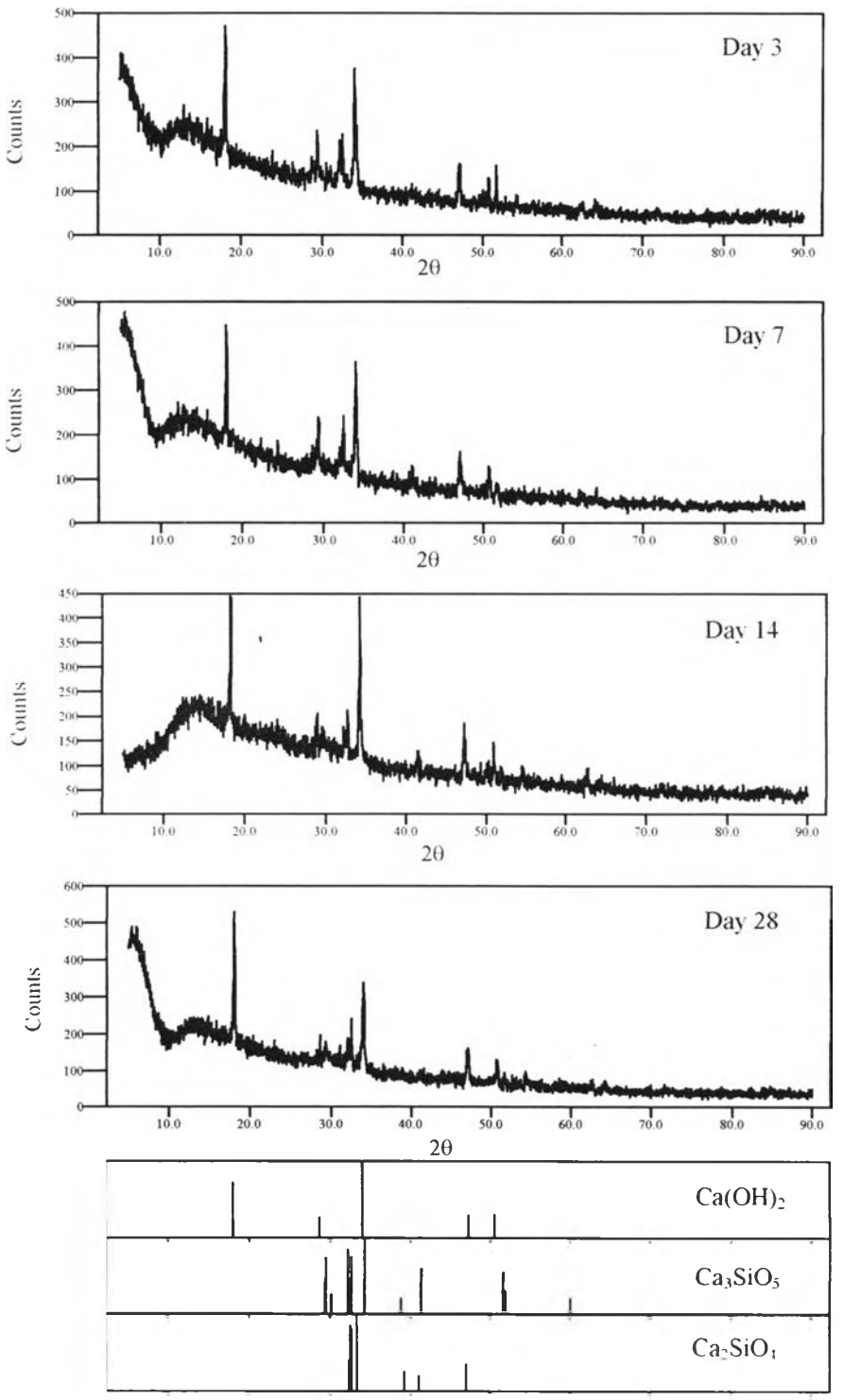

Figure 4.89 X-Ray Diffraction patterns of CW4-S00-L00 at the age of 3, 7, 14, 28, respectively, as well as their possible phases according to 1996 JCPDS International Center for Diffraction Data

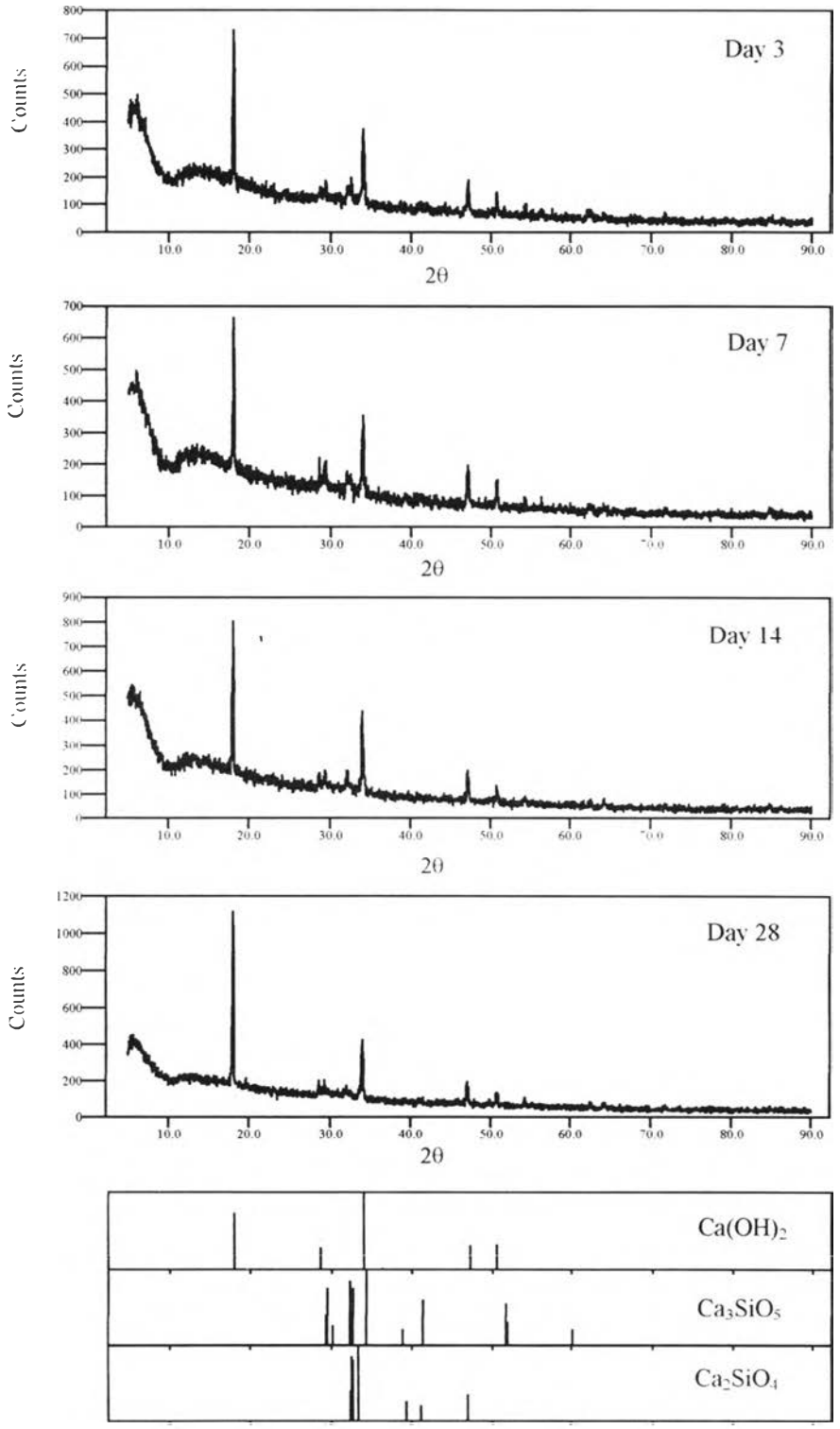

Figure 4.90 X-Ray Diffraction patterns of CW6-S00-L00 at the age of 3, 7, 14, 28, respectively, as well as their possible phases according to 1996 JCPDS-International Center for Diffraction Data

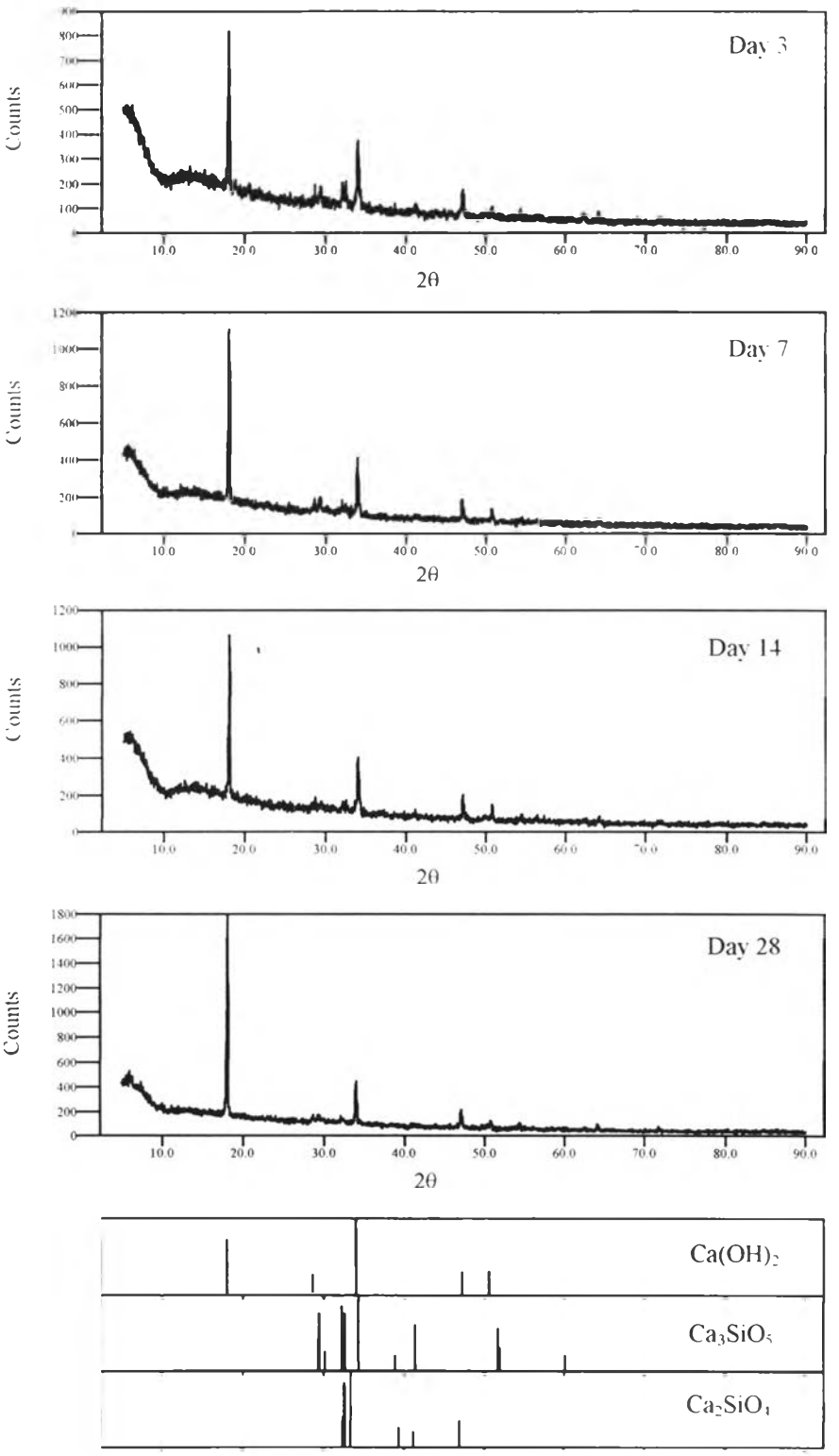

Figure 4.91 X-Ray Diffraction patterns of CW9-S00-L00 at the age of 3, 7, 14, 28, respectively, as well as their possible phases according to 1996 JCPDS-International Center for Diffraction Data

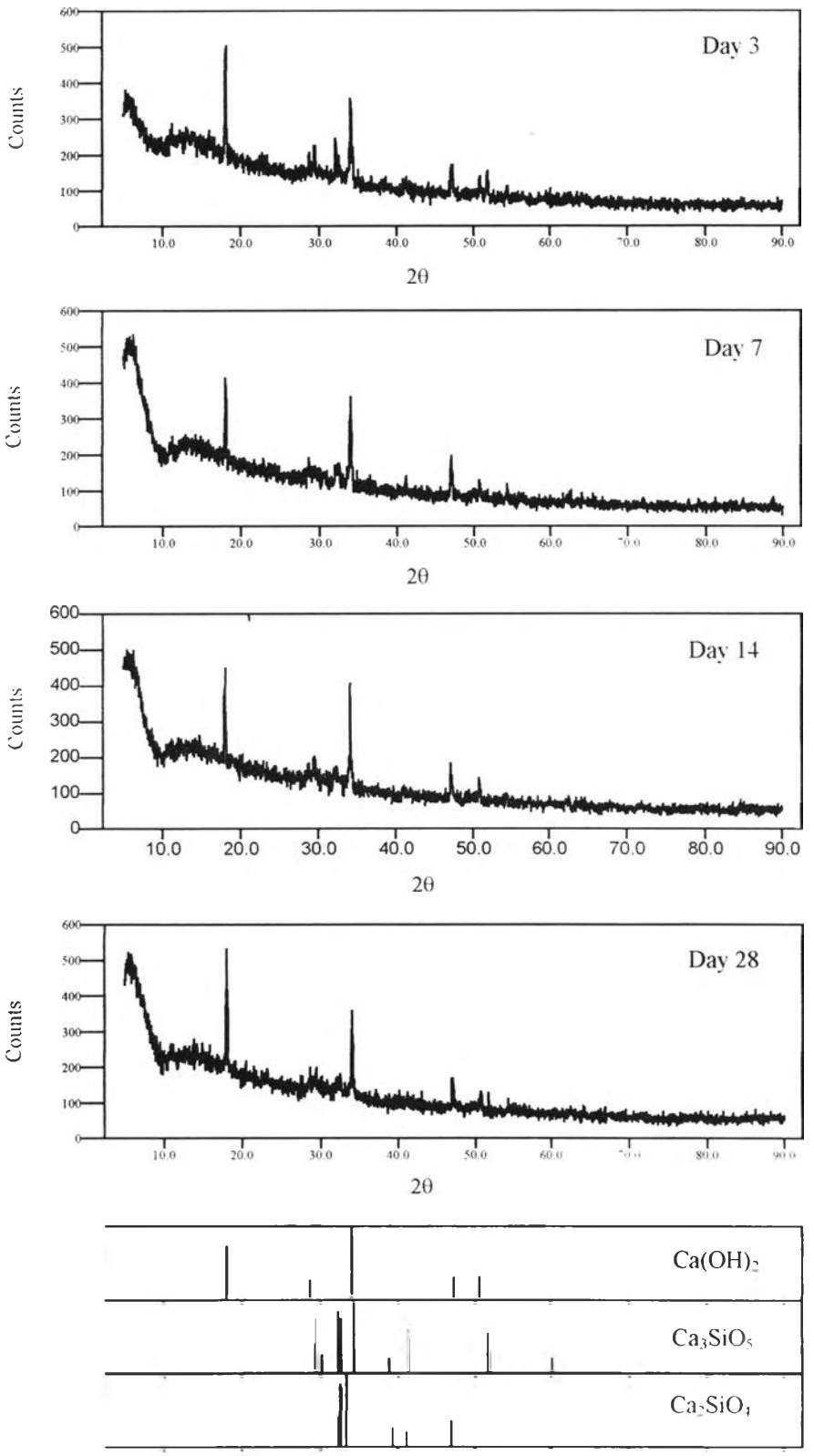

Figure 4.92 X-Ray Diffraction patterns of SW4-S00-L00 at the age of 3, 7, 14, 28, respectively, as well as their possible phases according to 1996 JCPDS-International Center for Diffraction Data

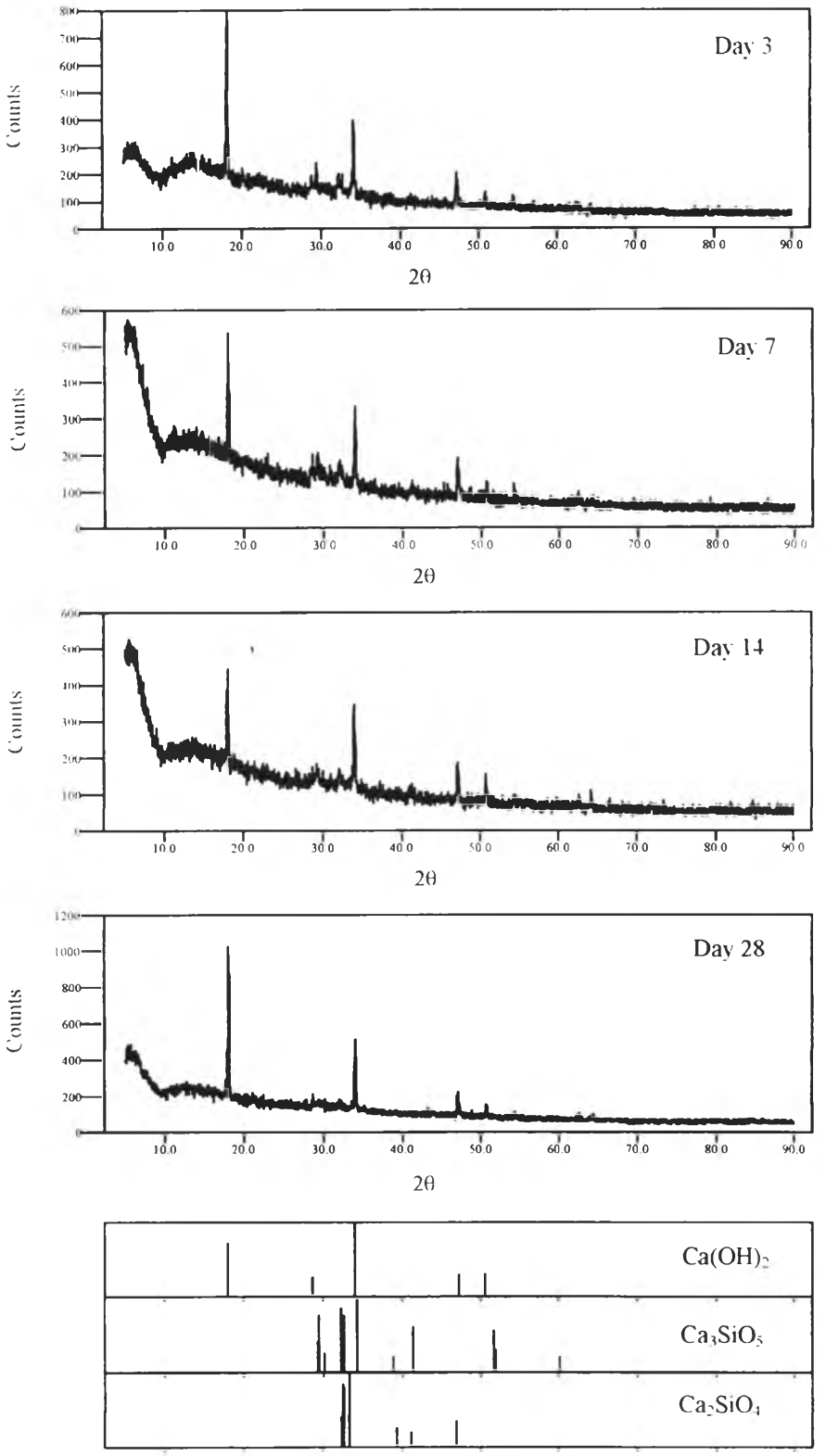

Figure 4.93 X-Ray Diffraction patterns of SW6-S00-L00 at the age of 3, 7, 14, 28, respectively, as well as their possible phases according to 1996 JCPDS-International Center for Diffraction Data

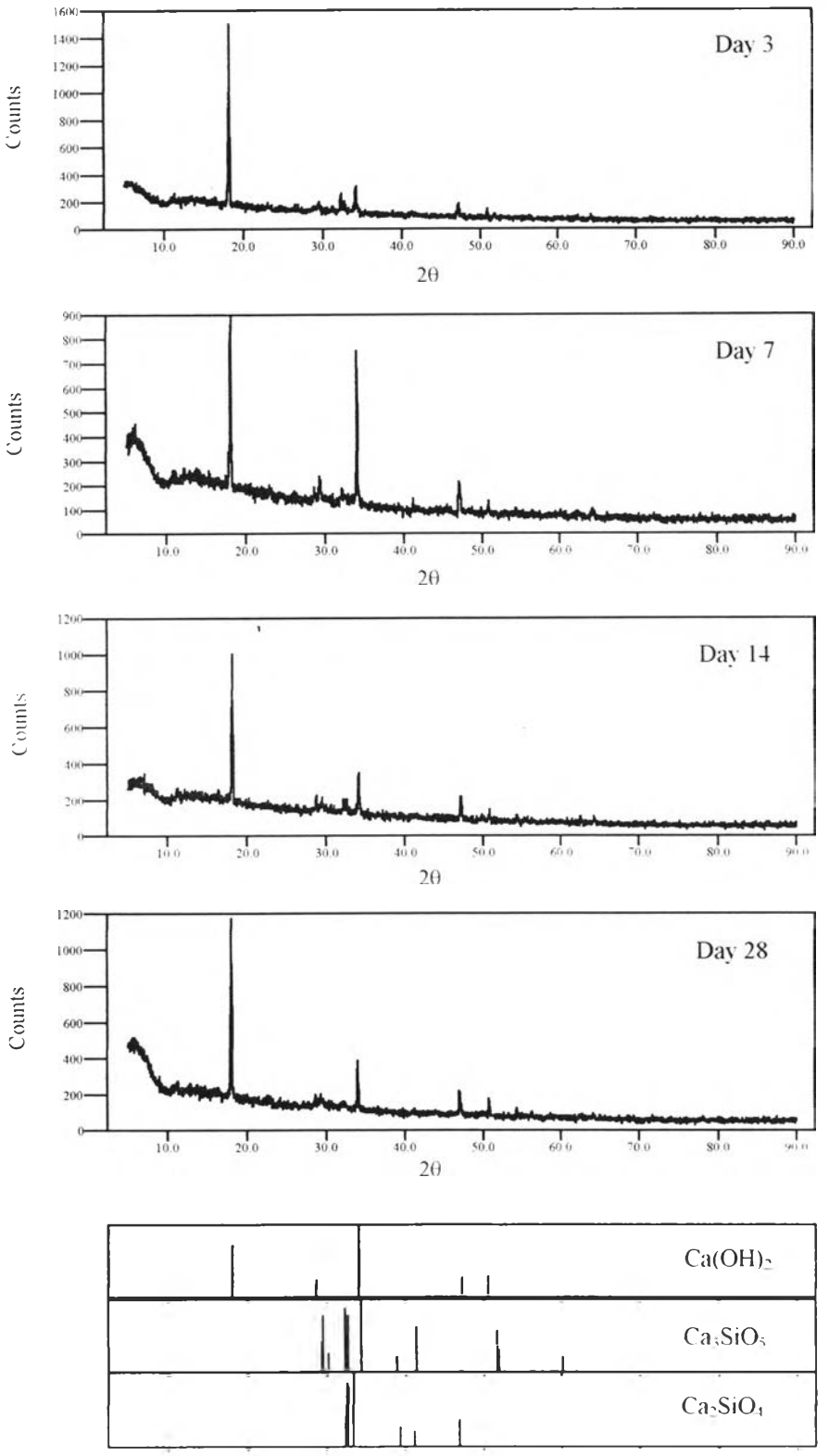

Figure 4.94 X-Ray Diffraction patterns of SW9-S00-L00 at the age of 3, 7, 14, 28, respectively, as well as their possible phases according to 1996 JCPDS International Center for Diffraction Data

Figures 4.95 to 4.97 illustrate the histograms comparing the intensities at 2.74 Å (32.5° 2θ) of the control samples to those of the S/S samples. According to Figure 4.95, although the normalized intensity at 2.74 Å (32.5° 2θ) of SW4-S25-L00 at the age of 3 days is more than that of the control samples at the same age, the intensities 2.74 Å (32.5° 2θ) of SW4-S25-L00 at the age of 7 and 28 days are slightly less than those of their control samples at the same age. This indicates that the average intensity of SW4-S25-L00 at all age might be not significantly different from that of CW4-S00-L00. Therefore, the hydration inhibition is not supposed to take place and the amount of the calcium-arsenic compounds possibly formed in the matrices might be too little to cause negative effects to the mechanical property of the solidified products. This observation is in good agreement with the conclusion in PART III concerning SW4-S25-L00 at 28 days.

In contrast, considering the histograms comparing the intensities at 2.74 Å (32.5° 2θ) of CW6-S00-L00 to those of SW6-S25-L00 shown in Figure 4.96 as well as the histograms comparing the intensities at 2.74 Å (32.5° 2θ) of CW9-S00-L00 to those of SW9-S00-L00 shown in Figures 4.97, it is clearly seen that the normalized intensities at 2.74 Å of SW6-S25-L00 as well as SW9-S25-L00 at all ages are more than those of their control samples at the same age. This indicates that the hydration inhibition might take place and the formation of the calcium-arsenic compounds was possible. This also implies that the amount of the calcium-arsenic compounds formed in these two samples was too little to be detected by XRD but enough to cause hydration inhibition.

This observation implies that not only the addition of lime but also the amount of water added influence the formation of the calcium-arsenic compounds in the solidified matrices. Without the addition of lime and at the same amount of waste added, the S/S recipes of which water-to binder are 0.6 and 0.9 show the formation potential of a significant amount of the calcium-arsenic compounds while the opposite is true for the S/S recipes of which water-to binder is 0.4. The rational explanation for the influence of a water-to-binder ratio on the formation of these insoluble compounds concerns the relationship between a water-to-binder ratio and porosity as well as the

pore size distribution in the cementitious system. On the ground that the more the water-to-binder ratio, the more porosity the system, the increase of porosity of the matrices by increasing water-to-binder ratios might facilitate transport of the desorbed arsenic to react with calcium ions in the system. The easier the transport of desorbed arsenic, the less competition for calcium with other hydration products, and the more possibility of the formation of calcium-arsenic compounds.

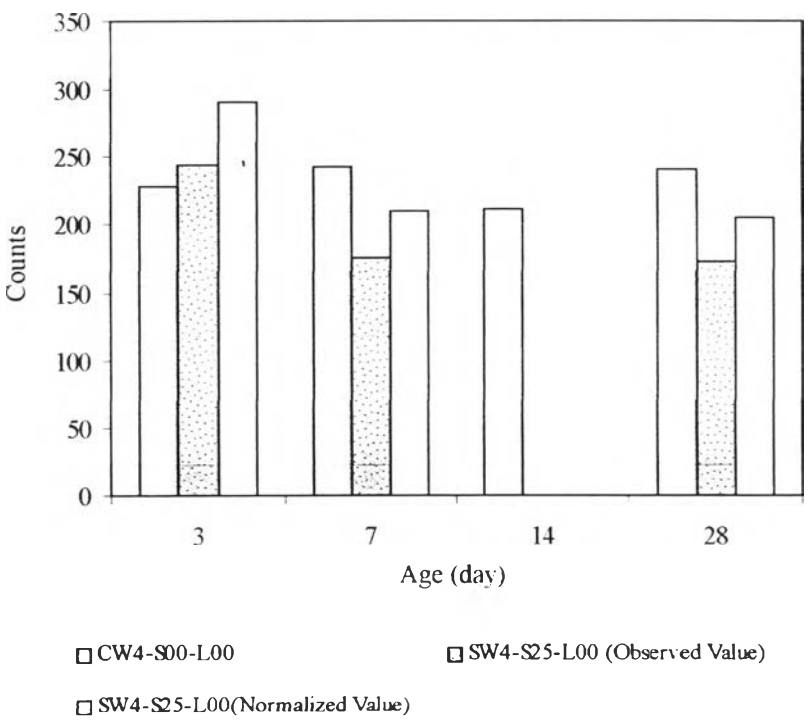

Figure 4.95 Histograms illustrating observed intensities at 2.74 Å of CW4-S00-L00 and SW4-S25-L00 as well as intensities at the same *d*-spacing of SW4-S25-L00 normalized by 0.837. The results are recorded at 3, 7, 14, 28 days.

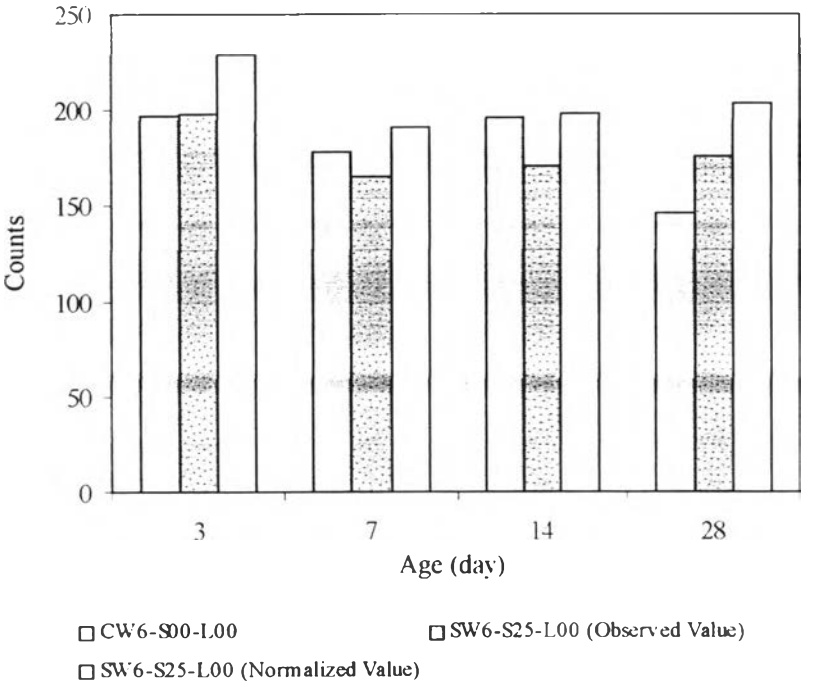

Figure 4.96 Histograms illustrating observed intensities at 2.74 Å of CW6-S00-L00 and SW6-S25-L00 as well as intensities at the same *d*-spacing of SW6-S25-L00 normalized by 0.865. The results are recorded at 3, 7, 14, 28 days.

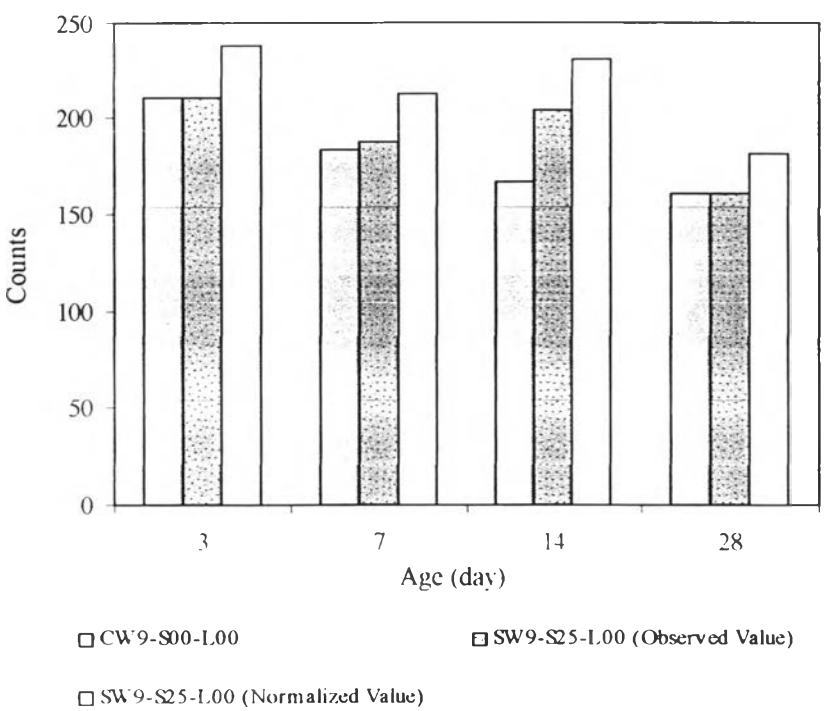

Figure 4.97 Histograms illustrating observed intensities at 2.74 Å of CW9-S00-L00 and SW9-S25-L00 as well as intensities at the same *d*-spacing of SW9-S25-L00 normalized by 0.884. The results are recorded at 3, 7, 14, 28 days.

Figures 4.98 to 4.100 illustrate the XRD spectra of all the control samples for the S/S recipes with the addition of lime. In the same way, The XRD spectra of the S/S samples with the addition of lime are shown in Figures 4.101 to 4.103. Like the spectra of the S/S recipes without the addition of lime and their control samples, the sets of peak corresponding to Portlandite, Alite, and Belite appear in all samples of the S/S recipes with the addition of lime and their controls. However, owning to the fact that forty- percent of cement in the S/S recipes with the addition of lime was substituted by lime, the amount of cement in these samples was relatively low. Therefore, not all of the peaks appearing in the S/S recipes without addition of lime exist in the S/S recipes with the addition of lime. For example, after undergoing hydration, the remaining amount of Alite and Belite was very limited, so the intensities of some peaks of these compounds, such as the peak at 2.74 Å, are lower than background and not present in the spectra. However, the other peaks of these compounds are present, so XRD is still able to identify these compounds. In addition, the absence of the peak at 2.74 Å in all the S/S recipes with addition lime makes it impossible to examine the hydration inhibition by comparing the intensity of this peak in the S/S samples to that in their control samples as done for the S/S recipes without the addition of lime.

However, the additional strong peak, approximately, at 7.9Å corresponding to the calcium-arsenic compounds appears in all the S/S recipes with lime, but it is absent in their control samples. This observation is in good agreement with conclusion in PART III in that addition of lime is the major factor encouraging the formation of calcium-arsenic compounds in the matrices. For this reason, the hydration inhibition is supposed to take place in all S/S recipes with lime due to the presence of the calcium-arsenic compounds.

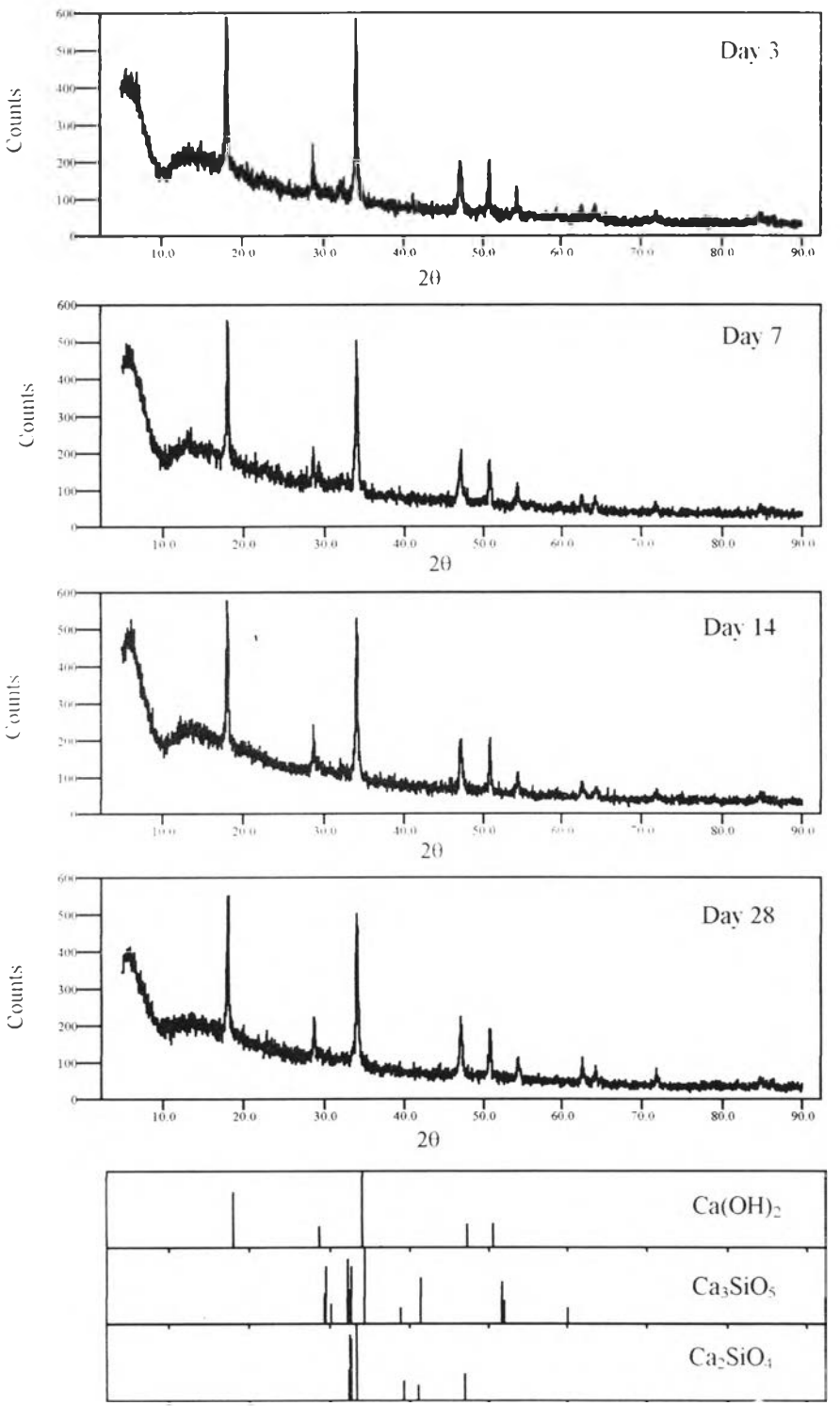

Figure 4.98 X-Ray Diffraction patterns of CW4-S00-L04 at the age of 3, 7, 14, 28, respectively, as well as their possible phases according to 1996 JCPDS-International Center for Diffraction Data

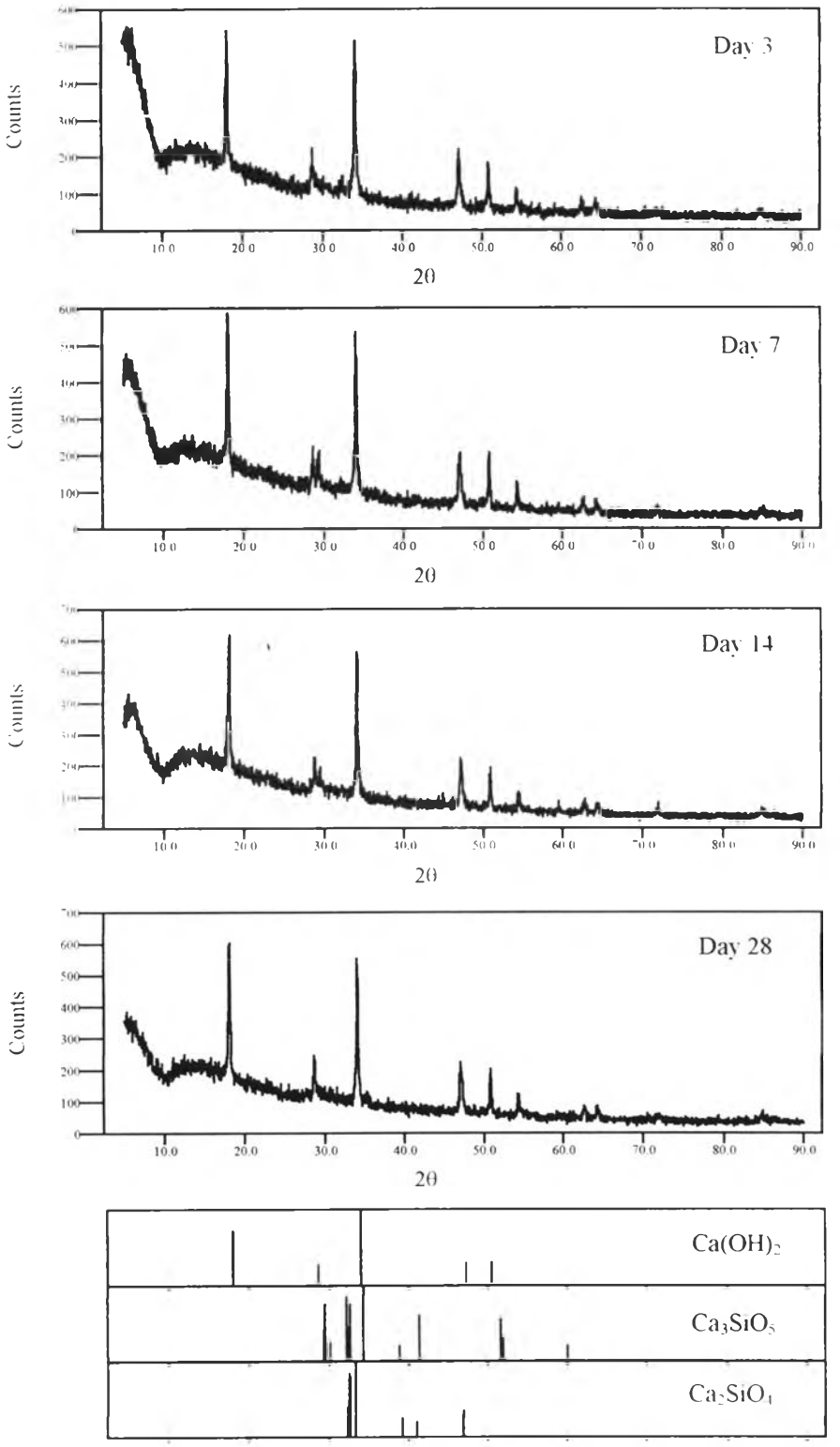

Figure 4.99 X-Ray Diffraction patterns of CW6-S00-L04 at the age of 3, 7, 14, 28, respectively, as well as their possible phases according to 1996 JCPDS-International Center for Diffraction Data

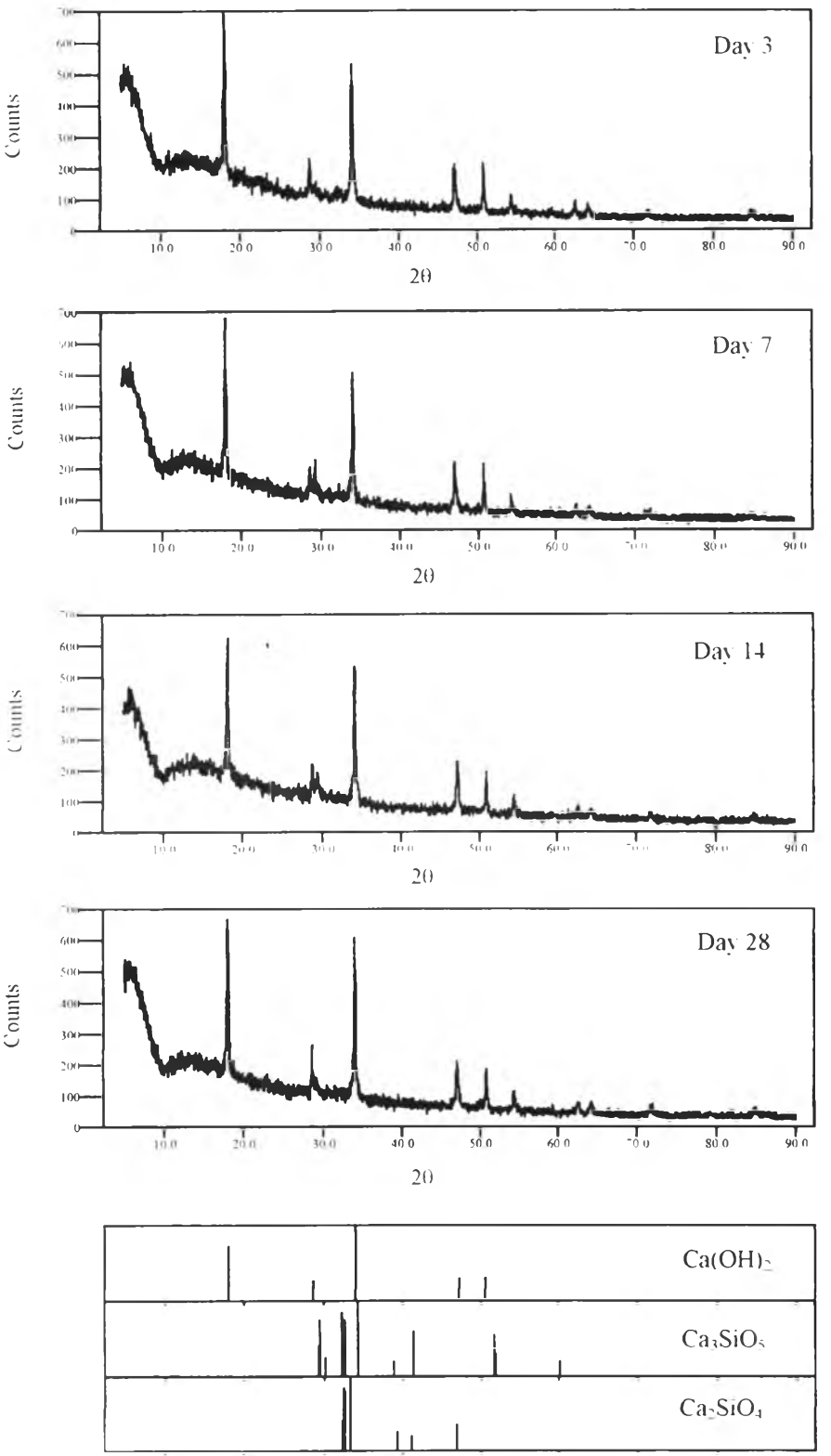

Figure 4.100 X-Ray Diffraction patterns of CW9-S00-L04 at the age of 3, 7, 14, 28, respectively, as well as their possible phases according to 1996 JCPDS-International Center for Diffraction Data

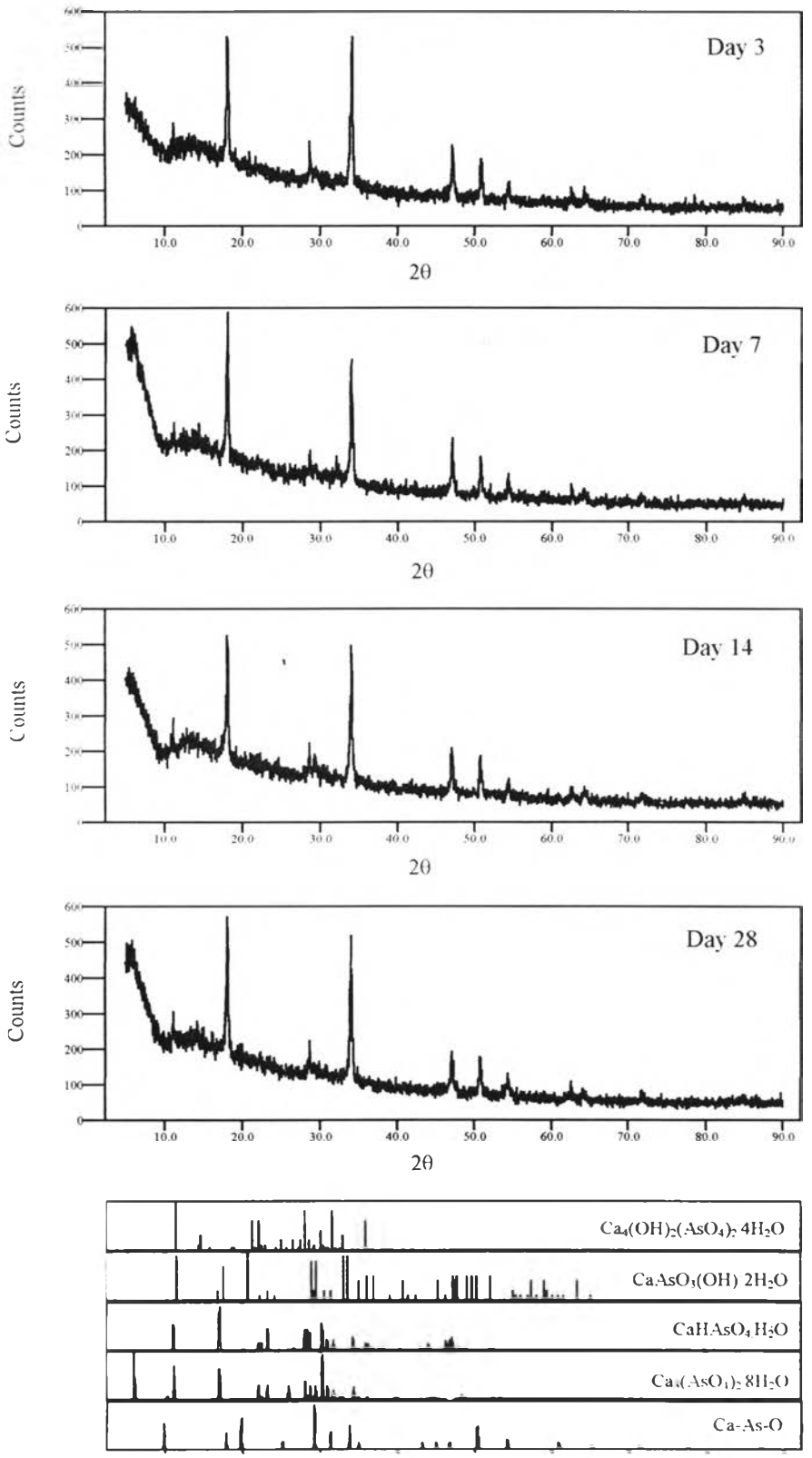

Figure 4.101 X-Ray Diffraction patterns of SW4-S25-L04 as well as their possible phases, besides $Ca(OH)_2$, Ca_3SiO_5, and Ca_2SiO_4, according to 1996 JCPDS-International Center for Diffraction Data

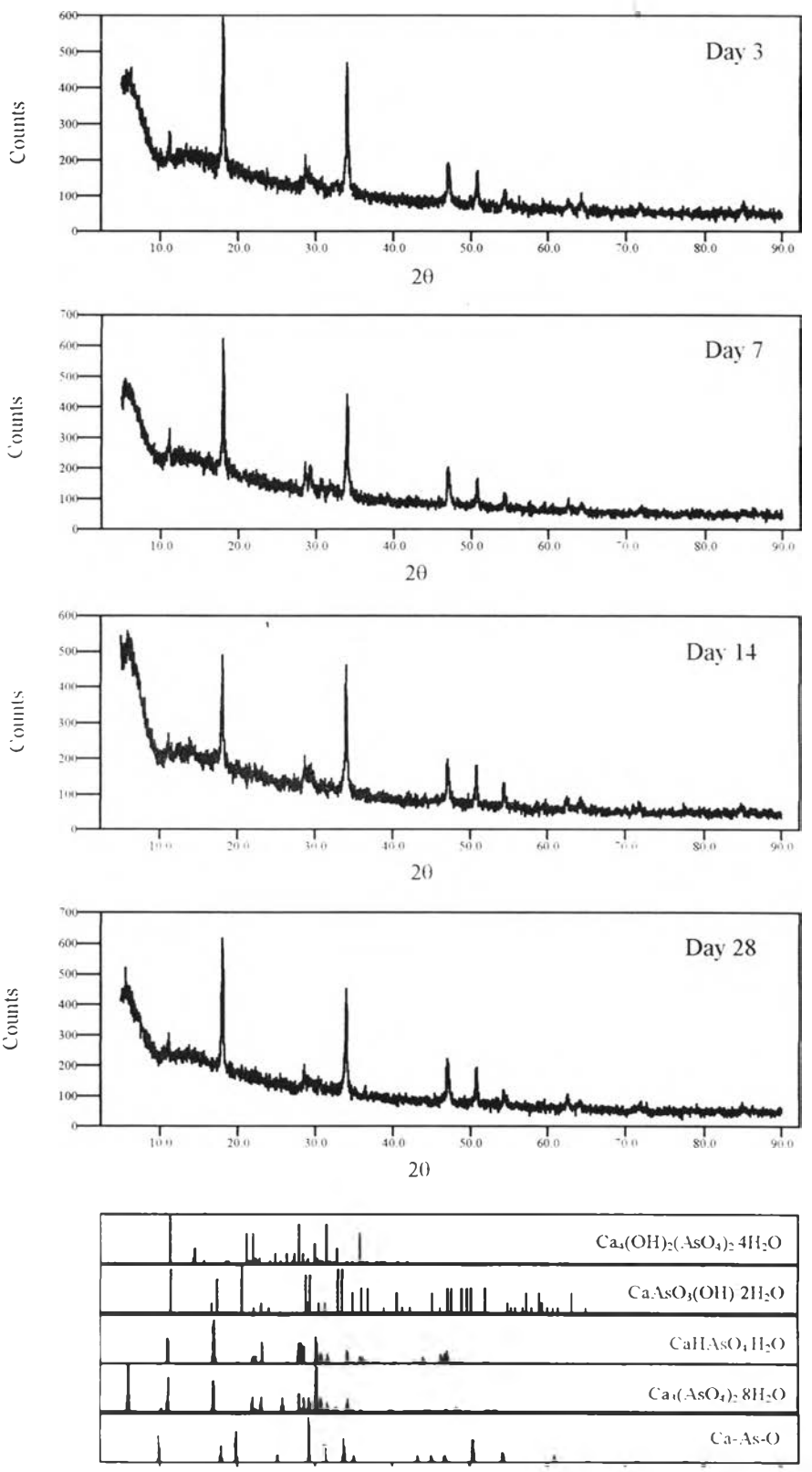

Figure 4.102 X-Ray Diffraction patterns of SW6-S25-L04 as well as their possible phases, besides $Ca(OH)_2$, Ca_3SiO_5, and Ca_2SiO_4, according to 1996 JCPDS-International Center for Diffraction Data

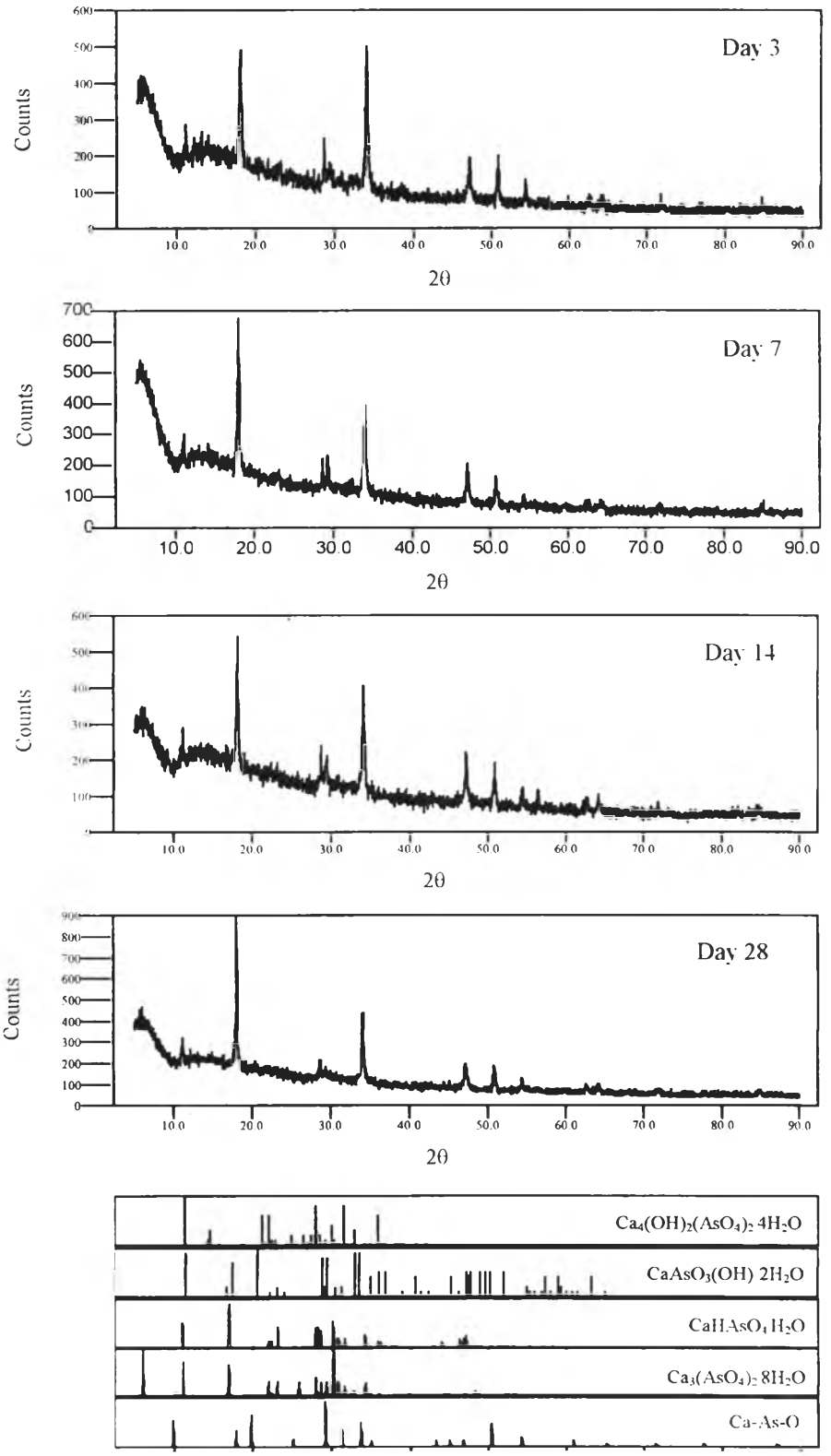

Figure 4.103 X-Ray Diffraction patterns of SW9-S25-L04 as well as their possible phases, besides $Ca(OH)_2$, Ca_3SiO_5, and Ca_2SiO_4, according to 1996 JCPDS-International Center for Diffraction Data

Considering Figures 4.104 and 4.105 illustrating the intensities of the peak at 7.9 Å as the function of time, it is evident that, at the age of 3 days, the intensities of this peak are around 95%, 84%, and 89% of the highest intensity at this *d*-spacing for SW4-S25-L04, SW6-S25-L04, and SW9-S25-L04, respectively. Moreover, from the age of 3 days to 28 days, the increase of the intensities at this peak is very limited. This implies that most of calcium-arsenic compounds were formed before the age of 3 days. Therefore, the remobilization mechanism of arsenic responsible for the formation of the calcium-arsenic compounds at the age of 3 days should be desorption of arsenic due to the influence of pH in the cementitious environment owning to the fact that the desorption by this mechanism is supposed to consume no long time and most of arsenic is supposed to remobilize by this mechanism. While the remobilization mechanism of arsenic responsible for the formation of the calcium-arsenic compounds from 3 days to 28 days might be diffusion and/or oxidation of arsenite to arsenate owning to the fact that they are supposed to consume longer time and only little of arsenic is supposed to remobilize by these mechanism

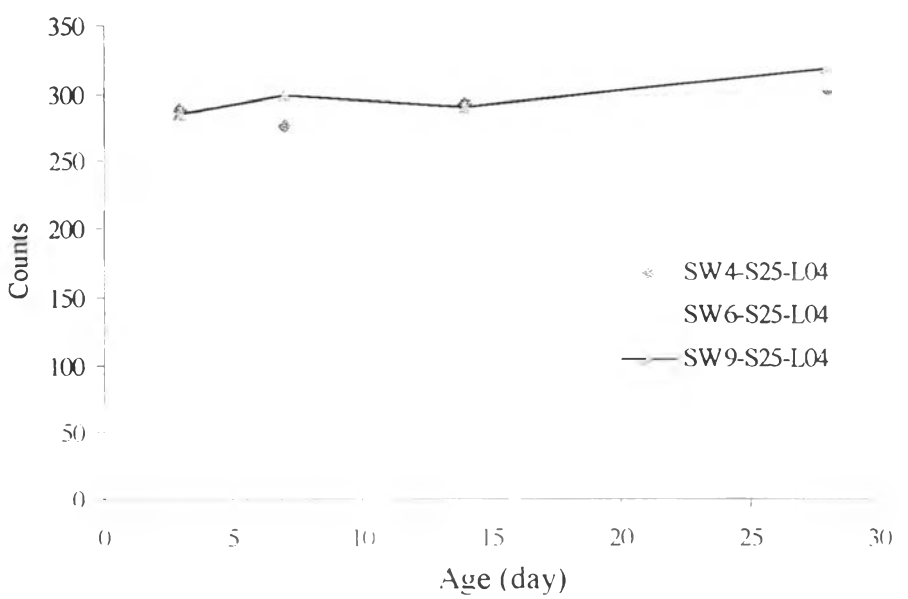

Figure 4.104 Comparison among intensity at 7.90 Å of SW4-S25-L04, SW6-S25-L04, and SW9-S25-L04

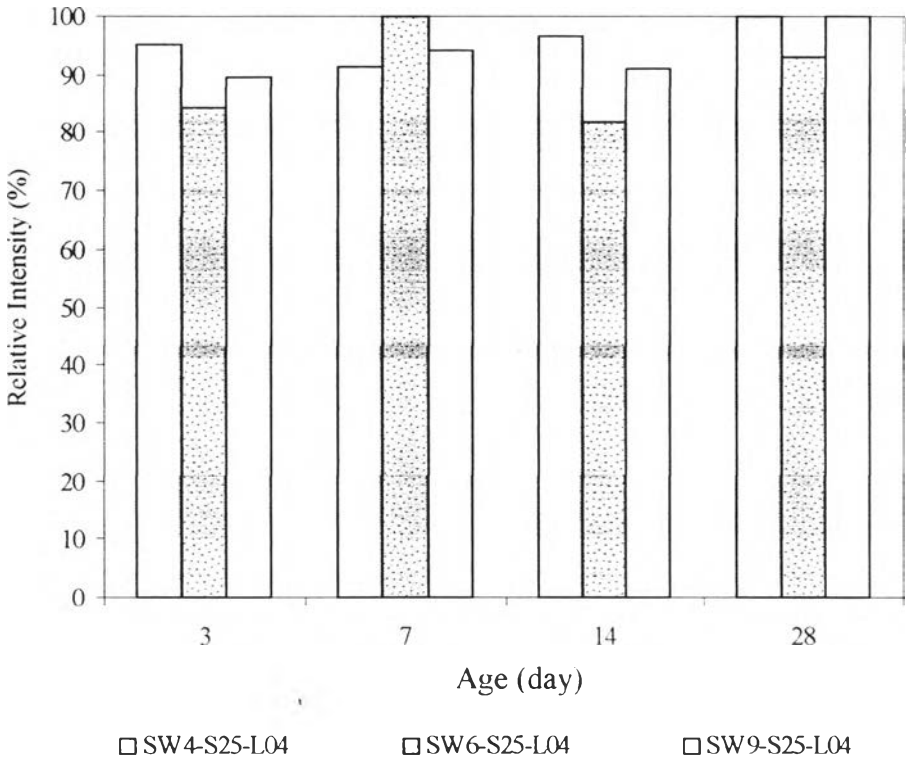

Figure 4.105 Comparison among relative intensity (%) at 7.90 A of SW4-S25-L04, SW6-S25-L04, and SW9-S25-L04

4.11 Compressive Strength Development of the Solidified/Stabilized Waste Form

Figure 4.106 illustrats the UCS of the S/S recipes of which the water-to-binder ratio is 0.4 as well as their control samples as a function of time at 3, 7, 14, and 28 days. In the same way, Figures 4.107 and 4.108 show the UCS of the S/S recipes of which the water-to-binder ratios are 0.6 and 0.9, respectively, as well as their control samples as a function time. Considering these graphs, it is clearly seen that for the S/S recipes of which the addition of lime is the same- for example SW4-S25-L04, SW6-S25-L04, and SW9-S25-L04 and so on- the higher the water-to-binder ratio, the lower the USC. This is due to the fact that the higher the water-to-binder ratio, the more porosity the matrices.

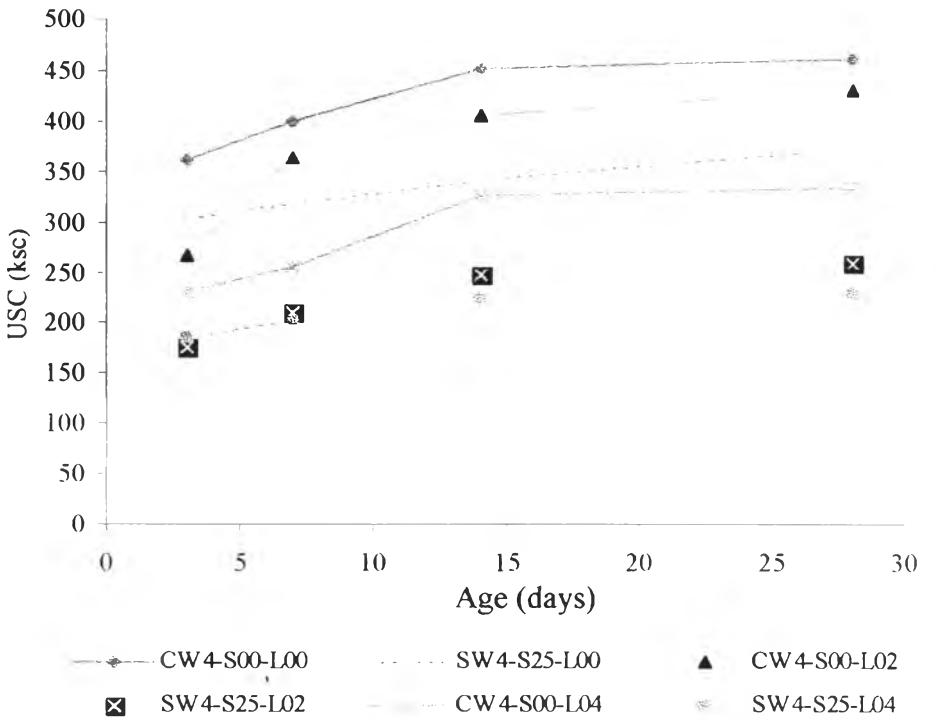

Figure 4.106 the USC of the S/S samples and their control samples of which water-to-binder ratio is 0.4 at 3, 7, 14, 28 days

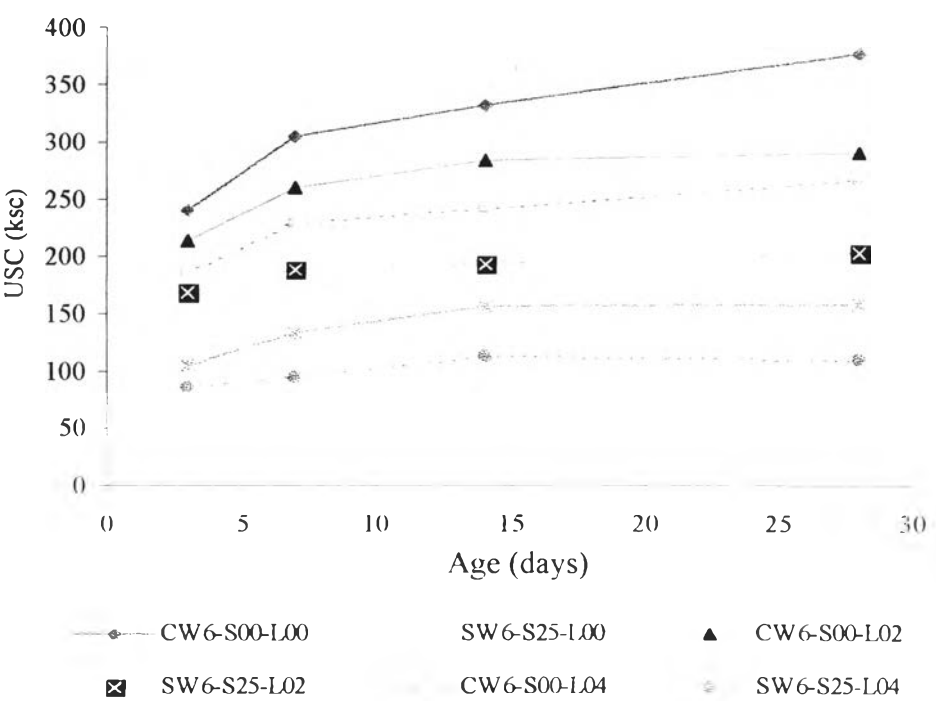

Figure 4.107 the UCS of the S/S samples and their control samples of which water-to-binder ratio is 0.6 at 3, 7, 14, 28 days

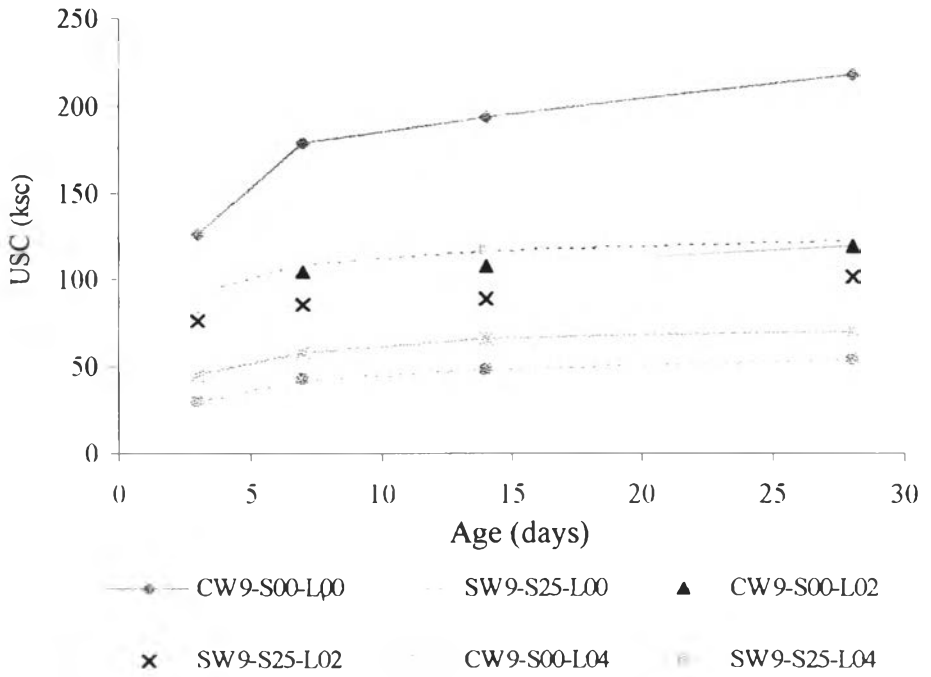

Figure 4.108 the UCS of the S/S samples and their control samples of which water-to-binder ratio is 0.9 at 3, 7, 14, 28 days

Similarly, according to the same graphs, it is evident that for the S/S recipes of which the water-to-binder ratio is the same- for example, SW4-S25-L00, SW4-S25-L02, and SW4-S25-L04 and so on-the more the addition of lime, the lower the USC. This is due to the fact that the more the addition of lime, the less the amount of cement undergoing hydration, and the higher the potential to form calcium-arsenic compounds.

According to PART III, it is concluded that the addition of arsenic containing sludge could reduce the UCS of the mortars in two manners: (1) as an inert substitute by reducing the amount of cement undergoing hydration and reducing baring areas by macroencapsulation, and (2) as an active substitute by the hydration inhibition. Considering Figure 4.109 illustrating the plotting of the reduction of the UCS of the S/S recipes of which water-to-binder ratio is 0.4 in comparison to their control samples at the same age, it is found that the reduction of the UCS of SW4-S25-L00 is

around 16 to 24%. According to the previous section, it is concluded that hydration inhibition is not supposed to occur in SW4-S25-L00. Therefore, This 16 to 24% of the UCS reduction should be a result of reducing the amount of cement undergoing hydration and reducing baring areas by macroencapsulation. In contrast, the reduction of the USC of SW4-S25-L04 is around 19 to 31% while the previous section concludes that the hydration inhibition possibly took place in these S/S recipes due to the formation of calcium-arsenic compounds. Therefore, this 3 to 7% surplus of the UCS reduction is supposed to be a result of hydration inhibition due to formation of calcium-arsenic compound.Similarly, as shown in Figures 4.110 and 4.111 the reductions of the UCS of SW6-S25-L00, SW6-S25-L04, SW9-S25-L00, and SW9-S25-L04 are 23 to 29%, 16 to 31%, 26 to 43%, and 23 to 31%, respectively, while the previous section suggests that the hydration inhibition possibly took place in these S/S recipes. Therefore, these surpluses (5 to 6% for SW6-S25-L00, 0 to 6% for SW6-S25-L04, 10 to 18% for SW9-S25-L00, and 7 % for SW9-S25-L04) are supposed to be a result of the hydration inhibition due to the formation of calcium-arsenic compounds.

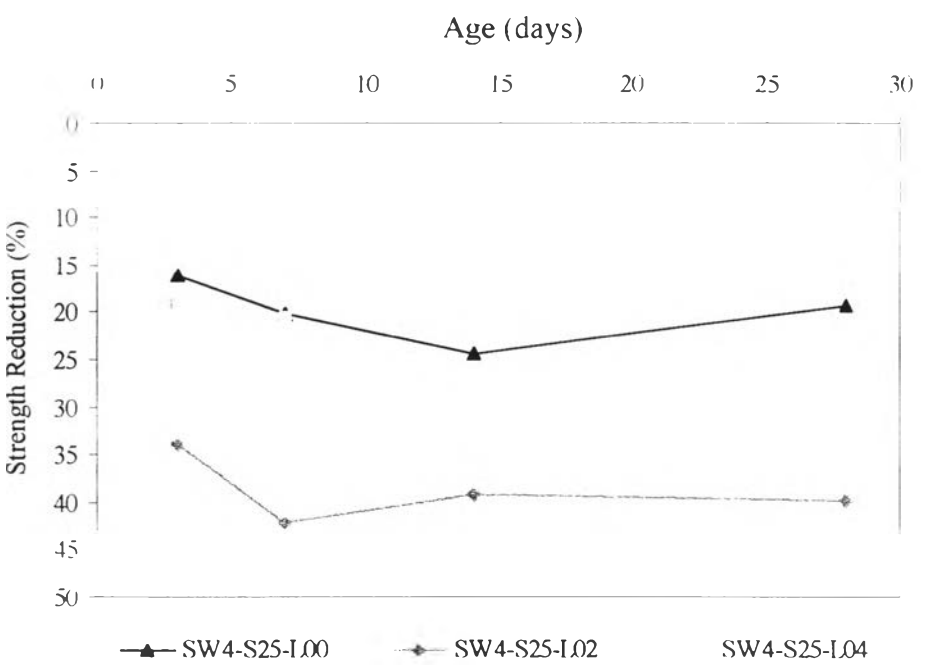

Figure 4.109 Reduction of the UCS of the S/S recipes of which water-to-binder ratio is 0.4 in comparison to their control samples at the same age

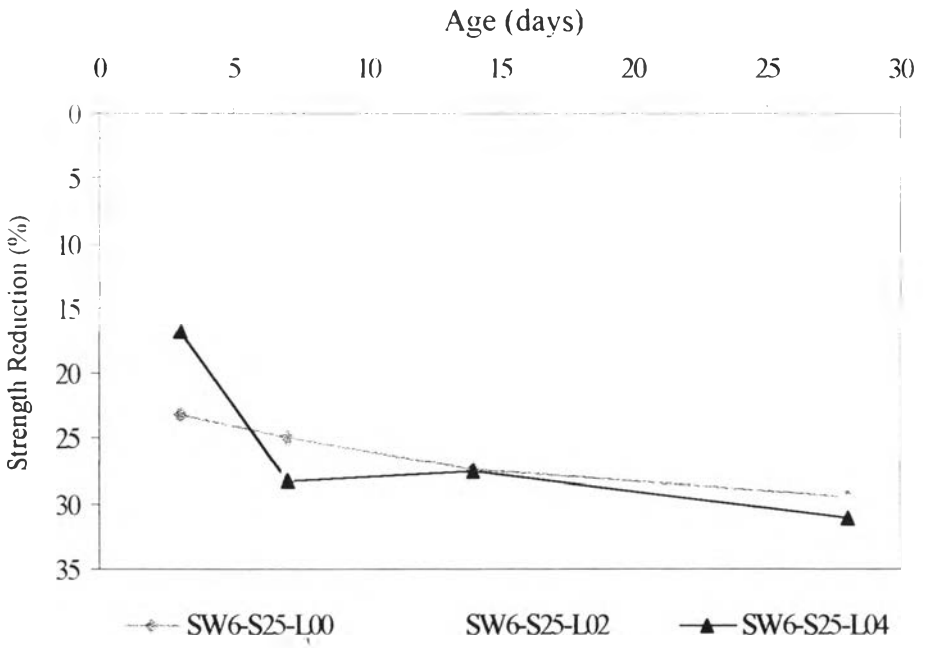

Figure 4.110 Reduction of the USC of the S/S recipes of which water-to-binder ratio is 0.6 in comparison to their control samples at the same age

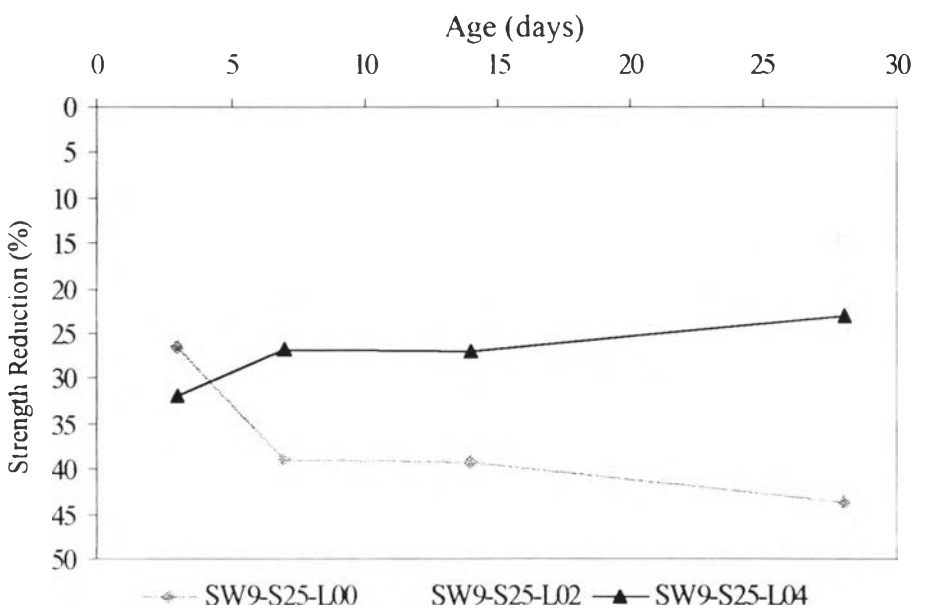

Figure 4.111 Reduction of the USC of the S/S recipes of which water-to-binder ratio is 0.9 in comparison to their control samples at the same age

4.12 Leaching Characteristics of the Solidified/Stabilized Sludge as a Function of Water-to Binder Ratio and Lime-to Binder Ratio

According to Part III, the leaching characteristics of the solidified/stabilized arsenic-iron hydroxide sludge as a function of waste-to-binder ratio have already been discussed. Therefore, the leaching characteristics of solidified/stabilized arsenic-iron hydroxide sludge as a function of water-to-binder ratios and lime-to-binder ratios at one fixed waste-to-binder ratio, which is 0.25, are discussed in this section.

The extraction results by the two types of leaching procedures on the nine different solidification/stabilization recipes are illustrated in Figures 4.112 to 4.113 in which the concentrations (mg/L) of As and Ca are given along with pH of the leachate. According to Figure 4.113 and 4.114, it is clearly seen that concentrations of calcium as well as the pH of the leachate from all S/S recipes are insignificantly different. This observation is in good agreement with the statistical analysis by SPSS 11.0.0, which indicates that there are no relationship among concentrations of calcium in leachate, water-to-binder ratios, and lime-to-binder ratios. The same conclusion is true for the pH of leachate. It should be noticed that the average concentration of calcium and the average pH in the leachate imply the saturation of calcium.

As concluded in Part III, the leachability of arsenic from the arsenic-iron hydroxide sludge is a function of waste-to-binder ratio, pH, and calcium reservoir. For this reason, owning to the fact that water-to-binder ratios and lime-to-binder ratios have no significant influence on calcium concentration and pH of leachate, as discussed in the previous paragraph, together with the fact that the pH of the leachate of all S/S recipes are the same, and calcium reservoir is available in all S/S recipes, it is not surprising that the arsenic concentrations in leachate of all S/S recipes are insignificantly different. This conclusion is in good agreement with the statistical analysis by SPSS 11.0.0, which indicates that there are no relationship between among concentration of arsenic in leachate, water-to-binder ratio, and lime-to-binder ratio

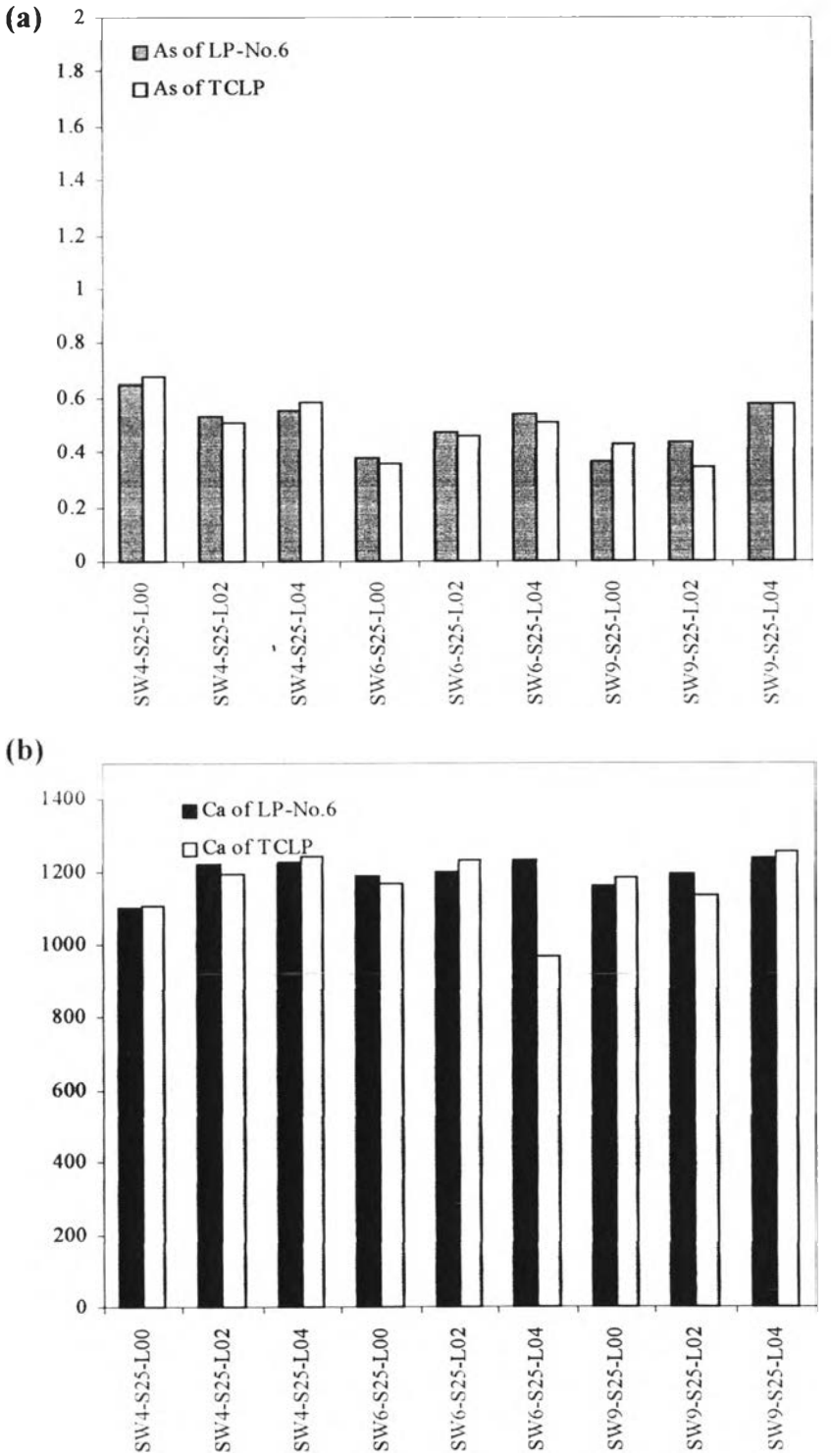

Figure 4.112 Histograms illustrating concentration of (a)arsenic and (b) calcium in leachate of nine different S/S recipes extracted by the TCLP and LP-No 6

In conclusion, the combination of examining the leachate characteristics in this section together that in Part III comes into the conclusion that, under the saturation of calcium of which pH is higher than 12 and calcium concentration is more than 1,200 mg/L, only waste-to-binder ratios influence the leachability of arsenic from the arsenic-iron hydroxide sludge. Moreover, it should be noticed that, as shown in Figures 4.112 and 4.113, the concentration of arsenic in the leachate subjected to TCLP is not significantly different from that submitted to LP-No.6 of the same recipe. This observation helps ensure the conclusion regarding indifference between arsenic extractability of TCLP and that of LP-No.6.

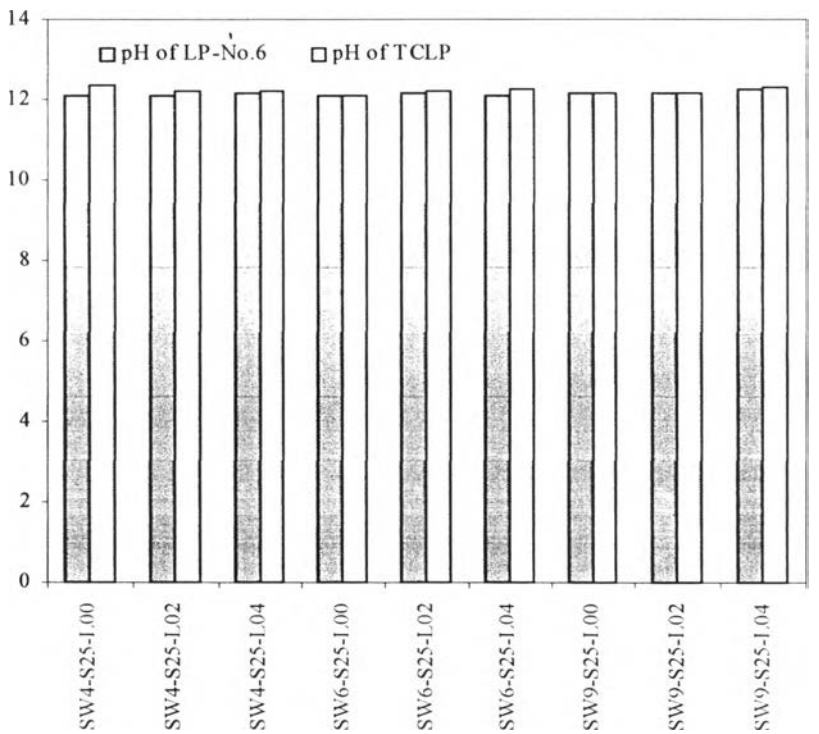

Figure 4.113 Histograms illustrating pH in leachate of nine different S/S recipes extracted by the TCLP and LP-No.6

Part VI

4.13 Framework for Evaluation of Arsenic-Iron Hydroxide Sludge Management Options

The studies of the leaching behavior of arsenic from the dewatered and the dried arsenic-iron hydroxide sludge discussed in Part I and the investigation of utilization potential of the solidified/stabilized arsenic-iron hydroxide sludge discussed in Part III help provide insight into some technical aspects regarding arsenic immobilization and remobilization due to the three different sludge management alternatives, which are the disposal of the dewatered arsenic-iron hydroxide sludge, the disposal of the dried arsenic-iron hydroxide sludge, and the utilization of the dried arsenic-iron hydroxide sludge. However, these studies do not answer the most important question concerning the practical application of the research which is " of these three management strategies which is most suitable?". There are several factors influencing the answer of such a question. The most important factor is the evaluation criteria. In this study, the economic and the environmental health considerations are used as evaluation criteria.

In addition to evaluation criteria, the other factors influencing the feasibility of these three management options are as follows: (1) amount of the sludge produced which is the function of the amount of people consuming contaminated water in the affected area, an initial arsenic concentration, and a finished water target; (2) the degree of hazard of arsenic-iron hydroxide sludge which is a function of a initial arsenic concentration, and a finished water target; and (3) the cost of each management alternative consisting of the capital, the operation, and the maintenance cost. It should be noted that these factors vary not only from region to region but also from time to time.

The variations of these factors together with the complexity of the calculation for feasibility study of these management options may make the evaluation consume a

great deal of time and a large number of efforts. Therefore, to make the evaluation easier and quicker, the framework for evaluating the sludge management options is converted to a flexible spreadsheet which is processed by Microsoft Excel together with Visual Basic for Applications. All the assumptions as well as the manual of the spreadsheet will be discussed below.

The most important caution which the author wants to emphasize is the fact that this spreadsheet is developed to illustrate how the results of this research can be put together for more practical application and to show how the interrelationships among factors mentioned in the previous paragraph. The purpose of this spreadsheet is not to develop the ultimate tool for real-life application owing to the fact that there are a number of vital limitations such as lack of reliable costs concerning disposal and transportation of waste in each country and lack of data of strength requirement for an interlocking concrete paving block in each country. Therefore, it is assumed that the strength requirement for an interlocking concrete paving block in every country is the same as that in Thailand. However, if the actual data is available in future, this spreadsheet can be modified to be more realistic.

Furthermore, it is very important to emphasize that, for economic consideration, the cumulative cost is used as an index to evaluate the feasibility of each option. The cumulative cost at n^{th} year of a management option is the summation of cost of that option from 1^{st} year to n^{th} year. For example, the cumulative cost of the dried sludge disposal at 3^{nd} year is the summation of annual cost of the dried sludge disposal from 1^{st} year to 3^{nd} year. Moreover, the annual cost of each management used to calculate its cumulative cost is not the actual total annual cost. In fact, it is only the summation of some cost components contributing to the comparative economic analysis of the three management options. For example, considering Figure 4.115 illustrating the whole process and the cost components of each management option, the total cost of the disposal of the dewatered sludge is the summation of the costs of 1.1 to 1.3. Similarly, the total cost of the disposal of the dried sludge is the summation of the costs of 2.1 to 2.4 while the total cost and benefit of the utilization of the dried sludge is the summation of the costs of 3.1 to 3.4. However, it is clearly seen that the cost of 1.1, 2.1, and 3.1 are the same; therefore, the cost components used to calculate

the cumulative cost of the disposal of the dewatered sludge are the costs of 1.2 and 1.3. In the same way, the cost components used to calculate the cumulative cost of the disposal of the dried sludge and the utilization of the dried sludge are the summation of the costs of 2.2 to 2.4 and the summation of the costs of 3.2 to 3.4, respectively. In conclusion, the purpose of economic analysis in the spreadsheet is not to estimate the total cost of each management but to compare the cumulative cost among the three options to identify the most cost-effective option.

Now, it is time to discuss the spreadsheet named " Feasibility Study of the Three Management Alternatives". This spreadsheet can be divided into 3 sections: the sludge evaluation section, the unit cost & benefit section, and the option evaluation section. The sludge evaluation section consists of four steps. The first step is selecting a population range. This step is very important because the amount of population in an affected area is related to the demand of water per day (million gallon per day, mgd) which influences the amount of arsenic-iron hydroxide sludge produced per day. The relationship between a population range and a water demand per day used in this spreadsheet is from USEPA water system categories (Amy et al., 2000: 220) shown in Table A1 in Appendix.

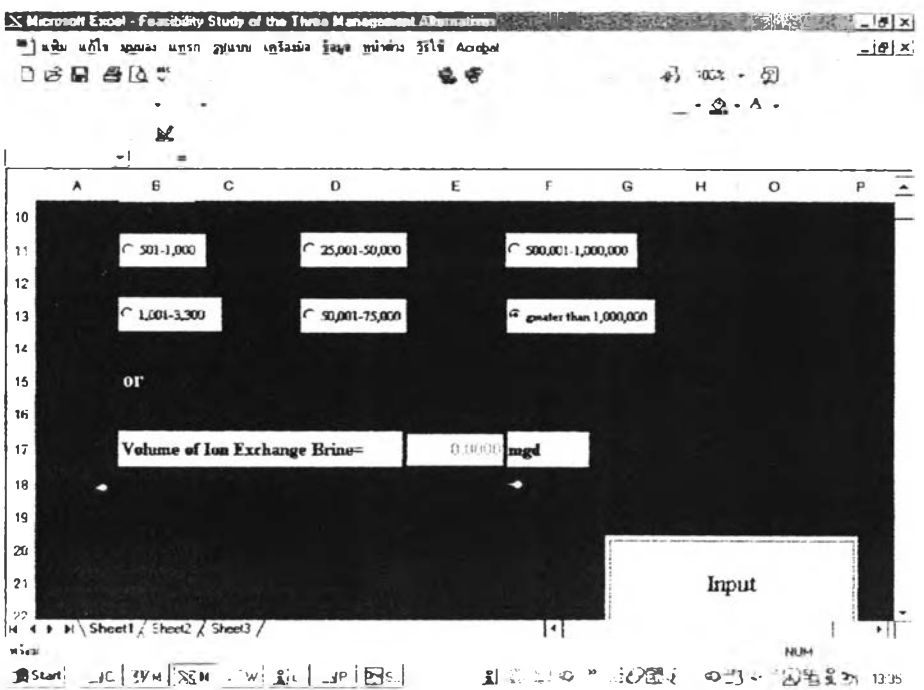

Figure 4.114 The first step of Feasibility Study of the Three Management Alternatives

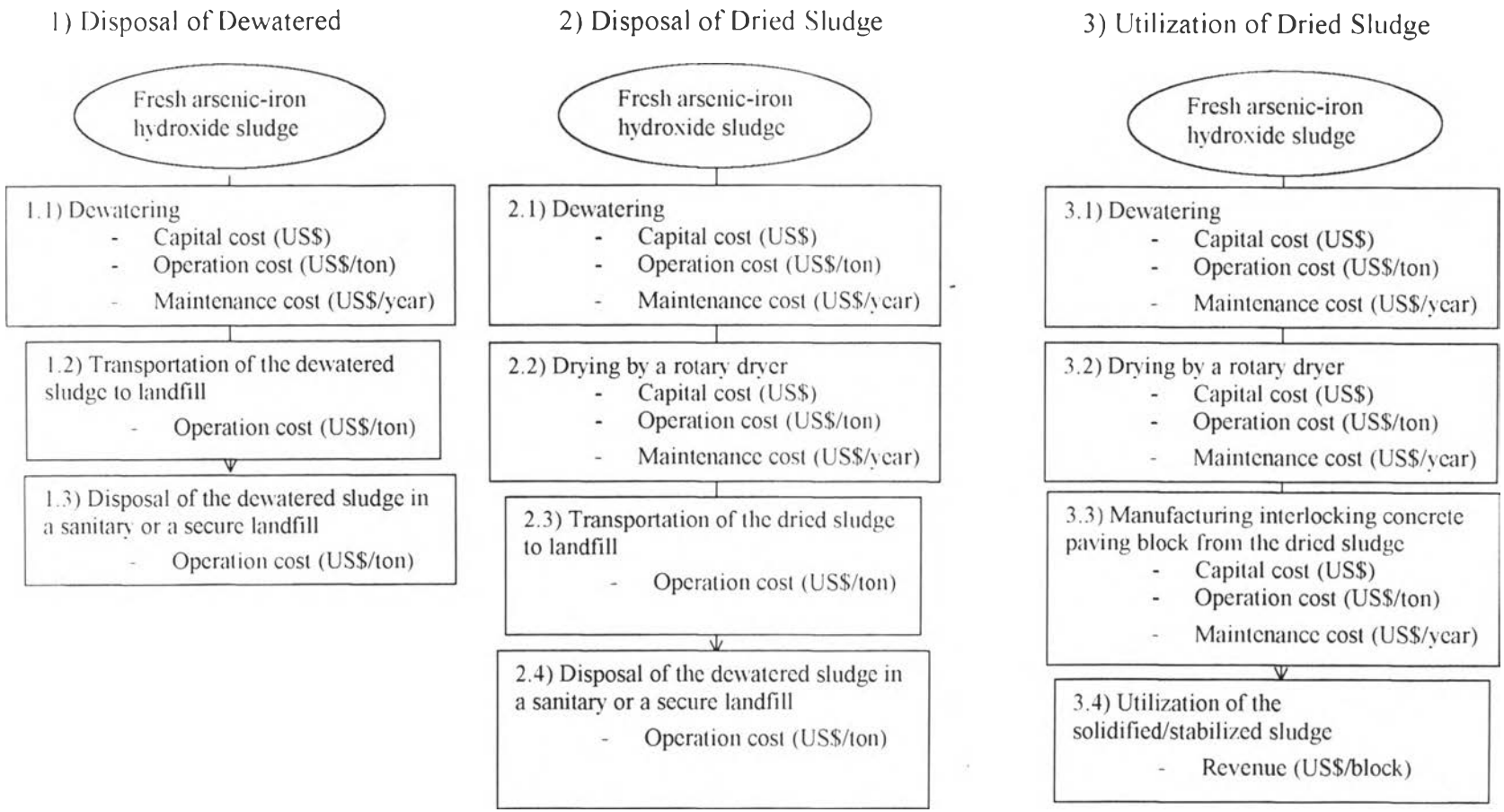

Figure 4.115 The whole process and cost components of each management option

For example, to apply this spreadsheet with the arsenic contamination in Bangladesh of which exposed population is $3x10^7$ according to Table 2.9, the first step is selecting "greater than 1,000,000" checkbox and push "Input" button as shown in Figure 4.114.

The second step is selecting the contaminated region. The contaminated region is also very important to the property and the amount of the sludge produced because MCLs of arsenic in drinking water vary from region to region as shown in Table 2.8. Therefore, select the forth checkbox containing Bangladesh and push "Input" button as shown in Figure 4.116

The third step is inputting maximum arsenic concentration (μg/L) in that contaminated area which is 2,500 μg/L in Bangladesh according to Table 2.9. Therefore, type 2,500 into the orange block as shown in Figure 4.117.

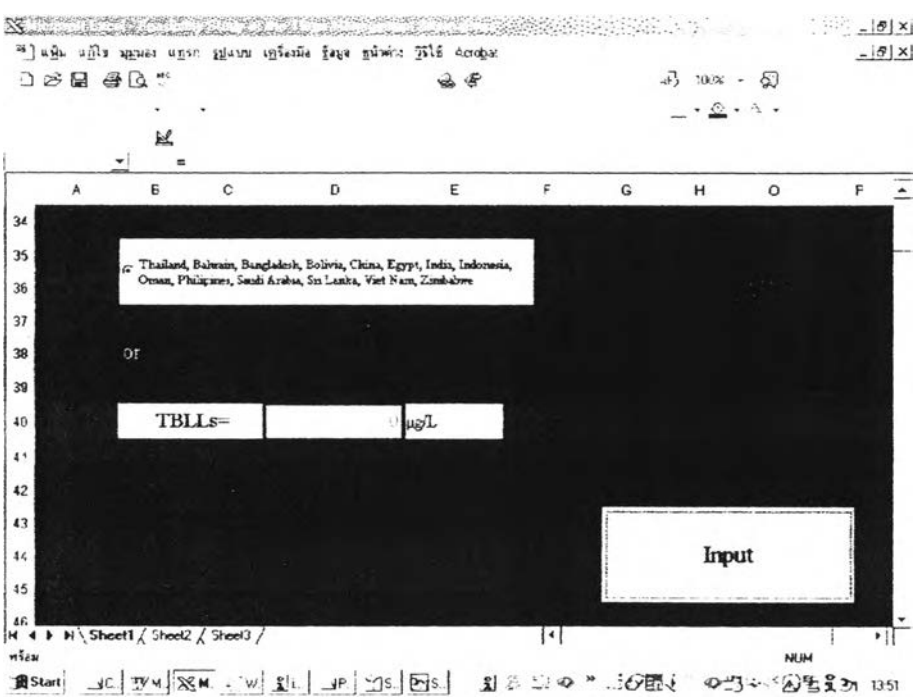

Figure 4.116 The second step of Feasibility Study of the Three Management Alternatives

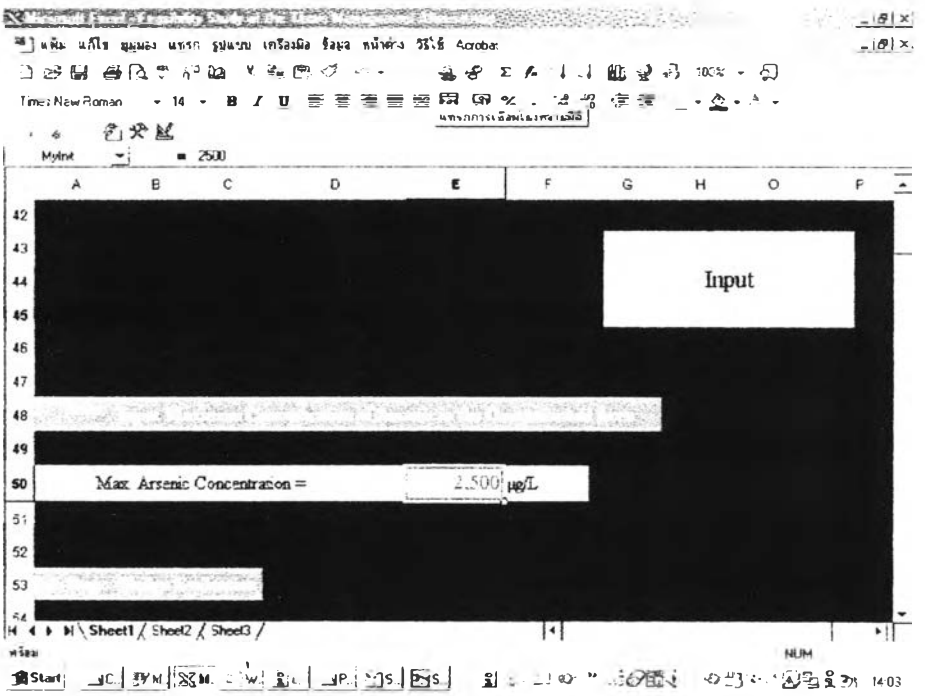

Figure 4.117 The third step of Feasibility Study of the Three Management Alternatives

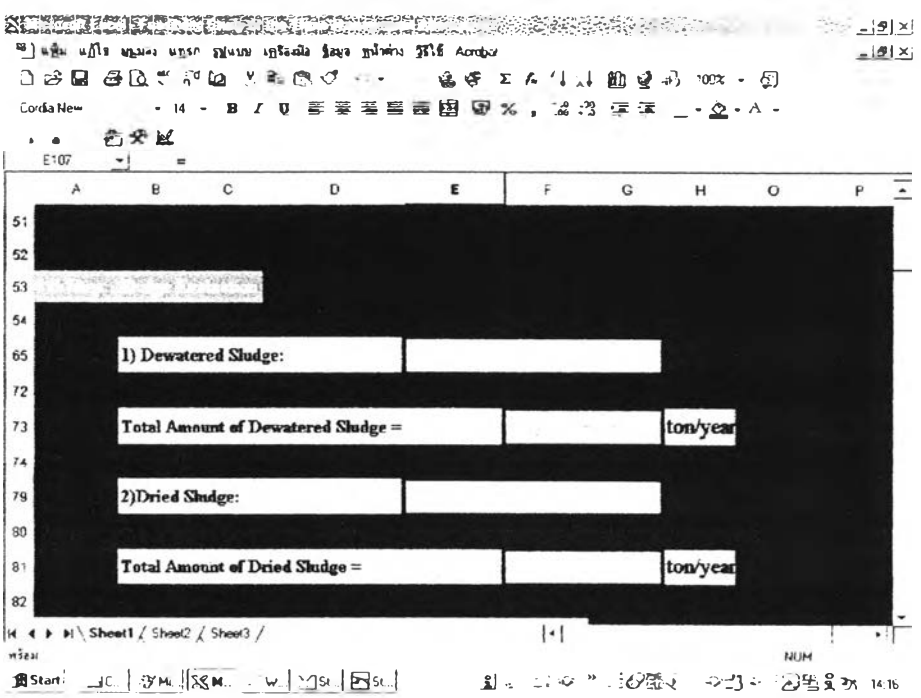

Figure 4.118 The forth step of Feasibility Study of the Three Management Alternatives

In the forth step, the spreadsheet will process the input data to determine whether the dewatered and the dried sludge are hazardous waste according to the empirical models in Part I, calculate amount of the sludge in each condition per year, and show the results in the yellow boxes as shown in Figure 4.118. It should be noted that the amount of dried sludge is calculated on the basis of mass balance concept according to Equation 2-26. Next, amount of dried sludge is multiplied by 100 and divided by (100 - water contain (%) in the dewatered sludge which is 78.1 % in this study) to obtain amount of dewatered sludge.

The next section is the unit cost and benefit section consisting of five steps, the fifth step to the tenth step. The fifth step is inputting the unit operation costs of the three management options. In reality, to obtain the best evaluation, these unit operation costs should have been the costs in Bangladesh. However, unfortunately, the author cannot find any of the unit operation costs in Bangladesh. For this reason, unit operation costs from other sources are used as an example to show how the spreadsheet works. All references of the costs inputted in the fifth step illustrated in Figure 4.119 are shown in Table A2 in Appendix.

The sixth step is selecting rotary dryers for drying the dewatered sludge. This step is very important for the dried sludge disposal and the dried sludge utilization. The specifications and the costs of the rotary dryers used in this spreadsheet are summarized in Table A3 and Figure A1 in Appendix. There are three steps in selecting the rotary dryers. First, consider volume of the sludge to be dried each day which is calculated by the spreadsheet and shown in a yellow box as shown in Figure 4.120(a). This value is derived from dividing total mass of the dewatered sludge per year with its specific gravity at moisture contain of 78.1% and working days in one year which is assumed to be 300 days. Select the rotary dryers to meet the required volume per day. In each checkbox are the code of a rotary dryer and its volume, so just select code of the rotary dryers and type amounts required in a yellow box; then push "Input" button as shown in Figures 4.120(b). However, if the volume of the selected rotary dryers cannot meet the requirement, the massage box will suggest selection of the additional rotary dryers as shown in Figure 4.120(c). Until the volume

of the selected rotary dryers is enough, the massage box will show "Finish Selection Go to Next Step" as shown in Figure 4.120(d).

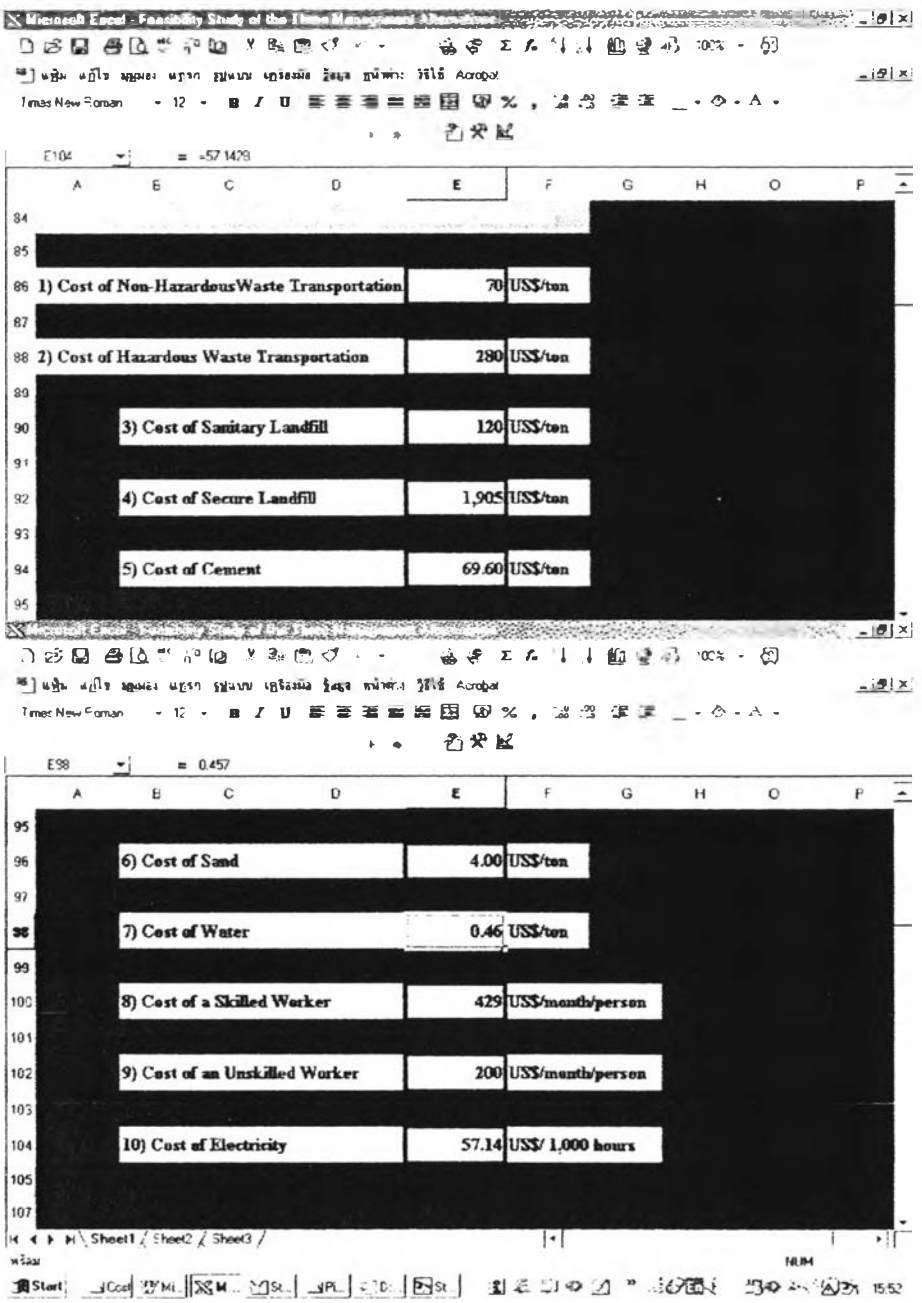

Figure 4.119 The fifth step of Feasibility Study of the Three Management Alternatives

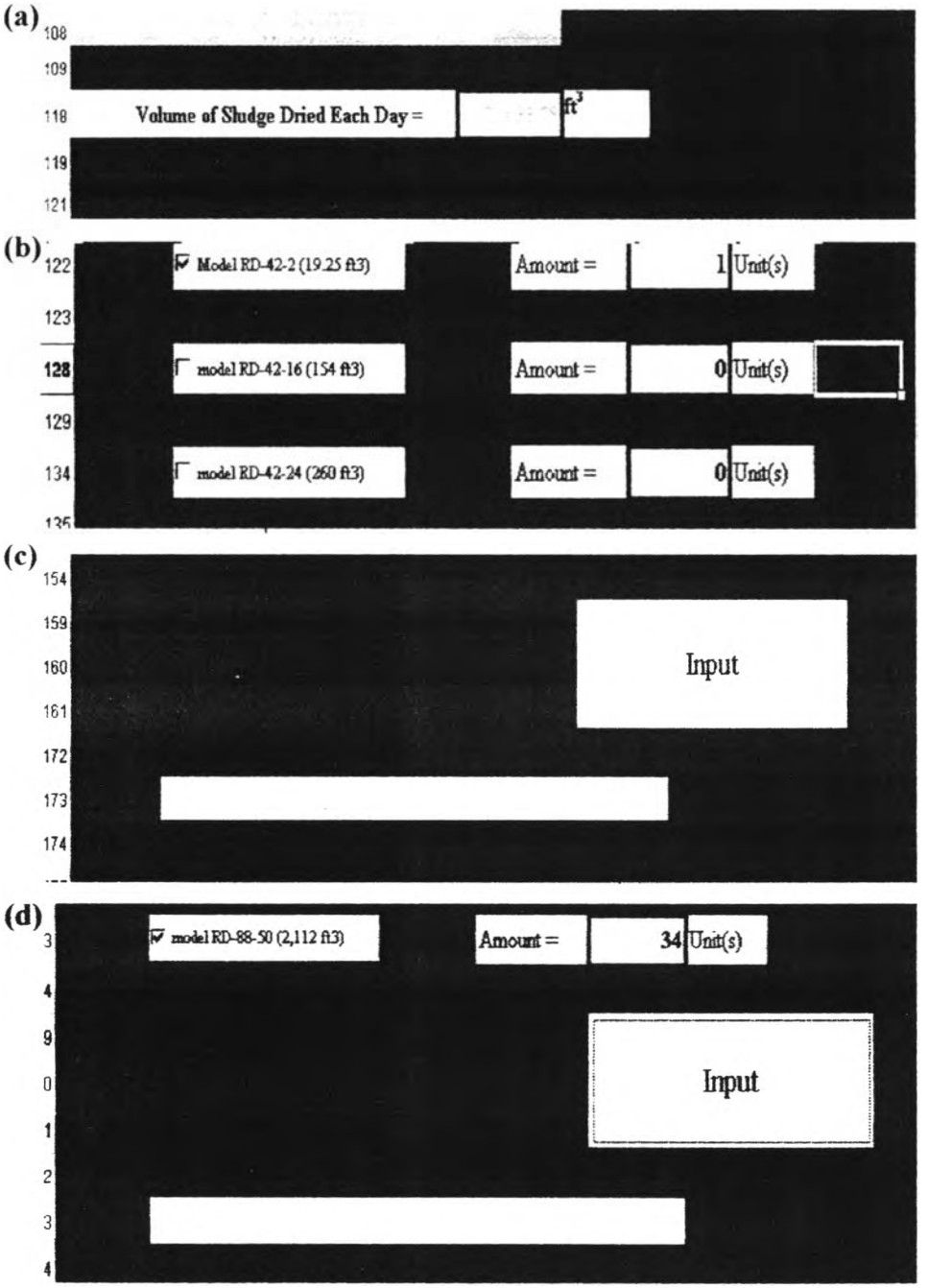

Figure 4.120 The sixth step of Feasibility Study of the Three Management Alternatives

The seventh step is inputting characteristics of the paving block making machine as shown in Figure 4.121. The paving block making machine is very important for the residual management by the utilization of the solidified/stabilized waste matrices. The specification of the paving block making machine used in this example is in Figure A2 and Table A4 in Appendix.

In the eighth step is the amount of the required paving block making machines calculated by the spreadsheet as shown in Figure 4.122. This amount is calculated by dividing the total concrete paving blocks which can be produced from the dried sludge per year by working days in one year (300 days) and the production rate of the machine. The ninth step is inputting the cost of interlocking concrete paving blocks for calculating revenue from the utilization. The cost of a concrete paving block used here is 0.1429 US$ according to CPAC (the Siam Cement, 2003). In addition, the interest rate (% of the capital cost) and maintenance cost (% of the capital cost) are considered in the tenth step as shown in Figure 4.122.

The last section, the option evaluation section, consists of only one step, the eleventh step, but it can be divided into two parts: the economic consideration and the environmental health consideration. The economic consideration of the three management options is evaluated by comparison among the cumulative cost and benefit of each option as shown in Figure 4.123. The positive value represents the cumulative benefit while the negative value represents the cumulative cost. Moreover, the details of the cumulative cost of benefit of the dewatered sludge disposal, the dried sludge disposal, and the utilization of the dried sludge are illustrated in Figures 4.124, 4.125 and 4.126, respectively. The components and formulas for calculating the capital, the operation, and the maintenance costs of each option are summarized in Table 4.25.

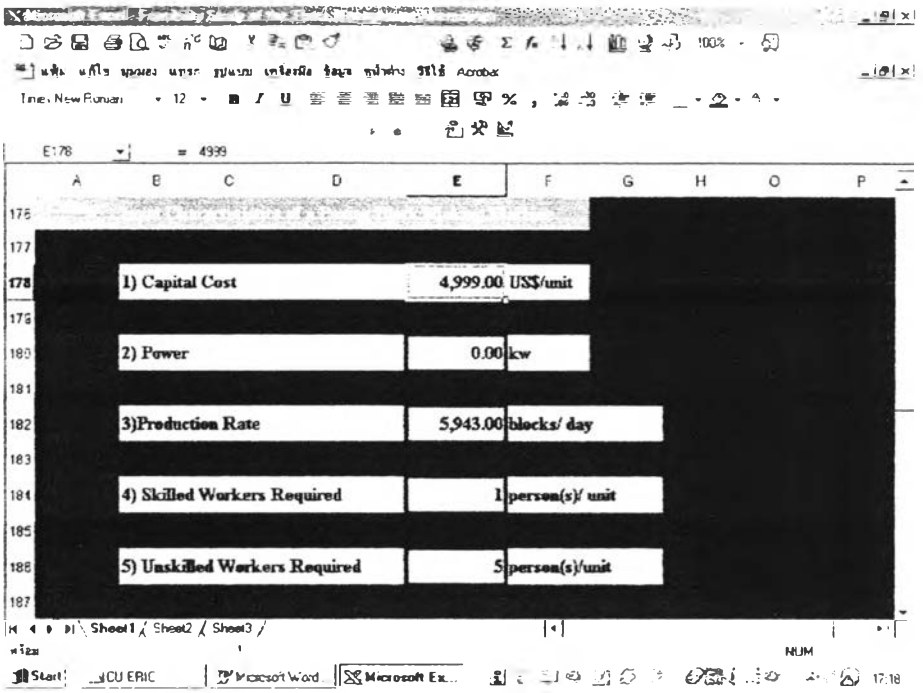

Figure 4.121 The seventh step of Feasibility Study of the Three Management Alternatives

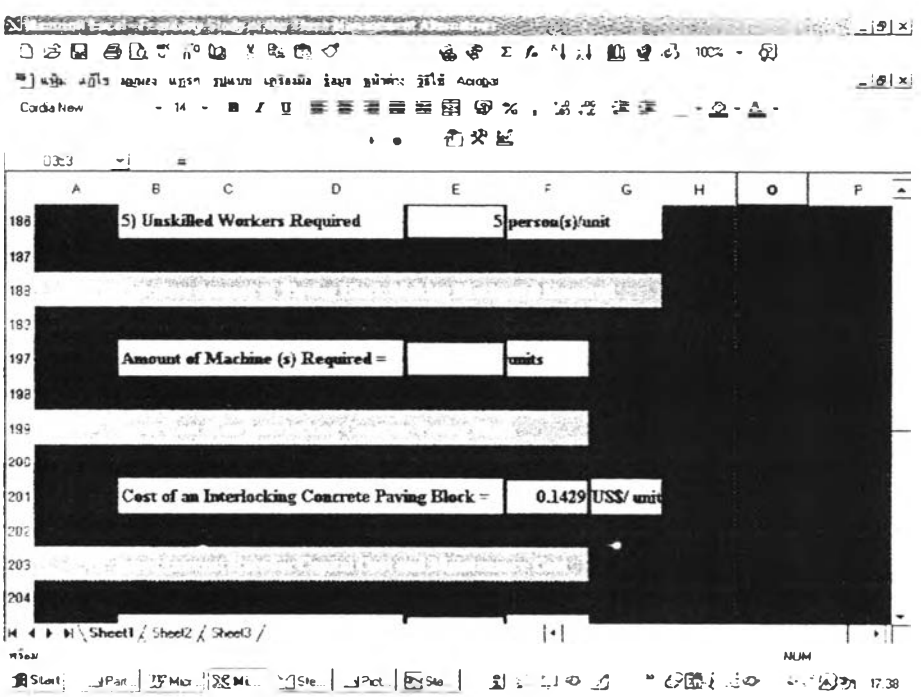

Figure 1.122 The eighth and the ninth steps of Feasibility Study of the Three Management Alternatives

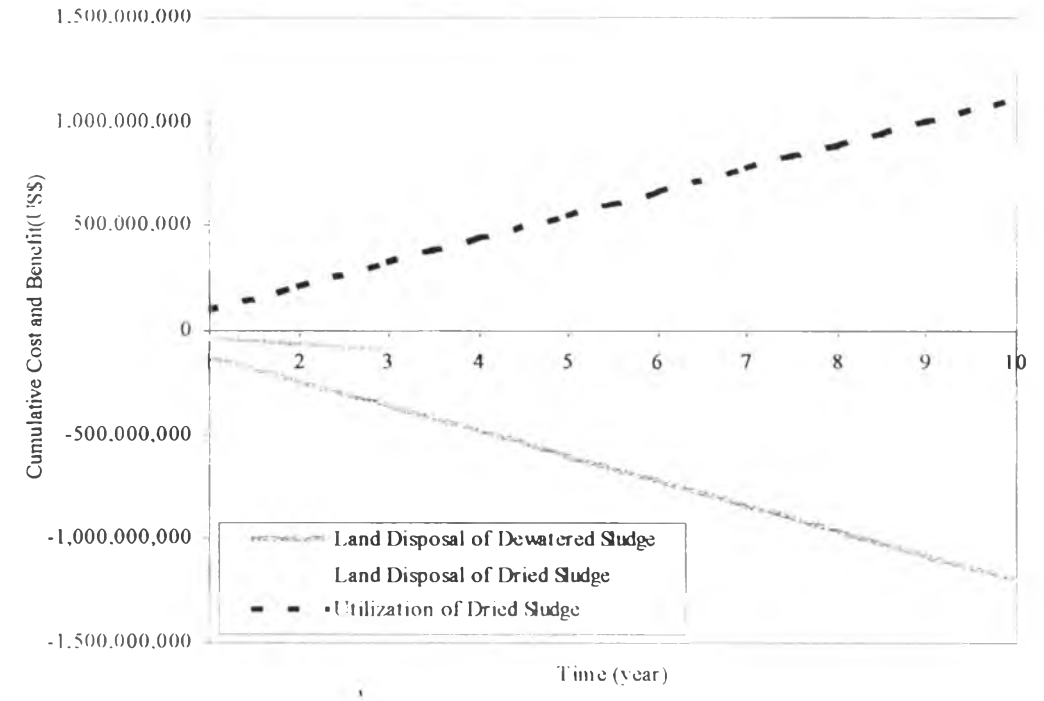

Figure 4.123 Economic consideration of sludge management alternatives for the first case study of which initial arsenic concentration is 2,500 μg/l and the affected population is greater than 1 million.

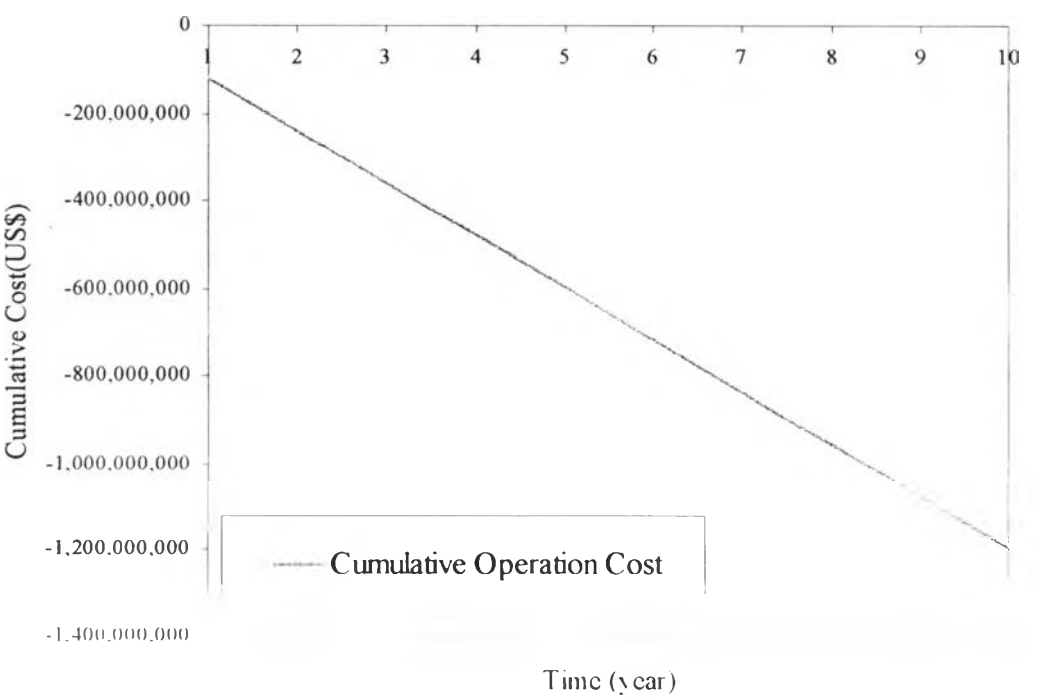

Figure 4.124 Cumulative cost and benefit analysis of dewatered sludge disposal of the same case as Figure 4.123

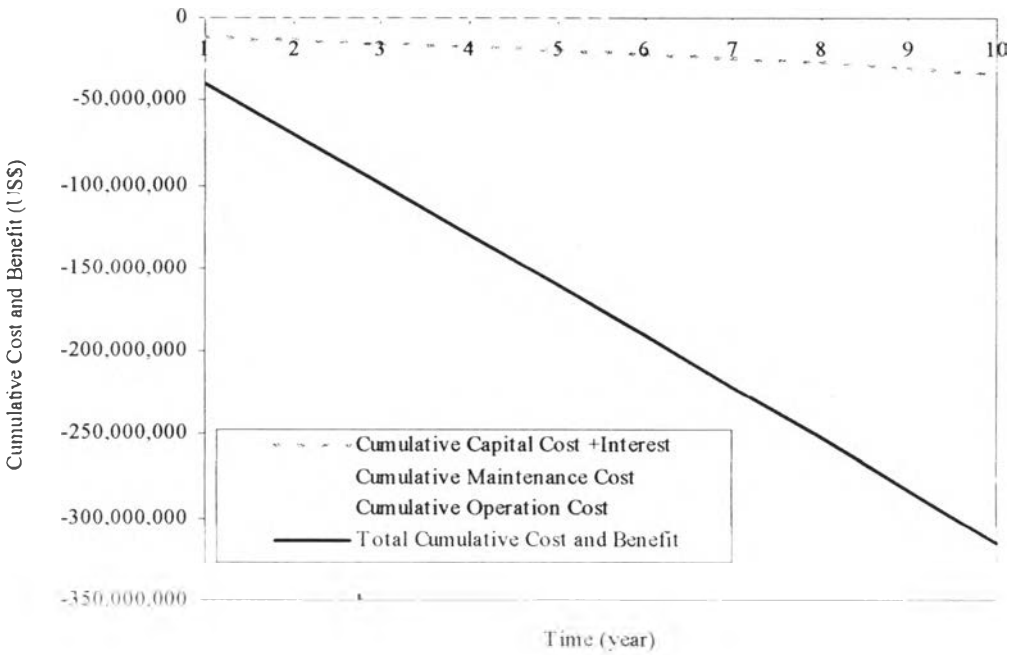

Figure 4.125 Cumulative cost and benefit analysis of dried sludge disposal of the same case as Figure 4.123

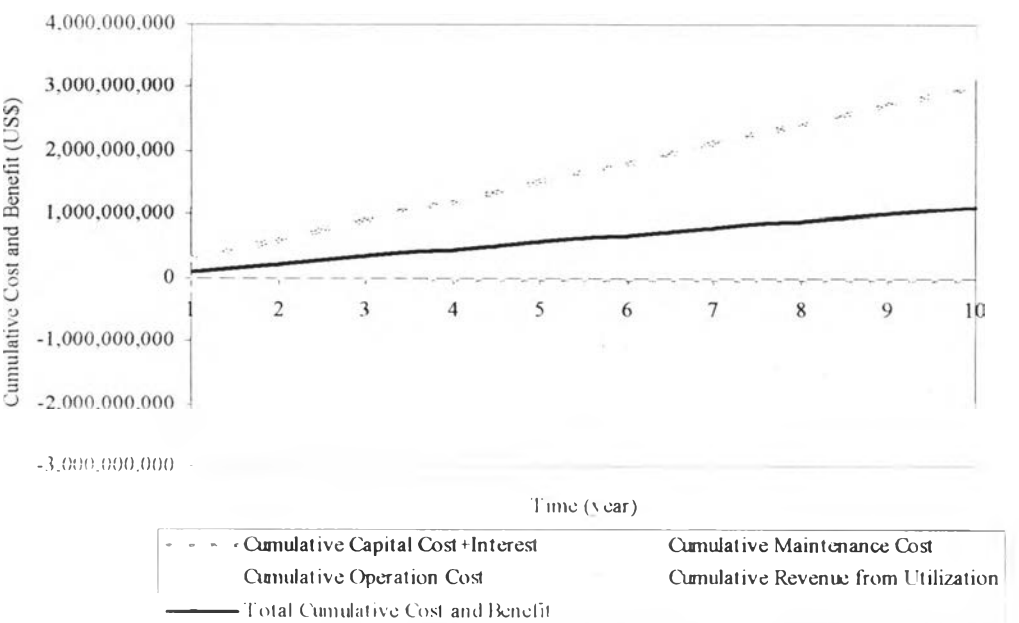

Figure 4.126 Cumulative cost and benefit analysis of dried sludge utilization of the same case as Figure 4.123

Table 4.25 The components and formulas for calculating the capital, the operation, and the maintenance costs of each option

Cost components Management option	Capital cost	Operation cost and benefit	Maintenance cost
Land disposal of dewatered sludge	-	Transportation cost + Disposal cost Transportation cost = [amount of dewatered sludge (ton/year) x unit transportation cost (US$/ton)] Disposal cost= (amount of dewatered sludge (ton/year) x unit disposal cost (US$/ton)	-
Land disposal of dried sludge	Cost of rotary dryers = [amount of rotary dryers required (unit) x unit cost of the dryers (US$/unit)]	Cost of workers for dryer operation + Cost of electricity for drying + Ttransportation cost + Disposal cost	Cost for dryers maintenance =[capital cost (US$) x percent of maintainance requirment (%/year)]

Table 4.25 (Cont)

Cost components Management option	Capital cost	Operation cost and benefit	Maintenance cost
Land disposal of dried sludge (Cont.)		Cost of workers for dryer operation = [1(person/unit)x amount of rotary dryers (unit) x salary of skilled-workers (US$/ month/person) x 12 months/ year] + [2 (person/ unit) x amount of rotary dryers (uint) x salary of unskilled workers (US$/ month/person) x 12 month per year] Cost of electricity for drying = [total power requirement of all dryers (kw) x 8 hours/day x unit cost of electricity US$/kw/ hour x 300 days per year] Transportation cost= [amount of dried sludge (ton/year) x unit disposal cost (US$/ton) Disposal cost=(amount of dried sludge (ton/year) x unit disposal cost (US$/ton)	

Table 4.25 (Cont.)

Cost components Management option	Capital cost	Operation cost and benefit	Maintenance cost
Utilization of dried sludge	Cost of dryers +Cost of paving block making machines Cost of rotary dryers= [amount of rotary dryers required (unit) x unit cost of the dryers (US$/unit)]	Cost of workers for dryer operation + Cost of electricity for drying + Cost of workers for making concrete blocks + Cost of cement for making blocks + Cost of sand for making blocks+ Cost of water formaking blocks + Revenue from block utilization	Cost for rotaryer maintenance + Cost for paving block making machine maintenance
	Cost of paving block making machines= [amount of paving block making machines required (unit) x unit cost of the machines (US$/unit)]	Cost of workers for dryer operation = [1(person/unit)x amount of rotary dryers (unit) x salary of skilled workers (US$/ month/person) x 12 months/year] + [2 (person/unit)x amount of rotary dryers (uint) x salary of unskilled workers (US$/ month/person) x12 months/year] Cost of electricity for drying = [total power requirement of all dryers (kw) x 8 hours/day x unit cost of electricity US$/kw/ hour x 300 days a year]	Cost for rotaryer maintenance = [capital cost of dryers (US$) x percent of maintainance requirment (%/year)] Cost for paving block making machine maintenance = [capital cost of the machines (US$) x percent of maintainance requirment (%/year)]

Table 4.25 (Cont.)

Cost components Management option	Capital cost	Operation cost and benefit	Maintenance cost
Utilization of dried sludge (Cont.)		Cost of workers for making blocks = [number of skilled worked required (person / machine) x amount of machines (machine) x salary of skilled workers (US$/ month/person) x 12 months per year] + [number of unskilled worked (person/machine) x machines (machine) x salary of unskilled workers (US$/ month/person) x 12 month/year] Cost of cement for making blocks = [amount of cement required to make one blocks (ton/block) x number of block produced per year (block/year) x unit cost of cement (US$/ton)] Cost of sand for making blocks =[amount of sand required to make one blocks(ton/block) x number of block produced per year(block/year) x unit cost of sand (US$/ton)]	

Table 4.25 (Cont.)

Cost components Management option	Capital cost	Operation cost and benefit	Maintenance cost
Utilization of dried sludge (Cont.)		Cost of water for making blocks = [amount of water required to make one blocks (ton/block) x number of block produced per year (block/year) x unit cost of water (US$/ton)]	
		Revenue from block utilization = [revenue from a block (US$/block) x number of block produce per year (blocks/ year)]	

Note: (+) for benefit and (-) for cost

Although Figure 4.123 seems to indicate that the dried sludge utilization is the best management option according to the economic consideration. It should be noted that this conclusion is not true for all cases. There are many factors that can alter the result as mentioned before. For example, if the arsenic contamination occurs in Thailand, but the exposed population are only 500 people. The initial arsenic concentration for this contamination is 5,000 mg/L. If the costs and the specifications of the dryers and the machines used in the previous example is still valid in this example, after finishing all eleven steps, it is found that the dried sludge utilization is not the best option as shown in Figure 4.127. Owing to the fact the amount of sludge produced in this example is minimal, the revenue from selling the concrete blocks produced from a little amount of dried sludge is not enough to compensate for the capital cost of the dryers and the block making machines. This is why the dried sludge utilization is not the cost-effective option in this case. This example is to emphasize that the best management option varies from case to case. Therefore, to select the best management option to deal with arsenic-iron hydroxide sludge as a result of arsenic contamination in drinking water sources, it is necessary to have the precise data of the contamination.

In the same way, the environmental health consideration of these three management options is evaluated by the comparison among the cumulative amount of leached arsenic according to the TCLP and LP-NO.6, the worst-case scenarios of leaching as shown in Figure 4.128. Amount of arsenic leached out of the sludge directly influences the environmental health in that if leached arsenic seeps to adjacent aquifers, in the presence of iron oxy-hydroxide coatings on soil particles, inorganic arsenic species are predominantly retained in such particles under oxidizing condition. However, onset of reducing conditions in such an environment can lead to the dissolution of iron-oxy hydroxide coating that can result in the release of iron(II), as well as arsenic present on such coating (Bose and Sharma, 2002; 4917). Finally, the arsenic contamination may take place again. For this reason, the best way to end or reduce the cycle of arsenic contamination is using the management strategy that allows the least leaching. According to Figure 4.128, the comparison between the cumulative leaching of arsenic estimated by the TCLP and LP-No.6 for the dewatered sludge disposal and that for the dried sludge disposal is the same trend as discussed in

Part I. However, it should be noticed that the cumulative leaching of arsenic estimated by the TCLP and LP-No.6 for the dried sludge utilization is higher than that of both the dewatered and the dried sludge disposal. This implies that immobilization efficiency of calcium-arsenic compounds is lower than that of arsenic-iron hydroxide surface complexation.

In addition, as mentioned in Part I, arsenic-iron hydroxide sludge is also produced from pretreatment of Ion Exchange brine by ferric chloride coagulation. This spreadsheet is applicable to management of such waste as well. For example, if concentration of arsenic in Ion Exchange brine is 10,000 μg/L, the volume of this brine is 0.004 mgd, and the TBLL of the contaminated area in the United States is 3,000μg/L, the concentration of arsenic, TBLL, and volume of brine are inputted to the orange boxes of the first, second, and third steps, respectively, as shown in Figures 4.129, 4.130, 4.131, and 4.132. Similarly, the forth step determines the volume and the degree of hazard of the sludge. It is found that the dried sludge is classified as hazardous as mentioned in Part I. Then, after the necessary data is inputted to the fifth step to the tenth steps, the results, both economic consideration and environmental consideration, are illustrated in Figure 4.133 and 4.134. According to Figure 4.133, it should be noted that owning to the fact that the cost of hazardous waste disposal is extremely expressive and the amount of sludge produced is so little that the revenue from the utilization cannot compensate the capital cost of the dryers and the machines, the dewatered sludge disposal seems to be the most cost-effective option in this case.

Last but not least, it is imperative to keep in mind that the present study serves to provide a extremely preliminary information on feasibility study of the three management option. In order to reach the point of practical application, a number of further studies have to be conducted, so the application of the result of this study should be done with great care.

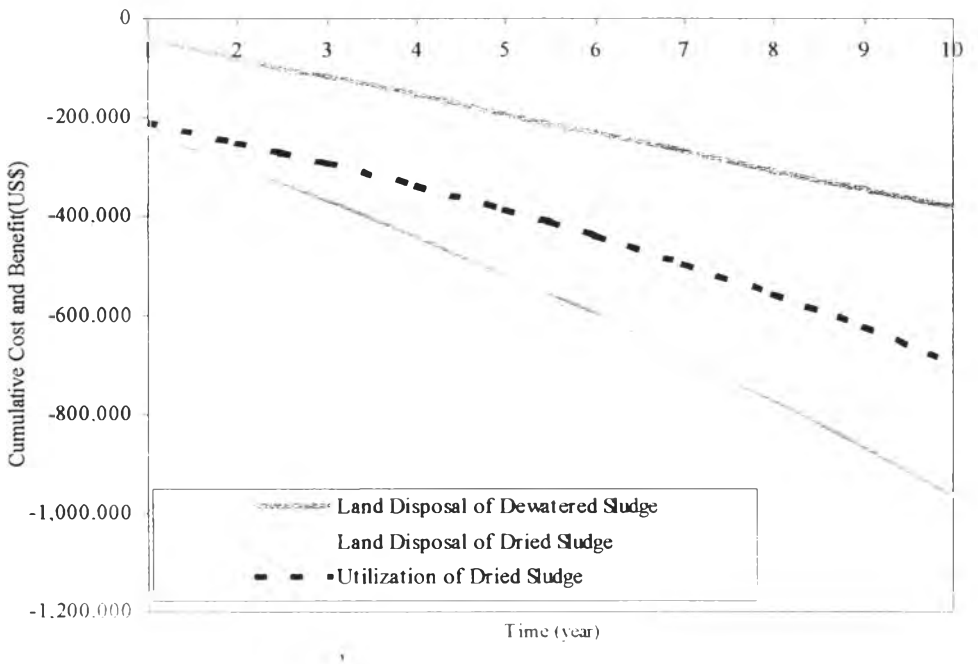

Figure 4.127 Economic consideration of sludge management alternatives for the first case study of which initial arsenic concentration is 5,000μg/l and the affected population is only 500 persons

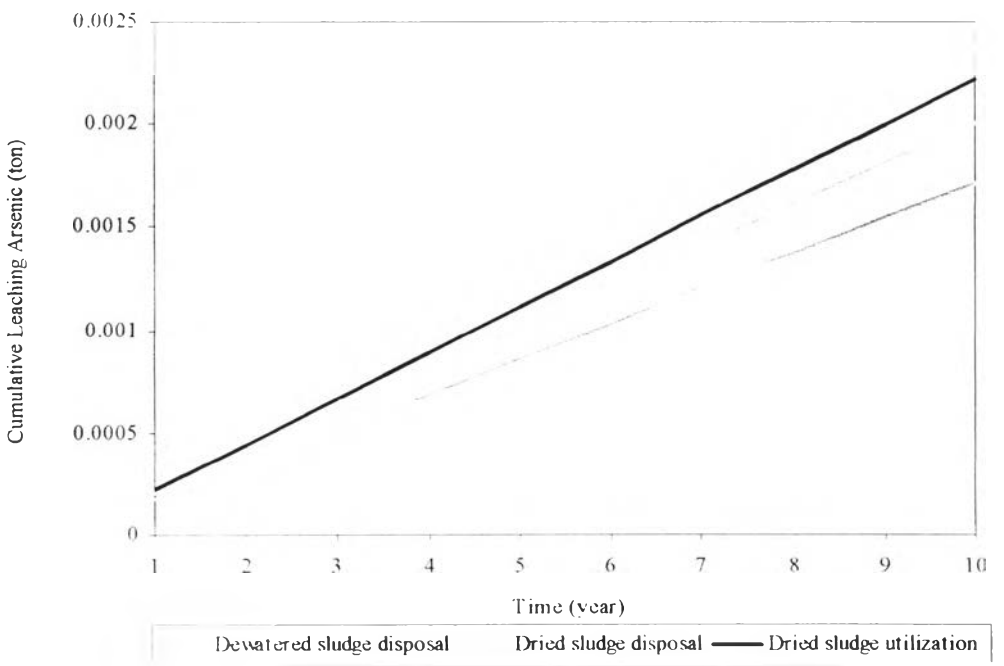

Figure 4.128 Environmental consideration of sludge management alternatives for the same case of Figure 4.123

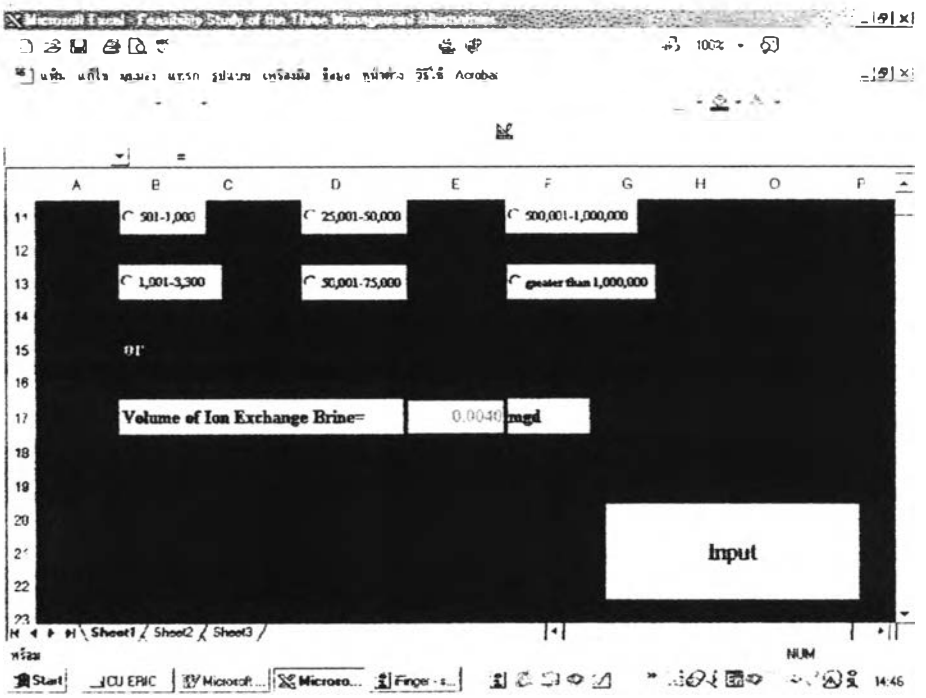

Figure 4.129 The first step for using the spreadsheet to evaluate management alternatives of sludge producing from pre-treatment of Ion Exchange brine of which arsenic concentration is 10,000 µg/L. TBLL is 3,000 µg/L, and volume of the brine is 0.004 mgd.

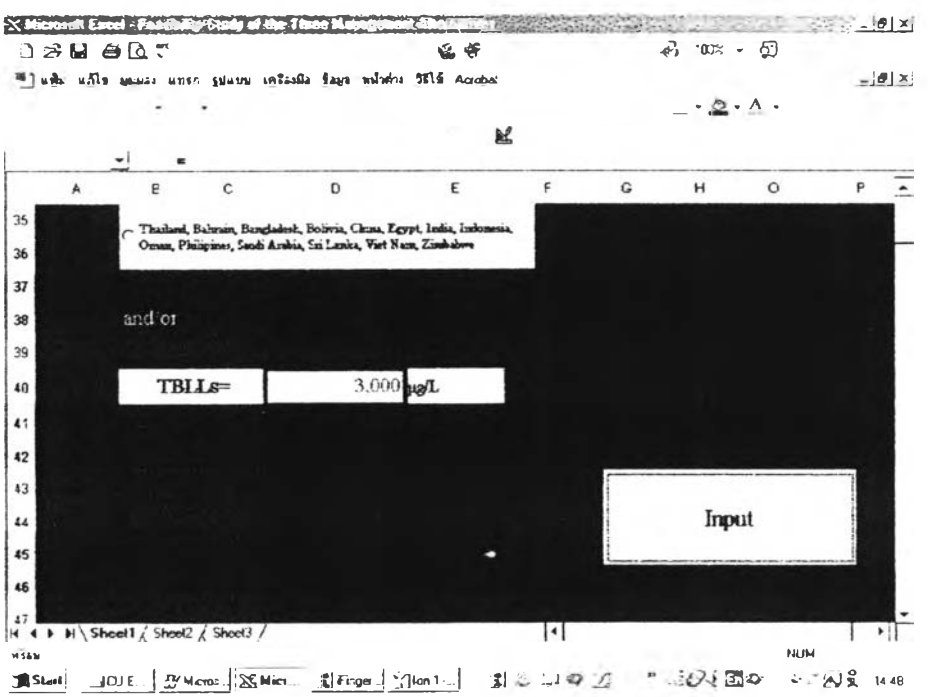

Figure 4.130 The second step for using the spreadsheet to evaluate management alternatives of same sludge as Figure 4.129

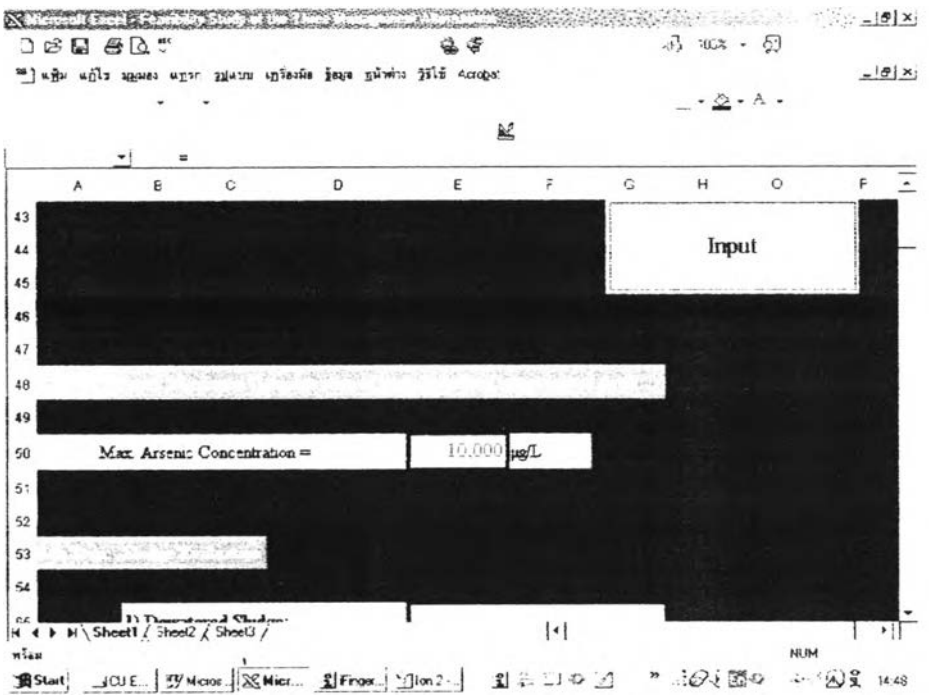

Figure 4.131 The third step for using the spreadsheet to evaluate management alternatives of same sludge as Figure 4.129

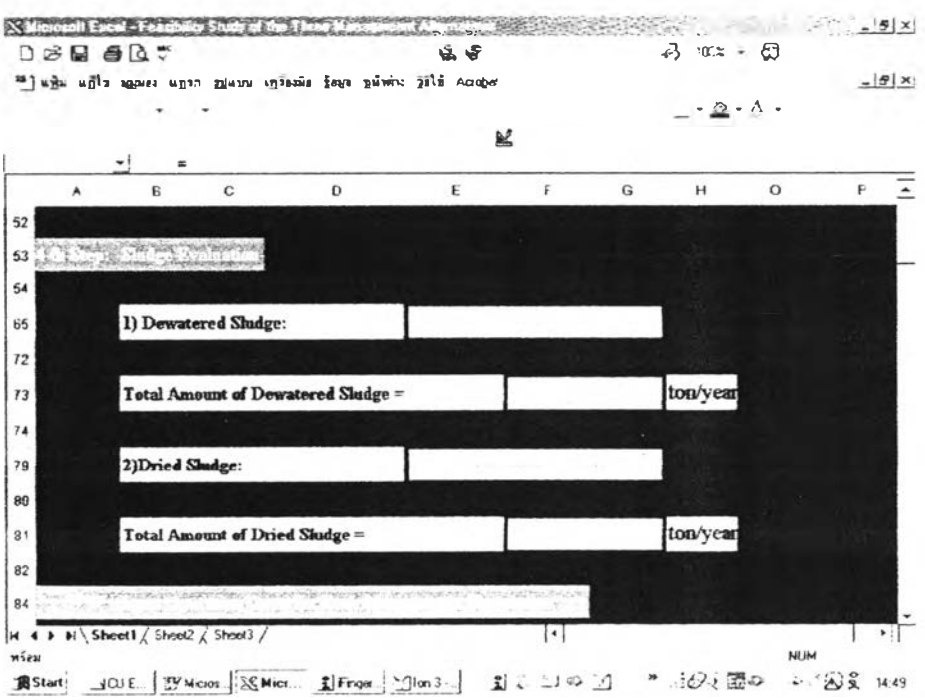

Figure 4.132 The forth step for using the spreadsheet to evaluate management alternatives of same sludge as Figure 4.129

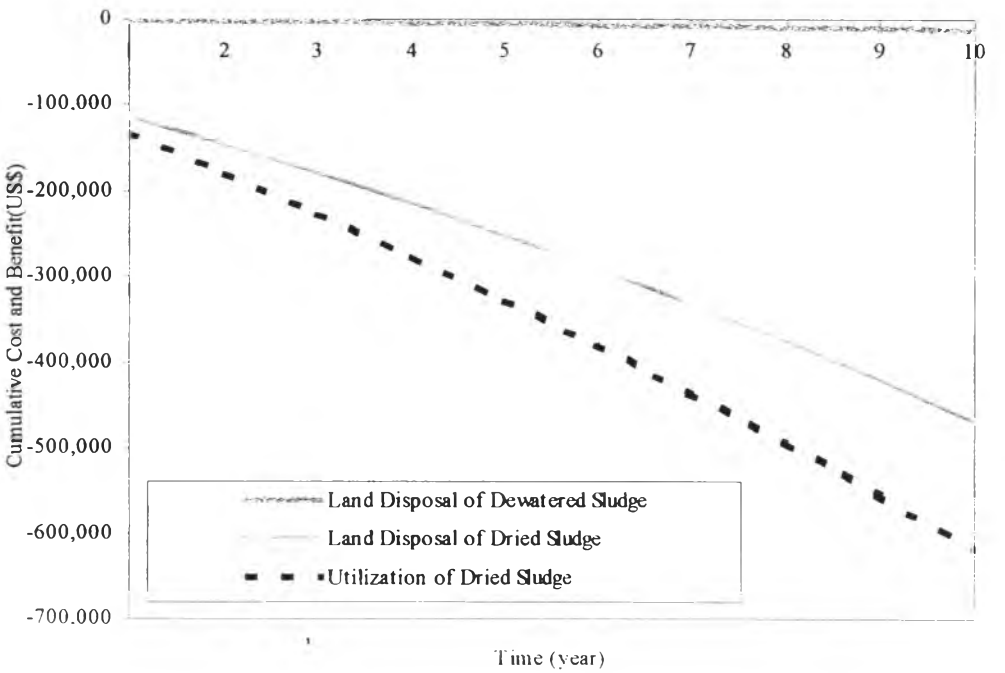

Figure 4.133 Economic consideration of the same sludge as Figure 4.129.

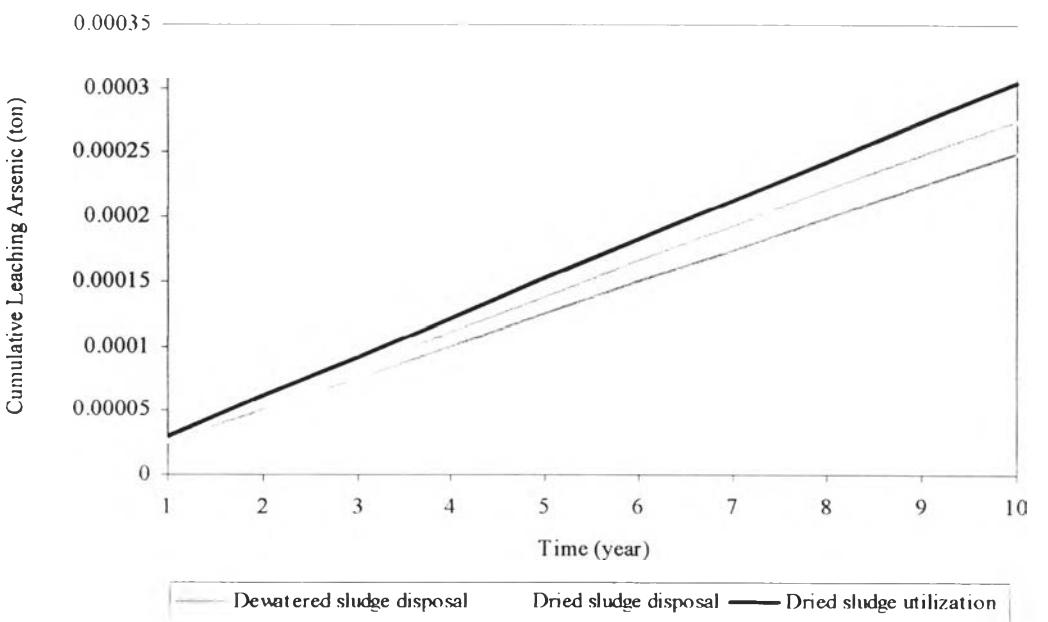

Figure 4.134 Environmental consideration of the same sludge as Figure 4.129.